The Dissertation Committee for Jeffrey Ryan Strahan certifies that this is the approved version of the following dissertation :

Advanced Organic Materials for Lithographic Applications

Committee:

C. Grant Willson, Supervisor

Eric V. Anslyn

Benny D. Freeman

Brent L. Iverson

Katherine A. Willets

Advanced Organic Materials for Lithographic Applications

by

Jeffrey Ryan Strahan, B.S.

Dissertation

Presented to the Faculty of the Graduate School of

The University of Texas at Austin

in Partial Fulfillment

of the Requirements

for the Degree of

Doctor of Philosophy

The University of Texas at Austin

August 2010

Dedication

I dedicate this dissertation to the influential teachers of my life. Among the multitude of people deserving my inexpressible gratitude, I specifically recognize Mrs. Pat Tyree, Mrs. Karen Mauldin, Prof. Kay Nakamaye, Prof. Jennifer Shepherd, and my parents.

Acknowledgements

nanos gigantium humeris insidentes

If I have seen a little further, it is by standing on the shoulders of Giants.

I begin by thanking one of the giants mentioned above: Prof. Grant Willson. I am honored to be the recipient of his support, encouragement, guidance, and mentoring throughout my five years in his group. I am a better chemist, engineer, scientist, employee, and man because of my time with him. Call it luck, chance, fate, or God's divine hand, our meeting in the spring of 2004 - followed by a phone call from Prof. Jennifer Shepherd at Gonzaga - led to Prof. Willson accepting me into his group, and I am forever thankful for this.

I also thank the second most important person in the Willson group: Mrs. Kathleen Sparks. The saying goes that behind every great man there is a great woman, and in our case, behind every great research group there is an irreplaceable team member like Kathleen. The completion of my graduate studies would not be possible without her.

From enlightening conversations, heated debates, and ferocious slide-editing at group meetings, all Willson group members have helped me during my five years. It began with the recommendation of former group members, Dr. Matt Pinnow and Dr. Brian Osborn, who solidified Prof. Willson taking me into his group. Once in the group, Dr. Brian Long and Dr. Jacob Adams invested significant effort into my scientific

training, and I will forever be in debt to them. Yukio Nishamura, Isao Nishamura, and Dr. Kane Jen patiently taught me the skills necessary for the engineering aspect of working in the Willson group. Current group members, Michael Jacobsson and Chris Bates, have been excellent resources on a day to day basis, and I wish them success in their upcoming careers.

Several members outside of the group have played important roles including Bielawski group members, Brent Norris, Dr. Kyle Williams, and Dr. Dan Coady. Dr. Peter Carmichael, Dr. Alex Liddle, and Dr. Kevin Yager from the National Institute of Standards and Technology provided much needed help when taking on new projects. I would also like to thank all of my committee members, and specifically Prof. Isaac Sanchez, Prof. Brent Iverson, and Prof. Eric Anslyn for their willingness to discuss scientific ideas. Additionally, Prof. Christopher Ellison has consistently treated me as a peer and colleague despite our different titles, and his door has always been open for my questions. UT staff members, Dr. Ben Shoulders, Steve Sorey, and Mike Ronalter, have been valuable resources whose expertise were called on multiple times.

I have had the privilege of working with a host of incredibly talented undergraduates who have amazed me with their ability to succeed in the classroom and work the number of hours they have in the laboratory. Without their hard work and input, my dissertation would remain noticeably incomplete. Although I did not break Michael Dickey's record of nine, I tried my best, and so I thank - in chronological order - Tim Rochelle, Colin Neikirk, Will Durand, Brennen Mueller, Jonathan Lee, Chad Webb, Jason Eubank, and Morgan Schulze. I hope I have shown each one of them the joys and pains of scientific research. Much more than any paper or patent I am a part of, I take pride and find great delight in their successes.

Dr. Jacob Adams, Dr. Adam Berro, Dr. Valerie Bradford, Dr. Bill Heath, Dr. Matt Pinnow, and Dr. Paul Zimmerman lent their wise council to me regarding finding employment. Each improved my résumé and interviewing skills and gave me confidence during the job search.

As mentioned in the dedication, teachers have played an important role in my life. Several high school teachers and college professors were instrumental in getting me into graduate school. I was a troubled youth, and without their constant pushing and challenging, I would not be here. Of note, Mrs. Tyree and Mrs. Mauldin are amazing teachers that introduced the joys of mathematics and chemistry to me. Prof. Kay Nakamaye and Prof. Jennifer Shepherd led me into the world of organic chemistry as an undergraduate, and I am most grateful for their encouragement and support to apply to graduate school.

It goes without saying that family has played the most influential role in my life. As I grow older and begin my professional career, I am continually amazed at my father's dedication and sacrifice to work sixty hour weeks for twenty-seven years with UPS. Truly only the purest of loves motivated and energized him. The same selfless love is found in my mother who spent countless hours teaching me up from down, one from two, and right from wrong. I can say with full confidence that my intelligence is due to in large part to my parents. Words cannot express my appreciation for their patience, discipline, and love.

This section would not be complete without acknowledging the blessings, grace, mercy, and love I have receieved from God. I find King David's words in Psalm 103 most appropriate to conclude.

Praise the Lord, O my soul;

all my inmost being, praise his holy name.

Praise the Lord, O my soul,
and forget not all his benefits-
who forgives all your sins
and heals all your diseases,
who redeems your life from the pit
and crowns you with love and compassion,
who satisfies your desires with good things
so that your youth is renewed like the eagle's.

Advanced Organic Materials for Lithographic Applications

Publication No._____

Jeffrey Ryan Strahan, Ph.D.

The University of Texas at Austin, 2010

Supervisor: C. Grant Willson

The microelectronics industry is driven by the need to produce smaller transistors at lower costs, and this requires an ever-changing approach to the chemistry involved in their fabrication. While photolithography has been able to keep pace with Moore's law over the past four decades, alternative patterning technologies are now receiving increased attention to keep up with market demand.

The first project describes work towards increasing the sensitivity of electron-beam resists by incorporating electron-withdrawing groups into the alpha position of methacrylates. After monomer design and synthesis, several polymers were synthesized that investigated the role of fluorine in the resists performance. G-values, electron-beam contrast curves, and EUV imaging showed that these fluorinated polymethacrylates outperformed current industrial resists.

The next project deals with the design, synthesis, and evaluation of a resist that seeks to decouple chemical amplification from acid diffusion. While work was shown that a system comprised of a photo-labile polyphthalaldehyde and

novolak could achieve this process, the high dose required to image was problematic. An aliphatic dialdehyde was envisioned to account for these issues, but its synthesis was never achieved. A polyethylene glycol aldehyde was synthesized and polymerized, but its material properties did not perform the intended function. Ultimately, the stability of aliphatic aldehydes proved to be too unstable for this project to continue.

While the synthesis was troublesome, a fundamental study of ceiling temperatures was undertaken. Numerical and analytical solutions were developed that describe the exact nature of the equilibrium constant on a living polymer system. These results were verified by a VT-NMR experiment, which accurately predicted the ceiling temperature of polythalaldehyde with a Van't Hoff plot.

Lastly, the self-assembly of block copolymers was investigated as a means to produce high resolution, high density nano-imprint lithography templates for bit patterned media. The first set of experiments involved synthesizing polymeric cross-linked surface treatments from substituted styrenes. The aryl substituent was shown to largely effect the surface energy, and after anionically synthesizing PS-b-PMMA, these materials were shown to effect block copolymer orientation. To produce a 3-D pattern of the self-assembled features, silicon was incorporated into one block to provide adequate etch resistance. Several monomers were investigated, and two, an isoprene and methacrylate analog, were successfully incorporated into two block copolymers. The silicon containing methacrylate derivative polymer was shown to successfully self-assemble in thin films under solvent annealing conditions.

Table of Contents

List of Tables

List of Figures

List of Schemes

Chapter 1: Photolithography

1.1 Societal Impact of Computers

The personal computer and the internet have completely revolutionized modern human existence. An average day in the life of a citizen in a westernized country includes scanning social networking websites, sending text messages and pictures via a cellular device, and "googling" any particular topic of interest for curiosity's sake. As a whole, industrialized society would cease to exist without the accessibility to information brought about by the personal computer and the internet. The twenty-four hour news updates, online stock trading, and global-positioning-system-guided travel would come to a crashing halt. Without computers the medical field could not offer such standard services such as magnetic resonance imaging, glucose monitors for diabetics, sonograms for pregnant mothers, and robot-stabilized hands for open heart surgery.

According to a 2007 article, "the number of personal computers in use worldwide will reach 1 billion by 2008 and 2 billion by 2015."[1] This prediction speaks not only of the widespread desire for computers but also the ability of the industry to produce this astounding amount of product. While other discoveries have led to world-wide paradigm shifts such as Plato's Republic, Galileo's heliocentric model, and Gutenburg's printing press, none of these have revolutionized human life on the same time scale as the personal computer and the internet.

1.2 Transistor and Integrated Circuit

The fundamental inventions that have led to the information age are the transistor and its incorporation into an integrated circuit. The transistor came about by the desire to replace vacuum tubes in electronic devices. Even after a half-century of improvements,

vacuum tubes were large, heavy, fragile, produced vast amounts of heat, and needed constant replacement because their filaments would only function for several hundred hours. Despite these limitations, the first general purpose electronic computer was announced in 1946 - ENIAC (Figure 1.1). Short for Electronic Numerical Integrator And Computer, it was financed by the United States Army during World War II and originally designed to calculate artillery firing tables. ENIAC was a true monster of a machine as it filled a 30 x 50 foot room and contained 17,468 vacuum tubes, 70,000 resistors, and 10,000 capacitors. This massive system weighed 30 tons, required 200 kilowatts of power, and over 2,000 tubes needed to be replaced each month.[2]

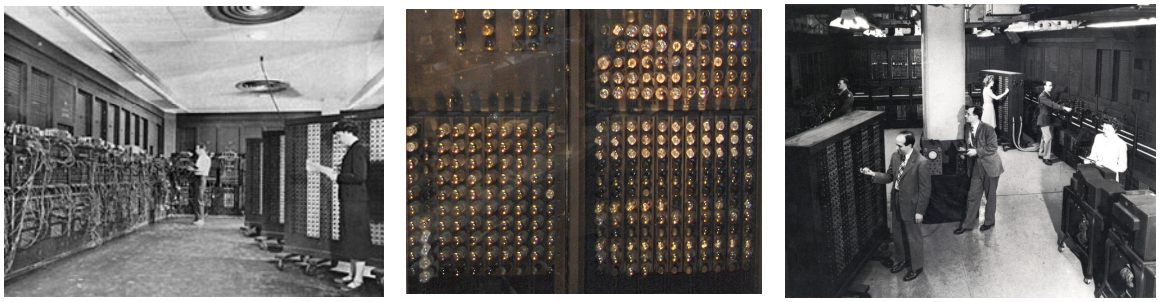

Figure 1.1: Pictures of ENIAC.[2]

Ironically, the invention that would make the ENIAC and all of its vacuum tubes obsolete within ten years was announced in 1947; the first solid-state transistor was demonstrated by William Shockley of AT&T Bell Labs.[3] Shockley and two of his co-workers, John Bardeen and Walter Houser Brattain, built a contraption that was able to amplify electric signals using a Germanium crystal and two gold contacts (Figure 1.2). Although still quite large at around half an inch tall compared to today's semiconductors, this technology vastly improved upon the tedious upkeep of vacuum tube amplification. The significance of this discovery has been properly recognized, and Shockley, Bardeen,

and Brattain received the 1956 Nobel Prize in Physics "for their research on semiconductors and their discovery of the transistor effect."[4]

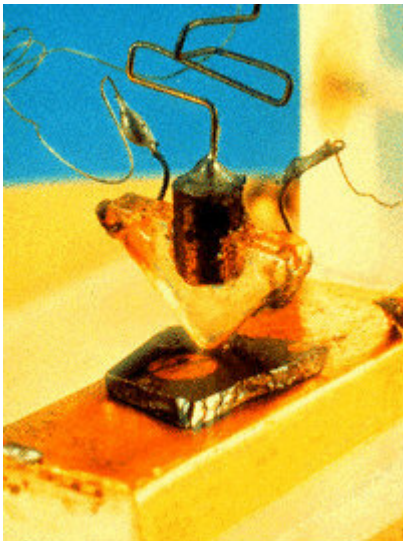

Figure 1.2: Shockley, Bardeen, and Brattain's point-contact germanium transistor.[3]

While the solid-state transistor was a massive improvement for amplification compared to vacuum tubes, Shockley's setup involved individual wires for each device of a circuit. This drawback was overcome in 1958 by Jack Kilby of Texas Instruments and Robert Noyce of Fairchild Semiconductor. Independently, these researchers successfully fabricated an integrated circuit (IC); a transistor, a capacitor, and a resistor all from silicon (Figure 1.3). Kilby continued in this field with great success; he held over sixty patents related to ICs and their applications. Ultimately he was awarded the National Medal of Science in 1970 and the Nobel Prize in Physics in 2000 "for his part in the invention of the integrated circuit."[4]

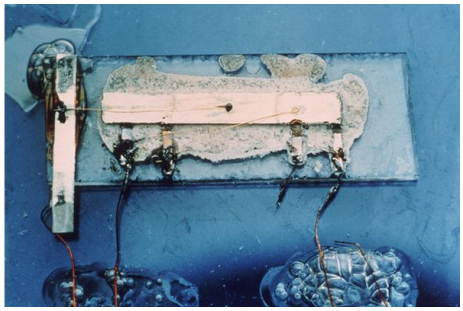

Figure 1.3: Jack Kilby's first Integrated Circuit (IC).[5]

1.3 MOORE'S LAW

The stage was set for the miniaturization of the IC. The smaller the individual components of an IC, the faster the capacitors can be charged and discharged. Furthermore since the devices are in such close proximity, the signal propagation time drastically decreases as size decreases. With the ability to mass-produce ICs from silicon substrates, the semiconductor industry was, is, and will continue to be driven by the need to decrease costs and increase the processing speed.[6]

The aggressive trend of increased transistor density was noted by a Fairchild Semiconductor employee, Gordon Moore, in 1965.[7] Eventually becoming CEO of Intel, a company founded by Robert Noyce, Moore's observation that the number of transistors on an IC doubles approximately every twelve months is now called, "Moore's Law." Now adjusted to an 18-24 month period, this doubling has remained true for the past forty years (Figure 1.4).

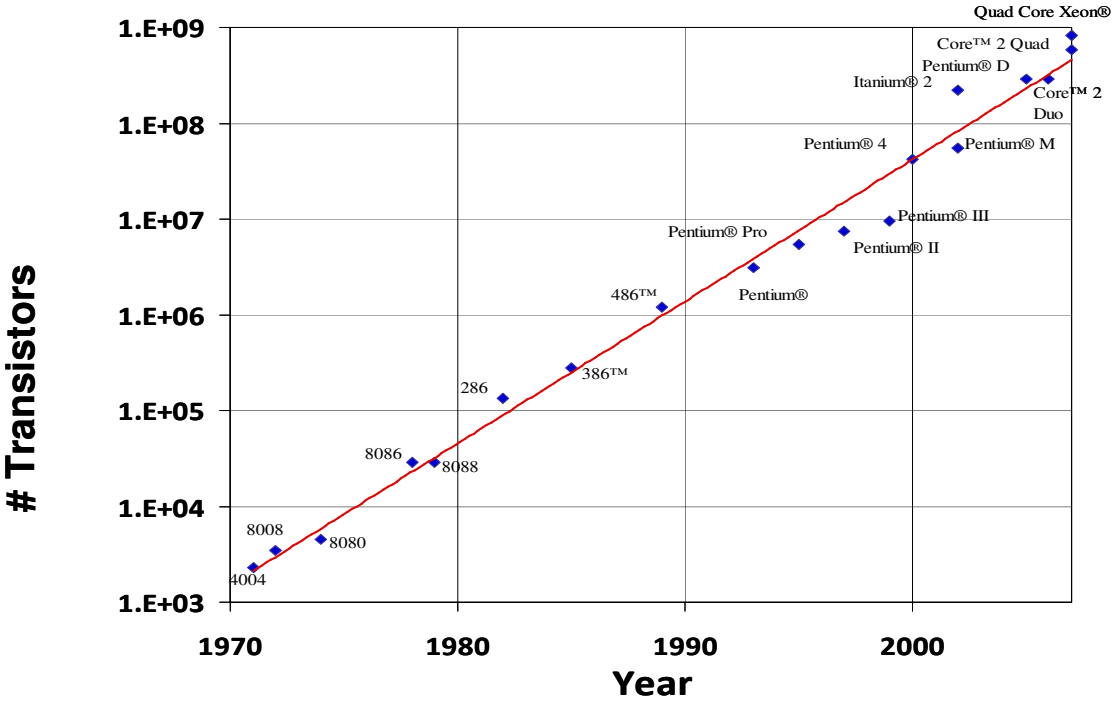

Figure 1.4: Moore's Law plotted as number of transistors vs time.

The ability of the semiconductor industry to keep this 'law' true is a testament to researchers across the world in multiple fields of science: physics, mathematics, optics, chemistry, chemical engineering, mechanical engineering, computer science, electrical engineering, etc.

1.4 PHOTOLITHOGRAPHY

From the 1970s to today, the ability to mass produce ICs has relied on the process of photolithography (Figure 1.5). This process can be simplified to five steps: prepare, expose, develop, etch, and strip. Each step has been studied in great detail and involves numerous variables, complex relationships, and requires tedious attention to detail at the manufacturing level. The general procedure begins with a flat silicon wafer. A planar layer to be patterned such as an oxide, polysilicon, or metal is deposited, followed by

spin-coating of an organic photoresist film. The wafer is selectively exposed to ultraviolet radiation in certain areas as dictated by a mask. Wherever photons reach the photoresist, they induce chemical reactions that change the solubility characteristics of the photoresist. This leads to two types of photoresists: positive tone and negative tone. The exposed areas of positive tone photoresists are more soluble in certain developers than the unexposed areas, while the opposite is true for negative tone resists. Once the wafer has been washed with developer to dissolve and remove the desired areas, the patterning layer is now accessible. The removal of the patterning layer is accomplished by a variety of etch chemistries, the most common being a reactive ion etch (RIE). It is crucial in this step for the photoresist to display a slower etch rate than the patterning layer. The photoresist actually derives its name from the fact it is both photosensitive (photo-) and can resist various etch chemistries that remove patterning layers (-resist). Once the patterning layer has been etched down to the substrate, the photoresist is stripped away to yield the first layer of an IC. This stripping is commonly accomplished by development in a solvent or an oxygen RIE that can remove organic materials.

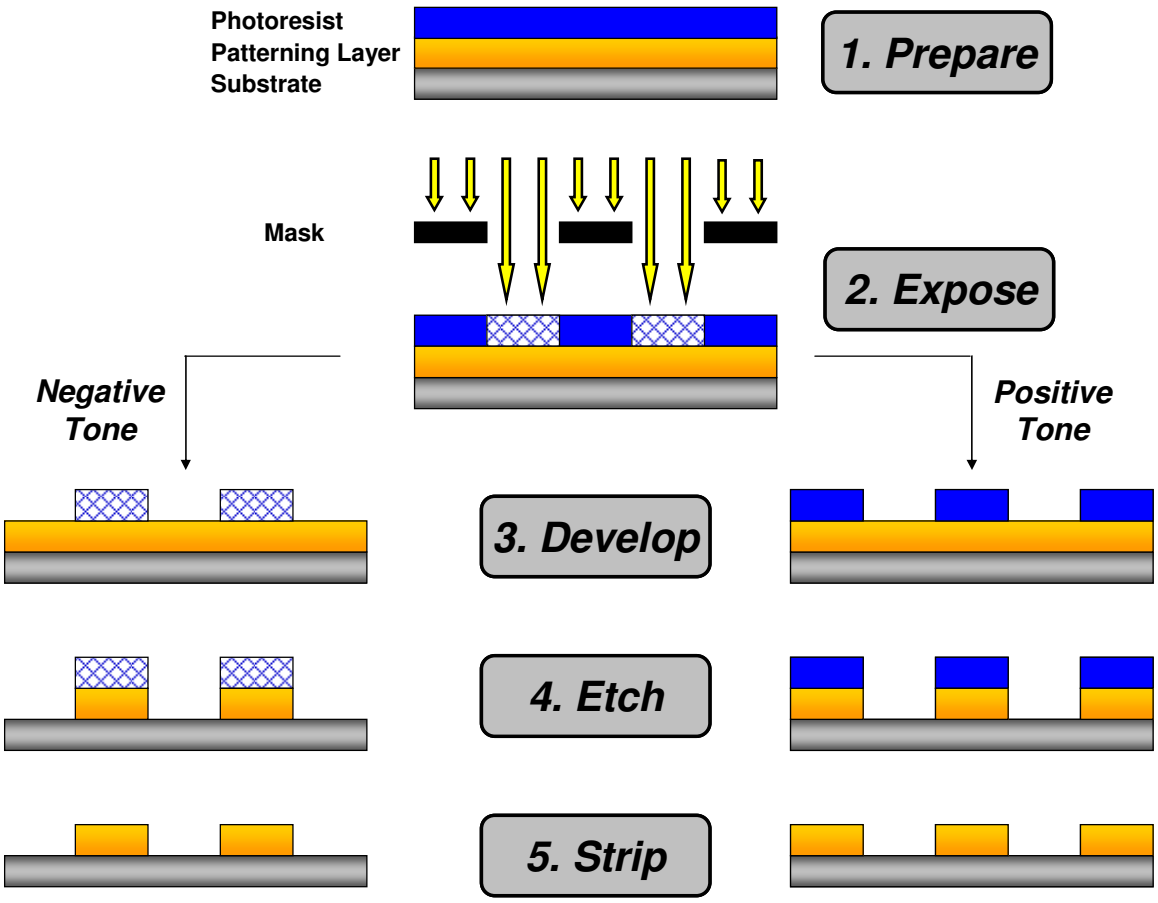

Figure 1.5: Simplified five step photolithographic process.

This process is repeated to produce a functioning IC with several layers of conductive and insulating materials. Current state-of-the-art microprocessors contain more than seven levels of wires intricately designed for the logic processes that give computers their unparalleled speed and computing power. It is quite remarkable this process is done around the clock and around the world to yield microprocessors. While numerous steps have been skipped for simplicity's sake, the overall process has been optimized to produce computer chips with over 2,000,000,000 transistors.[8]

1.5 RAYLEIGH EQUATION

The Rayleigh equation states the minimum feature size that can be printed with projection lithography (R) is directly proportional to the exposure wavelength (λ) and a process-dependent factor (k_1) and inversely proportional to the numerical aperture of the lens (NA) (eq (1.1)).

$$R = \frac{k_1 \lambda}{NA} \qquad (1.1)$$

Optical engineers have made tremendous strides in increasing the NA of lens systems to decrease the minimum feature size. The projection lithography systems of the 1970s had NAs of approximately 0.16, and this was improved to 0.28 in the 1980s.[9] Current lens systems have an NA of 1.3, but this comes at an enormous price. The entire optics system costs many millions of dollars and requires months to produce. While no image could be taken of an actual machine's optics system for proprietary reasons, Figure 1.6 below gives an idea of just how complex the system is.

Figure 1.6: Simplified cartoon version of optics within a current stepper.[10]

While increases in the NA of the optics system decrease the minimum feature size, the depth of focus decreases (eq (1.2)).[11] A small depth of focus decreases the process window and increases the complexity of the process.

$$DOF = k_2 \frac{\lambda}{NA^2} \quad (1.2)$$

Therefore researchers have approached the need to decrease transistor size by decreasing the exposure wavelength. This mandates materials that have low optical densities at these exposure wavelengths.

With highly absorbent materials, photons never reach the bottom of the photoresist film (Figure 1.7). This leads to incomplete chemical reactions within the photoresist, poorly resolved features, and eventually a failed device due to poor connections between conductive wires. The SEMs below display not only residual photoresist left by incomplete development but irregular rounded edges.

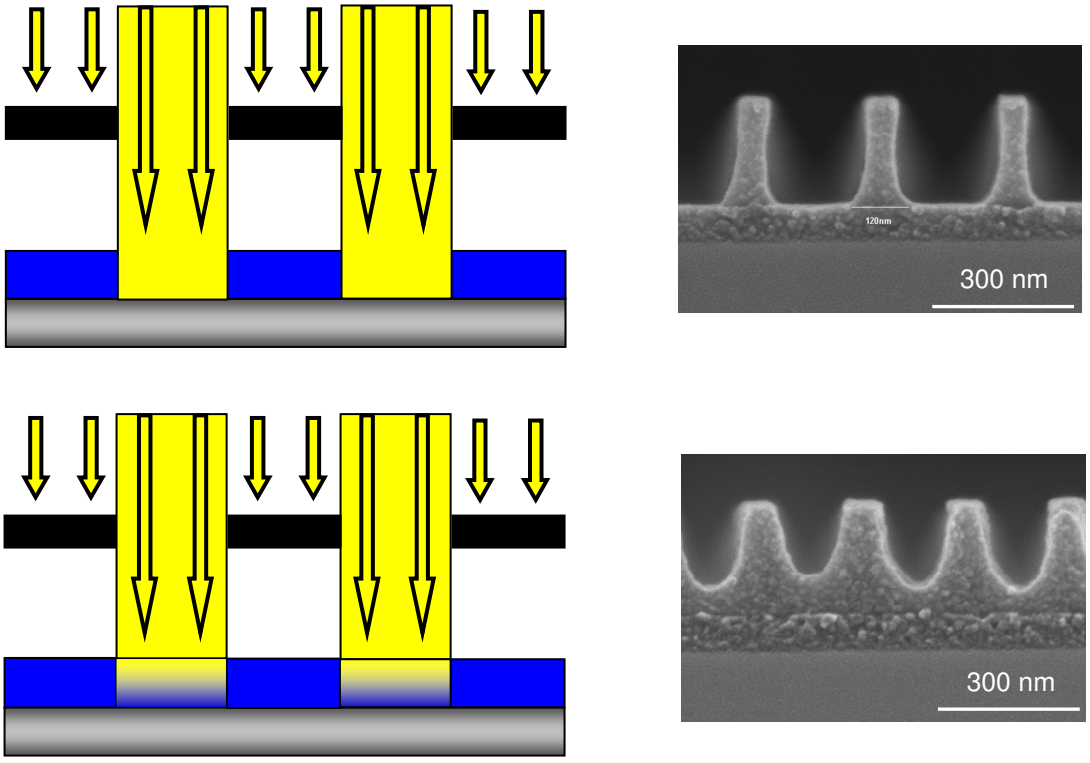

Figure 1.7: Impact of an absorbent photoresist upon features.

1.6 EXPOSURE WAVELENGTH

The exposure wavelengths used by the semiconductor industry have been chosen historically for one simple reason - power. Without a lot of cheap photons, devices cannot be produced on a massive scale. If the source is cheap but inefficient at delivering exposure photons, then exposure time increases driving up costs and consumer prices.

Likewise if the source is efficient at delivering photons but is itself expensive, costs rise as well. What is truly desired is a cheap source that efficiently converts input energy into exposure photons. A mercury arc lamp meets these requirements, and its emission spectrum is shown below (Figure 1.8).[12]

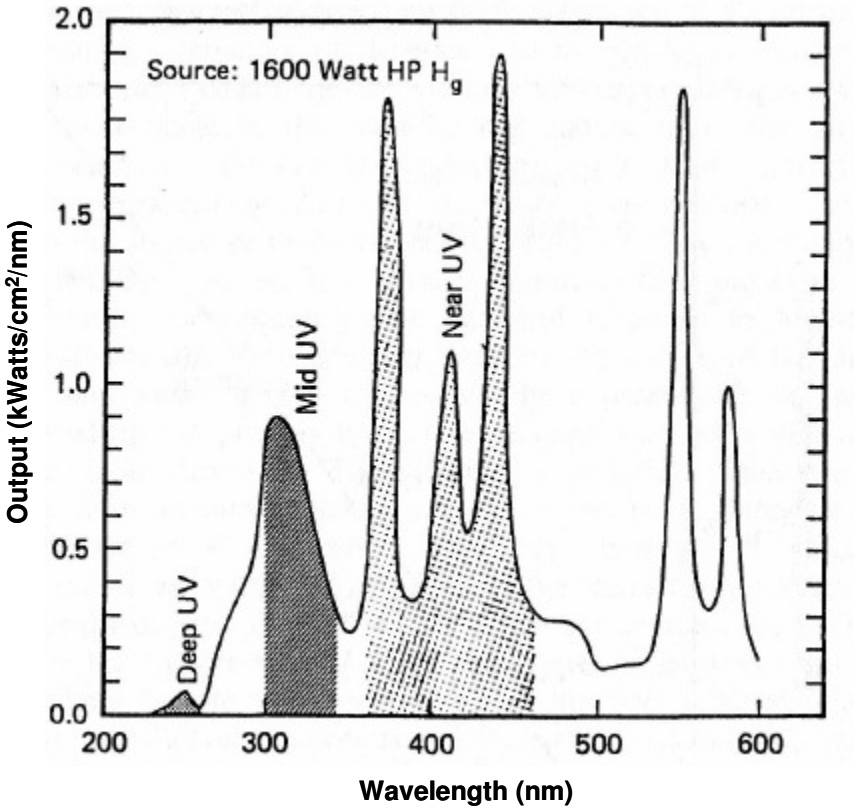

Figure 1.8: Output in watts/cm^2/nm of a mercury arc lamp.

The most prominent exposure wavelengths utilized from a mercury arc lamp have been 436 nm (g-line) and 356 nm (i-line). The major chemistries tuned to these exposure wavelengths will be discussed later. Once the industry demanded resolution beyond what could be manufactured from 356 nm, a KrF excimer laser was chosen as the viable source with a large output of 248 nm radiation. The progression continued when 193 nm was

determined to be the next exposure wavelength due to the availability of an efficient ArF excimer laser. When the industry once again tried to keep pace with Moore's Law by reducing the exposure wavelength, an F_2 excimer laser with a reasonable 157 nm output was chosen. For a variety of reasons, the industry abandoned research into 157 nm materials and has reverted back to 193 nm. The ability for the traditional photolithographic process to keep pace with Moore's Law is being questioned and an overview of alternative manufacturing techniques will be provided later.

1.7 THE CHEMISTRY OF PHOTORESISTS

1.7.1 Negative-Tone

KTRF (Kodak Thin Film Resist) has been one of the most successful negative tone resists. It is based on the cross-linking chemistry of bis-aryl azides with poly(isoprene).[13] The poly(isoprene) is soluble in common organic solvents, but the highly absorbent bis-aryl azides form nitrenes upon exposure that cross-link the matrix. This cross-linked material has minimal solubility in the original developer (Scheme 1.1). This large change in solubility provides the contrast necessary for the production of viable features.

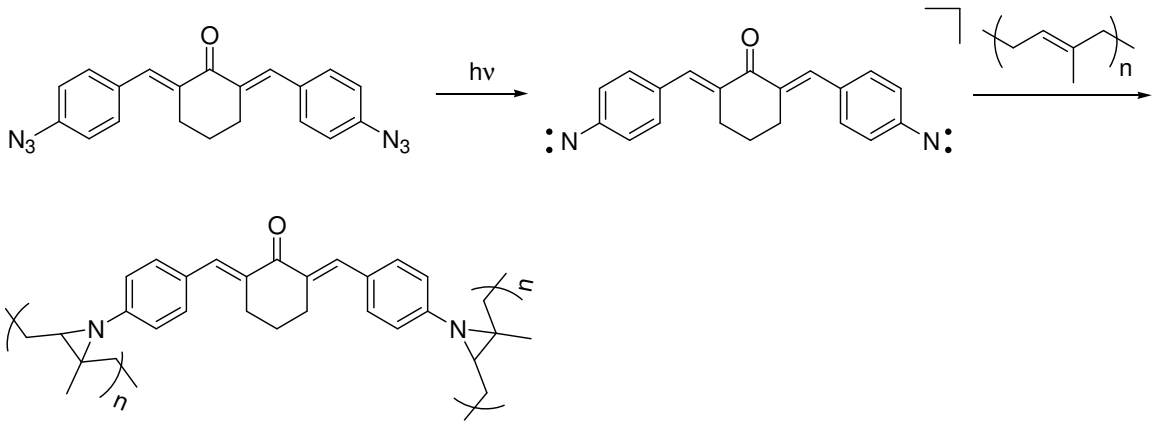

Scheme 1.1: Cross-linking reaction of bis-aryl azides and polyisoprene.

While this concept was used until the early 1980s, the system was only capable of producing features greater than two microns. The root cause of the limited resolution was due to the swelling of features upon development in organic solvents (Figure 1.9).

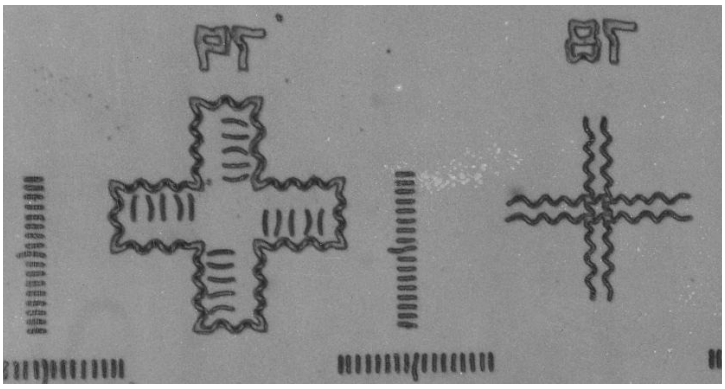

Figure 1.9: Swollen features of a cross-linked film.

1.7.2 Novolac/DNQ Resists

The problem of swelling was addressed by the development of a positive-tone resist formulation that consists of novolac, a poly(phenol) resin, and a photoactive diazonapthoquinone (DNQ). DNQs are small molecules that dramatically alter the solubility characteristics of novolac in aqueous base developers. Referring to Figure 1.5, the film is not soluble in basic developers in unexposed regions, however when exposed to g-line or i-line radiation, the DNQ undergoes a photochemical Wolff rearrangement leading to a ketene that reacts with adventitious water to form an indene carboxylic acid (Scheme 1.2). This small molecule has no dissolution inhibition properties, and therefore the matrix is soluble in exposed areas. Typical DNQs are loaded any where from 5-20 wt% compared to novolac and provide several orders of magnitude difference in dissolution rates upon exposure.

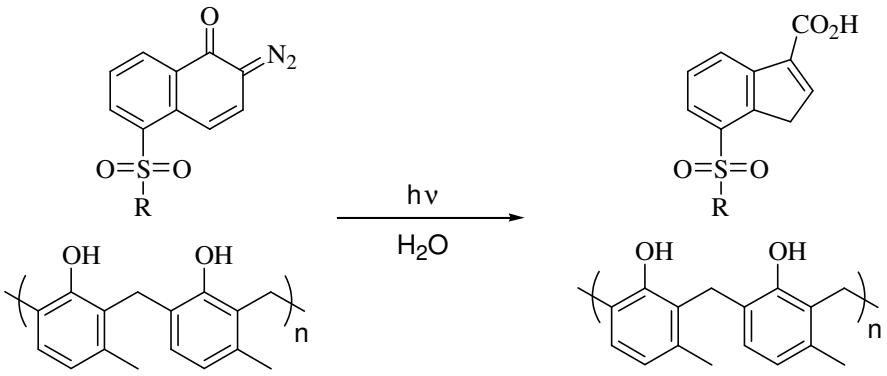

Scheme 1.2: Photochemical Wolff rearrangement of DNQ in novolac.

Marketed first by Azoplate, novolac/DNQ resist formulations accounted for nearly 90% of the world's photoresist market from 1972 to 1990.[13] In fact due to its ease of handling, novolac/DNQ is still used to produce the larger back-end-of-the-line (BEOL) features on today's microprocessors.

1.7.3 Chemical Amplification

The need to improve upon the resolution of the novolac/DNQ resists while cutting costs dictated a fundamental change in resists due to several reasons. First, DNQs are extremely absorbent at the next functional wavelength provided by a mercury arc lamp, 248 nm due to their highly conjugated pi-system (Figure 1.8). Secondly, the quantum efficiency of the Wolff rearrangement is 0.1-0.3. While the output of 436 and 365 nm light from a mercury arc lamp is efficient at these wavelengths, the power output at 248 nm is drastically less (10%). This means that each photon is much more expensive to produce and cannot be wasted in a 10-30% efficient photochemical reaction.

The concept of chemical amplification was brought about by the research team of Willson, Fréchet, and Ito at the IBM Almaden Research Center in the 1980s. Instead of relying on one photon to produce a single chemical reaction as in the Wolff

rearrangement, chemical amplification comes about by the acid-catalyzed deprotection of tert-butyloxycarbonyloxy (tBoc) groups. Scheme 1.3 displays the fundamentals of chemically amplified resists (CARs).

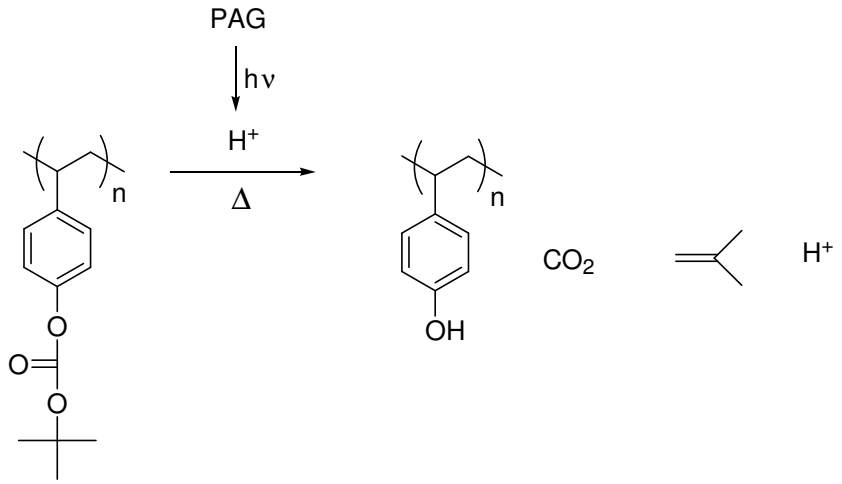

Scheme 1.3: Deprotection of poly(tert-butyloxycarbonyloxy styrene) in a typical CAR.

Instead of novolac, typical 248 nm CARs use poly(tert-butyloxycarbonyloxy styrene) (PBOCST) as the resin. Due to the aliphatic tBoc group, this polymer is not soluble in basic developers, however when exposed to a small amount of acid and heat, the tBoc group is removed yielding two products: a phenol or more accurately poly(hydroxy styrene) (PHOST), and secondly, a single molecule of acid brought about by the E1 reaction between the tert-butyl carbocation and the acid's conjugate base (Scheme 1.3).[14] This means with no termination, a single molecule of acid should be able to deprotect an infinite number of tBoc groups. Of course there are termination events for the acid, but the concept represented a way around the power problems associated with moving to 248 nm exposure radiation. Photoacid generators (PAGs) were readily available due to work by Crivello and coworkers at General Electric[15], and a model

system was reported in 1983.[16] This work displayed an improvement in sensitivity by two orders of magnitude as well as the ability to be a positive and negative tone resist. The formulation also had excellent etch resistance and remarkable resolution. Chemical amplification was truly a stepping stone in photolithography.

1.7.4 193 nm

Around the turn of the millennium, the resolution limits of 248 nm CARs were being pushed, and so to keep pace with Moore's law, the microelectronic industry once again decreased the exposure wavelength to 193 nm. Readily accessible from an ArF excimer laser, 193 nm radiation presented a large challenge in resist design because aromatic groups were too absorbent. This eliminated not only styrene and its readily available derivatives but also the phenol group used for the acid labile solubility switch. While aliphatic polymers such as poly(methyl methacrylate) were available that met the optical density properties needed for a 193 nm resist, there were no obvious choices for the solubility switch nor etch resistance. The answer came in the form of copolymers with tert-butyl protected acids for a solubility switch and alicyclic groups for etch resistance, such as norbornene and adamantyl. While countless numbers of variations exist, two representative polymers shown below (Scheme 1.4) display the functional groups used in a typical 193 nm resists.

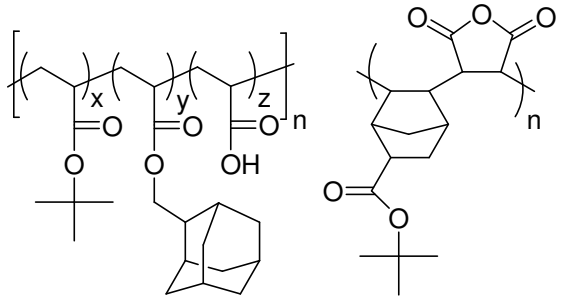

Scheme 1.4: Representative 193 nm photoresists.

1.8 KEEPING PACE

The case has been presented that the microprocessor industry is driven by the need to keep pace with Moore's Law by reducing the size of transistors while keeping costs down. This brutal pace has left many technologies behind not because there was a fundamental flaw, but simply because the process was too expensive for mass scale production or because the technology would not be ready in time to produce features small enough for Moore's law. This is particularly true of 157 nm lithography, which will not be covered here but is the topic of many dissertations in the Willson group.[17,18]

Several new technologies and re-workings of old techniques have been proposed to replace 193 nm lithography. While some like Immersion lithography have seen production-level integration, others like Extreme Ultra Violet (EUV) have yet to meet stated goals on time. The remainder of this dissertation focuses on the design, synthesis, and application of organic materials for alternative patterning technologies; chapter 2 describes work on fluorinated electron-beam resists, chapters 3 and 4 describe research directed at photo-labile, non-chemically amplified, polymeric dissolution inhibitors, and chapter 5 deals with block copolymers for nano-imprint lithography.

1.9 REFERENCES

1. http://www.inc.com/news/articles/200707/computers.html. **2007**.

2. http://www.pbs.org/transistor/index.html. **1999**.

3. http://www.computerhistory.org/timeline/?year=1947. **2006**.

4. www.nobelprize.org. **2010**.

5. Moreau, W. M. *Semiconductor Lithography: Principles, Practices, and Materials*; Pelnum Press: New York, 1998,

6. Moore, G. In *Electronics Magazine* 1965.

7. http://www.intel.com/technology/architecture-silicon/2billion.htm. **2009**.

8. Hibbs, M. S. *Microlithography: Science and Technology*; Marcel Dekker: New York, 1998, 1-108.

9. Taylor, J. C., *Advanced lithographic patterning technologies: Materials and processes*, The University of Texas at Austin, **2007**.

10. Heath, W. H., *Design, synthesis, and evaluation of materials for microelectronics applications*, The University of Texas at Austin, **2006**.

11. Willson, C. G.; Dammel, R. A.; Reiser, A. *Proc. SPIE-Int. Soc. Opt. Eng.* **1997**, *3050*, 38-51.

12. Ichikawa, R.; Hata, M.; Okimoto, N.; Oikawa-Handa, S.; Tsuda, M. *J. Polym. Sci., Part A: Polym. Chem.* **1998**, *36*, 1035-1042.

13. Crivello, J. V. *J. Polym. Sci., Part A: Polym. Chem.* **1999**, *37*, 4241-4254.

14. Frechet, J. M. J.; Eichler, E.; Ito, H.; Willson, C. G. *Polymer* **1983**, *24*, 995-1000.

15. Trinque, B. C., *Synthesis, copolymerization studies and 157 nm photolithography applications of 2-trifluoromethylacrylates*, The University of Texas at Austin, **2003**.

16. Osborn, B. P., Dissertation, *Vacuum ultraviolet directed design, synthesis and development of 157 nm photoresist materials*, The University of Texas at Austin, **2004**.

Chapter 2: Fluorinated Polymethacrylates as Highly Sensitive Non-Chemically Amplified Electron-Beam Resists

2.1 ELECTRON BEAM LITHOGRAPHY

Electron-beam lithography (EBL) is a direct-write, serial exposure lithography technique that utilizes high energy electrons with accelerating voltages on the order of tens of keV to change the solubility of a resist. This is in contrast to a full field exposure of photons in photolithography where multiple features can be exposed at once. While the potential resolution of EBL is much greater than photolithography, the serial nature of writing features has prevented it from full-scale production of semiconductors.

Despite these limitations, EBL has found its niche in the production of masks and reticles. A gate-level mask requires approximately twenty-four hours to write using a state-of-the-art, fifteen to twenty-five million dollar variable beam shape e-beam exposure tool. A fully functioning mask set for 65 or 45 nm production can total one to two million dollars and requires forty to fifty masks with many rewrites.[19,20]

While mask writing is the most prominent use of EBL, new 'maskless' technologies have emerged in recent years that take advantage of its resolution capabilities. In 2008, Slot reported the use of 13,000 simultaneous electron beams controlled by an electrostatic lens array to produce sub-45 nm lines and spaces.[21] This technology could make a significant contribution in the industry and lead to actual semiconductor devices, not just masks, being produced by EBL. In the same year, Samsung Electronics reported the fabrication of 40 nm lines and spaces with line width roughness of $3\sigma = 3.7$ nm.[22] Resolution on this order is needed to produce templates for nano-imprint lithography. If EBL is to expand to full-scale production for these

technologies, throughput must increase. Improvements in resist sensitivity could lead to shorter exposure times per wafer and thus, higher throughput.

2.2 EBL RESIST CHEMISTRY

Poly(methyl methacrylate) (PMMA) has long served as the benchmark for e-beam resists in regard to its resolution and ease of handling, but its etch resistance and sensitivity are not acceptable for current processing requirements.[23,24] Scheme 2.1 displays the accepted chain-scission mechanism. The first step is a Norrish I cleavage of the α carbonyl bond followed by rearrangement through a beta scission. The final products are carbon monoxide, carbon dioxide, methyl and methoxyl radicals, and most importantly, two distinct polymer chains.[23] This decrease in molecular weight is advantageous because it leads to a drastic change in the dissolution rate. This generic relationship is shown in Figure 2.1.

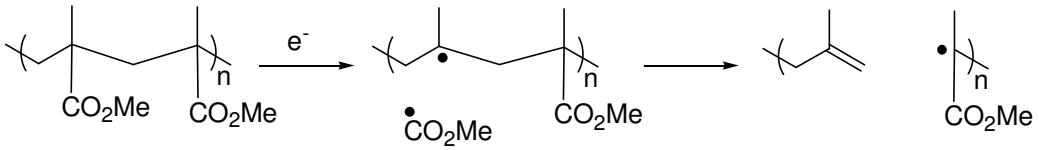

Scheme 2.1: Main-chain scissioning mechanism for PMMA.

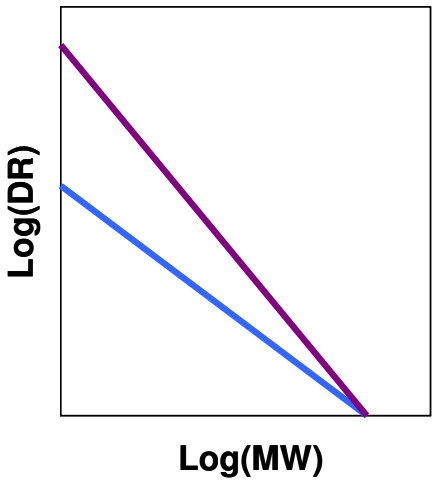

Figure 2.1: General relationship between the dissolution rate (DR) and molecular weight (MW) for a given polymer in a developer. The blue line represents a less sensitive resist than the purple line.

Efforts were made to improve the sensitivity of PMMA, and extensive work by Pittman demonstrated that α-halogen, electron-withdrawing substituents increase the backbone-scission efficiency. However, this substituent also undergoes dissociative-electron capture leading to the undesirable evolution of HCl and cross-linking within the resist (Scheme 2.2).[25]

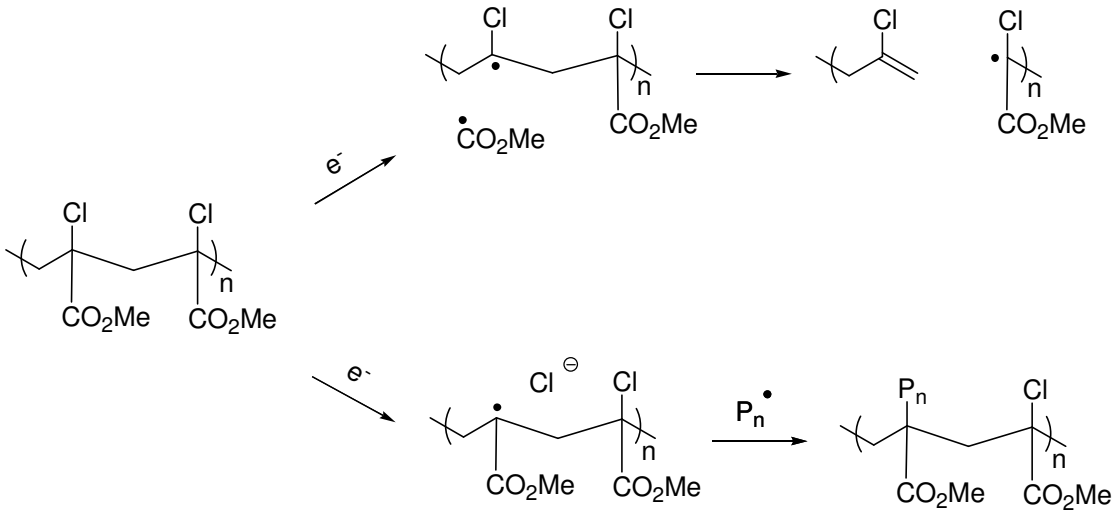

Scheme 2.2: Main-chain scission (top) and dissociative-electron capture (bottom) mechanisms for poly(α-chloroacrylate).

2.3 RESIST IMPROVEMENTS

Desiring to take advantage of Pittman's findings, Willson and Ito introduced the concept of utilizing α-CF_3 substituents in e-beam resists.[26] They proposed the α-CF_3 should preclude dissociative-electron capture and cross-linking but due to its electron-withdrawing character still enhance the main-chain scission efficiency, thereby reducing the time required for imaging. While their initial images were promising, this material never seemed to attract the attention of commercial vendors in the 1980s.

ZEP-520A, a one to one copolymer of methyl α-chloroacrylate and α-methyl styrene produced by Nippon Zeon Company, is a non-chemically amplified e-beam resist (Scheme 2.3).[27] It is used extensively in the literature and industry as an EBL resist because of its much improved sensitivity, brought about by the incorporation of α-chloro acrylate, and etch resistance, due to the α-methyl styrene.

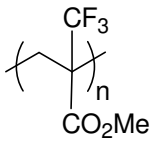

poly(2.1)

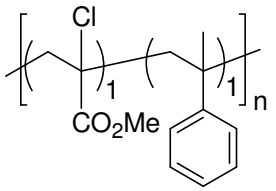

ZEP-520A

Scheme 2.3: Poly(methyl α-trifluoromethacrylate) (poly(2.1)) and Nippon Zeon's ZEP-520A

This chapter describes the synthesis and material evaluation of various non-chemically amplified e-beam resists attempting to further the work of Pittman, Willson and Ito, and Nippon Zeon Co.

2.4 MONOMER SYNTHESIS

The synthesis of an MMA analog with an α-CF_3 substituent (2.1) began with the nucleophilic addition of sodium cyanide to commercially available 1,1,1-trifluoroacetone 2.2 under basic conditions; this yielded 2.3 in 60% yield, which after hydrolysis with acidic methanol gave the methyl ester 2.4 in 48% yield. To convert the hydroxyl group to a better leaving group, 2.4 was acylated to give 2.5 in 92% yield. Finally, 2.5 was converted to monomer 2.1 via pyrolysis in 46% yield. The key to the pyrolysis process was accurately measuring the temperature with properly placed temperature probes and carefully controlling the speed at which 2.5 was passed through the quartz column. This 4-step previously published process yields 2.1 in 12% overall yield (Scheme 2.4).[17] Desiring a more efficient route, commercially available 2-bromo-3,3,3-trifluoropropene was converted to acid 2.5 by a palladium catalyzed carbonylation in 38% yield.[28] Needing to convert the acid to a methyl ester, acid 2.5 was subjected to several methylating conditions including Fisher esterification, diazomethane, amine bases with methyl iodide, DCC coupling, and Meerwein's salt with no detectable formation of

product due to the base sensitivity of 2.1, but the ester was recovered in 55% yield when the acid was reacted with neat dimethyl sulfate at 120 °C for 48 h.[29]

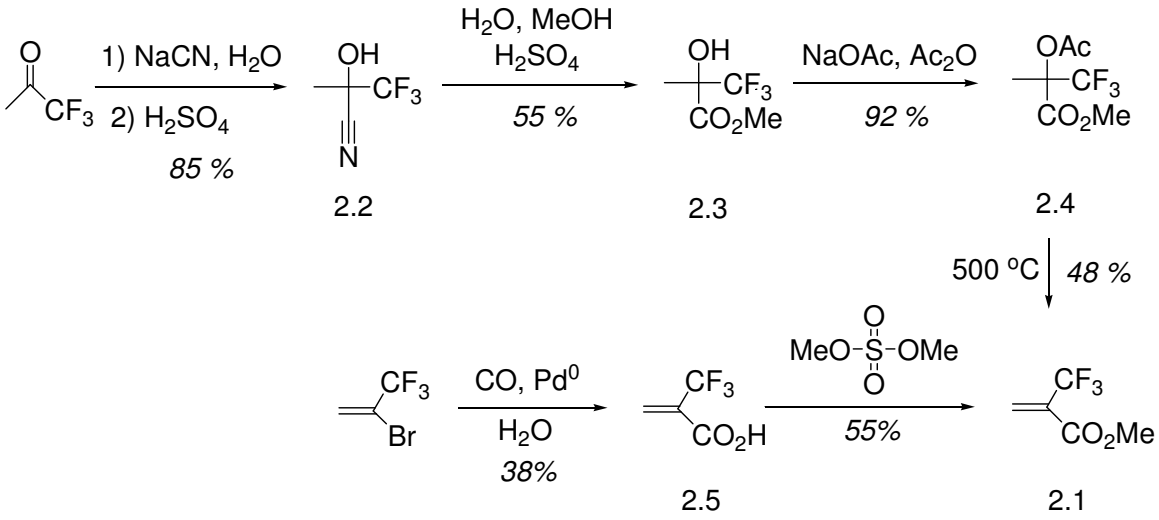

Scheme 2.4: Synthesis of methyl α-trifluoromethacrylate (2.1) via two different routes.

2.5 POLYMER SYNTHESIS

While synthesizing methyl α-trifluoromethacrylate, ethyl α-trifluoromethacrylate (ETFMA), 2,2,2-trifluoroethyl methacrylate (TFEMA), and 2,2,2-trifluoroethyl α-trifluoromethacrylate (TFETFMA) were obtained as generous gifts from Central Glass Co. Their corresponding polymers were compared to PMMA (poly(2.5)) and poly(2.1) to determine the effects of an α-CF_3 and/or CH_2CF_3 alkoxy substituent on a polyacrylate (Scheme 2.5).

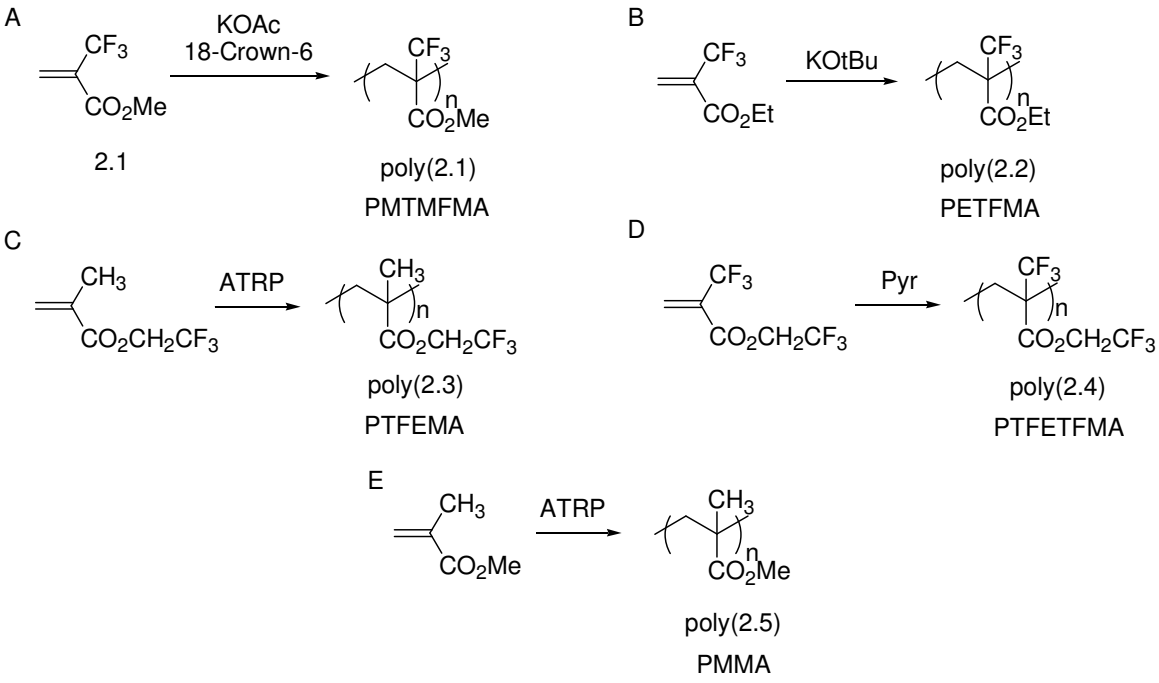

Scheme 2.5: Polymerization conditions for A) Poly(methyl α-trifluoromethacrylate) (poly(2.1)) B) Poly(ethyl α-trifluoromethacrylate) (poly(2.2)) C) Poly(2,2,2-trifluoroethyl methacrylate) (poly(2.3)) D) Poly(2,2,2-trifluoroethyl α-trifluoromethacrylate) (poly(2.4)) E) Poly(methyl methacrylate) (poly(2.5))

2.5.2 Homopolymers

Delaire noted that a resist's sensitivity is inversely proportional to its polydispersity index,[30] therefore monomers without an α-CF_3 substituent were polymerized via ATRP to obtain polymers with lower PDI than can be obtained by traditional radical polymerization.[31,32] Poly(2.5) was desired for comparative purposes to understand the effect of the fluorine introduction while poly(2.3) was envisioned as a means to determine the effect of fluorine incorporation in a position believed not to effect chain scission.

The remaining fluorinated monomers required their own unique and specific polymerization conditions as recently noted by Hamana.[33] Monomer 2.1 was polymerized using potassium acetate and 18-crown-6 according to a procedure developed by Ito (Scheme 2.5).[34] Narita reported the anionic polymerization of ETFMA;[35,36] however, these experimental conditions did not provide polymer. Different initiators including potassium acetate with 18-crown-6, n-butyllithium, and pyridine among others were tested without success, however potassium tert-butoxide (KOt-Bu) was determined to be an effective initiator at -78 ^{o}C.

n-Butyllithium and n-butylmagnesium chloride were reported to polymerize TFETFMA[37], but reproduction of these conditions yielded no polymer. Pyridine was used as the initiator at -78 °C in THF[38], but all attempts to polymerize this monomer produced an insoluble material with a high affinity for Teflon® stir bars. Due to the material's intractable nature, no characterization data is available.

2.5.3 Copolymers

Replacement of methyl α-chloroacrylate monomer in ZEP with 2.1 was initially targeted; unfortunately, attempts to polymerize 2.1 and α-methyl styrene via traditional radical polymerization conditions failed. Copolymerizations of 2.1 and various ratios of styrene produced materials with less than 5% incorporation of 2.1 as determined by ^{1}H-NMR. Due to this difficulty and given that current acrylate-based 193 nm resists display adequate etch resistance, incorporation of a more etch resistant monomer was determined not to be a fundamental necessity to compare resist performance.

To further investigate its unusual reactivity, 2.1 was radically copolymerized with MMA. As has been noted elsewhere a maximum 50% incorporation of 2.1 was obtained in copolymers regardless of feed ratios.[26] Acrylate 2.1 was also radically copolymerized

with TFEMA. The resulting materials were less soluble in THF and common casting solvents possibly due to the $-CH_2CF_3$ alkoxy functionality.

2.6 CONTRAST CURVES

Resist sensitivity was investigated by subjecting a film of each polymer to varying doses of e-beam radiation then developing the wafer. The depth of the features was measured using profilometry and compared to the original film thickness. As shown in Figure 2.2, the contrast for poly(2.5) and ZEP are very similar, however poly(2.1) and poly(2.2) are much more sensitive requiring nearly two orders of magnitude less dose to develop.[24] Although the contrast for poly(2.1) with the investigated conditions is poor, subsequent work by Gronheid was able to demonstrate good imaging contrast.[39] poly(2.2) displays higher contrast than poly(2.5) and ZEP.

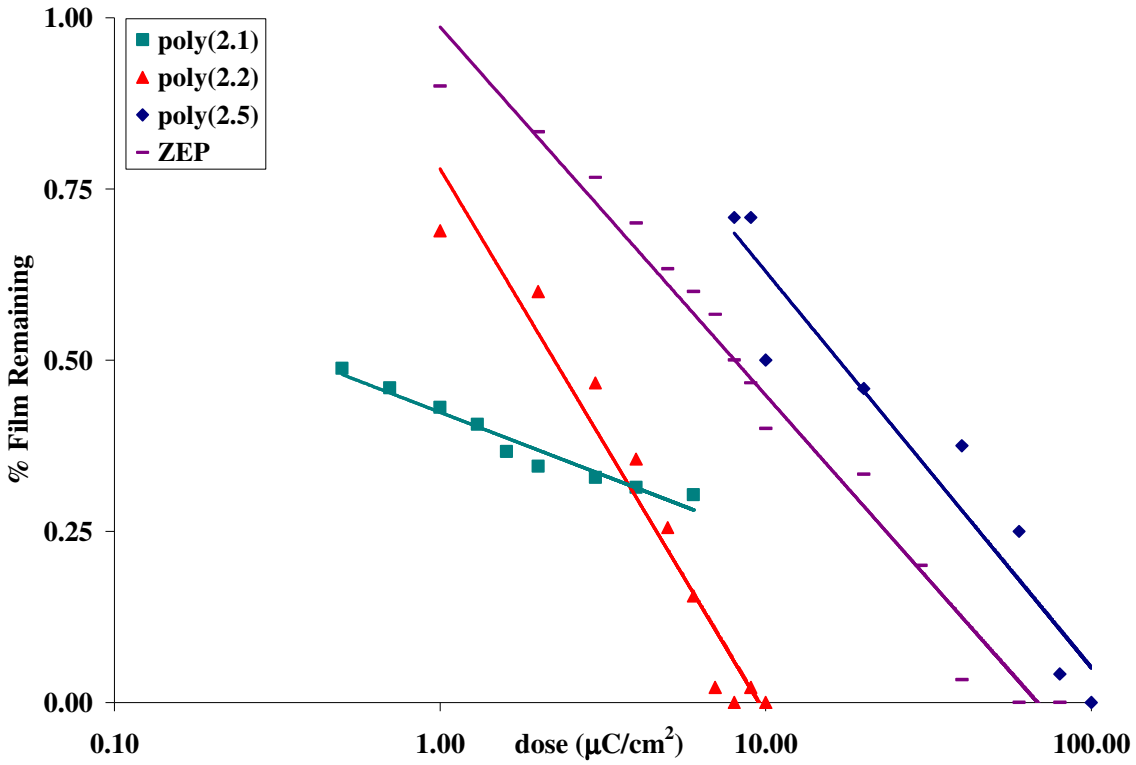

Figure 2.2: e-beam contrast curves for poly(2.1) (green square), poly(2.2) (red triangle), poly(2.5) (blue diamond), and ZEP (purple dash).

2.7 G(S) AND G(X) DETERMINATION

2.7.1 Polymer Characterization

As noted by Romack, fluorinated polymers have unique properties including low Refractive Indices (RIs) that make molecular weight determination by a lone RI detector prone to error.[40,41] While fluorinated solvents can increase the solubility of the polymer and improve the signal-to-noise ratio of an RI detector, these solvents are expensive and environmentally unfriendly.[42] To accurately determine the molecular weights of these polymers, a triple detection method that utilizes an RI detector, right-angle light scattering, and low-angle light scattering (λ_0 = 670 nm) detectors, and a four-capillary, differential viscometer was employed.

It was determined that acetone was an appropriate solvent for poly(2.1), poly(2.2), and poly(2.3) while THF was used for poly(2.5) and ZEP.[43] Through serial dilutions the dn/dc of each polymer was determined (Figure 2.3), and Table 2.1 lists these values including error analysis and correlation coefficients. The dn/dc calculated for poly(2.5) is in good agreement with literature, and all data show an extremely high linear correlation.[44] The dn/dc of each polymer was then used to determine the absolute M_w and M_n of each unique polymer sample. If conventional calibration techniques with polystyrene standards were used, the relative M_w, M_n, and PDI were significantly different than those obtained with the unique dn/dc method. The inherent error of conventional calibration when characterizing a novel polymer cannot be overstated.

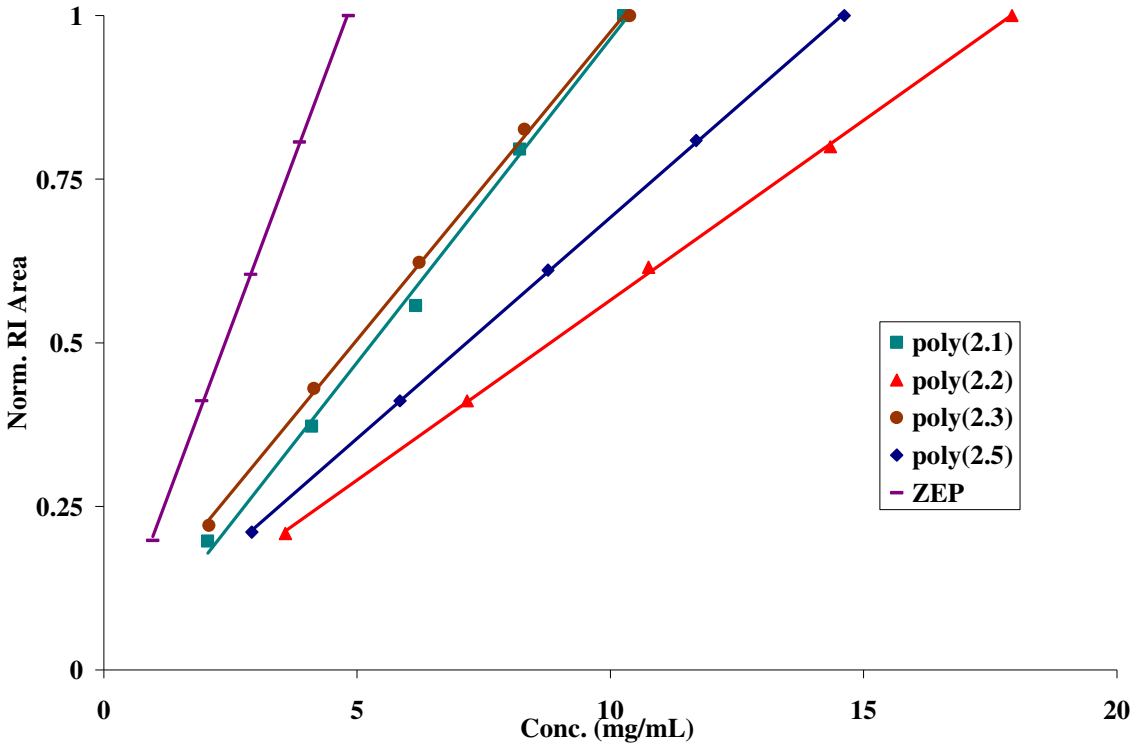

Figure 2.3: Normalized RI area versus concentration for calculating dn/dc of poly(2.1) (green square), poly(2.2) (red triangle), poly(2.3) (brown circle), poly(2.5) (blue diamond), and ZEP (purple dash) polymers.

Table 2.1**:** dn/dc data for poly(2.1), poly(2.2), poly(2.3), poly(2.5), and ZEP

Polymer	dn/dc	Error	% Error	R^2	Solvent
poly(2.1)	0.0404	0.0013	3.3%	1.00	Acetone
poly(2.2)	0.0355	0.0004	1.0%	1.00	Acetone
poly(2.3)	0.0319	0.0005	1.7%	1.00	Acetone
poly(2.5)	0.0674	0.0004	0.6%	1.00	THF
ZEP	0.1124	0.0011	1.0%	1.00	THF

2.7.2 G(s) and G(x)

While contrast curves are a valuable way to test a resist's viability, the experiment contains several variables including solution concentration, spin speed, PAB bake time

and temperature and, perhaps most importantly, developer that all play a role in a resist's contrast. To determine an absolute value of these resists' sensitivity to radiation, the G-values were determined. The sensitivity of a polymer to backbone scission may be quantified by irradiating samples with γ-radiation from a cobalt-60 source then measuring the change of the M_n and M_w of the samples.[23] Equation 2.1 and 2.2 display the linear relationships between a material's change in M_w and M_n as a function of dose and its G(s) and G(x) values.[23] G(s) represents the number of backbone scissions per 100 electron-volts (eV) absorbed while G(x) is the cross-linking efficiency per 100 eV absorbed. A polymer's sensitivity to this method has been shown to correlate well to e-beam sensitivity.[23]

2.1
$$\frac{1}{M_w{}^o} = \frac{G(s) - 4 * G(x)}{200 * N_A}(dose) + \frac{1}{M_w{}^i}$$

2.2
$$\frac{1}{M_n{}^o} = \frac{G(s) - G(x)}{100 * N_A}(dose) + \frac{1}{M_n{}^i}$$

Samples of poly(2.1), poly(2.2), poly(2.3), poly(2.5), and ZEP were sealed in glass vials under Argon and exposed at NIST to varying doses of ^{60}Co γ-radiation. Utilizing the previously described GPC detection system, the M_n and M_w of the initial and irradiated polymer samples were determined. These values were analyzed using the relations shown above where the dose is expressed in units of eV, NA is Avagadro's number, M_n^o and M_n^i are the number-average molecular weights of the irradiated and initial polymer samples, respectively, and M_w^o and M_w^i are the weight-average molecular weights of the irradiated and initial polymer samples, respectively.

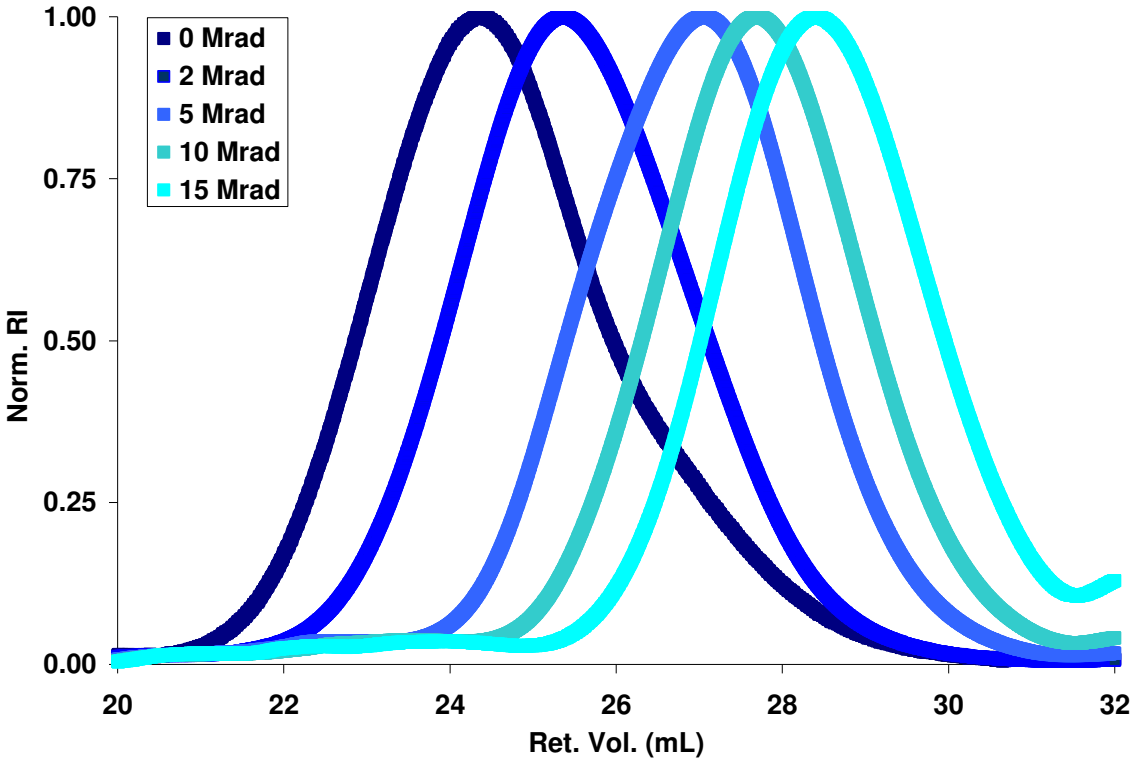

Figure 2.4: GPC chromatograms of irradiated poly(2.1).

Figure 2.4 is representative data from GPC chromatograms of irradiated poly(2.1). As dose increased, the retention volume increased indicating a decrease in molecular weight. By substituting the experimental values into Eq 2.1 and Eq 2.2, the G(s) and G(x) values for each of the polymers were determined (Figure 2.5, Figure 2.6, and Table 2.2).

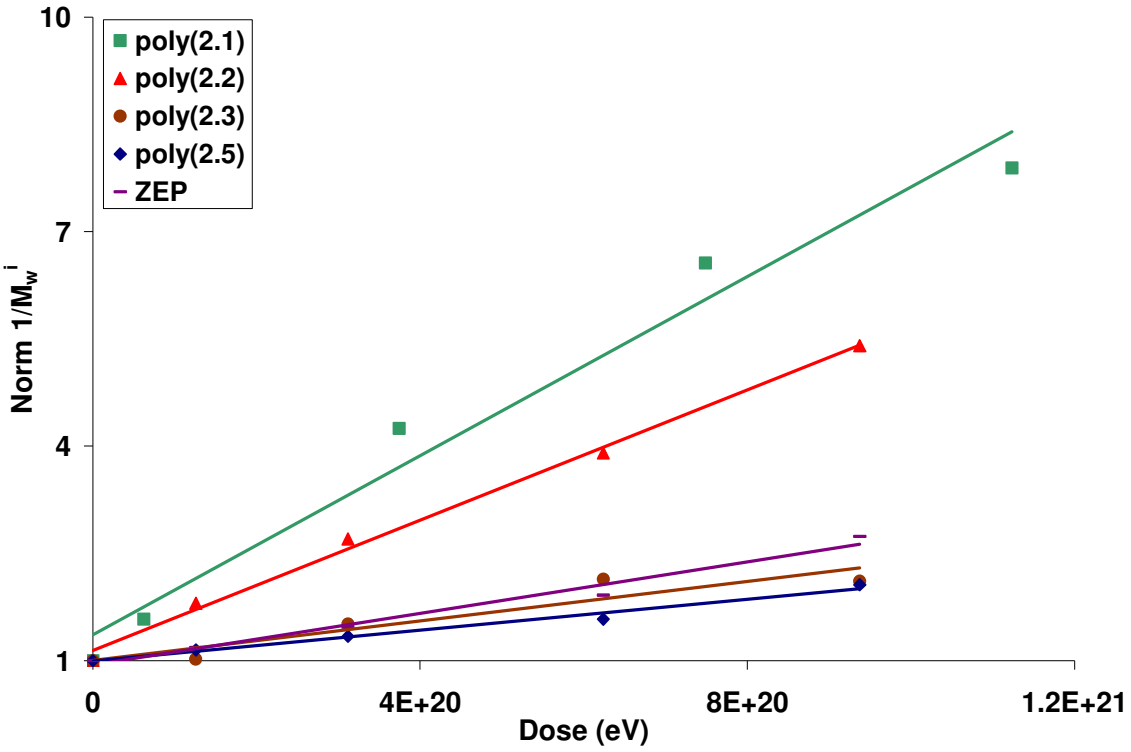

Figure 2.5: Normalized $1/M_w^i$ vs dose for poly(2.1) (green square), poly(2.2) (red triangles), poly(2.3) (brown circle), poly(2.5) (blue diamond), and ZEP (purple dash).

Table 2.2 displays the polymers' G(s) and G(x) values with error analysis. The experimentally determined G(s) and G(x) values for poly(2.5) (1.26, 0.12) are in good agreement with literature values (1.3, 0.0),[23] however, the G(s) value for poly(2.1) determined by these experiments of 3.19 is higher than the previously reported value of 2.5,[26] which could be attributed to a more accurate determination of M_n and M_w. Overall, the G(s) values for the fluorinated polymers are higher than that of both poly(2.5)'s 1.26 and ZEP's 1.71. None of the fluorinated polymers have a significant G(x) component, as expected by eliminating the dissociative-electron capture mechanism. In fact, poly(2.1) and poly(2.5) display a negative G(x) value that has no physical meaning, but these

values are within error of a zero value so they can be regarded as zero. A surprising find was the similarity of the G(s) values for poly(2.2) and poly(2.3), 2.75 and 2.80 respectively. It was hypothesized that poly(2.3) would have a lower scission efficiency than poly(2.2) due to the lack of an α-CF_3 substituent; The effect of the -CH_2CF_3 alkoxy substituent on the G(s) warrants further study. Given that poly(methyl α-chloroacrylate) has a reported G(x) value of 0.8[45], it was expected that ZEP, which has 50 mol% methyl α-chloroacrylate, would exhibit a significant cross-linking component. It is notable the G(x) value for ZEP (0.01) is negligible, indicating the effect of the α-methyl styrene must be significant. The high linear correlations confirm these polymers are responding to the radiation as expected.

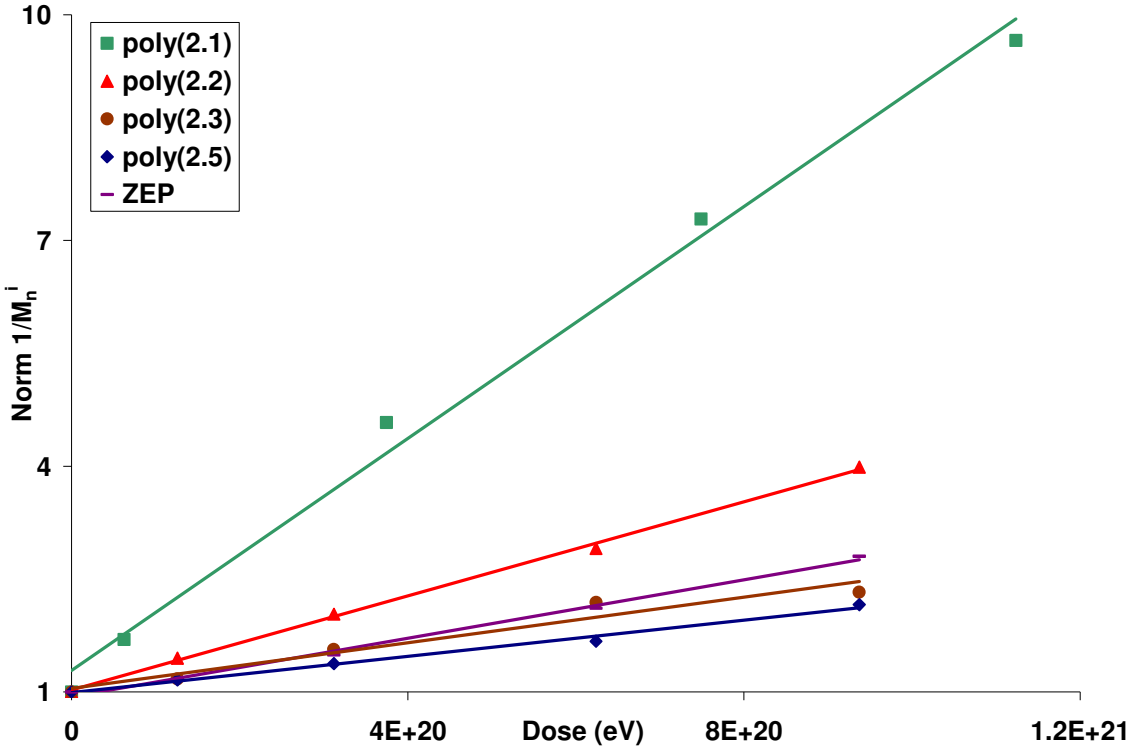

Figure 2.6: Normalized $1/M_n^i$ vs dose for poly(2.1) (green square), poly(2.2) (red triangle), poly(2.3) (brown circle), poly(2.5) (blue diamond), and ZEP (purple dash).

Table 2.2: G(s) and G(x) values for poly(2.1), poly(2.2), poly(2.3), poly(2.5), and ZEP.

	G(s)	Error	R^2	G(x)	Error	R^2
poly(2.1)	3.19	0.15	0.99	-0.02	0.00	0.98
poly(2.2)	2.75	0.20	0.98	0.07	0.01	0.94
poly(2.3)	2.80	0.34	0.95	0.09	0.01	0.86
poly(2.5)	1.26	0.12	0.97	-0.03	0.00	0.98
ZEP	1.71	0.10	0.99	0.01	0.00	0.98

2.7.3 GPC Method Comparison

As noted earlier, the detection method used to obtain the M_w and M_n for the polymer samples is vitally important to obtaining accurate G values.

Table 2.3 and Figure 2.7 display analysis of several polymer samples using different detection methods. The calculated G(s) values for poly(2.5) using a conventional calibration (CC) curve with PMMA standards and a triple detection method (Trip) are both 1.28. This translates to similar slopes in Figure 2.7. This result is not surprising given that poly(2.5) is PMMA, and therefore the CC curve was made of standards of the same polymer with all of the same physical constants, specifically hydrodynamic volume. However, the Trip and CC methods give very different G(s) values for poly(2.1) and poly(2.3). In particular, the slopes of poly(2.1)-Trip and poly(2.1)-CC are visibly different in Figure 2.7. This is primarily due to differences in hydrodynamic volumes compared to the PMMA standards used to make the CC curve. Because the Trip method uses the polymer's dn/dc and collects four signals, refractive index, viscometer, low-angle light scattering, and right-angle light scattering, these data are a more accurate representation of the polymer's M_w and M_n.

Table 2.3: Comparative G(s) values for poly(2.1), poly(2.3), and poly(2.5) using a triple detection (Trip) and conventional calibration method (CC).

	G(s)
poly(2.1)-Trip	3.16
poly(2.1)-CC	4.55
poly(2.3)-Trip	2.35
poly(2.3)-CC	1.79
poly(2.5)-Trip	1.28
poly(2.5)-CC	1.28

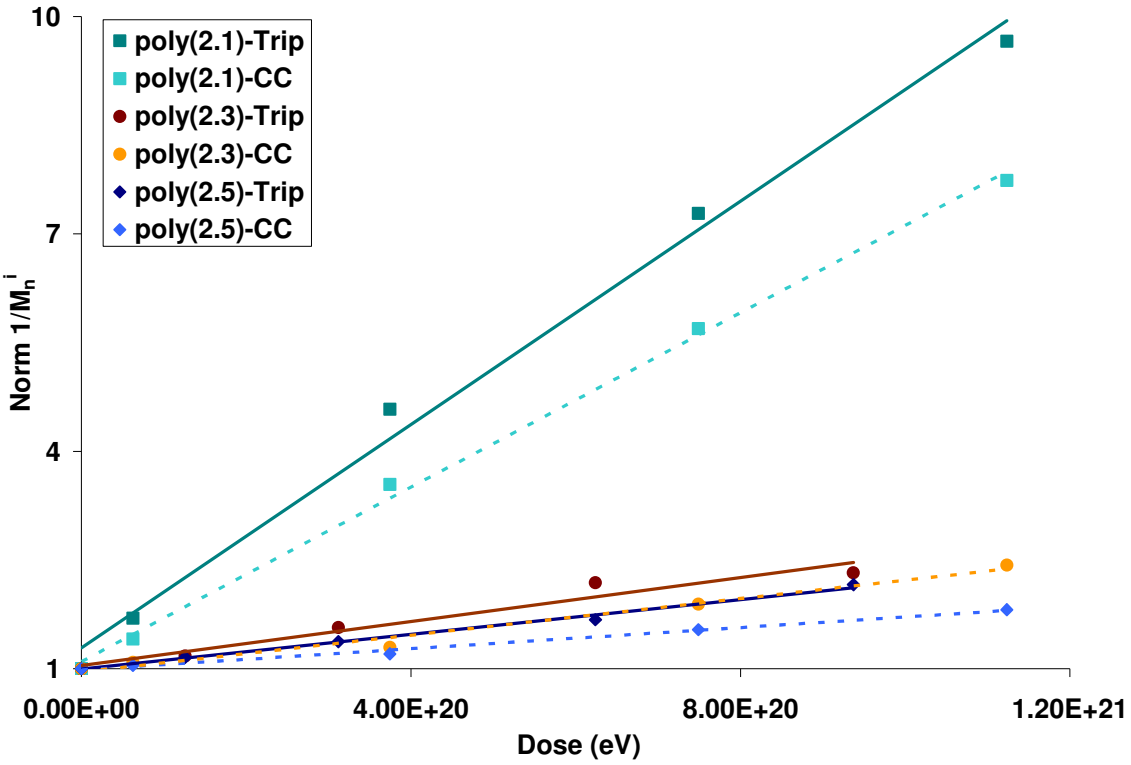

Figure 2.7: Comparison of poly(2.1) (green diamonds), poly(2.3) (brown circles), and poly(2.5) (blue diamonds) using triple detection (Trip) and conventional calibration (CC) vs. normalized $1/M_n^i$.

2.8 EUV

It has been noted that as fluorine content of MMA increases, the optical density of the resulting polymeric resist to extreme ultra-violet (EUV) irradiation (13.4 nm) increases significantly. This allows for a thinner optimal film thickness, which will be necessary for the production of 22 nm and smaller features.[39]

To compare the rate of response to exposure or photospeed of poly(2.5) and poly(2.1), films of nearly identical thickness were spin coated and exposed to varying doses of e-beam and EUV irradiation. These films were then developed in the same developer. This was a challenge as the vastly different solubility characteristics of these materials made it difficult to find an effective developer for both systems. Scanning electron microscopy (SEM) images were collected, and the e-beam photospeed of poly(2.1) was determined to be 2.8x faster than that of poly(2.5) (Figure 2.8). The EUV photospeed of poly(2.1) compared to poly(2.5) was found to be 4.0x, of which 1.5x can be attributed to the increase in EUV absorbance. A more thorough discussion of the e-beam and EUV photospeed of poly(2.1) and poly(2.5), including images, has been reported elsewhere.[39]

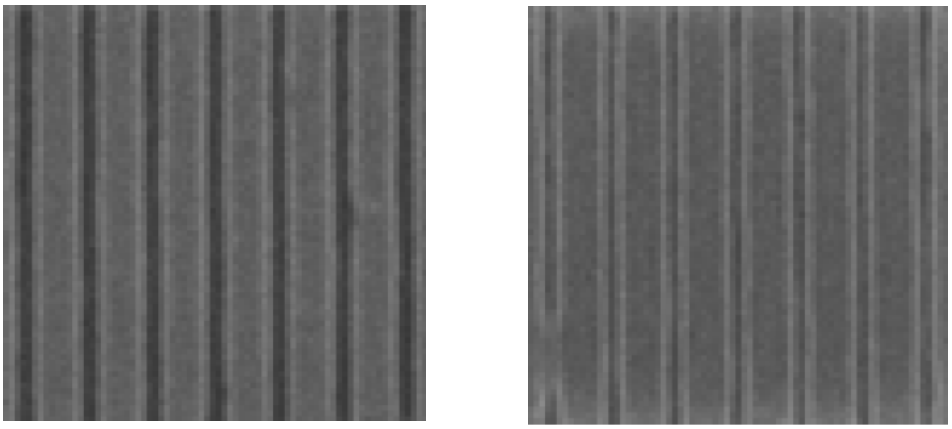

Figure 2.8: SEMs of 100 nm pitch lines and spaces of poly(2.1) and poly(2.5) exposed with EUV.

2.9 CONCLUSION

A variety of fluorinated polyacrylates have been shown to be more sensitive than poly(2.5) and ZEP to e-beam, cobalt-60 γ-radiation, and EUV irradiation. This was demonstrated quantitatively in e-beam contrast curves that showed poly(2.1) and poly(2.2) required nearly a 100x less dose to develop than poly(2.5) and 10x less dose than ZEP. The G(s) value for poly(2.1), poly(2.2), and poly(2.3) was higher than poly(2.5) and ZEP, confirming the e-beam sensitivity results. In addition, no polymer had a significant G(x) value, meaning there was no measurable cross-linking upon ^{60}Co γ-irradiation. Finally, the EUV photospeed of poly(2.1) compared to poly(2.5) was found to be 4.0x, of which 1.5x can be attributed to the increase in EUV absorbance due to the incorporation of fluorine. The biggest area for improvement for these materials is the control of MW and PDI and reproducible development of sub 100 nm thin films. These materials, including copolymers with more fluorine content, will continue to be investigated for their applicability as both e-beam and EUV non-chemically amplified resists.

2.10 ACKNOWLEDGMENTS

The authors would like to thank Central Glass Co. for their donations of fluorinated monomers, Dr. Peter Carmichael of NIST for his help with the ^{60}Co irradiations, Mike Ronalter of UT for his help with sample preparations, and Brent Norris of UT, David Kiddy of Agilent, and Michael Murphy of Viscotek for their help with the GPC analysis. We would also like to thank Prof. Bruce Smith of RIT for his simulation data, and NSF R05-0126, Applied Materials, and the Texas Advanced Materials Research Center for their generous support of this research.

2.11 EXPERIMENTAL

2.11.1 General Methods and Materials

All chemicals were purchased from Sigma-Aldrich and used as received unless otherwise stated. ZEP-520A was purchased from Nippon Zeon Co (T_g = 143 °C). After precipitating in 0 °C MeOH, the polymer was isolated by filtration and dried *in vacuo*. AP410 was purchased from Silicon Resources, Inc. All reactions were conducted under a positive nitrogen atmosphere with oven-dried glassware unless otherwise stated. Dry DCM, TEA, and pyridine were obtained by distillation over CaH_2 while dry THF was obtained by distillation over Na/benzophenone. All ^{1}H, ^{13}C, and ^{19}F NMR spectra were recorded on a Varian Unity Plus 300 MHz instrument. All chemical shifts are reported in ppm downfield from TMS using the residual protonated solvent as an internal standard ($CDCl_3$, ^{1}H 7.26 ppm and ^{13}C 77.0 ppm; DMSO-d_6, ^{1}H 2.49 ppm and ^{13}C 39.5 ppm). HRMS (CI) was obtained on a VG analytical ZAB2-E instrument. IR data were recorded on a Nicolet Avatar 360 FT-IR and all peaks are reported in cm^{-1}. All molecular weights were measured using an Agilent 1100 Series Isopump and Autosampler, and a Viscotek Model 302 TETRA Detector Platform with 3 I-series Mixed Bed High MW columns. Films were spin coated and baked on a Brewer CEE 100CB Spincoater & Hotplate. A 50 keV JEOL-6000FS/E-based e-beam tool was used for exposures, and a Veeco Dektak 6M Stylus Profiler was used to determine film thicknesses. Glass transition temperatures (T_g) were recorded on a TA Q100 Differential Scanning Calorimeter (DSC).

2.11.2 Monomer Synthesis

Trifluoracetone cyanohydrin, 2.2

A 500 mL round bottom flask (RBF) equipped with a stir bar was charged with sodium cyanide (65.5 g, 1.3 mol) and H_2O (190 mL). After cooling the reaction flask in

an ice-water bath, 2 (13 mL, 0.14 mol) was added. The reaction was stirred for 1 h and then added to 700 mL of 6 M sulfuric acid and stirred for an additional hour. Addition to the acid resulted in release of cyanide gas; hence this reaction should be carried out in a well tested fume hood. The reaction mixture was extracted with ether (3x200 mL) and the combined organic layers were washed with a saturated aqueous solution of sodium bicarbonate, rinsed with brine, dried over $MgSO_4$, filtered, and concentrated *in vacuo*. Vacuum distillation (35 torr, 49-55 ^oC) yielded 2.3 as a clear liquid (11.46 g, 60%). ^1H NMR (CDCl3) δ 4.52 (s, 1H), 1.76 (s, 3H); ^{13}C NMR(CDCl3) δ 20.87 (s), 69.29 (q) 115.77 (s), 122.17 (q); ^{19}F NMR (CDCl3) δ -82.43; IR (NaCl) 3400, 1706; HRMS (CI) M+1 calc = 140.0323, found 140.0326.

Methyl α-hydroxy-α-(trifluoromethyl) propionate, 2.3

A 500 mL RBF equipped with a stir bar and condenser was charged with conc. H_2SO_4 (60 mL, 1.1 mol). In a separate flask, 2.2 (90.1 g, 0.65 mol) was mixed with MeOH (54 mL), and the mixture was slowly added by syringe to the acid. After drop-wise addition of H_2O (11.7 mL, 0.65 mol), the reaction mixture was heated at 105 °C for 8.5 h then cooled to 80 °C for another 13.75 h. Upon cooling to rt, H_2O (20 mL) was added to the mixture. The crude mixture was extracted with ether (3x250 mL) and the combined organic layers were washed with water, brine, dried over $MgSO_4$, filtered, and concentrated *in vacuo*. Vacuum distillation (55 torr, 55-58 °C) yielded 2.3 as a clear liquid (53.63 g, 48%). ^1H NMR (CDCl3) δ 1.69 (s, 3H) 1.86 (s, 3H) 8.37 (s, 1H); ^{13}C NMR(CDCl3) δ 18.79(s), 54.02(s), 75.37(q), 123.55(q), 170.77(s); ^{19}F NMR (CDCl3) δ -80.731; IR (NaCl) 3492, 3013, 2964, 1741; HRMS (CI) M+1 calc = 173.0426, found 173.0433.

Methyl α-acetoxy-α-(trifluoromethyl) propionate, 2.4

A 500 mL RBF equipped with a stir bar and condenser was charged with 2.3 (53.6 g, 0.31 mol), acetic anhydride (92 mL, 0.97 mol), and sodium acetate (4.6 g, 56 mmol). This was heated to 110 °C and stirred for 8 h. After cooling to rt, the reaction mixture was added to ice (700 g) and stirred for 1 h. The crude mixture was extracted with ether (3x200 mL) and the combined organic layers were washed with 200 mL portions of saturated sodium bicarbonate solution until neutral. The organic layers were washed with brine (200 mL), dried over $MgSO_4$, and concentrated *in vacuo*. Vacuum distillation (60 torr, 90-95 °C) yielded 5 as a clear liquid (85.4g, 92%). ^{1}H NMR ($CDCl_3$) δ 1.79 (s, 3H), 2.13 (s, 3H), 3.79 (s, 3H); ^{13}C NMR($CDCl_3$) δ 16.47(s), 20.60(s), 53.389(s), 79.30 (q), 120.73(s), 165.50(s), 168.60(s); ^{19}F NMR (CDCl3) δ -79.10; IR (NaCl) 3502, 3015, 2962, 1829, 1772, 1717; HRMS (CI) M+1 calc = 215.0531, found 215.0528.

Methyl α-trifluoromethacrylate, 2.1

A quartz pyrolysis column (42 cm (heated length) with 4 cm outer diameter (OD)) packed with 20 feet of 5 mm OD, 3 mm inner diameter (ID) quartz tubing and 44 feet of 3 mm OD, 1 mm ID quartz tubing cut into lengths of 0.5 cm to 1 cm. and wrapped with heating tape (HTS/Amptek Co Model AWH-051-0600) was used. Two temperature probes were positioned about 1/3 of the column from the top and bottom respectively. These probes were secured with the tips directly between the heating tape and the column. The column was wrapped with two layers of insulation tape (Wale Apparatus Co. 151508) and aluminum foil. An addition funnel was added to the top of the column, and a cold finger and collection flask were attached at the bottom. The column was brought to 500 °C under nitrogen, and 2.4 (79.7 g, 0.37 mol) was introduced at approximately four drops per second. Nitrogen was flowed through the system at four bubbles per second, regulated by a needle valve at the beginning of the system and a

bubbler at the end. Product 4 was added over 35 min while paying careful attention to minimize the build up of any smoke at the top of the column. Immediately after the last drop of 4 was added, the addition funnel was shut. The heat and nitrogen were continued to ensure a complete reaction. The collected product was washed three times with brine (200 mL) and dried over $MgSO_4$. This was distilled from the drying agent to give 2.1 as a clear liquid. The first fraction (14.3 g, 25.0%) was collected with a 9" Vigreaux column wrapped with cotton and aluminum foil at atmospheric pressure from 83-87 ºC. A second fraction (12.1 g, 21.0%) was collected with a 3" Vigreaux column at 60 torr and 103-107◦ C. ^{1}H NMR ($CDCl_3$) δ 3.80 (s, 3H), 6.60 (s, 1H), 6.68 (s, 1H); ^{13}C NMR($CDCl_3$) δ 52.44(s), 121.22 (q, J = 270.4 Hz), 132.85(s), 161.72(s); ^{19}F NMR (CDCl3) δ-66.47; IR (NaCl) 3136, 3014, 2962; HRMS (CI) M+1 calc = 155.0318, found 155.0320.

2-(trifluoromethyl)acrylic acid, 5 (75 g, 0.54 mol), prepared by palladium catalyzed carbonylation of 2-Bromo-3,3,3-trifluoro-propene[28], was dissolved in dimethylsulfate (500 mL) and the reaction vessel was heated to 120 °C under an atmosphere of nitrogen for 48 h. The color of the reaction changed to dark brown over 6 h. After the reaction was cooled to rt, the crude reaction was subjected to vacuum distillation by heating the still pot to 120 °C and cooling the receiving flask with dry ice (-78 °C). The pressure was gradually reduced to 100 millitorr over 1 h, maintaining the temperature of the still head at ~100 °C to obtain 60 g (73%) of clear liquid. The ^{1}H NMR analysis of the liquid indicated the material collected consisted of desired product 2.1 with approximately 6 mol% of dimethyl sulfate impurity. Second distillation with a Vigreaux column was performed at atmospheric pressure and a fraction boiling at 75-80 °C was collected to obtain the desired product (45 g, 55%) with no detectable impurities.

2.11.3 Polymer Synthesis

Poly(methyl α-trifluoromethacrylate), poly(2.1)

A 50 mL RBF equipped with a stir bar was charged with oven-dried potassium acetate (23.6 mg, 0.28 mmol) and 18-crown-6 (63.4 mg, 0.24 mmol). These were dissolved in THF (20 mL) and cooled to -5 °C in an ice/brine bath. Upon addition of 2.1 (5 mL, 39.0 mmol), the reaction was stirred for 3 h. To precipitate the polymer, the reaction solution was slowly dripped into 500 mL of ice-cold vigorously stirring MeOH in an Erlenmeyer flask. The polymer was isolated using a Hirsch funnel and filter paper. The polymer was then dissolved in THF (50 mL) and precipitated again as described above using roughly ten times the volume of MeOH as THF. This procedure gave excellent yields (5.48 g, 91 %) of a fine white powder. T_g = 101 °C.

Poly(ethyl α-trifluoromethacrylate), poly(2.2)

A 25 mL RBF equipped with a stir bar was charged with potassium tert-butoxide (6.7 mg, 0.06 mmol) in a glove box. After removing the flask from the glove box, THF (5 mL) was added to the flask. The flask was then chilled to -78 °C with an acetone/dry ice bath, and ethyl α-trifluoromethacrylate (0.5 mL, 3.6 mmol) was added. The reaction flask was stirred and warmed to rt overnight, and poly(2.2) was precipitated using the same procedure as poly(2.1) precipitation but using hexanes instead of MeOH. T_g = 67 °C.

Poly(2,2,2-trifluoroethyl methacrylate), poly(2.3)

A 10 mL RBF equipped with a stir bar was loaded with Cu(I)Br (20.65 mg, 0.144 mmol) in a glove box. After removing the flask from the glove box, TFEMA (2 mL, 14.0 mmol) was added. After hexamethyltriethylenetetramine (TREN) (31.969 µl, 0.144 mmol) and ethyl 2-bromoisobutyrate (E2BIB) (17.79 µl, 0.12 moles) were added via micro syringe, the flask was taken through two freeze, pump, thaw cycles and then heated to 80 oC for 4.5 h. The reaction solution formed a gelatinous solid, so it was dissolved in

THF for removal. The polymer was precipitated in MeOH as described for poly(2.1). T_g = 66 °C.

Poly(2,2,2-trifluoroethyl α-trifluoromethacrylate), poly(2.4)

A 100 mL RBF equipped with a stir bar was charged with TFETFMA (1.5 mL, 8.6 mmol), and THF (50 mL). This flask was chilled to -78 °C with an acetone/dry ice bath and stirred for at least 10 min. Separately, pyridine (0.67 mL, 8.3 mmol) was diluted in 20 mL THF. This solution (0.1 mL) was added to the chilled monomer solution. The reaction was stirred for 3 h followed by precipitation of poly(2.4) in distilled water.

Poly(methyl methacrylate), poly(2.5)

A 25 mL RBF with a stir bar was loaded with Cu(I)Br (16.9 mg, 0.12 mmol) and Cu(II)Br (1.0 mg, 0.01 mmol) in a glove box. After removing the flask from the glove box, diphenyl ether (5 mL) was added to the flask. Methyl methacrylate (5 mL, 47.1 mmol) was filtered through neutral alumina and injected into the reaction vessel via syringe. N,N,N',N',N''-pentamethyldiethylenetriamine (PMDETA) (24.6 μl, 0.12 mmol) was added via a micro syringe. After E2BIB (14.0 μL, 0.09 mmol) was added, the flask was immediately taken through two freeze, pump, thaw cycles and then heated to 40 °C for 8 h. To precipitate the polymer, the reaction solution was slowly dripped into 250 mL of ice-cold vigorously stirring MeOH in an Erlenmeyer flask. The polymer was isolated using a Hirsch funnel and filter paper. The polymer was then dissolved in THF (50 mL) and filtered through neutral alumina to remove any residual copper. This solution was precipitated again as described above using roughly ten times the volume of MeOH as THF.

2.11.4 Contrast Curves

Each polymer was dissolved in propylene glycol methyl ether acetate (PGMEA) (6 wt%) and filtered (0.22 μm PTFE). poly(2.5) films were spin coated at 2000 rpm for 60 sec with a 90 °C 60 sec post-application bake (PAB). Fluoropolymers were spin coated on wafers pre-treated with AP410 at 3000 rpm for 60 sec with a 90 °C 60 sec PAB. The resulting films were 200-400 nm thick. Optimized developers were 1:1 methyl isobutyl ketone (MIBK):IPA for poly(2.5), 7:3 MIBK:IPA for poly(2.1), 2:8 MIBK:IPA for poly(2.2), and 6:4 MIBK:methyl ethyl ketone for ZEP. Films were exposed to a dose array ranging from 0.1 to 100 $\mu C/cm^2$, developed for 60 sec, and the film thicknesses of the resulting features were determined by profilometry and normalized to the original film thickness.

2.11.5 dn/dc Determination

A sample of polymer (40-200 mg) was dissolved in THF (10 mL), and five gel permeation chromatography (GPC) chromatograms were collected by varying the overall concentration through variation of injection volumes. The dn/dc was then determined by calculating the slope of the RI area vs concentration line. The eluent for poly(2.5) and ZEP analysis was THF while acetone was used for poly(2.1), poly(2.2), and poly(2.3).

2.11.6 G(s) and G(x) Determination

A sample of each polymer (~200 mg) was placed into a small glass vial. After purging with Argon for 5 min, the vial was flame sealed. The samples were irradiated with a cobalt-60 γ-radiation source in collaboration with the National Institute of Standards and Technology (NIST) with 2, 5, 10, and 15 Mrad of γ-radiation. Three 1 wt% samples in THF were prepared for each sample and analyzed by GPC.

2.12 REFERENCES

1. LaPedus, M. In *EE Times* 2008, p 1-5.

2. http://www.itrs.net/reports.html. **2007**.

3. Slot, E.; Wieland, M. J.; de Boer, G.; Kruit, P.; ten Berge, G. F.; Houkes, A. M. C.; Jager, R.; van de Peut, T.; Peijster, J. J. M.; Steenbrink, S. W. H. K.; Teepen, T. F.; van Veen, A. H. V.; Kampherbeek, B. J. *Proc. SPIE* **2008**, *6921*, 69211P/69211-69211P/69219.

4. Yeo, J.; Kim, H.; Eynon, B. *Proc. SPIE* **2008**, *6921*, 692107/692101-692107/692109.

5. Thompson, L. F.; Willson, C. G.; Bowden, M. J.; Editors *ACS Symposium Series, Vol. 219: Introduction to Microlithography: Theory, Materials, and Processing*, 1983, 139-267.

6. Medeiros, D. R.; Aviram, A.; Guarnieri, T. C.; Huang, W.-S.; Kwong, R.; Magg, C. K.; Mahorowala, A. P.; Moreau, W. M.; Petrillo, K. E.; Angelopoulos, M. *IBM J. Res. Dev.* **2001**, *45*, 639-650.

7. Helbert, J. N.; Chen, C.-Y.; Pittman, C. U., Jr.; Hagnauer, G. L. *Macromolecules* **1978**, *11*, 1104-1109.

8. Willson, C. G.; Ito, H.; Miller, D. C.; Tessier, T. G. *Polym. Eng. Sci.* **1983**, *23*, 1000-1003.

9. Nishida, T.; Notomi, M.; Iga, R.; Tamamura, T. *Jpn. J. Appl. Phys., Part 1* **1992**, *31*, 4508-4514.

10. Trinque, B. C., Dissertation, *Synthesis, copolymerization studies and 157 nm photolithography applications of 2-trifluoromethylacrylates*, The University of Texas at Austin, **2003**.

11. Fuchikami, T.; Yamanouchi, A.; Ojima, I. *Synthesis* **1984**, 766-768.

12. Khramov, D. M., Dissertation, *Novel N-heterocyclic carbenes: Applications in materials chemistry and catalysis*, The University of Texas at Austin, **2008**.

13. Delaire, J. A.; Lagarde, M.; Broussoux, D.; Dubois, J. C. *J. Vac. Sci. Technol., B* **1990**, *8*, 33-38.

14. Wang, J.-L.; Grimaud, T.; Matyjaszewski, K. *Macromolecules* **1997**, *30*, 6507-6512.

15. Wang, J.-L.; Grimaud, T.; Shipp, D. A.; Matyjaszewski, K. *Macromolecules* **1998**, *31*, 1527-1534.

16. Umino, Y.; Narita, T.; Hamana, H. *J. Polym. Sci., Part A: Polym. Chem.* **2008**, *46*, 7011-7021.

17. Ito, H.; Schwalm, R. *Recent Adv. Anionic Polym., Proc. Int. Symp.* **1987**, 421-430.

18. Narita, T.; Hagiwara, T.; Hamana, H.; Nara, T. *Makromol. Chem., Rapid Commun.* **1985**, *6*, 301-304.

19. Narita, T.; Hagiwara, T.; Hamana, H.; Nara, T. *Polym. J. (Tokyo)* **1988**, *20*, 277-279.

20. Narita, T.; Hagiwara, T.; Hamana, H.; Maesaka, S. *Polym. J. (Tokyo)* **1988**, *20*, 519-523.

21. Personal Communication, Satoshi Kikichi, Y. S., *Central Glass Polymerization of TFETFMA*, **2006.**

22. Gronheid, R.; Fonseca, C.; Leeson, M. J.; Adams, J. R.; Strahan, J. R.; Willson, C. G.; Smith, B. W. *Proc. SPIE* **2009**, *7273*, 727332/727331-727332/727338.

23. Romack, T. J.; Harrison, Z. J.; French, D. V.; Amin, D. H.; Hartsell, J. L.; Meyer, J. D. *Macromolecules (Washington, DC, U. S.)* **2007**, *40*, 7180-7183.

24. Netopilik, M.; Kratochvil, P. *Polymer* **2003**, *44*, 3431-3436.

25. Isemura, T.; Kakita, R.; Kawahara, K. *J. Chromatogr., A* **2004**, *1026*, 109-116.

26. Personal Communication, Viscotek, *Solvents for Fluorinated Polymers*, **2008.**

27. Brandrup, J. *Polymer Handbook*; 4th ed.; Wiley-Interscience, 1999, 432.

28. Chen, C.-Y.; Pittman, C. U., Jr.; Helbert, J. N. *J. Polym. Sci., Polym. Chem. Ed.* **1980**, *18*, 169-178.

Chapter 3: Polymeric Dissolution Inhibitors

3.1 CARs AND LER

As discussed in Chapter 1, the predominant system used to achieve small features while maintaining a high throughput of product is the chemically amplified resist (CAR). CARs consist of a photo-acid generator (PAG) and a polymer possessing an acid-sensitive functional group, which serves as a solubility switch. The sensitivity of the CAR is advantageous because a single photochemical event causes a large number of chemical reactions, however this gain leads to a decrease in resolution – a blur. Several dissertations from the Willson group include writing on the issue, and without their fundamental work, this project would not have been possible.[46-48] To oversimplify, acid diffuses into areas of the resist that were not exposed to light during the fabrication process, specifically during the post-exposure bake (PEB) (Figure 3.1).[48]

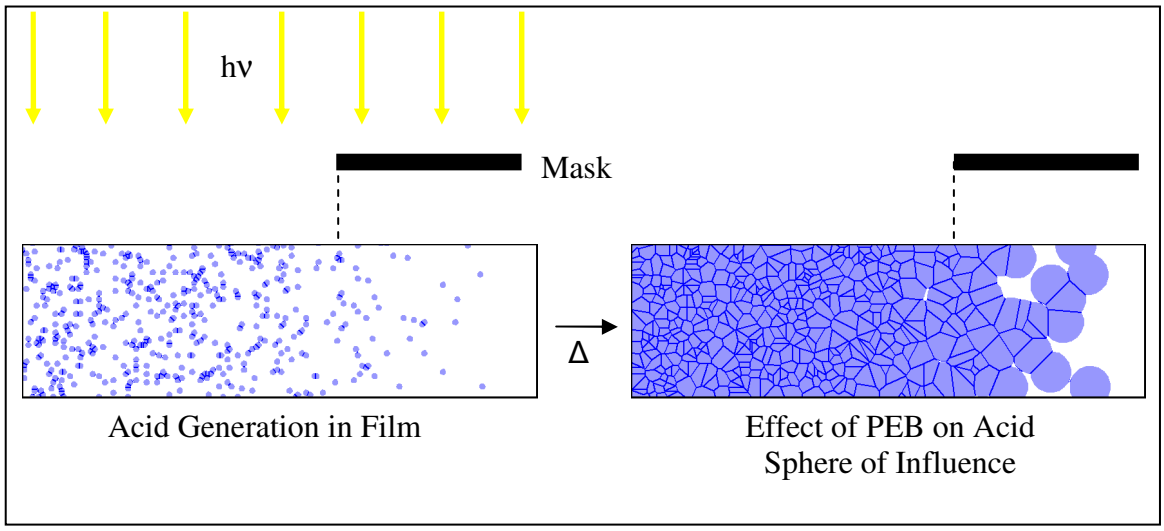

Figure 3.1: Effect of PEB on acid diffusion into dark film.[48]

The developed features on the device therefore end up wider than originally intended (bias), and they are not smooth (line-edge roughness, LER) as shown in Figure 3.2. Both the bias and LER affect the minimum attainable feature size that ultimately limits a microprocessor's capacity and performance.[49,50]

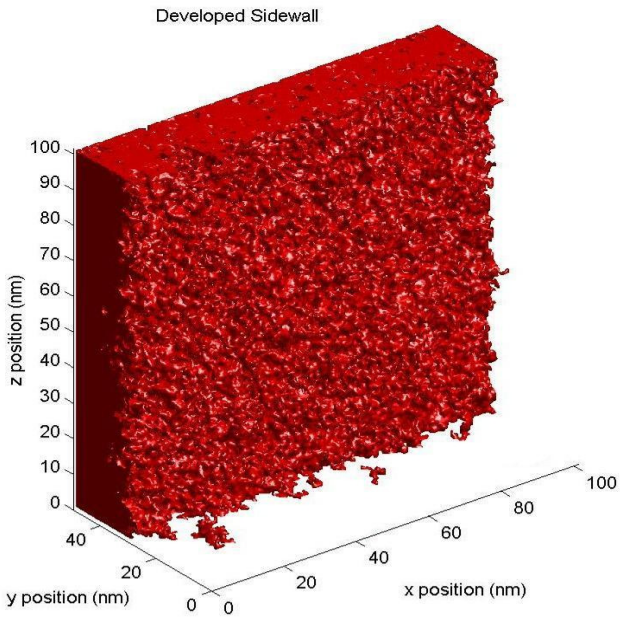

Figure 3.2: Simulated developed sidewall of a feature showing bias and LER.[48]

The International Technology Roadmap for Semiconductors (ITRS) is a public document written by representatives from many semiconductor corporations that outlines the problems and targets of the industry. In 2001, the ITRS officially recognized LER as a specification that needed to be addressed.[20] This including the necessary control of LER (Figure 3.3). Currently, no process exists which can meet the LER requirements outlined by the ITRS.

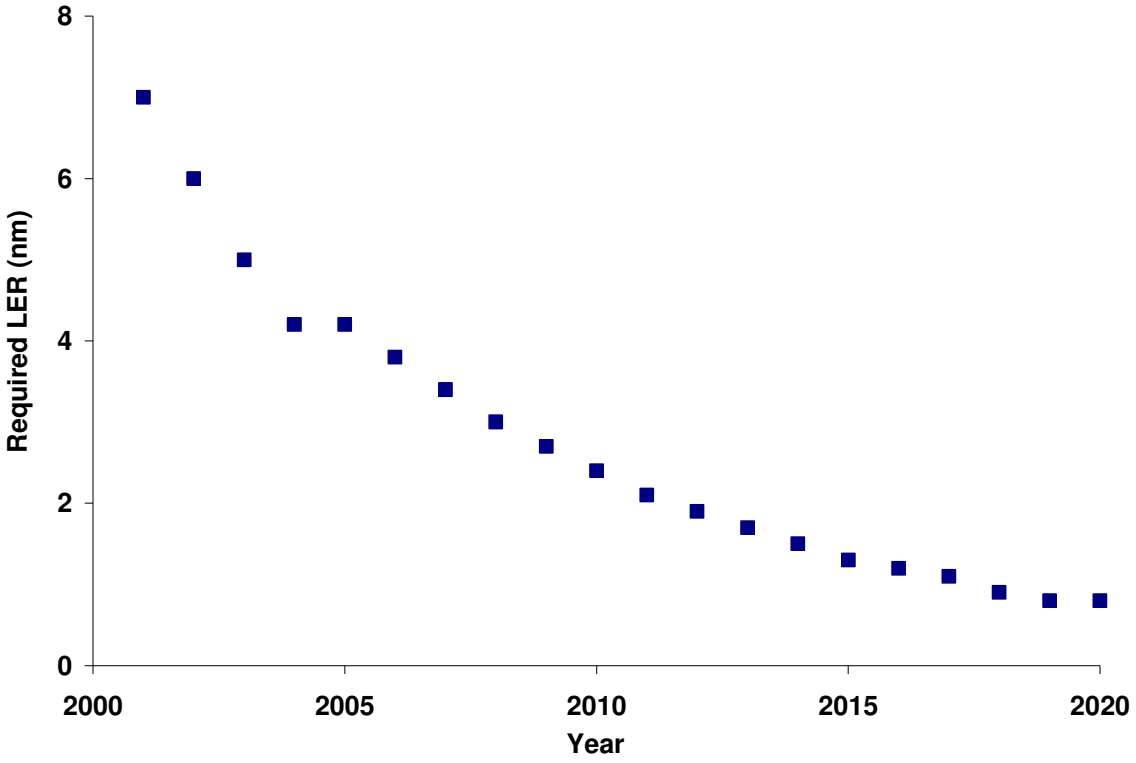

Figure 3.3: ITRS roadmap for LER.

3.2 GAIN WITHOUT BIAS

To remove the problem of acid diffusion in CARs, a system is needed that maintains chemical amplification, the breaking of many bonds with one photochemical event, while not relying on the mass transport of a small molecule catalyst - simply stated, a system that has gain without blur. This would combine the best features of non-chemically amplified resists (NCAR) and chemically amplified resists (CAR).

A photosensitive polymeric dissolution inhibitor (PDI) might be utilized to achieve these goals. The PDI must undergo a photochemical change through chemical amplification that removes its dissolution inhibition capabilities, exhibit phase

compatibility with a resin of choice, and function as a dissolution inhibitor of the resin in aqueous base developer.

3.3 POLY(PHTHALALDEHYDE)

One material that has been investigated for this role is poly(phthalaldehyde) (PPHA). Commercially available PHA readily undergoes anionic polymerization at -78 °C, and end-capping at low temperatures with subsequent purification provides a fine white powder that is soluble in common organic solvents. Willson and Ito first reported in the 1980s the use of PPHA as a polymeric dissolution inhibitor of the base soluble resin novolac. This was a breakthrough because up to this point, dissolution inhibitors had been small molecules like DNQ and not polymers. Photolithographic features were produced with a film of novolac, PPHA, and a photoacid generator via exposure to 248 nm light. It is presumed the photogenerated acid hydrolyzes the polyacetal backbone of PPHA creating an uncapped polymer. This uncapped polymer depolymerizes or 'unzips' to monomeric PHA, which does not function as a dissolution inhibitor of novolac (Scheme 3.1), so exposed areas dissolve in base while unexposed areas do not.[51-55]

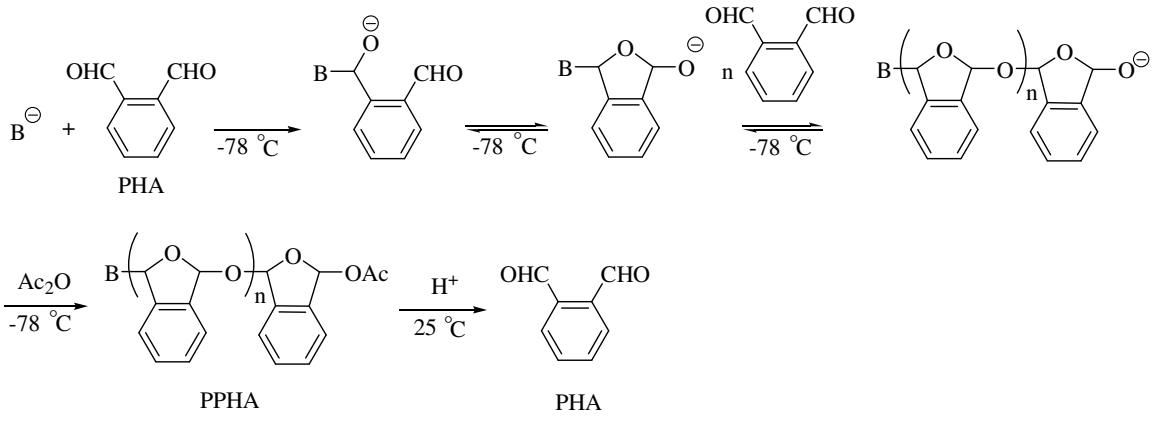

Scheme 3.1: Anionic polymerization, end-capping, and acidic 'unzipping' of PPHA.

3.4 CEILING TEMPERATURE

The fundamental polymeric principle that produced the images by Willson and Ito is termed ceiling temperature (T_c). T_c is described in various ways in numerous polymer textbooks with the same overall theme. Odian defines T_c as the temperature "at which the propagation and depropagation rates are equal,"[56] while Stevens states the T_c is the point at which "the forward and back reactions are equal," and "ΔG of polymerization is zero."[57] According to Allcock, "no polymer can exist" above the T_c.[58] Chapter 4 will discuss details of these definitions further, but as it pertains to PDIs, a low ceiling temperature provides the gain mechanism. The chemical amplification of a CAR is derived from one molecule of acid leading to multiple bonds being broken, but with a low ceiling temperature PDI, the un-capping of a single end group above T_c leads to depolymerization, which is really a large number of bonds being broken and hence another kind of amplification. This 'unzipping' does not rely on a small catalyst molecule and, therefore, will not have the fundamental bias caused by acid migration by mass transport during the PEB process.

3.5 PHOTOLABILE END GROUP

While PPHA's low T_c represents a chemical potential to break many bonds with one event, Willson and Ito's first report used acid to hydrolyze the polyacetal backbone and initiate depolymerization. To remove acid from the system, an o-nitrobenzyl photolabile end group was incorporated into PPHA (Scheme 3.2). The o-nitrobenzyl group is a common photolabile moiety and is well represented in the literature.[59,60] For incorporation into a PDI, o-Nitrobenzyl alcohol (NBA) was deprotonated with NaH, and the resulting anion was used to initiate PHA. Interestingly, this anion was not stable at -78 °C for more than an hour. Stirring the anion at -78 °C followed by protonation with water showed significant decomposition in the recovered material. Less than 10% NBA

starting material was recovered under the same conditions when n-BuLi was used to deprotonate this alcohol.

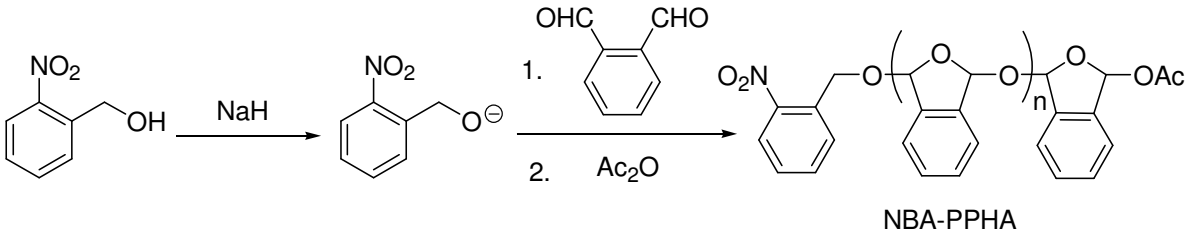

Scheme 3.2: Synthesis of o-nitrobenzyl capped PPHA (NBA-PPHA).

3.6 PHASE COMPATIBILITY

Phase compatibility between two polymers is frequently difficult to achieve due to unfavorable enthalpic and entropic interactions.[61,62] In some of these cases, phase compatibility can be achieved by decreasing the molecular weight of one of the components in the blend as described by Flory-Huggins theory.[61,62] While PPHA >20 kDa resulted in optically phase separated films, phase compatibility of PPHA with novolac was achieved by decreasing the molecular weight to <5 kDa.

3.7 DISSOLUTION INHIBITION

Novolac/PPHA formulations were made in PGMEA, and the dissolution inhibition properties were studied as shown in Figure 3.4.

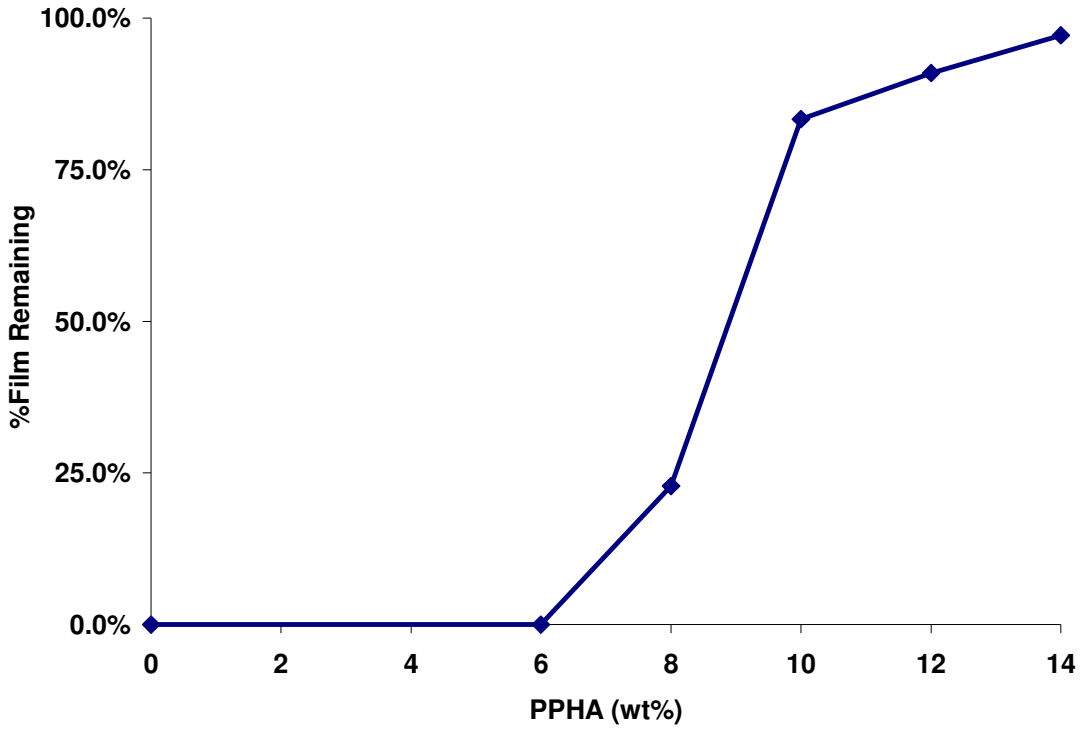

Figure 3.4: %Film remaining vs PPHA wt% for novolac.

While 6 wt% PPHA showed no inhibition of novolac in standard TMAH, 14 wt% completely inhibited with a 60 sec development.

3.8 IMAGING PPHA

To confirm NBA-PPHA functioned as a photolabile PDI, two formulations were made: one with novolac, NBA-PPHA, and PAG and another with novolac and NBA-PPHA. Films were coated and visibly phase compatible. Upon exposure to 248 nm light and subsequent development, features were successfully imaged in both formulations (Figure 3.5).

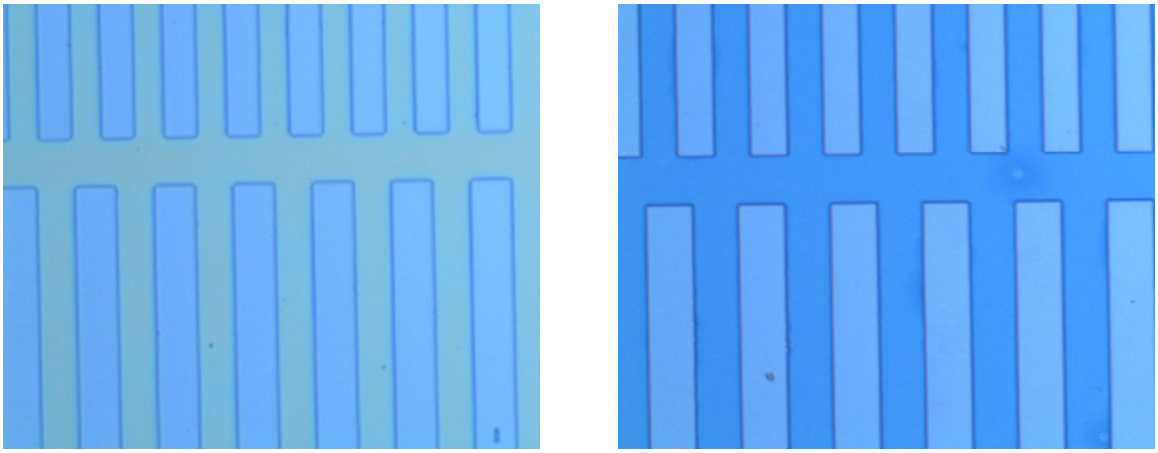

10 wt% with PAG
160 mJ/cm^2

10 wt% without PAG
1800 mJ/cm^2

Figure 3.5: 248 nm exposure features of novolac/NBA-PPHA/PAG formulation (left) and novolac/NBA-PPHA formulation (right).

While exposing the formulation with the PAG generated acid to 'unzip' the NBA-PPHA, the formulation without any PAG relied on the o-nitrobenzyl group to remove NBA-PPHA's dissolution inhibition properties. These images are a proof of principle that photolabile PDIs can successfully image commercially available resins such as novolac.

3.9 DOSE ISSUES

With this initial success, one issue that needed to be addressed before proceeding was the dose required to image. While 160 mJ/cm^2 is high but not an unreasonable dose for the formulation containing PAG, the formulation without the PAG required 1800 mJ/cm^2. Upon scanning the literature for doses of other o-nitrobenzyl containing compounds, it was found that the exposure dose in this experiment was on par with other reports. In a 2007 report from Blanc and Bochet, o-nitrobenzyl compounds were exposed in solution with a Rayonet reactor for 48 h.[63] Several groups have incorporated o-nitrobenzyl groups into various polymer architectures, and for a linear polymer the

exposure time for measurable o-nitrobenzyl cleavage was 4-8 h.[64] It was 2 d for a star polymer[65] and 180 min for a dendrimer with a Xenon arc lamp.[66] Given the exposures in these studies were in dilute solution, the high dose for the novolac/NBA-PPHA films seems reasonable.

Additionally, UV-vis experiments were conducted to further probe the high dose issue. First, the extinction coefficients of each species were calculated using Beer's Law (Figure 3.6). The molecular weight used to calculate the ε_{PPHA} was determined from GPC, which is not an exact method, so there is some inherent error in these calculations. However, the ε_{PHA} is more precise, and Figure 3.6 shows that ε_{PPHA} was consistently two to three orders of magnitude less than ε_{PHA} at λ <275 nm.

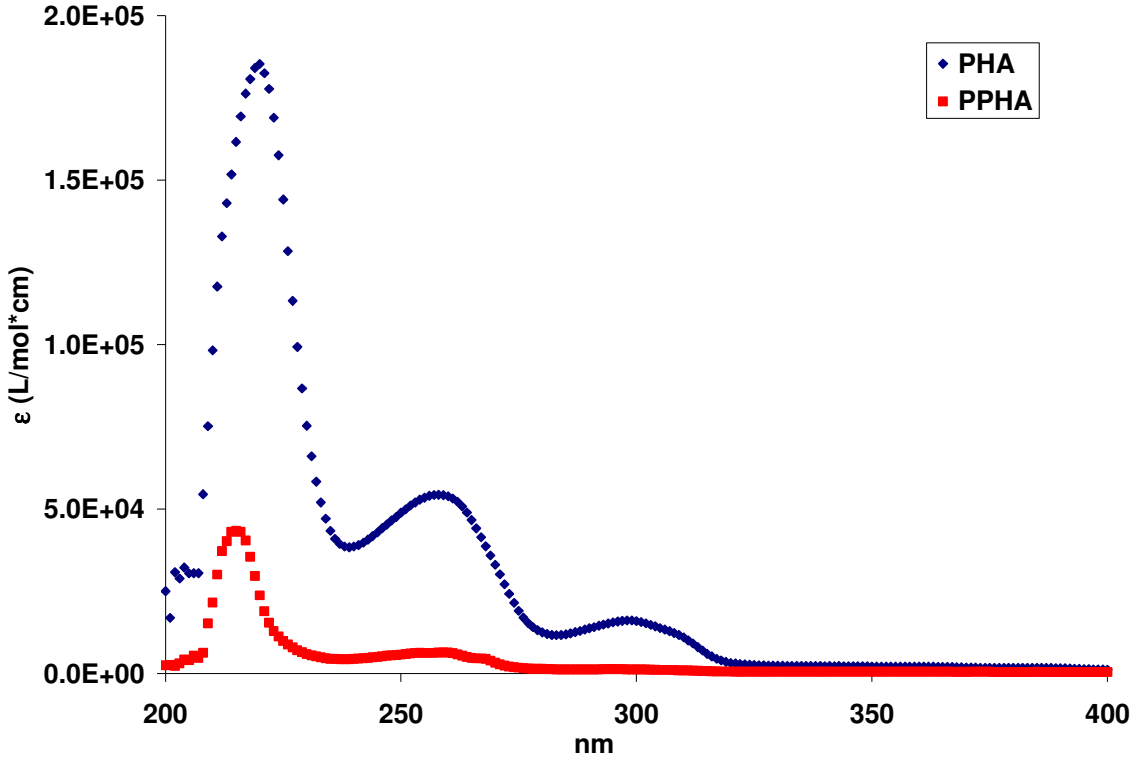

Figure 3.6: Molar extinction coefficients (ε) vs. wavelength for PHA (blue) and PPHA (red).

This is one reason why the NBA-PPHA/novolac resist required such a high dose to properly develop; once the NBA-PPHA on top of the resin unzipped, it formed a layer of monomer that then absorbed strongly preventing further light from penetrating to the NBA-PPHA below. It is also worth noting that Figure 3.6 is the molar extinction coefficient; therefore, an x molar PPHA solution will unzip to a solution an x*(degree of polymerization) molar solution of PHA. This further increases the effect of the large difference between ε_{PPHA} and ε_{PHA}. The NBA-PPHA/novolac/PAG resist did not require such a high dose because the absorption spectra of the PAG did not overlap with the PHA while the *o*-nitrobenzyl photolabile group did.

To confirm the results of this experiment, PPHA was dissolved in THF with a catalytic amount of acid, and UV-Vis spectra of this solution were collected over time. They showed the absorbance of the solution increasing as the PPHA unzipped; in particular, note the change in absorbance of the solution at 248 nm (Figure 3.7). The solution's absorbance at t = 120 min was greater than two, meaning that over 99% of the light was absorbed. These data are consistent with the hypothesis that the photoproducts of unzipping are one reason for high dose required for the development of the NBA-PPHA system.

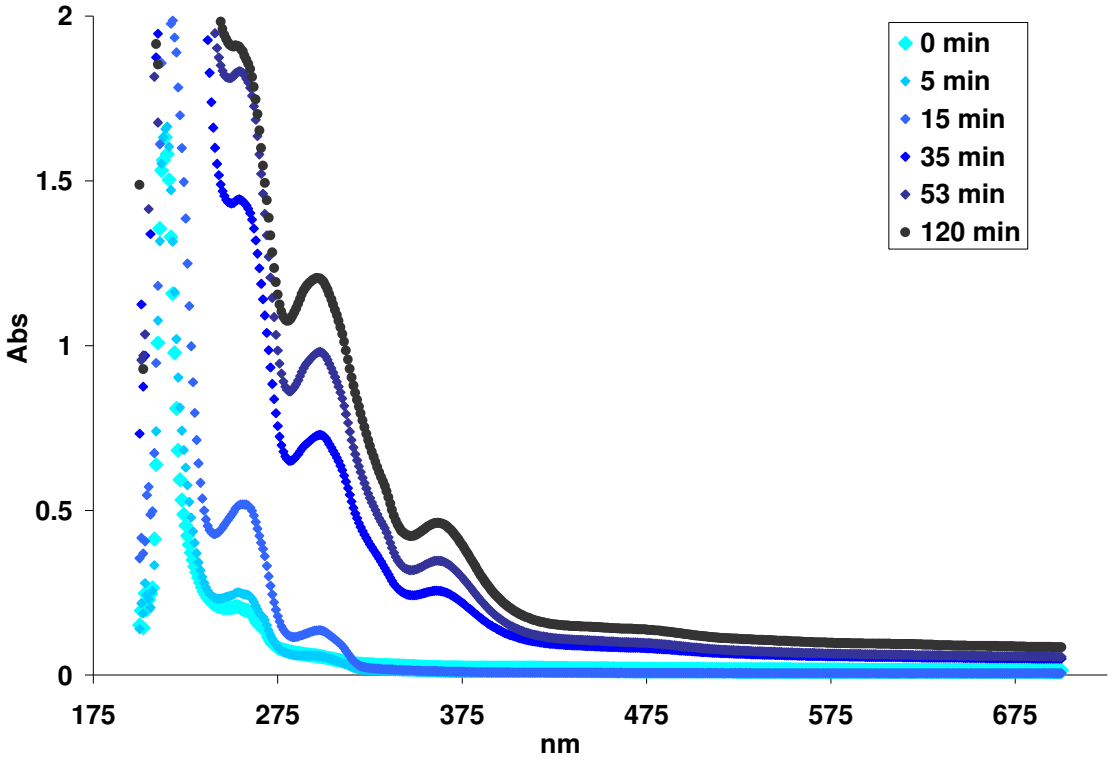

Figure 3.7: UV-vis spectra of PPHA unzipping in acidic THF.

3.10 EXPANDING TO 193 NM RESISTS

To expand the application of this chemistry, PPHA was tested as a polymeric dissolution inhibitor with poly(norbornenehexafluoroalcohol) (PNBHFA). Initial experiments showed these two polymers were not reproducibly phase compatible despite low molecular weight PPHA. A monomer containing a 1,4-dialdehyde functionality necessary for polymerization and a norbornane carbon skeleton for phase compatibility and lower optical density was envisioned (Scheme 3.3). Poly(3.1) could be accessed from dialdehyde 3.1, which due to the steric strain of the norbornane ring would require the aldehydes to be on the same face (3.1(bis-endo) or 3.1(bis-exo)). It was proposed the resulting polymer would be phase compatible with PNBHFA because of the similar

aliphatic structure and the lack of conjugation would decrease the optical absorption problems associated with PPHA and PHA.

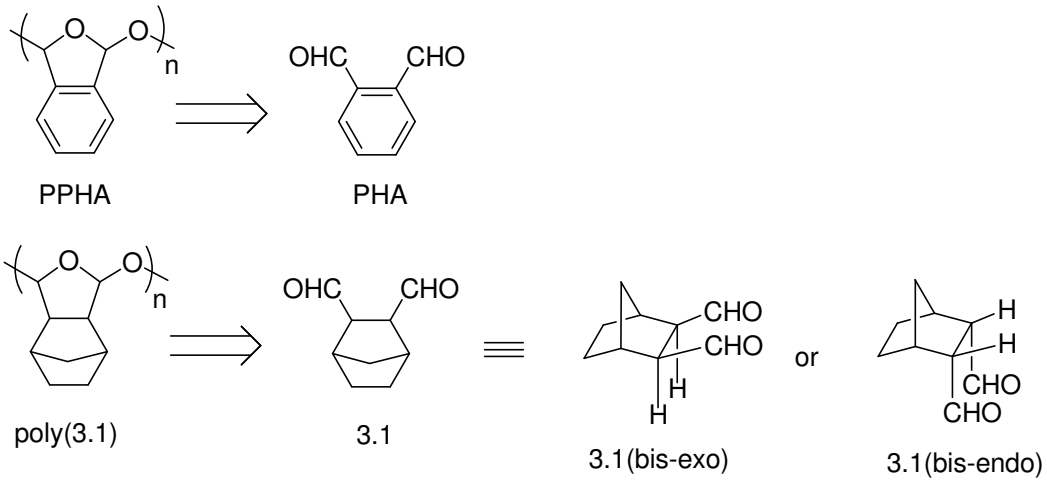

Scheme 3.3: Desired norbornane analog of PPHA and PHA.

3.11 NORBORNANE DIALDEHYDE

3.11.1 Oxidative and Reductive Routes

Initial efforts to synthesize 3.1 started with the reduction of the Diels-Alder adduct of cyclopentadiene and maleic anhydride[67] (3.2) with LAH to give bis-endo-diol 3.3. After hydrogentation of the double bond, diol 3.4 was submitted to standard oxidative PCC conditions. Unfortunately, no detectable amount of bis-endo-dialdehyde 3.1 was isolated but only lactone 3.5 in good yield (Scheme 3.4).

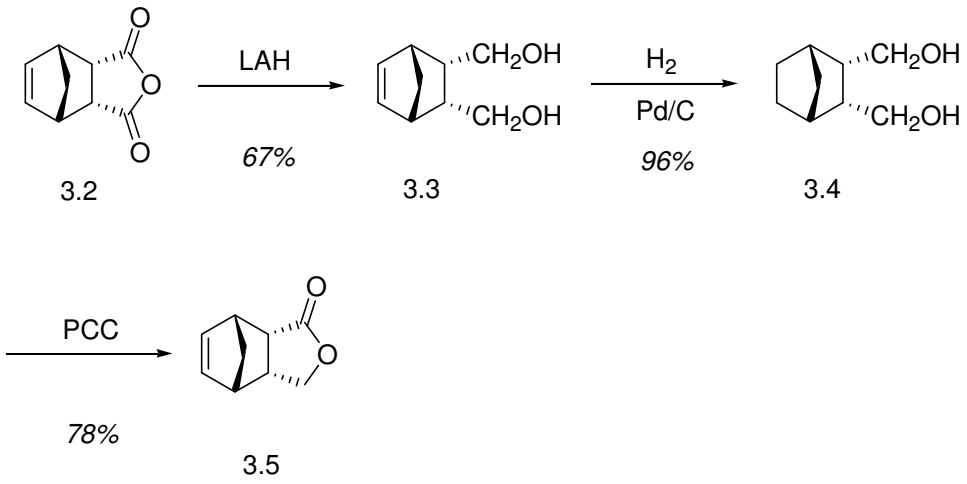

Scheme 3.4: Attempted oxidative route at bis-endo-aldehyde 3.1

Scheme 3.5 shows a route that was designed to circumvent the oxidative cyclization. First, the Diels-Alder adduct of fumaric acid and cyclopentadiene was formed (3.6) followed by reduction with LAH to yield endo-exo-diol 3.7. Upon oxidation with PCC, endo-exo-dialdehyde 3.8 was recovered in poor yield, but this was an important intermediate towards a bis-endo or bis-exo norbornene dialdehyde. Upon hydrogenation with Pd on carbon, only 68% of a crude material was recovered, which did contain endo-exo-dialdehyde 3.9 by ^{13}C-NMR and HRMS, however the product decomposed upon further attempts at purification. Desiring to continue on, this crude reaction mixture was submitted to acidic and basic epimerization conditions. Unfortunately, only the crude starting material was recovered and more rigorous conditions led to sample decomposition. This route was abandoned due to these purification issues.

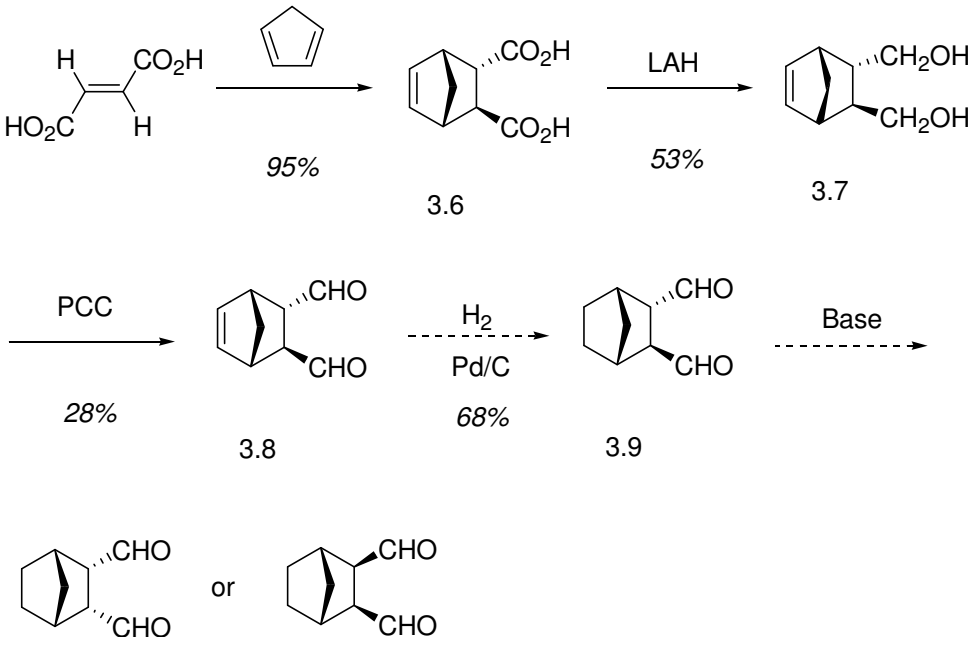

Scheme 3.5: Attempted route to 3.1 via an endo-exo dialdehyde (3.9)

Since the oxidation step in the first two routes was seen as the limiting step, a route was attempted that relied on reduction of a methyl ester to obtain the desired dialdehyde. As shown in Scheme 3.6, the Diels-Alder adduct of dimethyl maleate and cyclopentadiene was formed to obtain 3.10. After hydrogenation, dimethyl ester 3.11 was submitted to various DIBAL-H conditions. With mild conditions, only starting material was recovered, but when the solution was heated with large excesses of DIBAL-H, the sample decomposed. This route was therefore abandoned.

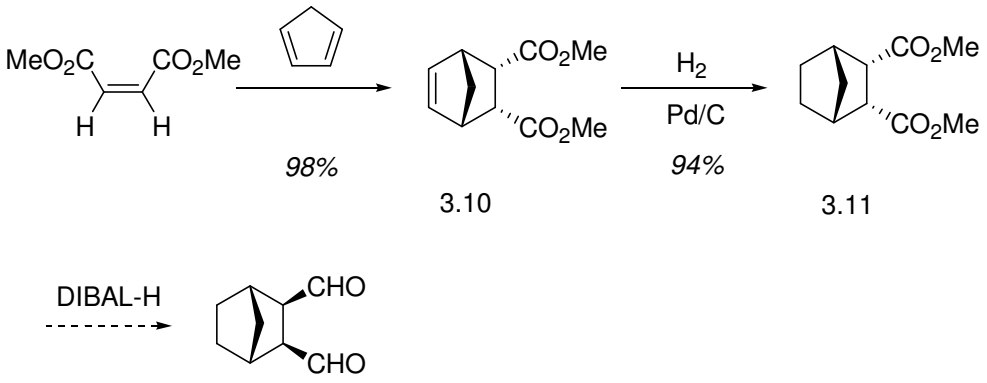

Scheme 3.6: Reductive route to dialdehyde 3.1.

3.11.2 Benzyl Protection Route

In a method inspired from Grayson et al.,[68] a fourth route was proposed that would rely on sequentially oxidizing the aldehydes via a benzyl protected alcohol (Scheme 3.7). This would allow the bis-endo or bis-exo stereochemistry to be set from the beginning of the synthesis while preventing the cyclic-oxidation to the lactone observed in Scheme 3.4. The first step was a transacetalization of dimethyl benzyl acetal and bis-endo-diol 3.4. The 7-membered cyclic acetal 3.12 was then reduced with DIBAL-H to yield the asymmetric 3.13 with a free hydroxyl group and a benzyl protected alcohol. The alcohol was oxidized to aldehyde 3.14 with PCC. Surprisingly, the ethylene glycol protection of the aldehyde was very troublesome. The ^{1}H-NMR of the crude isolated material displayed no aldehyde proton or protons around 3.3 ppm associated with ethylene glycol acetals. Given the multi-step approach in this route and continued observed instability of norbornane aldehydes, this route was abandoned.

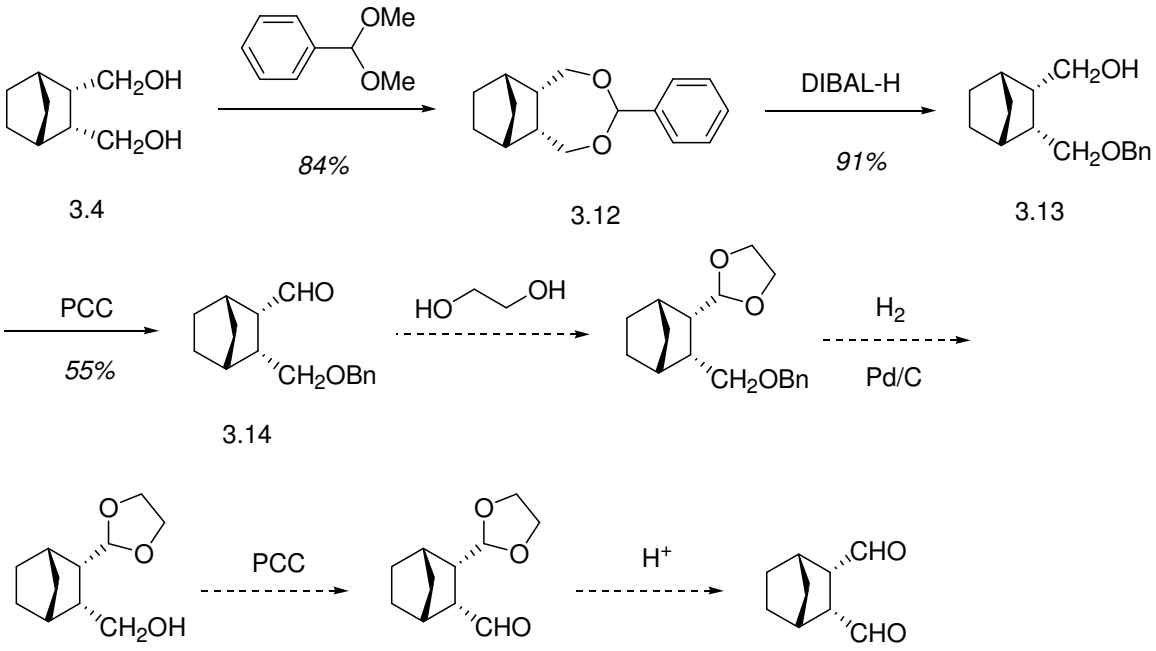

Scheme 3.7: Benzyl protection route to dialdehyde 3.1.

3.11.3 Dienophile Route

Up to this point, the proposed routes focused on synthesizing the 1,4-dialdehyde on a norbornane skeleton. Given the lack of success with these routes, another route was proposed that synthesized the 1,4-dialdehyde component separately, and then subjected it to cyclopentadiene to produce the norbornane skeleton via a Diels-Alder reaction. A scan of the literature showed that maleic dialdehydes[69] and acetylene dicarboxaldehyde[70] are very unstable and cannot be isolated. Fortunately, a 2004 report was found in which large quantities of 4,4-dimethoxybut-2-ynal were synthesized,[71] and it was proposed that this could act as a dienophile in a Diels-Alder reaction (Scheme 3.8).

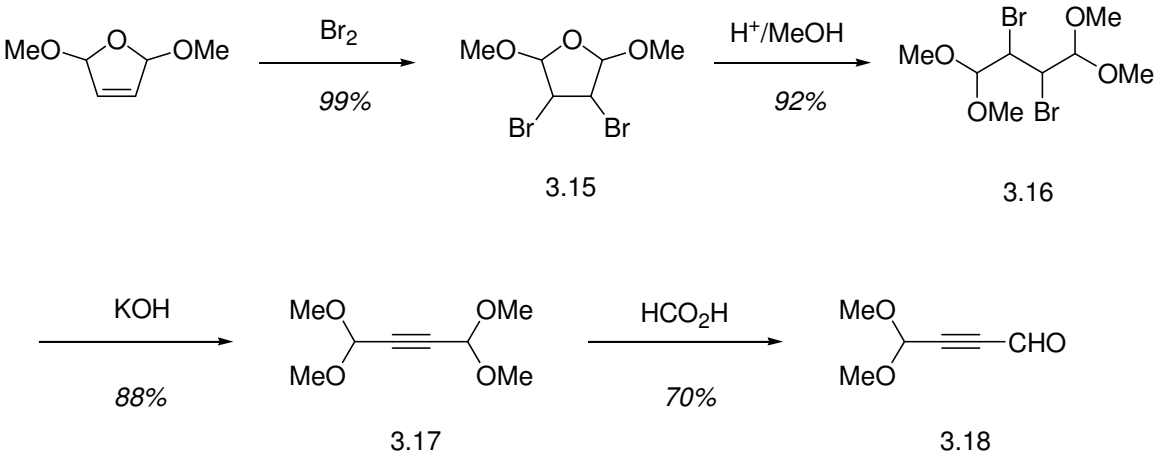

Scheme 3.8: Synthetic route towards butynal 3.18.

The synthesis began by brominating the commercially available 2,5-dimethoxy-2,5-dihydrofuran. Compound 3.15 was hydrolyzed in acidic methanol to produce the dimethyl diacetal 3.16, followed by elimination of the bromines with KOH to produce alkyne 3.17. The hydrolysis of 3.17 proved to be a very sensitive reaction, and initial attempts at this reaction gave poor yields. It was determined the temperature and purity of the formic acid needed to be precisely controlled.[72] When a temperature regulated water bath and 96% pure formic acid were used, the reaction proceeded as reported to give butynal 3.18 in good yields.

With appreciable quantities of butynal 3.18 in hand, the Diels-Alder adduct was formed with cyclopentadiene in water to give norbornadiene dialdehyde 3.19; the water hydrolyzed the dimethyl acetal *in situ*. The next step was to reduce each of the double bonds. The hydrogenation of the double bond between the two methynes was easily accomplished under standard reduction conditions to give 3.20 however, the reduction of the double bond between the two aldehydes was never accomplished (Scheme 3.8). A catalyst screening confirmed the delicate nature of diene 3.19 towards hydrogenation. As shown in Table 3.1 a variety of standard hydrogenation catalysts and solvents including

Pd on carbon, Pd on $BaSO_4$, Pt, rhodium on carbon, Wilkinsons's, Crabtree's, and Lindlar's catalysts would yield starting material 3.19, conjugated dialdehyde 3.20, or decomposition products as determined by IR and ^{1}H-NMR spectroscopy. This was interpreted as once the system achieved enough reduction potential to reduce the conjugated double bond, it reduced the aldehydes as well.

Table 3.1: Catalyst and solvent screen for hydrogenation of diene 3.19

Exp	Catalyst	Solvent	IR	^{1}H-NMR	Result
1	Pd/C (5%)	DCM	-CHO	-CHO	3.20
2	Pd/C (10%)	DCM	No -CHO	No –CHO or vinyl	Decomp
3	Pd/C (10%)	EtOH	-OH	No –CHO or vinyl	Decomp
4	Pd/C (10%)	H+/EtOH	-OH	No –CHO or vinyl	Decomp
5	Pd/C (10%)	AcCN	-OH	No –CHO or vinyl	Decomp
6	Pd/$BaSO_4$	DCM	-CHO	-CHO	3.20
7	Pd/$BaSO_4$	EtOH	-CHO	-CHO	3.20
8	Pd/$BaSO_4$	H+/EtOH	-CHO	-CHO	3.20
9	Pd/$BaSO_4$	AcCN	-CHO	-CHO	3.20
10	Lindlar's	DCM	-CHO	-CHO	3.20
11	Raney Nickel	DCM	No -CHO	No –CHO or vinyl	Decomp
12	Raney Nickel	EtOH	No -CHO	No –CHO or vinyl	Decomp
13	Pt/C	DCM	-OH	No –CHO or vinyl	Decomp
14	Pt/C	EtOH	-OH	No –CHO or vinyl	Decomp
15	Wilkinson's	DCM	-CHO	-CHO	3.19
16	Crabtree's	DCM	-CHO	-CHO	3.19
17	Rh/C	DCM	-CHO	-CHO	3.19

Believing the conjugation was stabilizing the dialdehyde and hence making it sensitive towards hydrogenation conditions, compound 3.21 was synthesized under anhydrous Diels-Alder condition with cyclopentadiene (Scheme 3.9). Unfortunately, it showed the same reactivity towards hydrogenation as 3.20. Several catalysts and solvents were screened, but product was never obtained.

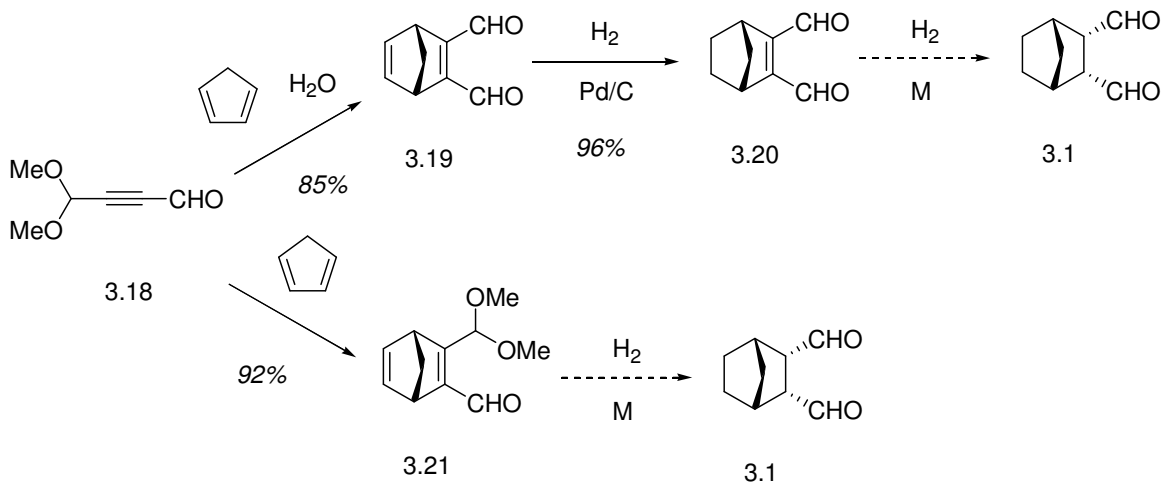

Scheme 3.9: Diels-Alder and hydrogenations of butynal 3.18.

3.11.4 1,2-Diol Cleavage

After much time and effort into dialdehyde synthesis, a last route was investigated that relied on oxidative cleavage of 1,2-diols. An aromatic model system was run concurrently with a norbornane skeleton as shown in Scheme 3.10. The dihydroxylation of commercially available indene was successful and yielded 3.22 as a white powder after purification by sublimation. Despite being subjected to several 1,2-diol cleavage conditions, the expected dialdehyde product was never isolated even though it is claimed in the literature.[73,74] The dihydroxylation of commercially available 5,6-dihydrodicyclopentadiene was carried out in fair yield to obtain diol 3.23 as a white powder after purification by sublimation. Unfortunately, the 1,2-diol cleavage was unsuccessful on this compound as well, and dialdehyde product was never isolated.

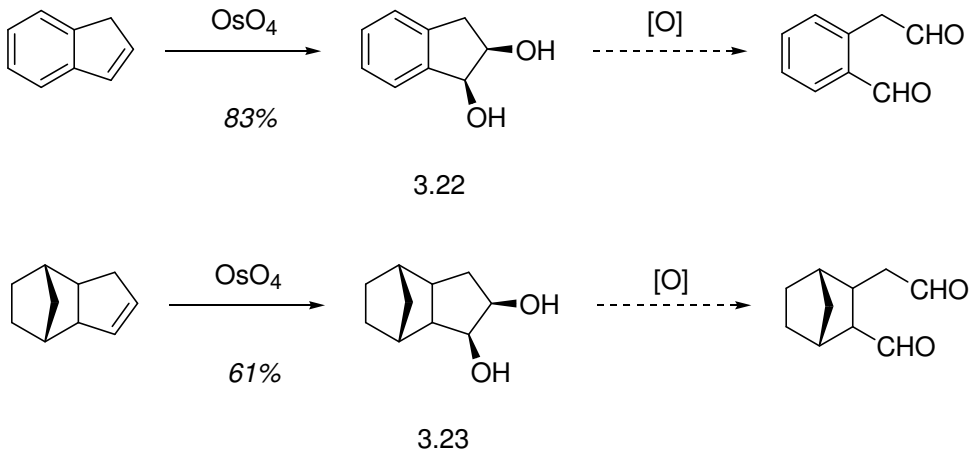

Scheme 3.10: 1,2-Diol cleavage routes towards dialdehydes.

3.12 POLY(ALIPHATIC) ALDEHYDES

Due to the synthetic difficulties encountered in preparing 1,4-dialdehydes, a much simpler approach was proposed that addressed both the absorbance and phase compatibility issues of PPHA while using commercially available or easily synthesized monoaldehydes. PPHA is amorphous; therefore it can be dissolved in common casting solvents used for photolithographic processes. However, the majority of polyaldehydes are crystalline and not soluble in solvents at room temperature.[75-78] It was proposed instead of synthesizing a new monomer, copolymers of short chain aliphatic aldehydes might have the necessary material properties to function as a PDI with PNBHFA. The optical absorbance of these polymers and the resulting unzipped monomers would be less than that of PPHA because of the lack of aromatic groups. While the homopolymers of aliphatic aldehydes are known to be crystalline,[77,78] random copolymers with different side chains might disrupt the polymer's crystallinity. The literature on the topic is very limited; one report was found which states that the random copolymers of several short chain aliphatic aldehydes are crystalline over all ranges.[79] This conclusion is based experimentally upon x-ray crystal data of several copolymers, and the authors conclude

this paper stating, "a more detailed discussion of this work is being reserved for forthcoming publications," which apparently do not exist outside of 1960s Japanese patent literature. Furthermore, this report exists as an island in the literature with only two reviews citing it in passing.[75,80]

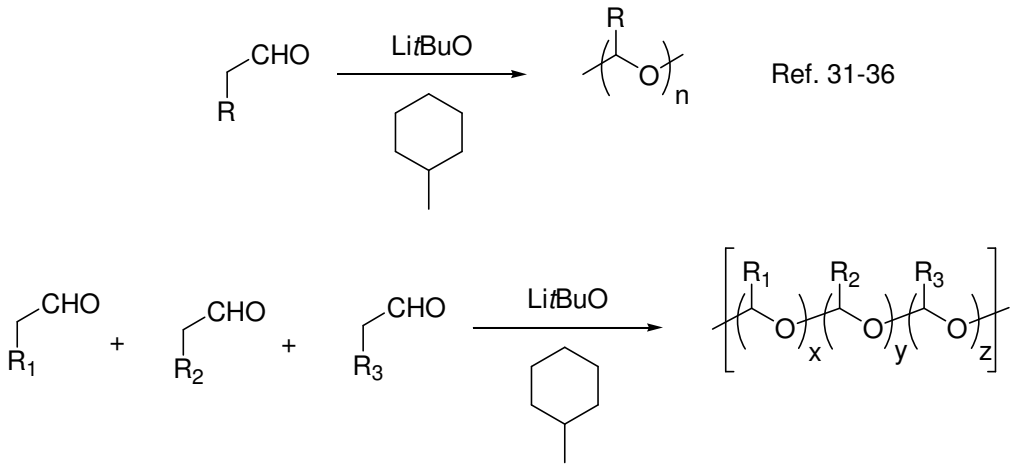

Scheme 3.11: Synthesis of aliphatic polyaldehydes.

Based on the knowledge of Vogl, who pioneered this field in the 1960s and 70s, copolymers of propanal, butanal, pentanal, hexanal, and 2-ethyl butyraldehyde were made by polymerization at -78 °C in freshly distilled methyl cyclohexane (MCH) using lithium t-butoxide as the initiator (Scheme 3.11). Upon addition of the monomer or monomers to the cold MCH/initiator solution, the solution became very viscous, and the stir bar stopped moving. A large excess of acetic anhydride and TEA were then added to cap the proposed polymer. Despite the addition of up to four different monomers, the resulting materials were never soluble in THF for GPC analysis nor in any common casting solvent to test as a PDI. Only a few of the resulting highly crystalline polymers were partially soluble in $CDCl_3$. ^{1}H-NMR was not helpful because all of the monomers were small alkyl chains, so copolymer ratios could not be determined. DSC and TGA

analysis of these materials showed low thermal decomposition temperatures and large T_m peaks. Due to these dismal material properties, this route was abandoned.

3.13 HETERO-ATOM CONTAINING MONO-ALDEHYDES

After observing the high amount of crystallinity in the proposed copolymers of aliphatic polyaldehdyes, it was envisioned that incorporating a hetero-atom, specifically oxygen, into a monoaldehyde monomer would break up the crystallinity of the resulting polymer. Scheme 3.12 represents a synthetic method to obtain one such monomer.[81] The synthesis began with the deprotonation and benzylation of commercially available cis-2-butene diol to yield dibenzyl ether 3.24. Benzyloxy-acetaldehyde (3.25) was isolated after ozonolysis and a reductive work up. Once obtained, polymerization was attempted using a variety of initiators in THF. MCH was not used due to the lack of solubility of benzyloxy-acetaldehyde in MCH. After many trials, a small amount of polymer was obtained that was soluble in THF and $CDCl_3$. GPC and ^{1}H-NMR analysis confirmed the material was a polyacetal. This result was consistent with the hypothesis that an oxygen in the beta position of the linear aldehyde would lead to a less crystalline, more amorphous polymer. Polymerization of the aliphatic analog phenylacetaldehyde with no β-oxygen was attempted, and a highly crystalline material was obtained which was not able to be characterized.

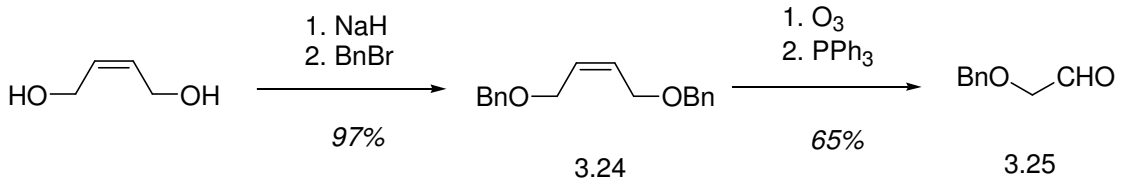

Scheme 3.12: Synthesis of benzyloxy-acetaldehyde 3.25.[81]

Despite being less crystalline, poly(benzyloxy-acetaldehyde) did not have the solubility properties desired for a PDI. Therefore, a mono-aldehyde was proposed that had two oxygen atoms to break up polymer crystallinity (Scheme 3.13). The first step was the mesyl protection of commercially available 2-ethoxy-ethanol to give mesylate 3.26. Compound 3.26 was then submitted to a Williamson-Ether reaction with commercially available cis-2-butene diol to give 3.27 followed by ozynolysis to yield aldehyde 3.28.

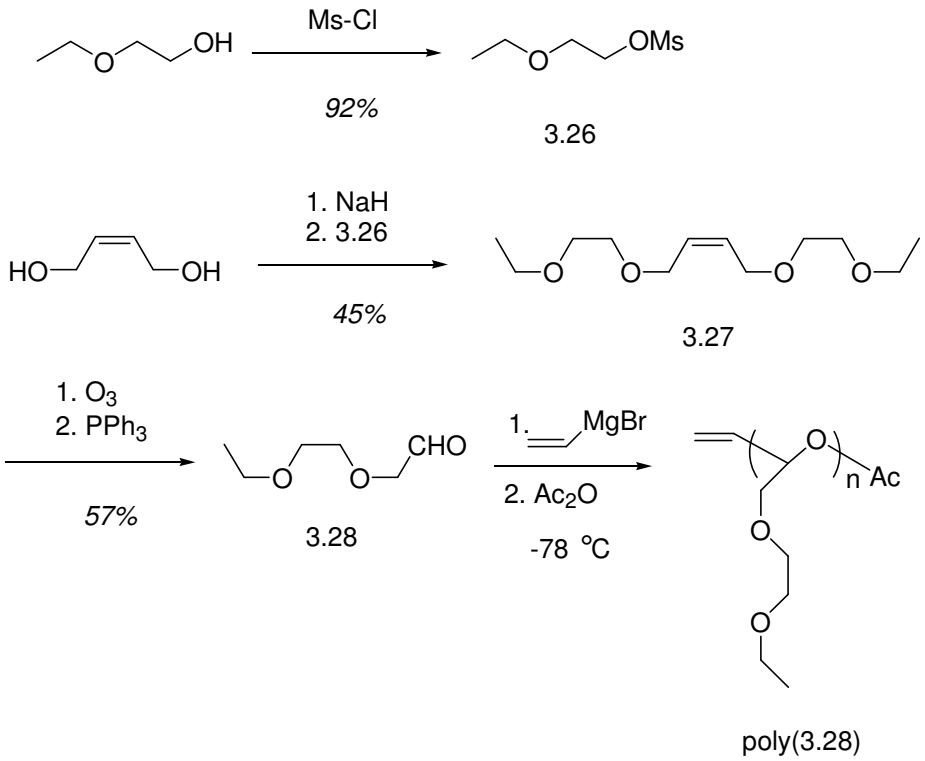

Scheme 3.13: Synthesis of hetero atom aldehyde 3.28 and poly(3.28).

After synthesizing an appreciable amount of this monomer, polymerization conditions were tested. Due to its similarity to an oligomeric polyethylene glycol this monomer was extremely difficult to keep dry. Alkyl lithium reagents and tert-butoxide salts yielded no polymer, but surprisingly, the only initiator that yielded polymer was

vinyl magnesium bromide. The selectivity of this initiator warrants further study. After polymerization, poly(3.28) was isolated by removing the THF, Ac_2O, and TEA *in vacuo*. GPC and ^{1}H-NMR analysis both showed the isolated material was polymeric.

To confirm that upon generation of an active chain end poly(3.28) would unzip, a film was spin coated from a 8 wt% solution of poly(3.28) in PGMEA with 2 wt% PAG. The photogenerated acid hydrolyzed the polyacetal backbone yielding an uncapped chain-end similar to earlier experiments with PPHA. No material remained after exposure to 248 nm light and a 90 °C PEB for 60 sec. This was consistent with a T_c below room temperature.

To test poly(3.28) as a PDI, various solutions were made of poly(3.28) and PNBHFA. While both components readily went into solution, films were regrettably cloudy and hazy upon spin coating. Despite the phase separation with PNBHFA, a 10 wt% solution of poly(3.28) to novolac was made in PGMEA. While this film was phase compatible to the eye, its dissolution rate was identical to that of novolac with no poly(3.28). Therefore although another novolac phase compatible polymer had been synthesized, it did not function as a PDI.

3.14 CONCLUSIONS

Poly(phthalaldehyde) served as a polymeric dissolution inhibitor of novolac. While PPHA relies on acid hydrolysis to unzip, a photolabile end group was incorporated via initiation with o-nitrobenzyl oxide. NBA-PPHA was shown to unzip upon exposure to 248 nm light without acid. UV-vis experiments showed that solutions of unzipping PPHA increased in optical density by several orders of magnitude, and this explains the high dose necessary to image NBA-PPHA/novolac formulations.

To expand this application to 193 nm photolithography, a norbornane dialdehyde was envisioned that would address the issues of phase compatibility and optical density

with PPHA and PNBHFA. Six different routes were attempted to make such a molecule relying on oxidation, reduction, and Diels-Alder chemistries, but the stability of aliphatic aldehydes was too great of an obstacle to overcome.

To circumvent dialdehyde synthesis, copolymers of aliphatic aldehydes were synthesized, but their material properties including low thermal stability, high crystallinity, and minimal solubility did not meet the specifications of a PDI. Heteroatoms were then incorporated into mono-aldehydes, and the resulting polymers had more attractive materials properties. A polyethylene glycol aldehyde analog was synthesized, but unfortunately the resulting polyacetal was not phase compatible with PNBHFA nor did it function as a PDI of novolac. Despite the lack of bottom-line success with this project, several interesting chemistries were explored, and information about PDIs was expanded.

3.15 EXPERIMENTAL

3.15.1 General Methods and Materials

All chemicals were purchased from Sigma-Aldrich and used as received unless otherwise stated. All reactions were conducted under a positive nitrogen atmosphere with oven-dried glassware unless otherwise stated. Dry DCM, TEA, and pyridine were obtained by distillation over CaH_2 while dry THF was obtained by distillation over Na/benzophenone. All ^{1}H and ^{13}C NMR spectra were recorded on a Varian Unity Plus 400 MHz instrument. All chemical shifts are reported in ppm downfield from TMS using the residual protonated solvent as an internal standard ($CDCl_3$, ^{1}H 7.26 ppm and ^{13}C 77.0 ppm; DMSO-d_6, ^{1}H 2.49 ppm and ^{13}C 39.5 ppm). HRMS (CI) was obtained on a VG analytical ZAB2-E instrument. IR data was recorded on a Nicolet Avatar 360 FT-IR and all peaks are reported in cm^{-1}. LRMS (GC/MS) were obtained on an Agilent 6890N

Network GC Systtem and Agilent 5973N Mass Selective Detector. All molecular weights were measured using an Agilent 1100 Series Isopump, Autosampler, and Refractometer and the following Pgel GPC columns: guard, 10^4 Å and 100 Å. Films were spin coated and baked on a Brewer CEE 100CB Spincoater & Hotplate. A Veeco Dektak 6M Stylus Profiler was used to determine film thicknesses.

3.15.2 Phthalaldehyde Compounds

Poly(phthalaldehyde), PPHA

A 10 mL RBF equipped with a stir bar was charged with phthalaldehyde (1.0 g, 7.5 mmol) and THF (3 mL). After cooling reaction flask to -78 °C in an isopropyl alcohol/dry ice bath, n-butyllithium (0.22 mL, 2.2 M in Hex, 0.50 mmol) was added dropwise. The reaction was stirred for 8 h followed by addition of freshly distilled acetic anhydride (0.14 mL, 1.5 mmol). The reaction mixture was slowly warmed to rt over 2 h, then precipitated into a vigorously stirring 1:1 MeOH:H_2O solution at 0 °C. The white polymer was then filtered and dried overnight to yield **PPHA** (487 mg, 49%). The M_w was 1,900 as determined by GPC with polystyrene standards.

o-Nitrobenzyl alcohol initiated poly(phthaladehyde), NBA-PPHA

A fritted glass funnel with a 14/20 female opening on top and a luer lock was constructed by University of Texas Glassblower, Mike Ronalter. After placing NaH (250 mg, 10.4 mmol), and a magnetic stir bar on top of the fritt funnel, THF was added (5 mL). *o*-Nitrobenzyl alcohol (34.1 mg, 0.2 mmol) was then added and the suspension was stirred for 15 min. This solution was then added to a previously prepared 10 mL RBF equipped with a stir bar, phthalaldehyde (1.0 g, 7.5 mmol), and THF (3 mL) at -78 °C. The reaction was stirred for 8 h and then quenched with acetic anhydride and precipitated as described for **PPHA**. **NBA-PPHA** was recovered (395 mg, 40%) with an M_w of 1,700 as determined by GPC with polystyrene standards.

3.15.3 Norbornane Dialdehyde Monomer Synthesis

bis-endo-(3-Hydroxymethyl-bicyclo[2.2.1]hept-5-en-2-yl)-methanol, 3.3

A 3-neck 500 mL RBF equipped with a stir bar, condenser, and an addition funnel was charged with $LiAlH_4$ (3.42 g, 90.1 mmol) and THF (80 mL). In a separate 250 mL RBF, endo-4-Oxa-tricyclo[5.2.1.02,6]dec-8-ene-3,5-dione 3.2 (10.0 g, 60.9 mmol, previously prepared by Pinnow methods[67]) was dissolved in THF (100 mL). After slow addition of this solution to the reaction flask via the addition funnel over a period of 20 min, the reaction was heated to reflux overnight. In the morning, the reaction was cooled to rt, quenched with a saturated solution of Rochelle's salt, and acidified to pH=1 with conc. HCl. Ether (300 mL) was added to this mixture and allowed to stir for 1 h. After removal of the ether, the aqueous layer was extracted again with ether (2x300 mL). The organic layers were then combined, rinsed with brine, dried with $MgSO_4$, filtered, and concentrated *in vacuo* to yield 3.3 as a white solid (6.3 g, 66.9 %). No further purification was required. Mp = 87-89 °C; ^{1}H NMR ($CDCl_3$) δ ppm: 1.39 (m, 2H), 2.52 (m, 2H), 2.79 (s, 2H), 3.36 (t, *J* = 10.8 Hz, 2H), 3.62 (m, 2H), 3.83 (s, 2H), 6.02 (m, 2H); ^{13}C NMR ($CDCl_3$) δ ppm: 134.76, 63.42, 49.89, 46.51, 45.06; IR (NaCl): 3313, 2928; HRMS (CI) M+1 calc = 155.1072, found = 155.1070.

bis-endo-(3-Hydroxymethyl-bicyclo[2.2.1]hept-2-yl)-methanol, 3.4

A 100 mL RBF equipped with a stir bar was then charged with 3.3 (3.0 g, 19.5 mmol), 5 wt% Pd/C (300 mg), and DCM (60 mL). After several minutes of stirring, the flask was placed in a 1L Parr reaction vessel, pressurized with H_2 to 500 psi, and stirred overnight. In the morning, the crude reaction mixture was filtered through celite and $MgSO_4$ and concentrated *in vacuo* to yield 3.4 as white solid (2.9 g, 96%). No further purification was required. Mp = 88-89 °C; ^{1}H NMR ($CDCl_3$) δ ppm: 1.28 (m, 4H), 1.38 (m, 2H), 2.16 (m, 2H), 2.20 (m, 2H), 3.59 (d, *J* = 9.3 Hz, 2H), 3.89 (m, 2H), 4.21 (br s,

2H); ^{13}C NMR ($CDCl_3$) δ ppm: 61.75, 43.07, 40.71, 40.01, 22.69; IR (NaCl): 3312, 3008; HRMS (CI) M+1 calc = 157.1229, found = 157.1229.

bis-endo- 4-Oxa-tricyclo[5.2.1.0^{2,6}]dec-8-en-3-one, 3.5

A 50 mL RBF quipped with a stir bar was charged with 3.4 (500 mg, 3.0 mmol), 4 Å molecular sieves (300 mg), and DCM (15 mL). Pyridinium chlorochromate (1.9 g, 9.0 mmol) was then slowly added and stirred for 5 h. The crude reaction mixture was filtered through a celite, charcoal, and silica plug with DCM and concentrated *in vacuo* to yield 3.5 as a colorless oil (375 mg, 78%). ^1H NMR ($CDCl_3$) δ ppm: 1.48 (m, 6H), 2.30 (m, 1H), 2.59 (m, 1H), 2.83 (m, 1H), 2.91 (m, 1H), 4.21 (m, 2H); ^{13}C NMR ($CDCl_3$) δ ppm: 178.64, 68.28, 46.55, 41.77, 41.72, 40.21, 39.65, 25.27, 21.37; IR (NaCl) 1738, 1102; HRMS (CI) M+1 calc = 153.0916, found 153.0913.

endo-exo-Bicyclo[2.2.1]hept-5-ene-2,3-dicarboxylic acid, 3.6

A 500 mL RBF equipped with a stir bar was charged with fumaric acid (19.32 g, 166.5 mmol), acetone (290 mL), and H_2O (29 mL).[82] Freshly distilled CPD (10 g, 151.5 mmol) was then added to the reaction mixture and stirred over night. After adding H_2O (200 mL) in the morning, the reaction mixture was extracted with EtOAc (2x300 mL). The organic layers were then combined, rinsed with brine, dried with $MgSO_4$, filtered, and concentrated *in vacuo* to yield 3.6 as a white solid (28.8 g, 95%). No further purification was required. Mp = 159-161 °C; ^1H NMR (DMSO) δ ppm: 12.30 (br s, 2H), 6.27 (d, *J* = 5.4 Hz, 1H), 6.04 (d, *J* = 5.4 Hz, 1H), 3.16 (s, 2H), 3.01 (s, 1H), 2.40 (s, 1H), 1.49 (d, *J* = 8.4 Hz, 1H), 1.32 (d, *J* = 7.8 Hz, 1H); ^{13}C NMR (DMSO) δ ppm: 175.34, 174.15, 137.50, 134.97, 47.44, 47.06, 46.99, 46.77, 44.95; IR (neat): 3428, 1690, 1658, 1641.

endo-exo-(3-Hydroxymethyl-bicyclo[2.2.1]hept-5-en-2-yl)-methanol, 3.7

A 3-neck 100 mL RBF equipped with a stir bar, addition funnel, and condenser was charged with $LiAlH_4$ (1.5 g, 43.9 mmol) and THF (20 mL). In another 50 mL RBF, 3.6 (1.0 g, 5.5 mmol) was dissolved in THF (20 mL). After slow addition of this solution to the LAH slurry via the addition funnel, the reaction was refluxed overnight. In the morning, the reaction was cooled to rt, quenched with a saturated solution of Rochelle's salt, and acidified to pH=1 with conc. HCl. Ether (100 mL) was added to this mixture and allowed to stir for 1 h. After removal of the ether, the aqueous layer was extracted again with ether (2x50 mL). The organic layers were then combined, rinsed with brine, dried with $MgSO_4$, filtered, and concentrated *in vacuo* to yield 3.7 as a clear oil (450 mg, 53%). No further purification was required. ^{1}H NMR ($CDCl_3$) δ ppm: 6.23 (m, 1H), 5.98 (m, 1H), 3.89 (br s, 2H), 3.78 (m, 1H), 3.66 (m, 1H), 3.41 (t, *J* = 10.2 Hz, 1H), 3.03 (t, *J* = 9.6 Hz, 1H), 2.82 (s, 1H), 2.58 (s, 1H), 1.39 (s, 2H), 1.21 (t, *J* = 6.3 Hz, 2H); ^{13}C NMR ($CDCl_3$) δ ppm: 137.82, 133.32, 66.16, 65.65, 47.60, 46.90, 46.65, 44.39, 44.29; IR (NaCl) 3389, 2987; HRMS (CI) M+1 calc = 155.1072, found = 155.1074.

endo-exo-Bicyclo[2.2.1]hept-5-ene-2,3-dicarbaldehyde, 3.8

A 50 mL RBF equipped with a stir bar was charged with 3.7 (490 mg, 3.1 mmol), 4 Å molecular sieves (150 mg), and DCM (20 mL). After addition of pyridinium chlorochromate (1.7 g, 7.8 mmol), the reaction mixture was stirred overnight. The crude reaction mixture was filtered through a celite, charcoal, and silica plug with DCM and concentrated *in vacuo* to yield 3.8 as a clear liquid (130.2 mg, 28%). No further purification was required. ^{1}H NMR ($CDCl_3$) δ ppm: 9.75 (s, 1H), 9.49 (s, 1H), 6.21 (m, 1H), 6.06 (m, 1H), 3.37 (m, 1H), 3.32 (m, 1H), 3.20 (m, 1H), 2.78 (m, 1H), 1.42 (m, 1H), 1.31 (m, 1H); ^{13}C NMR ($CDCl_3$) δ ppm: 201.03, 200.55, 137.16, 134.88, 53.44, 53.15, 46.56, 44.58, 43.94; IR (NaCl) 2972, 1738; HMRS (CI) M+1 calc = 151.0759, found = 151.0755.

endo-exo- Bicyclo[2.2.1]heptane-2,3-dicarbaldehyde, 3.9

A 25 mL RBF equipped with a stir bar was then charged with 3.8 (50 mg, 0.3 mmol), 5 wt% Pd/C (5 mg), and DCM (10 mL). After several minutes of stirring, the flask was placed in a 250 mL Parr reaction vessel, pressurized with H_2 to 500 psi, and stirred overnight. In the morning, the crude reaction mixture was filtered through celite and $MgSO_4$ and concentrated *in vacuo* to yield 3.9 as a clear liquid (34.4 mg, 68%). Full characterization of this compound was not accomplished due to decomposition of product upon purification; ^{13}C NMR ($CDCl_3$) δ ppm: 202.07, 200.80, 53.34, 38.69, 37.82, 37.38, 29.67, 28.96, 24.62; IR (NaCl) 3002, 1741; HMRS (CI) M+1 calc = 153.0916, found 153.0922.

bis-endo-Bicyclo[2.2.1]hept-5-ene-2,3-dicarboxylic acid dimethyl ester, 3.10

A 500 mL RBF equipped with a stir bar was charged with dimethylmaleate (48.4 mL, 387.5 mmol), zinc chloride (5.3 g, 38.9 mmol), and DCM (70 mL). After slowly adding freshly distilled CPD (28.13 g, 426.3 mmol), the reaction was stirred for 8 h. The reaction mixture was filtered through a small alumina/ $MgSO_4$ plug concentrated *in vacuo* to yield 3.10 as a white solid (80.6 g, 98%). No further purification was required. Mp = 53-54 °C; ^1H NMR ($CDCl_3$) δ ppm: 6.23 (s, 2H), 3.59 (s, 6H), 3.28 (m, 2H), 3.13 (m, 2H), 1.44 (d, J = 9 Hz, 1 H), 1.31 (d, J = 8.7 Hz, 1 H); ^{13}C NMR ($CDCl_3$) δ ppm: 173.12, 134.83, 51.55, 48.60, 48.02, 46.16; IR (NaCl) 3001, 1742, 1082; HRMS (CI) M+1 = 211.0892 calc, 211.0890 found.

bis-endo-Bicyclo[2.2.1]heptane-2,3-dicarboxylic acid dimethyl ester, 3.11

A 100 mL RBF equipped with a stir bar was then charged with 3.10 (4.0 g, 18.8 mmol), 5 wt% Pd/C (400 mg), and DCM (60 mL). After several minutes of stirring, the flask was placed in a 1 L Parr reaction vessel, pressurized with H_2 to 500 psi, and stirred overnight. In the morning, the crude reaction mixture was filtered through celite and

$MgSO_4$ and concentrated *in vacuo* to yield 3.11 as a white solid (3.7 g, 94%). No further purification was required. Mp = 54-55 °C; ^{1}H NMR ($CDCl_3$) δ ppm: 3.61 (s, 6H), 2.94 (s, 2H), 2.52 (m, 2H), 1.73 (m, 2H), 1.42 (m, 4H); ^{13}C NMR ($CDCl_3$) δ ppm: 172.92, 51.23, 46.63, 40.20, 39.74, 23.95; IR (NaCl): 2954, 2882, 1739, 1435, 1201, 737; HMRS (CI) M+1 calc = 213.1127, found = 213.1134.

endo-5-Phenyl-4,6-dioxa-tricyclo[7.2.1.02,8]dodecane, 3.12

A 100 mL RBF was charged with 3.4 (1.0 g, 6.5 mmol), dimethyl benzyl acetal (1.17 mL, 7.8 mmol), *p*-toluene sulfonic acid monohydrate (61.6 mg, 0.32 mmol), and toluene (30 mL). The reaction mixture was stirred under reduced pressure (65 torr) at 0 °C by connecting it to a rotary evaporator. After 3 h, the reaction mixture was quenched with a saturated solution of sodium bicarbonate, extracted with DCM (3x50 mL), dried with $MgSO_4$, and concentrated *in vacuo* to yield 3.12 as a clear viscous oil (1.3 g, 84%). No further purification was required. ^{1}H NMR ($CDCl_3$) δ ppm: 7.56 (m, 5H), 5.45 (s, 1H), 4.08 (d, *J* = 29.7 Hz, 4 H), 2.51 (m , 2H), 2.25 (s, 2H), 1.51 (m, 4H), 1.24 (m, 2H); ^{13}C NMR ($CDCl_3$) δ ppm: 134.39, 128.31, 128.10, 125.89, 108.18, 71.34, 43.63, 41.68, 39.67, 22.92; IR (NaCl):2939, 2878, 1701, 1451, 1002, 695; HRMS (CI) M+1 calc = 245.1542, found = 245.1539.

bis-endo-(3-Benzyloxymethyl-bicyclo[2.2.1]hept-2-yl)-methanol, 3.15

A 100 mL RBF equipped with a stir bar was charged with 3.14 (1.0 g, 4.1 mmol) and toluene (20 mL). After addition of DIBAL-H (10.9 mL, 1 *M* in tol, 10.9 mmol) over a 5 min period, the reaction was stirred for 5 h and then quenched with a saturated solution of Rochelle's salt (100 mL). The solution was acidified to pH=1 with conc. HCl, and extracted with ether (3x75 mL). The organic layers were combined, rinsed with brine, dried with $MgSO_4$, and concentrated *in vacuo*. The crude mixture was subjected to flash column chromatography (9:1 Hex:EtOAc then 100% DCM) to yield 3.15 as a

clear liquid (917.5 mg, 91 %). ^{1}H NMR ($CDCl_3$) δ ppm: 7.32 (m, 5H), 4.52 (q, *J* = 11.4 Hz, 2H), 3.78 (m, 2H), 3.51 (br s, 1H), 3.48 (m, 2H), 2.27 (m, 2H), 2.10, (m, 2H), 1.27 (m, 6H); ^{13}C NMR ($CDCl_3$) δ ppm: 137.22, 128.38, 128.08, 126.68, 73.27, 69.82, 61.12, 43.46, 40.49, 39.78, 22.75, 22.28; IR (NaCl):3390, 3030, 2954, 1496, 1071, 698; HRMS (CI) M+1 calc = 247.1698, found = 247.1703.

bis-endo-3-Benzyloxymethyl-bicyclo[2.2.1]heptane-2-carbaldehyde, 3.16

A 100 mL RBF equipped with a stir bar was charged with 3.15 (500 mg, 2.0 mmol), 4 Å molecular sieves (150 mg), and DCM (20 mL). The reaction flask was placed in a 0 °C ice bath followed by addition of pyridinium chlorochromate (657 mg, 3.0 mmol). After stirring the solution overnight, the crude reaction mixture was filtered through a celite, charcoal, and silica plug with DCM and concentrated *in vacuo*. This oil was then dissolved in toluene (7 mL) with a catalytic amount of NaOH in a 25 mL RBF equipped with a stir bar and a condenser. After refluxing for 12 h, a drop of water was added to the reaction mixture which was then filtered through a small $MgSO_4$ plug and concentrated *in vacuo* to yield 3.16 as a clear liquid (266.6 mg, 55 %). No further purification was required. ^{1}H NMR ($CDCl_3$) δ ppm: 9.632 (s, 1H), 7.31 (m, 5H), 4.52 (s, 2H), 3.47 (d, *J* = 8.4 Hz, 2H), 2.55 (m, 2H), 2.41 (s, 1H), 1.86 (d, *J* = 5.7 Hz, 2H), 1.46 (m, 6H); ^{13}C NMR ($CDCl_3$) δ ppm: 202.48, 138.36, 128.29, 127.47, 127.43, 72.89, 71.25, 58.84, 40.82, 38.35, 38.18, 37.75, 29.28, 22.54; IR (NaCl): 3030, 2957, 1719, 1453, 1096, 698:HRMS (CI) M+1 calc = 245.1542, found = 245.1544.

3,4-Dibromo-2,5-dimethoxytetrahydrofuran, 3.15

2,5-dimethoxy-2,5-dihydrofuran (50 mL, 412 mmol) and DCM (150 mL) were added to a 1 L RBF equipped with a large stir bar and an addition funnel. This system was placed in an ice bath followed by a slow drop-wise addition of bromine (22.2 mL, 435 mmol) via the addition funnel over 20 min. After complete addition of the bromine,

the reaction was stirred for 1.5 h. A small aliquot was then taken and analyzed by GC/FID to monitor the reaction's progress. Upon complete consumption of starting material, the reaction mixture was concentrated by a rotary evaporator with a 0 °C water bath. The resulting slightly orange colored mass was then placed on the high vacuum giving 3.15 (118 g, 99%) as mixture of several isomers. No further purification was needed. ^{1}H NMR ($CDCl_3$) δ ppm: 41% [3.48 (s, 3H), 3.50 (s, 3H), 4.16 (dd, J = 9.6, 3.9 Hz, 1H), 4.26 (dd, 9.6, 3.9 Hz, 1H), 4.94 (d, J = 3.9 Hz, 1H), 5.21 (d, J = 3.9 Hz, 1H)], 7% [3.47 (s, 6H), 4.42 (dd, J = 1.9, 0.7 Hz, 2H), 5.23 (dd, 1.9, 0.7 Hz, 2H)], 52% [3.50 (s, 6H), 4.18 (dd, J = 2, 1.3 Hz, 2H), 5.29 (dd, 2, 1.3 Hz, 2H)]; ^{13}C NMR ($CDCl_3$) δ ppm: 110.38, 110.24, 109.37, 102.52, 56.55, 56.48, 56.12, 55.57, 53.07, 52.54, 51.75, 51.53; IR (NaCl): 2936, 2835, 1779, 1447, 1116, 815: HRMS (CI) M+1 calc = 286.8918, found 286.8921.

2,3-Dibromo-1,1,4,4-tetramethoxybutane, 3.16

A 3-L 3-neck RBF equipped with a large magnetic stir bar and two condensers was loaded with 3.15 (118 g, 408 mmol) and MeOH (2 L). After slow addition of concentrated H_2SO_4 (22.7 mL, 408 mmol), the reaction mixture was refluxed for 72 h. GC/MS was used to monitor the reaction, and upon complete consumption of starting material, the reaction was cooled to rt. TEA (58 mL, 416 mmol) was added and stirred for 1 h to neutralize the acid. The solution was then concentrated by a rotary evaporator at 25 °C giving a red/orange viscous liquid that was extracted with heptane (3x250 mL). The organic layers were combined and concentrated *in vacuo* giving 3.16 as a slightly yellow liquid (126 g, 92%). No further purification was needed. ^{1}H NMR ($CDCl_3$) δ ppm: 4.51 (d, *J* = 15.0 Hz, 2H), 4.26 (d, *J* = 12.0 Hz, 2H), 3.34 (s, 12H); ^{13}C NMR ($CDCl_3$) δ ppm: 104.67, 55.06, 52.96; IR (NaCl): 2937, 2835, 1781, 1444, 1115, 815: HRMS (CI) M+1 calc = 302.9231, found = 302.9229.

1,1,4,4-Tetramethoxybut-2-yne, 3.17

A 2-L 3-neck RBF equipped with a large magnetic stir bar and a condenser was loaded with 3.16 (110 g, 327 mmol), THF (600 mL), and tris[2-(2-methoxyethoxy)-ethl]amine (10.5 mL, 30 mmol). KOH pellets (73.5 g, 1.31 mol) were slowly added to the vigorously stirring solution over a 10 min period. The reaction mixture was then refluxed for 72 h. Once GC/MS confirmed all of the starting material had been consumed, the reaction was cooled to rt. After removal of the THF by rotary evaporation, H_2O (300 mL) and ether (500 mL) were added. The aqueous layer was extracted by ether two more times (2x300 mL), and then the organic layers were combined, dried with $MgSO_4$, filtered, and concentrated *in vacuo* to give a slightly yellow liquid. Vacuum distillation with a 9" Vigreux column (0.7 torr, 67-69 °C) yielded 3.17 (50.2 g, 88%) as a clear liquid; ^{1}H NMR ($CDCl_3$) δ ppm: 5.06 (s, 2H), 3.27 (2, 12H); ^{13}C NMR ($CDCl_3$) δ ppm: 92.36, 79.86, 52.03; IR (neat) 2997, 2938, 2832, 2361, 2338, 1456, 1340, 1139, 1058, 966; HRMS (CI) M+1 calc = 175.0970, found 175.0970.

4,4-Dimethoxybut-2-ynal, 3.18

A 500 mL RBF equipped with stir bar was loaded with 3.17 (25 g, 144 mmol) and DCM (75 mL) and brought to 0 °C in an ice bath. Another 250 mL RBF was loaded with 96% Formic Acid (140 g, 3.0 mol) and DCM (75 mL) and brought to 0 °C in an ice bath. After pouring the acidic solution into the solution of 3.17, the reaction vessel was placed into a pre-cooled temperature regulated water bath at 15 °C and covered with a towel and foil. This solution was slowly stirred for 30 h. GC/MS was used to monitor the reaction, but the most effective method was to collect an aliquot, concentrate it *in vacuo* at 0 °C, and then collect an ^{1}H NMR spectrum. The aldehyde and monoacetal proton of the product have chemical shifts of 9.3 and 5.3 ppm respectively while 3.17's acetal protons have chemical shifts of 5.2 ppm. Once the reaction was determined to be complete by

^{1}H-NMR, the reaction was partitioned with 0 °C H_2O (3x200 mL). The aqueous layers were combined, rinsed with 0 °C DCM (3x200 mL), and then added to the original organic layer. The combined organic layers were then rinsed with 0 °C H_2O (2x150 mL), dried with a 10:1 mixture of $MgSO_4$/$NaHCO_3$, filtered, and concentrated *in vacuo*. This procedure yielded 3.18 as an orange/brown liquid (12.9 g, 70%). Attempts at purification of 3.18 by column chromatography or vacuum distillation were not successful and led to decomposition; therefore, this product was carried on to the next step without further purification. Compound 3.18 must be stored in fridge. ^{1}H NMR ($CDCl_3$) δ ppm: 9.22 (s, 1H), 5.27 (s, 1H), 3.36 (s, 6H); ^{13}C NMR ($CDCl_3$) δ ppm: 175.97, 92.534, 88.09, 82.82, 52.87; IR (NaCl): 2984, 2368, 1723. HRMS (CI and ESI): failed several attempts.

Bicyclo[2.2.1]hepta-2,5-diene-2,3-dicarbaldehyde, 3.19

A 250 mL RBF equipped with a large stir bar was charged with 3.18 (5.0 g, 39 mmol) and 100 mL H_2O. After adding freshly distilled cyclopentadiene (5.2 g, 78 mmol), the reaction was vigorously stirred for 5 h. GC/MS was used to monitor the reaction, and once all of 3.18 was consumed and all of the intermediate norbornadiene monoaldehyde monoacetal was hydrolyzed, the reaction was rinsed with ether (3x200 mL). The combined organic layers were dried with $MgSO_4$, filtered, and concentrated *in vacuo*. Although 3.19 can be purified by vacuum distillation (0.2 torr, 57-60 °C), the yield was less than 30% due to decomposition, so product was recovered by column chromatography (9:1 Hex:EtOAc) as a yellow oil (4.9 g, 85%). ^{1}H NMR ($CDCl_3$) δ ppm: 10.41 (s, 2H), 6.76 (s, 2H), 4.06 (s, 2H), 2.11 (q, J = 0.03 Hz, 2 H); ^{13}C NMR ($CDCl_3$) δ ppm: 185.24, 164.92, 142.14, 72.03, 49.23; IR (NaCl) 2980, 2945, 2871, 1661, 1591, 1558, 1329, 1285, 1213, 1139, 873, 675; HRMS (CI) M+1 calc = 149.0603, found 149.0606.

Bicyclo[2.2.1]hept-2-ene-2,3-dicarbaldehyde, 3.20

A 25 mL RBF was charged with a stir bar, 3.19 (50 mg, 33.7 mmol), 5 wt% Pd/C (5 mg), and DCM (2 mL). The system was placed under 1 atm of H_2 and stirred overnight at rt. The reaction mixture was filtered through a small magnesium sulfate/cotton plug using DCM as the eluent in the morning. Solvent was then removed *in vacuo* to yield 3.20 as a yellow liquid (49 mg, 96%); ^{1}H NMR ($CDCl_3$) δ ppm: 10.405 (s, 1H), 3.505 (m, 2H), 1.898 (d, J = 9.3 Hz, 2H), 1.533 (d, J = 9 Hz, 1H), 1.321 (d, J = 9 Hz, 1H), 1.131 (m, 2H); ^{13}C NMR ($CDCl_3$) δ ppm: 186.250, 156.325, 46.536, 41.795, 24.819; IR (NaCl): 2983, 2872, 1662, 1587, 1329, 1289, 1208, 678; HRMS (CI) M+1 calc = 151.0759, found 151.0755.

3-Dimethoxymethyl-bicyclo[2.2.1]hepta-2,5-diene-2-carbaldehyde, 3.21

A 50 mL RBF was charged with a stir bar, 3.18 (1.0 g, 7.8 mmol), freshly distilled CPD (1.0 g, 15.7 mmol), and DCM (12 mL). The reaction was stirred at rt overnight, and then reduced *in vacuo* to yield 3.21 as a pale yellow oil (1.4 g, 92%); ^{1}H NMR ($CDCl_3$) δ ppm: 10.063 (s, 1H), 6.729 (dd, J = 3 Hz, J = 8.4 Hz, 2H), 5.296 (s, 1H), 3.996 (s, 1H), 3.697 (s, 1H), 3.250 (s, 6H), 1.983 (s, 2H); ^{13}C NMR ($CDCl_3$) δ ppm: 187.590, 169.761, 152.807, 142.866, 141.402, 100.465, 71.043, 53.069, 52.850, 52.814, 48.138; IR (NaCl): 2981, 2864, 1668, 1329, 1272, 1213, 703; HMRS (CI) M+1 calc =195.1021, found 195.1022.

syn-Indan-1,2-diol, 3.22

A 250 mL RBF was charged with 4-methylmorpholine *N*-oxide (3.5 g, 29.9 mmol), H_2O (50 mL), THF (6 mL), and a stir bar. After addition of 1*H*-Indene (3.0 mL, 25.8 mmol), OsO_4 was added (1.0 mL, 1.3 mmol, 2.5 wt% in 2-methyl 2-propanol) to the reaction flask. After stirring for 72 h at rt, the THF was removed under reduced pressure. Brine (100 mL) was added to the remaining brown mixture, and it was then extracted

with EtOAc (3x150 mL). The organic layers were combined, dried over $MgSO_4$, and concentrated *in vacuo*. Diol 3.22 was recovered by sublimation (0.25 torr, 90 °C) as a white solid (3.2 g, 83%); ^{1}H NMR ($CDCl_3$) δ ppm: 7.346 (dd, *J*=5.1 Hz, 1.8 Hz, 1H), 7.196 (m, 3H), 4.909 (d, *J*=3.9 Hz, 2H), 4.403 (m, 1H), 3.036 (dd, *J*= 12 Hz, 3.9 Hz, 1H), 2.865 (dd, *J*= 12.3 Hz, 2.4 Hz, 1H) 2.629 (s, 2H); ^{13}C NMR ($CDCl_3$) δ ppm: 141.920, 140.117, 128.821, 127.179, 125.361, 125.041, 75.938, 73.441, 38.606; Mp = 99-100 °C, Lit.= 94-96 °C [83]; IR (KBr); 3298, 1103, 1062; HRMS (CI) 151.0759 calc, 151.0762 found.

syn-Octahydro-4,7-methano-indene-1,2-diol, 3.23

A 250 mL RBF was charged with 4-methylmorpholine *N*-oxide (3.0 g, 25.6 mmol), H_2O (50 mL), THF (6 mL), and a stir bar. After addition of 3α,4,5,6,7,7α-Hexahydro-1*H*-4,7-methano-indene (3.0 g, 22.4 mmol), OsO_4 was added (1.0 mL, 1.3 mmol, 2.5 wt% in 2-methyl 2-propanol) to the reaction flask. After stirring for 72 h at rt, the THF was removed under reduced pressure. Brine (100 mL) was added to the remaining brown mixture, and then extracted with EtOAc (3x150 mL). The organic layers were combined, dried over $MgSO_4$, and concentrated *in vacuo*. Octahydro-4,7-methano-indene-1,2-diol was recovered by sublimation (0.25 torr, 110 °C) as a white solid (1.8 g, 61%); ^{1}H NMR ($CDCl_3$) δ ppm: 4.206 (q, *J* = 3.6 Hz, 1H), 3.904 (m, 1H), 2.536 (m, 1H), 2.514 (br s, 2H), 2.306 (d, *J* = 4.8 Hz, 2H), 2.126 (s, 1H), 1.793 (dt, *J* = 8.7 Hz, 1.5 Hz, 1H), 1.629 (m, 1H), 1.475 (d, *J* = 6.9 Hz, 1H), 1.362 (m, 4H), 1.260 (d, *J* = 8.1 Hz, 1H); ^{13}C NMR ($CDCl_3$) δ ppm: 76.633. 74.006, 51.727, 42.249, 41.630, 40.836, 39.156, 32.068, 24.216, 22.781; Mp 98-103 °C; IR (KBr); 3358, 2951, 2877, 1457, 1097, 1027; HRMS (CI) 167.1072 calc, 167.1076 found.

But-2-ene-1,4-diol dibenzyl ether, 3.24

A 250 mL RBF was charged with NaH (1.3 g, 53.4 mmol) and a stir bar followed addition of THF (75 mL). After cooling the suspension to 0 °C, but-2-ene-1,4-diol (2 mL, 24.3 mmol) was slowly added. This solution was stirred for 1 h followed by addition of benzyl bromide (6.4 mL, 53.4 mmol). After stirring overnight, the solution was quenched with NH_4Cl (aq) and extracted with ether (3x200 mL). The organic layers were combined, dried over $MgSO_4$, and concentrated *in vacuo*. Flash chromatography (Hex to 8:2 Hex:EtOAc) yielded 3.24 as a colorless liquid (6.3 g, 97%); ^{1}H NMR ($CDCl_3$) δ ppm: 7.278 (m, 10H), 5.777 (t, J = 9.0 Hz, 2H), 4.461 (s, 4H), 4.039 (d, J = 3.3 Hz, 4H); ^{13}C NMR ($CDCl_3$) δ ppm: 137.994, 129.356, 128.248, 127.622, 127.561, 127.508, 72.066, 65.597; IR (NaCl) cm^{-1}: 3063, 3028, 2855, 1072, 1028; HRMS (CI): 269.1542 calc, 269.1545 found.

Benzyloxy-acetaldehyde, 3.25

A 500 mL RBF was charged with 3.24 (10.0 g, 37.3 mmol), DCM (150 mL), and MeOH (50 mL). After bringing the solution to -78 °C, ozone was vigorously bubbled through the solution until it turned a pale blue (approximately 3 h). After adding a stir bar, triphenylphosphine (29.4 g, 111.9 mmol) was slowly added to the solution while nitrogen was bubbled through it. Upon complete addition of triphenylphosphine, the solution was warmed to rt and stirred overnight. Solvent was removed *in vacuo*, and benzyloxy-acetaldehyde was recovered by distillation (0.50 torr, 67-72 °C) in good yield (7.6 g, 65%); ^{1}H NMR ($CDCl_3$) δ ppm: 9.702 (s, 1H), 7.354 (m, 5H); 4.616 (s, 2H), 4.805 (s, 2H); ^{13}C NMR ($CDCl_3$) δ ppm: 200.325, 136.749, 128.500, 128.111, 127.943, 75.175, 73.525; IR (NaCl) cm^{-1}: 2864, 1735, 1273, 1119, 1029, 699; HRMS (CI): 151.0759 calc, 151.0759 found.

Methanesulfonic acid 2-ethoxy-ethyl ester, 3.26

A 1 L RBF was charged with DCM (450 mL), TEA (28.8 mL, 206.6 mmol), N,N-dimethylamino pyridine (10 mg, 0.1 mmol), 2-ethoxy-ethanol (20.0 mL, 206.6 mmol), and a stir bar. After cooling this solution to 0 °C with an ice bath, methanesulfonylchloride (16.8 mL, 217.0 mmol) was slowly added over 30 min. The solution was warmed to rt, stirred for 5 h, and quenched with $NaHCO_3$ (aq) (300 mL). The aqueous layer was extracted with DCM (2x200 mL), and the organic layers were combined, dried over $MgSO_4$, and concentrated *in vacuo*. 3.26 was recovered by distillation (110-112 °C, 5.0 torr) in excellent yield (32.0 g, 92.1 %) as a colorless liquid; ^{1}H NMR ($CDCl_3$) δ ppm: 4.296 (m, 2H), 3.269 (m, 2H), 3.484 (qd, *J* = 7.5, 1.2 Hz, 2H), 3.000 (s, 3H), 1.145 (td, *J* = 6.9, 1.2 Hz, 3H); ^{13}C NMR ($CDCl_3$) δ ppm: 69.287, 67.955, 66.476, 37.352, 14.797; IR (NaCl) cm^{-1}; 3026, 2977, 1456, 1351, 1017; HMRS (CI) M+1 calc =169.0535, found = 169.0537.

1,4-Bis-(2-ethoxy-ethoxy)-but-2-ene, 3.27

A 500 mL RBF was charged with NaH (3.6 g, 89.1 mmol, 60% dispersion in mineral oil) and a stir bar followed addition of THF (180 mL). After cooling the suspension to 0 °C, but-2-ene-1,4-diol (3.3 mL, 40.5 mmol) was slowly added. This solution was stirred for 1 h followed by addition of 3.26 (15.0 g, 89.1 mmol). Upon addition of a condenser, the solution was heated to 75 °C for 4 d. The reaction was cooled, and the solvent removed *in vacuo*. Ether was added to the solid reaction mixture, and the salts were removed by filtration. After removal of ether *in vacuo*, 3.27 was isolated by vacuum distillation (88-90 °C, 0.27 torr) in moderate yield (4.7 g, 45%) as a colorless liquid; ^{1}H NMR ($CDCl_3$) δ ppm: 5.605 (m, 2H), 3.989 (m, 4H), 3.453 (m, 8H), 3.397 (qd, *J* = 6.9, 3.6 Hz, 4H), 1.090 (td, *J* = 7.2, 2.1 Hz, 6H); ^{13}C NMR ($CDCl_3$) δ ppm:129.058, 69.528, 69.193, 66.505, 66.272, 14.797; IR (NaCl) cm^{-1}: 2974, 2865, 1008; HRMS (CI): calc = 233.1753, found = 233.1755.

(2-Ethoxy-ethoxy)-acetaldehyde, 3.28

A 500 mL RBF was charged with 3.27 (15.0 g, 64.6 mmol), DCM (180 mL), and MeOH (60 mL). After bringing the solution to -78 °C, ozone was vigorously bubbled through the solution until it turned a pale blue (approximately 3 h). After adding a stir bar, triphenylphosphine (33.9 g, 129.1 mmol) was slowly added to the solution while nitrogen was bubbled through it. Upon complete addition of triphenylphosphine, the solution was warmed to rt and stirred overnight. Solvent was removed *in vacuo*, and (2-Ethoxy-ethoxy)-acetaldehyde was recovered by distillation (1.0 torr, 33-35 °C) in moderate yield (9.8 g, 57%); ^{1}H NMR ($CDCl_3$) δ ppm: 9.629 (t, *J* = 2.4 Hz, 1 H), 4.057 (d, *J* = 2.4 Hz, 2 H); (s, 2H), 3.624 (m, 2H); 3.532 (m, 2H); 3.428 (dq, *J* = 5.4 Hz, 2.7 Hz, 2 H); 1.109 (dt, *J* = 5.1 Hz, 3.0 Hz, 3H); ^{13}C NMR ($CDCl_3$) δ ppm: 200.722, 76.557, 71.027, 69.653, 66.430, 14.837; IR (NaCl) cm^{-1}: 2976, 2870, 1736, 1118; HRMS (CI): 133.0865 calc, 133.0866 found.

Poly((2-Ethoxy-ethoxy)-acetaldehyde), poly(3.28)

A 10 mL RBF equipped with a stir bar was charged with 3.28 (1.0 g, 7.6 mmol) and THF (8 mL). After cooling reaction flask to -78 °C in an isopropyl alcohol/dry ice bath, vinyl magnesium bromide (0.22 mL, 1 *M* THF, 0.22 mmol) was added dropwise. The reaction was stirred for 8 h followed by addition of freshly distilled acetic anhydride (0.14 mL, 1.5 mmol). The reaction mixture was slowly warmed to rt over 2 h, and poly(3.28) was isolated *in vacuo*. The resulting rubbery material isolated in poor yield (210 mgs, 21%) was confirmed to be polymeric by ^{1}H-NMR in $CDCl_3$ and GPC in THF.

3.15.4 Dissolution Inhibition

Samples of PPHA and NBA-PPHA were dissolved with novolac in PGMEA. The weight percentage of PPHA to novolac was varied (6, 8, 10, 12, and 14 wt%) but the final solution was kept constant at 7 wt%. These solutions were then spin coated on wafers at

3000 rpm for 30 sec with a 60 sec post application bake at 90 °C. Part of the wafer was then developed in standard 2.38 wt% tetramethylammonium hydroxide for a given period of time (70 sec or 120 sec). The developed part of the wafer was rinsed with water and dried. The initial and developed film thicknesses were then measured by profilometry.

3.15.5 Exposures

A wafer was spin coated for 30 seconds at 3000 rpm with a 60 sec 90 °C post application bake with a 7 wt% solution of novolac:NBA-PPHA:PAG (80:20:5 wt %). The PAG used was trifluorosulfonium nonafluorobutylsulfonate. This wafer was then exposed with a KrF excimer laser until a dose of 160 mJ/cm^2 was achieved. The wafer was then immersed in standard developer for 70 seconds, rinsed with H_2O, and dried. This procedure was repeated with a 7 wt% of novolac:NBA-PPHA (80:20) with a dose of 1800 mJ/cm^2.

3.16 REFERENCES

1. Schmid, G. M., Dissertation, *Understanding molecular scale effects during photoresist processing*, The University of Texas at Austin, **2003**.

2. Stewart, M. D., Dissertation, *Catalyst diffusion in positive-tone chemically amplified photoresists*, The University of Texas at Austin, **2003**.

3. Meiring, J. E., Dissertation, *Mesoscale simulation of the photoresist process and hydrogel biosensor array platform indexed by shape*, The University of Texas at Austin, **2005**.

4. Leunissen, L. H. A.; Lawrence, W. G.; Ercken, M. *Microelectron. Eng.* **2004**, *73-74*, 265-270.

5. Orji, N. G.; Vorburger, T. V.; Fu, J.; Dixson, R. G.; Nguyen, C. V.; Raja, J. *Meas. Sci. Technol.* **2005**, *16*, 2147-2154.

6. http://www.itrs.net/reports.html. **2007.**

7. Willson, C. G.; Ito, H.; Frechet, J. M. J.; Tessier, T. G.; Houlihan, F. M. *Journal of the Electrochemical Society* **1986**, *133*, 181-187.

8. Ito, H.; Willson, C. G. *Polym. Eng. Sci.* **1983**, *23*, 1012-1018.

9. Ito, H.; Ueda, M.; Schwalm, R. *J. Vac. Sci. Technol., B* **1988**, *6*, 2259-2263.

10. Ito, H.; Flores, E.; Renaldo, A. F. *J. Electrochem. Soc.* **1988**, *135*, 2328-2333.

11. Ito, H.; England, W. P.; Ueda, M. *J. Photopolym. Sci. Technol.* **1990**, *3*, 219-233.

12. Odian, G. *Principles of Polymerization*; 4th ed.; Wiley-Interscience: New York, 2004, 279-282, 444-447.

13. Stevens, M. P. *Polymer Chemistry: An Introduction*; 3rd ed.; Oxford UP: New York, 1999, 191-194.

14. Allcock, H. *Contemporary Polymer Chemistry*; Prentice Hall: Upper Saddle River, 1990, 236-240.

15. Pelliccioli Anna, P.; Wirz, J. *Photochem Photobiol Sci* **2002**, *1*, 441-458.

16. Falvey, D. E.; Sundararajan, C. *Photochem. Photobiol. Sci.* **2004**, *3*, 831-838.

17. Munk, P.; Aminabhavi, T. M. *Introduction to Macromolecular Science*; 2nd ed.; John Wiley and Sons: New York, 2001, 241-250.

18. Coleman, M. M.; Graf, J. F.; Painter, P. C. *Specific Interactions and the Miscibility of Polymer Blends*; Technomic: Landcaster, 1991, 1-45.

19. Blanc, A.; Bochet, C. G. *Org. Lett.* **2007**, *9*, 2649-2651.

20. Jiang, X.; Lavender, C. A.; Woodcock, J. W.; Zhao, B. *Macromolecules (Washington, DC, U. S.)* **2008**, *41*, 2632-2643.

21. Johnson, J. A.; Baskin, J. M.; Bertozzi, C. R.; Koberstein, J. T.; Turro, N. J. *Chem. Commun. (Cambridge, U. K.)* **2008**, 3064-3066.

22. Kevwitch, R. M.; McGrath, D. V. *Synthesis* **2002**, 1171-1176.

23. Pinnow, M. J., Dissertation, *Design and synthesis of materials for 157 nm photoresists applications*, The University of Texas at Austin, **2005**.

24. Grayson, S. M.; Long, B. K.; Kusomoto, S.; Osborn, B. P.; Callahan, R. P.; Chambers, C. R.; Willson, C. G. *J. Org. Chem.* **2006**, *71*, 341-344.

25. Hufford, D. L.; Tarbell, D. S.; Koszalka, T. R. *J. Am. Chem. Soc.* **1952**, *74*, 3014-3018.

26. Gorgues, A.; Simon, A.; Le Coq, A.; Hercouet, A.; Corre, F. *Tetrahedron* **1986**, *42*, 351-370.

27. Akue-Gedu, R.; Rigo, B. *Tetrahedron Lett.* **2004**, *45*, 1829-1832.

28. Personal Communication, Rigo, B., *Hydrolysis of acetal with formic acid*, **2006.**

29. Emmanuvel, L.; Shaikh, T. M. A.; Sudalai, A. *Org. Lett.* **2005**, *7*, 5071-5074.

30. Wuensch, B.; Zott, M. *Synthesis* **1992**, 927-928.

31. Vogl, O. *J. Polym. Sci., Part A: Polym. Chem.* **2000**, *38*, 2293-2299.

32. Vogl, O. *Makromol. Chem.* **1974**, *175*, 1281-1308.

33. Negulescu, I.; Vogl, O. *J. Polym. Sci., Polym. Chem. Ed.* **1976**, *14*, 2415-2431.

34. Negulescu, I.; Vogl, O. *J. Polym. Sci., Polym. Chem. Ed.* **1976**, *14*, 2995-3012.

35. Tanaka, A.; Hozumi, Y.; Hatada, K.; Endo, S.; Fujishige, R. *J. Polym. Sci.* **1964**, *2*, 181-186.

36. Auriemma, F.; De Rosa, C.; Corradini, P. *Adv. Polym. Sci.* **2005**, *181*, 1-74.

37. Pollex, A.; Millet, A.; Mueller, J.; Hiersemann, M.; Abraham, L. *J. Org. Chem.* **2005**, *70*, 5579-5591.

38. Moore, J. D.; Byrne, R. J.; Vedantham, P.; Flynn, D. L.; Hanson, P. R. *Org. Lett.* **2003**, *5*, 4241-4244.

39. Gagis, A.; Fusco, A.; Benedict, J. T. *J. Org. Chem.* **1972**, *37*, 3181-3182.

Chapter 4: Modeling and VT-NMR Spectroscopy of a Complex Polymer Equilibrium: Reinvestigating Ceiling Temperature

4.1 POLYACETALS

The polymerization of small molecule aldehydes via carbonyl addition to produce polyacetals was first reported in the 19th century.[56] Roughly one hundred years later in 1956, DuPont™ patented Delrin®, a polyacetal resin, with production beginning in the early 1960s and continuing to present day.[84] Despite this commercially successful and functional material, extensive work by Vogl in the 1970s concluded few functional polyaldehydes could be produced on appreciable scales since these polymerizations required stringent purification of starting materials, extremely low reaction temperatures, and specific combinations of solvent and initiator depending on the size of the aliphatic aldehyde. The resulting insoluble, semi-crystalline polymers were obtained in low yields, could not be characterized by ^{1}H-NMR or gel permeation chromatography, and showed poor material properties with particularly low thermal stability.[75-78,85]

4.2 POLY(PHTHALALDEHYDE)

As discussed in chapter 3, one exception to this trend is the material poly(phthalaldehyde) (PPHA). Commercially available PHA readily undergoes anionic polymerization at -78 °C, and end-capping at low temperatures with subsequent purification provides a fine white powder that is soluble in common organic solvents. Willson and Ito first reported in the 1980s the use of PPHA as a dissolution inhibitor of the base soluble resin Novolac. Photolithographic features were produced with a film of Novolac, PPHA, and a photoacid generator via exposure to 248 nm light. It is presumed the photogenerated acid hydrolyzes the polyacetal backbone of PPHA creating an uncapped polymer. This uncapped polymer depolymerizes or 'unzips' to monomeric

PHA, which does not function as a dissolution inhibitor of novolac (Scheme 4.1), so exposed areas dissolve in base while unexposed areas do not.[51-55]

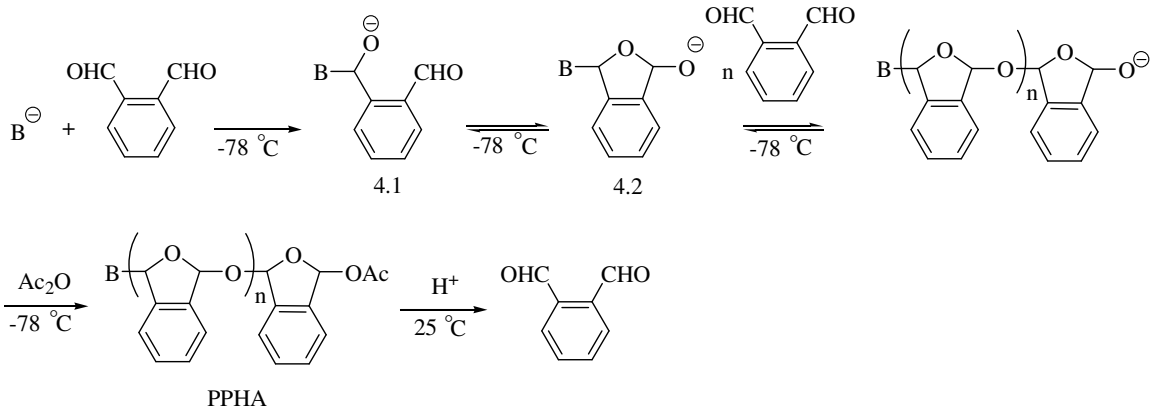

Scheme 4.1: Anionic polymerization, end-capping, and acidic 'unzipping' of PPHA.

4.3 CEILING TEMPERATURE

The fundamental polymeric principle that dictates the low reaction temperatures necessary for polymerization of aldehydes and produced the images by Willson and Ito is termed ceiling temperature (T_c). T_c is described in various ways in numerous polymer textbooks with the same overall theme. Odian[56] defines T_c as the temperature "at which the propagation and depropagation rates are equal," while Stevens[57] states the T_c is the point at which "the forward and back reactions are equal," and "ΔG of polymerization is zero." According to Allcock[58], "no polymer can exist" above the T_c. These commonly used texts show the following equations regarding T_c.

$$M_n + M \underset{k_{dp}}{\overset{k_p}{\rightleftharpoons}} M_{n+1} \qquad (4.1)$$

Eq. (4.1)is the equilibrium expression for the propagation step of an active chain (M_n) and monomer (M) with the extended active polymer chain (M_{n+1}).

$$k_p[M_n][M] = k_{dp}[M_{n+1}] \;\Rightarrow\; K_{eq} = \frac{k_p}{k_{dp}} = \frac{[M_{n+1}]}{[M_n][M]} = \frac{1}{[M]} \qquad (4.2)$$

Eq. (4.2) is the equilibrium constant as defined by the ratio of the propagation and depropagation rate constants, k_p and k_{dp}, respectively. As is customary, brackets denote molar concentrations. In Odian's textbook, the $[M_n]$ and $[M_{n+1}]$ terms are cancelled, which leaves the term $[M]^{-1}$.[56] This will be discussed later.

In the Gibbs free-energy equation (eq.(4.3)), T_c is also defined as the ratio of the remaining thermodynamic terms, ΔH and ΔS, when $\Delta G = 0$ (eq. (4.4)).

$$\Delta G = \Delta H - T\Delta S \qquad (4.3)$$

$$T_c = \frac{\Delta H}{\Delta S} \qquad (4.4)$$

To further exploit the chemical potential of T_c, several items needed to be addressed:

1) The concentration of monomer at T_c given an initial ratio of monomer to initiator.
2) The distribution of polymeric species (M_n and M_{n+1} in eq. (4.2)) in terms of their molar concentration and mass fraction at T_c.
3) The effect of temperature on these equilibrium concentrations above and below T_c.

Surprisingly little literature exists to date on this topic[86], and herein efforts are described towards developing an equilibrium model that is solved numerically via an

iterative technique as well as solving the system analytically to address these topics. The results describe the molar concentrations and mass fractions of monomer and polymeric species for a given K_{eq} and initial monomer and initiator concentrations.

To validate the solution, a variable temperature NMR (VT-NMR) experiment was conducted on a living PPHA system, and the spectra showed the equilibrium monomer concentration at various temperatures. Plots of the resulting data are consistent with the Van't Hoff equation as well as accurately described the T_c of PHA.

4.4 METHODS

4.4.1 Numerical Solution

The model has two basic chemical reactions; the initiation (eq. (4.5)) and the propagation (eq. (4.1)).

Initiation:

$$I + M \rightarrow M_1 \qquad (4.5)$$

Propagation:

$$M_n + M \underset{k_{dp}}{\overset{k_p}{\rightleftharpoons}} M_{n+1} \qquad (4.1)$$

The model assumes the reaction between an initiator (I) and monomer (M) leading to an active polymer chain end (M_1) is quantitative with no side reactions such as butyl lithium addition to an aldehyde similar to anions 4.1 or 4.2 in Scheme 4.1. Therefore, $[I]_0 = [M_1]_0$. The propagation reaction is described as a multiple equilibrium system in which all of the equilibrium constants are equal as stated by Flory's principle of equal reactivity.[87] Additionally, the model assumes there are no termination events. The model requires three inputs: the equilibrium constant of the propagation step (K_{eq}), the initial monomer concentration ($[M]_0$), and the initial concentration of active ends/initiator ($[M_1]_0$). Theoretically, the number of propagation steps is unlimited leading to an infinite

number of equilibrium reactions between monomer, active polymer containing n repeat units (M_n), and active polymer containing n+1 repeat units (M_{n+1}). However in order to facilitate a numerical solution, only a limited number of equilibria were considered after which chain growth and consumption of monomer were assumed to be negligible. Thus, another important input was the maximum degree of polymerization (DP) calculated; the maximum DP used in the calculations was 1000.

$$\frac{[M_{n+1}]+\Delta}{([M_n]-\Delta)([M]-\Delta)} = K_{eq} \quad (4.6)$$

$$K_{eq}(\Delta)^2 - \left[K_{eq}([M]+[M_n])+1\right]\Delta + [M_n][M]K_{eq} - [M_{n+1}] = 0 \quad (4.7)$$

Each equilibrium reaction was considered individually and described by an equation of the form of eq. (4.6) where Δ is the change in concentration required to reach equilibrium from the initial conditions. Eq. (4.6) was then rearranged to quadratic form, eq. (4.7). Given $[M]_0$, $[M_1]$, and K_{eq}, the first equilibrium expression was solved for Δ to find the dimer concentration ($[M_2]$). Using $[M_2]$ and the resulting $[M]$ ($[M]_0$ - Δ), the second equilibrium expression was solved to find $[M_3]$. The process was repeated iteratively from the beginning using the most recent $[M]$ and $[M_n]$ values until all the equilibria expressions were solved. Once the last equilibrium was solved, the most recent $[M]$, $[M_1]$, and $[M_2]$ were used as initial values for the first equilibrium; the above process was repeated incorporating the newest values of $[M]$ and $[M_n]$. Finally, the model compared the most recent solution matrix to the previous solution every ten iterations. If there was no concentration change of any individual species >0.001% over ten iterations the model terminated. As an additional check, a material balance was performed by multiplying the concentration of each polymer species by its DP, summing that value,

and adding the unconsumed monomer. This value was compared to the sum of the $[M]_0$ and $[I]_0$. If the two were not equal, the results were discarded; generally this occurred only when the maximum calculated DP specified was too low for the input K_{eq}.

It was also noted if the equilibrium concentration of monomer ($[M]_{eq}$) and initiator ($[M_1]_{eq}$) are known, then all equilibrium concentrations can be calculated using the following equations.

$$M_1 + M \rightleftharpoons M_2 \qquad (4.8)$$

Eq. (4.8) is the chemical reaction between M_1, M, and M_2.

$$K_{eq} = \frac{[M_2]}{[M_1][M]} \qquad (4.9)$$

Eq (4.9) is the equilibrium expression for the reaction and has been rearranged to solve for $[M_2]$ (eq. (4.10)).

$$[M_2] = K_{eq}[M_1][M] \quad (4.10)$$

$$M_2 + M \rightleftharpoons M_3 \qquad (4.11)$$

Eq. (4.11) is the chemical reaction between M_2, M, and M_3.

$$K_{eq} = \frac{[M_3]}{[M_2][M]} \qquad (4.12)$$

Eq (4.12) is the equilibrium expression for eq. (4.11) and has been rearranged to solve for [M_3] (eq. (4.13)). Noting eq. (4.10), eq. (4.13) describes [M_3] in terms of K_{eq}, [M], and [M_1].

$$[M_3] = K_{eq}[M_2][M] = K_{eq}^{2}[M_1][M]^2 \qquad (4.13)$$

Therefore any propagation equilibrium of the form shown in eq. (4.14) can be rewritten to eq. (4.15), which describes [M_n] in terms of K_{eq}, [M_1], and [M].

$$K_{eq} = \frac{[M_{n+1}]}{[M_n][M]} \qquad (4.14)$$

$$[M_{n+1}] = K_{eq}^{n}[M_1][M]^n \qquad (4.15)$$

Once the numerical model converged on a solution for [M_1] and [M] for a given set of inputs, eq. (4.15) was used to find the theoretical molar concentration distribution and mass fraction distribution by multiplying the concentration of each species by its DP and dividing by the total mass of the system.

4.4.2 Analytical Solution

An analytical solution derived by Prof. Isaac Sanchez from the Department of Chemical Engineering at the University of Texas at Austin is described in Appendix A. The numerical model and analytical solution give the same results.

4.4.3 VT-NMR

All compounds were purchased from Sigma-Aldrich and used as received. PHA (140 mg, 1.0 mmol) and a catalytic amount of potassium *tert*-butoxide (95%) were dissolved in THF-d_8 (1.0 mL) under a nitrogen cone. After all materials were dissolved,

the solution was transferred to a NMR tube, sealed with Parafilm®, and immediately analyzed with a Varian INOVA 500 MHz NMR spectrometer. ^{1}H spectra were collected with a 15 degree flip angle and a 6 sec relaxation delay. After cooling the probe to the given temperature, the sample was equilibrated for 15 min. A spectra was collected at 27, -10, -20, -30, -40, -50, -60, -70, and again at 27 °C.

4.5 RESULTS AND DISCUSSION

4.5.1 Numerical Results

Numerical results were generated for various $[I]_0$ conditions with $[M]_0$ = 1 M. A range of K_{eq} values from 0.01 to 100 was considered, and the effects of $[I]_0$ and K_{eq} on both the equilibrium monomer concentration and the resulting distribution of polymer species were examined. These results were compared to those predicted by the analytical solution fully described in Appendix A, eq. (A.13) and (A.15), and found to be consistent.

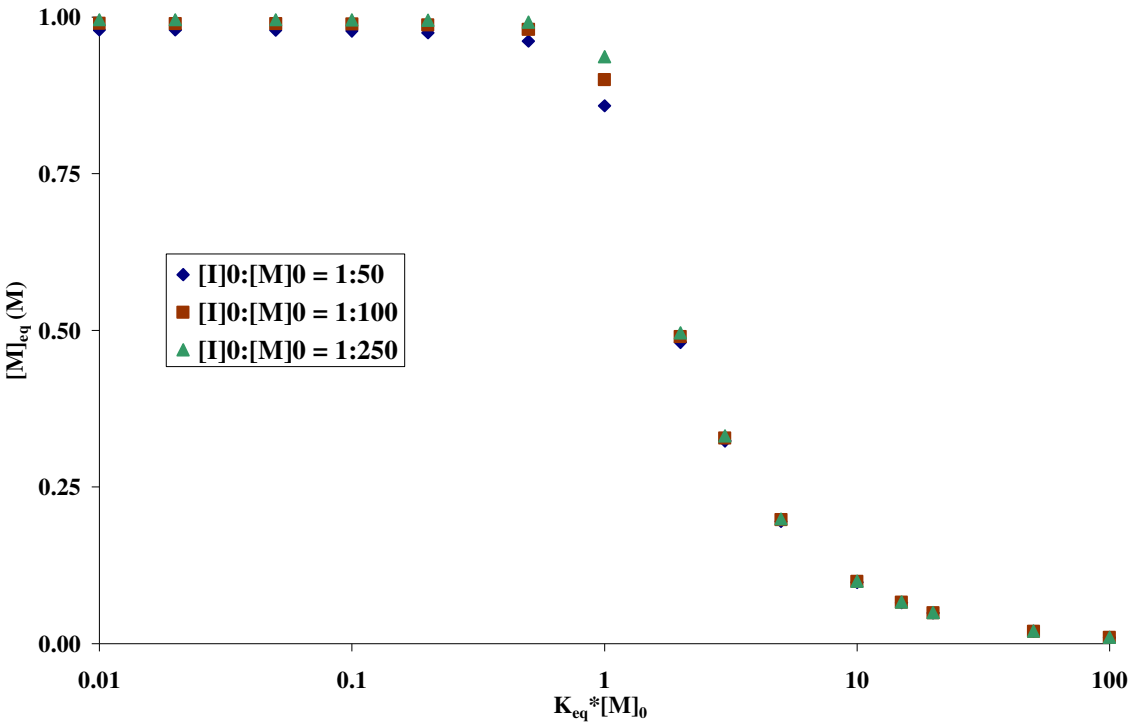

Figure 4.1: $[M]_{eq}$ vs. $K_{eq}[M]_0$ for $[M]_0$ = 1 M and $[I]_0$ = 0.02 (blue diamond), 0.01 (brown square), and 0.004 M (green triangle).

Figure 4.1 shows $[M]_{eq}$ vs. $K_{eq}[M]_0$ for three different initiator to monomer concentration ratios ($[I]_0/[M]_0$) 1:50, 1:100, and 1:250 with $[M]_0$ = 1 M. The data show three distinct regions as described by the analytical solution (eq. (A.13)). Within the first region, where $K_{eq}[M]_0$ <1, the system is predominantly monomer with no significant amount of polymeric species. The transition value, where $K_{eq}[M]_0$ =1, is when the propagation of a theoretically infinite number of equilibriums must be satisfied. The system is still predominantly monomer, but the concentration of oliogomeric species begins to rise. Once $K_{eq}[M]_0$ >1, the third region, the system favors polymer resulting in significant consumption of monomer.

The contrast of the regions is further displayed by observing if the propagation step was disfavored by 2:1, $K_{eq}[M]_0 = 0.5$ for 1:100 $[I]_0/[M]_0$, $[M]_{eq}$ was 0.98 M, however if the propagation was favored 2:1, $K_{eq}[M]_0 = 2$, then $[M]_{eq}$ was 0.49 M. This dramatic change can be rationalized by noting if $K_{eq}[M]_0 < 1$, the system is predominantly controlled by the first propagation step; the equilibrium between M_1, M, and M_2. However once propagation becomes even slightly favorable, $K_{eq}[M]_0 > 1$, a theoretically infinite number of equilibria must be satisfied between M_n, M_{n+1}, and M, and each one of these reactions decreases the monomer pool. Also worth noting was that even when $K_{eq}[M]_0 = 20$, $[M]_{eq}$ was still approximately 0.05 M, 5% of $[M]_0$. The surprisingly high amount of monomer remaining even for high $K_{eq}[M]_0$ values can be rationalized by realizing each propagation step requires a small amount of monomer to satisfy the equilibrium and no propagation step can proceed to complete conversion.

Figure 4.1 also shows the low sensitivity of a living polymer system to $[I]_0/[M]_0$. For instance when $K_{eq}[M]_0 = 0.1$, $[M]_{eq}$ for 1:50, 1:100, and 1:250 $[I]_0/[M]_0$ were 0.98, 0.99, and 1.00 M, respectively; this range of 0.02 M was only a 1.8% variation. Likewise with large $K_{eq}[M]_0$ values, $[M]_{eq}$ for the three $[I]_0/[M]_0$ ratios only varied by less than 2.5%. The only $K_{eq}[M]_0$ values that showed significant variation of $[M]_{eq}$ were near $K_{eq}[M]_0 = 1$; $[M]_{eq}$ at $K_{eq}[M]_0 = 1$ for $[I]_0/[M]_0$ 1:50, 1:100, and 1:250 were 0.86, 0.90, and 0.94 M, respectively, which was a 8.4% variation.

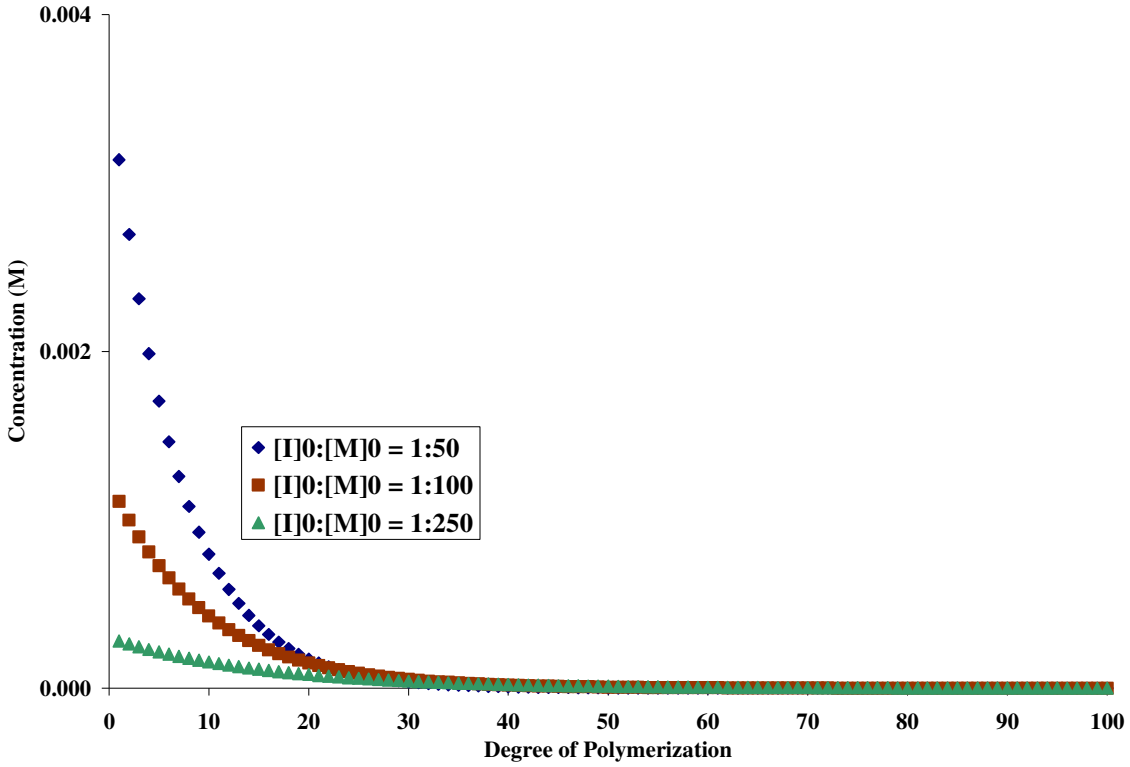

Figure 4.2: $[M_n]$ vs. n for $K_{eq}[M]_0 = 1$, $[M]_0 = 1$ M, $[I]_0 = 0.02$ (blue diamond), 0.01 (brown square), and 0.004 M (green triangle).

Figure 4.2 shows $[M_n]$ vs. n for a system at the transitional value of $K_{eq}[M]_0 = 1$ for the three starting conditions. The concentration of each individual species was very small given $[M]_0$. For instance, $[M_{10}]$ in each of the scenarios was 0.97, 0.48, and 0.16 mM, respectively, while monomer composed 86%, 90%, and 94% respectively of the total mass in each system as described by eq. (A.13). The mass fraction of each polymer species with respect to the total polymer mass for several different initial $[I]_0/[M]_0$ ratios is shown in Figure 4.3.

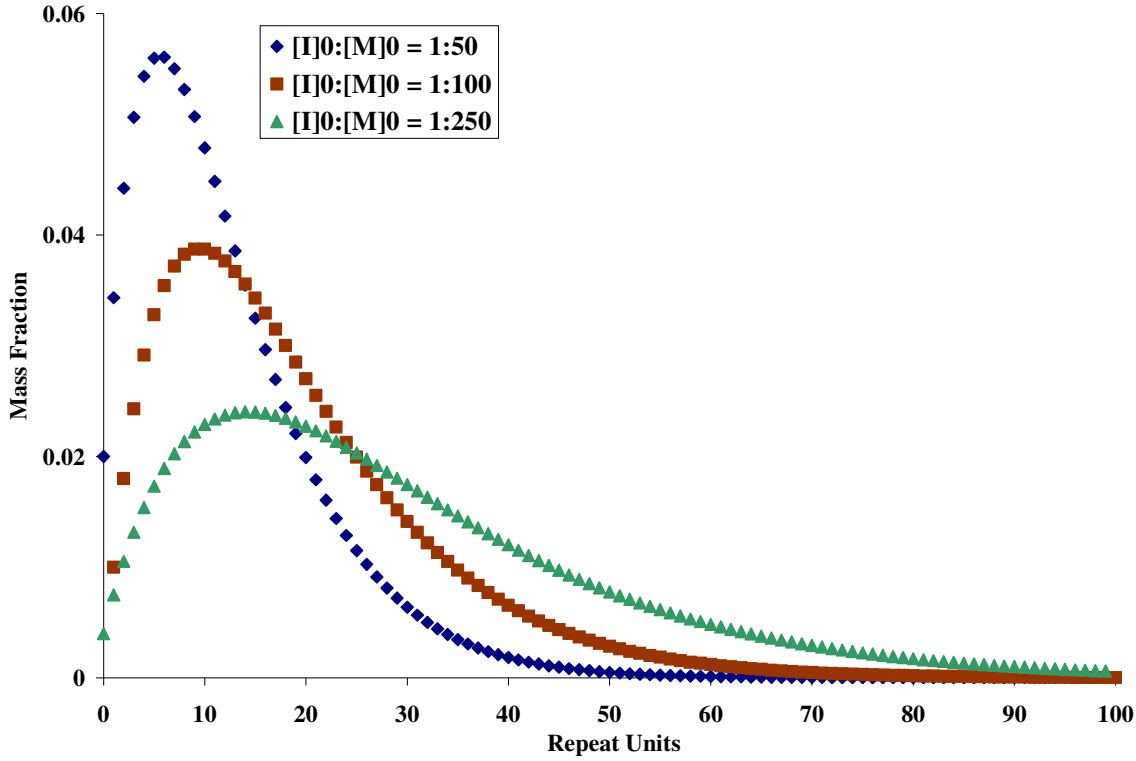

Figure 4.3: Mass fraction of M_n vs. n for $K_{eq}[M]_0 = 1$, $[M]_0 = 1$ M, $[I]_0 =$ 0.02 (blue diamond), 0.01 (brown square), and 0.004 M (green triangle).

After analyzing Figure 4.1 and noting Odian's derivation (eq. (4.2)), the reciprocal of $[M]_{eq}$ vs. $K_{eq}[M]_0$ was plotted (Figure 4.4). The three distinct regions were very evident here; the first region where $K_{eq}[M]_0 <1$ had a slope ≈ 0 as described by eq. (A.13). Likewise $[M]_{eq}^{-1}$ values were a perfect linear fit ($R^2 = 1$) for $K_{eq}[M]_0 >2$, however there were significant deviations from this function when $K_{eq}[M]_0 \approx 1$. Given the solutions' data, it is our conclusion the most accurate descriptor of these types of systems is the term $K_{eq}[M]_0$ and $K_{eq}[M]$ and not just K_{eq}. The cancellation of the terms $[M_n]$ and $[M_{n+1}]$ found in the common derivation for T_c (eq. (4.2)) is only valid for $K_{eq}[M]_0 >2$. There the difference between $[M_2]$ and $[M_3]$ and any $[M_n]$ and $[M_{n+1}]$ is negligible, and

therefore the cancellation of these terms is valid; however, when approaching and above T_c this assumption is no longer valid.

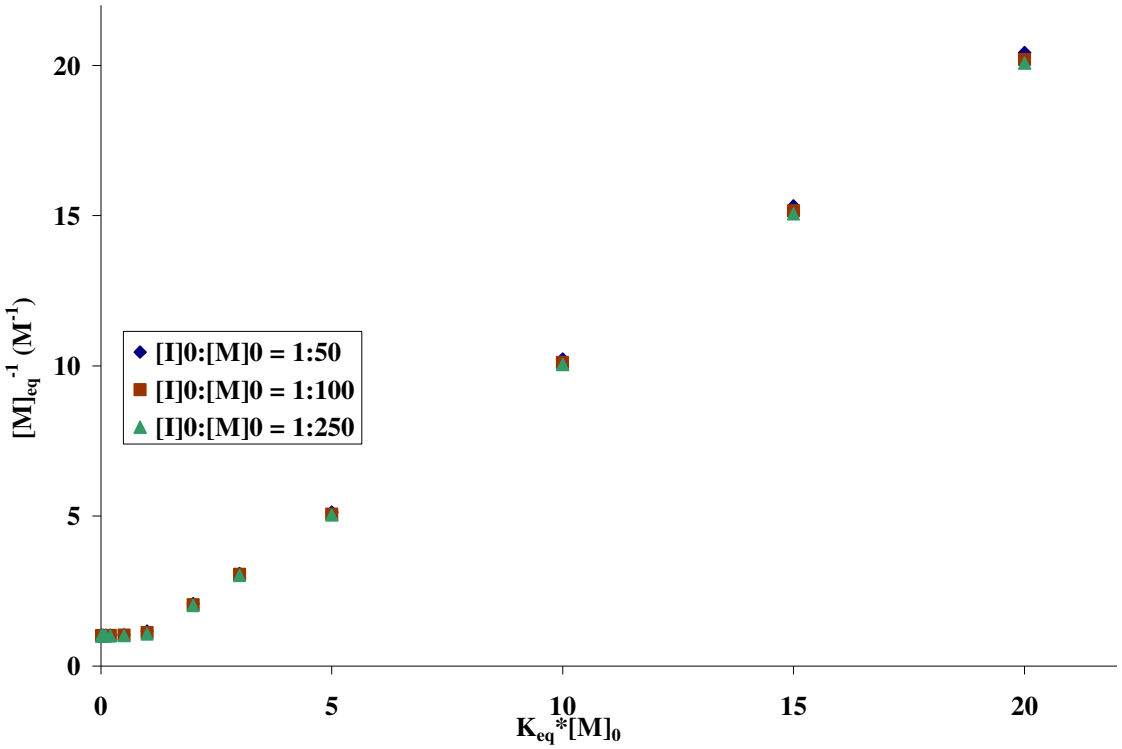

Figure 4.4: $[M]_{eq}^{-1}$ vs. $K_{eq}[M]_0 = 1$, $[M]_0 = 1$ M, $[I]_0 = 0.02$ (blue diamond), 0.01 (brown square), and 0.004 M (green triangle).

Finally, the molar concentration and mass fraction distributions of the initial 1:100 $[I]_0/[M]_0$ conditions at various $K_{eq}[M]_0$ values were investigated (Figure 4.5 and Figure 4.6). As $K_{eq}[M]_0$ increased, the molar distribution shifted towards larger DP, although in all cases the species with the highest molar concentration was M_2. When examining the mass fraction distribution of $[M_n]$ where n >1, the species with the highest mass fraction was M_{10}, $M_{50,}$ and M_{96} for $K_{eq}[M]_0$ = 1, 2, and 20; this is accurately described by the analytical solution (eq. (A.27)). For a $[I]_0/[M]_0$ ratio of 1:100, the DP of the most abundant species (by mass) approached 100 as $K_{eq}[M]_0$ increased. The

polydispersity index for each of these systems was >1.9 as calculated by the distribution of the numerical solution and described by the analytical solution (eq. (A.30)).

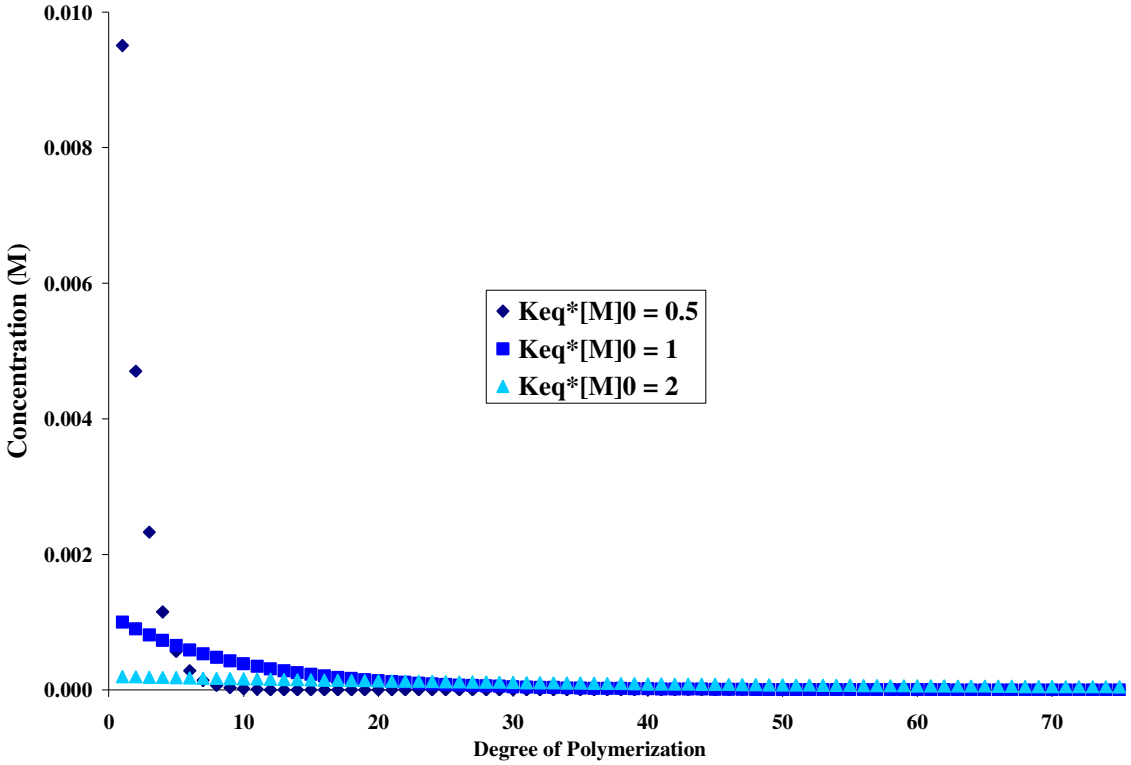

Figure 4.5: $[M_n]$ vs. n for $K_{eq}[M]_0 = 0.5$ (diamond), 1 (square), and 2 (triangle), $[M]_0 = 1$ M, and $[I]_0 = 0.01$ M.

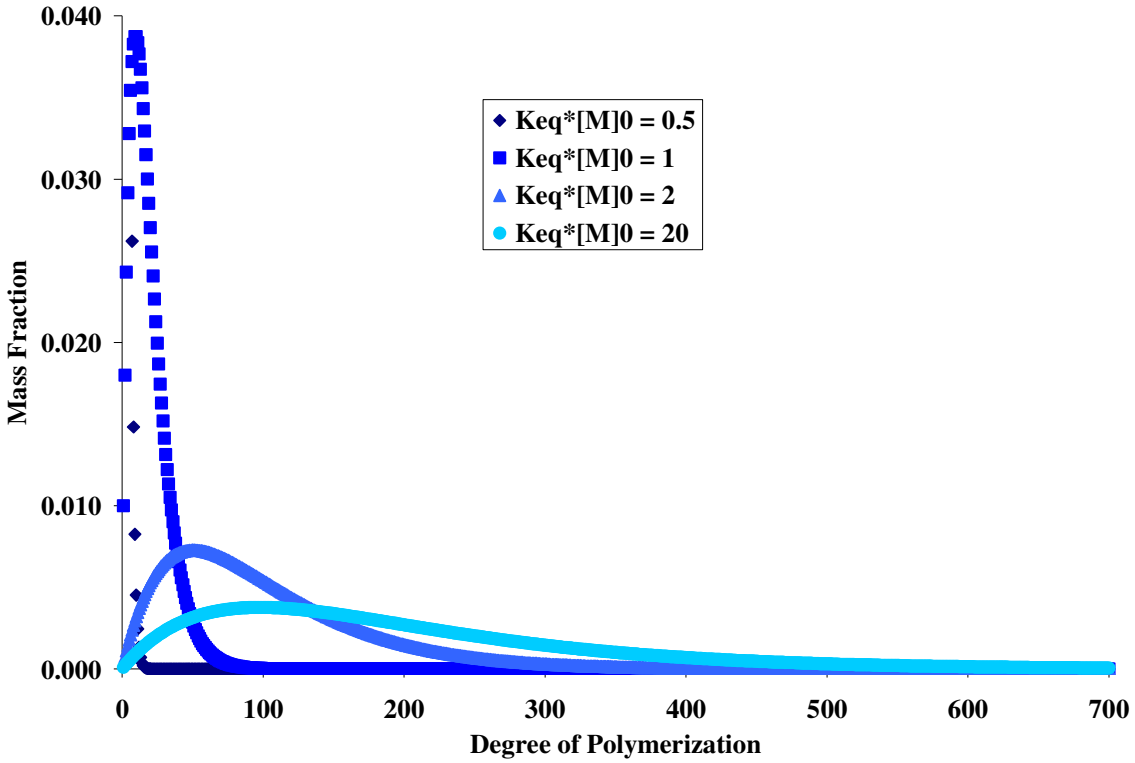

Figure 4.6: Mass fraction of M_n vs. n for $K_{eq}[M]_0 = 0.5$ (diamond), 1 (square), 2 (triangle), and 20 (circle), $[M]_0 = 1$ M, and $[I]_0 = 0.01$ M.

4.5.2 VT-NMR

Desiring to confirm the predictions made by the solutions, a VT-NMR experiment was conducted to study the response of $[M]_{eq}$ at various temperatures. Radical polymer systems were not a valid option because the model assumes no termination events. Cationic and anionic polymerization of styrene and its derivatives were also ruled out due to the high number of possible side reactions between the propagating polymer chain with the monomer and/or the solvent. Anionic polymerization of PHA was chosen as an optimal system because the T_c is known (-40 °C[52]), the propagating anion will not react with THF, and spectra could be collected above and below its T_c.

Figure 4.7 and Figure 4.8 display the VT-NMR spectra. As shown in Figure 4.7, monomer 4.4's aldehyde (orange box) and aromatic (blue box) peaks at 10.5 ppm and 8.0 and 7.8 ppm, respectively, decreased in area as the temperature decreased but returned to their initial state upon warming back to 27 °C. This confirms a living polymer system.

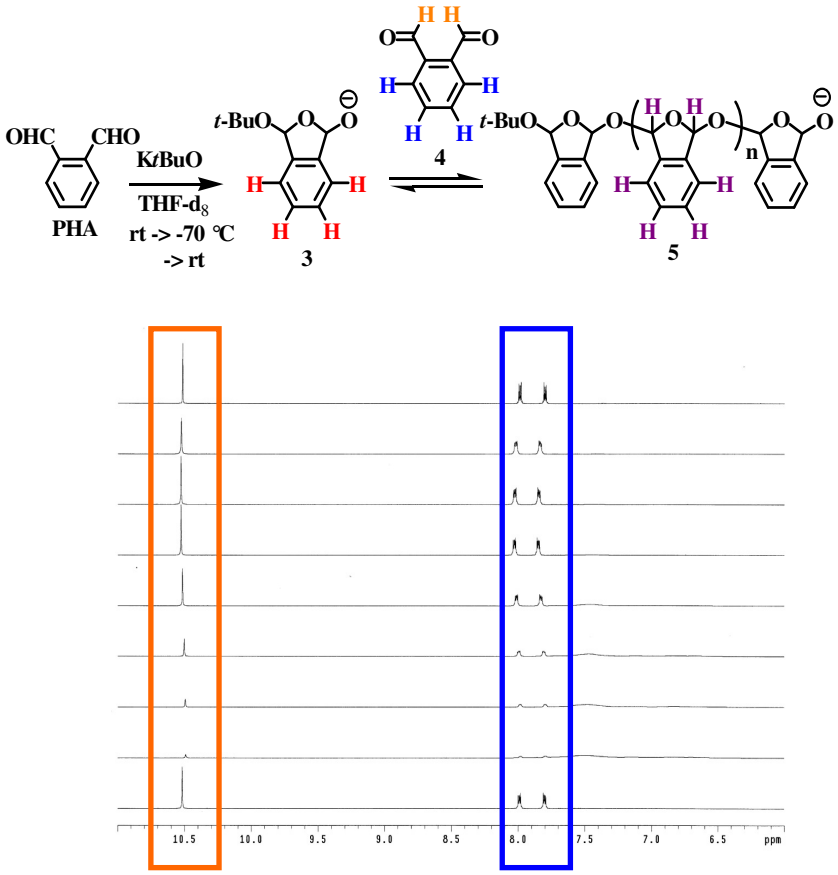

Figure 4.7: VT-NMR spectra of living PPHA system: top to bottom; 27, -10, -20, -30, -40, -50, -60, -70, and 27 °C.

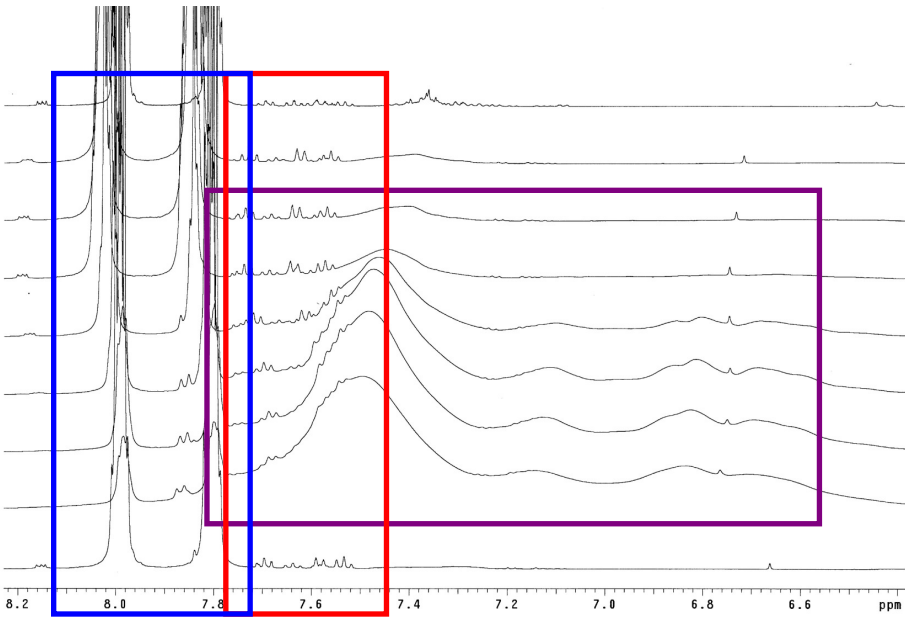

Figure 4.8: Expanded view of VT-NMR spectra in the aromatic region from top to bottom 27, -10, -20, -30, -40, -50, -60, -70, and 27 °C.

Figure 4.8 is the expanded aromatic region of the VT-NMR spectra. The red box outlines the initiator peaks (anion 4.3) and the purple box outlines the polymeric peaks (compound 4.5). As the temperature decreased, the aromatic monomer peaks (blue box) decreased in area while the broad polymer peaks increased; the polymer peaks were minimal at -10 and -20 °C but became more prominent starting at -30 °C and -40 °C. While the peaks do begin to overlap at lower temperatures, the system returned to its initial state upon warming to 27 °C.

To investigate the time required for the system to achieve equilibrium, spectra were collected immediately after the probe had been chilled (t = 0) and at 10, 20, 30, 40 and 95 min. The area of the aldehyde peak displayed minimal change (<4%) over this

time period, so it was assumed all spectra represent the system at equilibrium. For other controls, VT-NMR spectra were collected with potassium *tert*-butoxide (K*t*-BuO) in THF-d_8 and PHA in THF-d_8; no side reactions or decomposition were visible in all spectra. Spectra collected at -80 °C were disregarded due to polymer chains precipitating in the NMR tube and the large difference in relaxation times between the monomer and polymer.

To compare these spectra with our solution, the initial monomer concentration $[M]_0$ was determined from the initial mass of PHA and the volume of the solution. The $[I]_0/[M]_0$ ratio was determined by comparing the area of the *t*-butyl peak of the K*t*-BuO to the aldehyde peak; for this experiment the ratio was 1:83.2. The equilibrium concentrations of aldehyde, $[M]_{eq}$, were calculated by relating the normalized aldehyde peak area at various temperatures to the initial aldehyde peak area (Table 4.1).

Table 4.1: VT-NMR and Solution Data

T (°C)	CHO Area	$[M]_{eq}$ (M)	$[M]_{eq}^{-1}$ (M^{-1})	K_{eq} (M^{-1})	$K_{eq}[M]_0$	T^{-1} (K^{-1})	$\ln(K_{eq}[M]_0)$
27	15.03	1.04	-	-	-	0.0033	-
-10	14.58	1.01	0.99	0.58	0.60	0.0038	-0.50
-20	14.16	0.98	1.02	0.76	0.80	0.0040	-0.23
-30	13.07	0.91	1.10	0.87	0.91	0.0041	-0.10
-40	8.83	0.61	1.63	1.59	1.65	0.0043	0.50
-50	4.85	0.34	2.97	2.92	3.03	0.0045	1.11
-60	2.37	0.16	6.08	6.00	6.24	0.0047	1.83
-70	1.11	0.08	12.97	12.84	13.35	0.0049	2.59

When $K_{eq}[M]_0 > 1$, $[M]_{eq}$ values were calculated from the VT-NMR data using a linear regression of $[M]_{eq}^{-1}$ vs. $K_{eq}[M]_0$ as determined by the numerical solution (similar to Figure 4.4). When $K_{eq}[M]_0 < 1$, the analytical solution was used to determine $[M]_{eq}$ (eq.

(A.13)); the area of the aldehyde peak for the 27 °C spectrum was used for $[M]_0$, therefore a K_{eq} value could not be calculated. The $K_{eq}[M]_0$ data were plotted and fit the expected linear Van't Hoff equation (eq. (16)), as shown in Figure 4.9. The plots show a clear change in slope and intersect around 0.0041 K^{-1} (-31 °C), which approximately corresponds to the reported T_c of PHA. Looking at the data points collected from 27 °C, -10 °C, and -20 °C where there was no significant polymer in the NMR spectra, there was a strong linear correlation between $\ln(K_{eq}[M]_0)$ and T^{-1} ($R^2 = 0.95$) with a y-intercept of -5.4 and slope of 1300. The data points of -30, -40, -50, -60, and -70 °C where large polymer peaks were evident in the ^{1}H-NMR spectra also had a high linear correlation ($R^2 = 1.00$) with a y-intercept of -14 and a slope of 3300. The y-intercept of these types of plots can be correlated with entropy,[88] and these data confirmed as the polymerization became favorable ($K_{eq}[M]_0 > 1$), the entropy of the propagation step became less favorable. The slope of these plots correlates to the enthalpy.[88] When below T_c and exothermic bond formation is favorable, the slope of the lines should be positive, which is indeed what was observed. When above T_c, there was minimal net bond formation. This correlates to the smaller slope of the red line in Figure 4.9. The error of each point was calculated by changing the integral area from the NMR +/- 5%[89,90] and proceeding with this number through the model calculations. As shown in Figure 4.9, the only point with a significant amount of error is the -10 °C spectrum. This is due to the small change of the integral value of the aldehyde peak on the ^{1}H-NMR spectra and the severe sensitivity of this region to changes in $K_{eq}[M]_0$ as shown in Figure 4.1, Figure 4.2, and eq. (A.13). The other data points have <0.1 error, which demonstrates the accuracy of the solutions. The chemical potential and entropy of the solvent also play roles in this equilibrium, and future work will be directed at investigating these issues.

$$\ln(K_{eq}) = -\frac{\Delta H^o}{RT} + \frac{\Delta S^o}{R} \qquad (4.16)^{88}$$

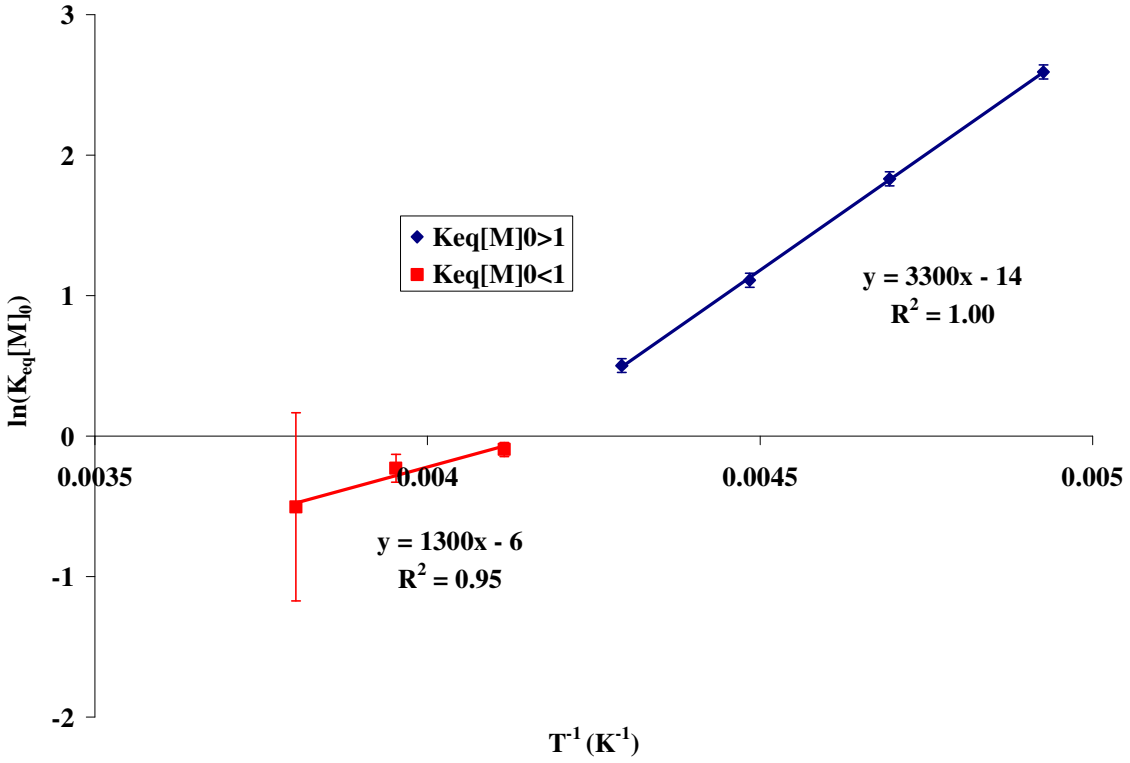

Figure 4.9: Temperature dependence of $K_{eq}[M]_0$ from VT-NMR and solution data; $K_{eq}[M]_0$ <1 (red square) and $K_{eq}[M]_0$ >1 (blue diamond).

4.6 CONCLUSION

A numerical model and an analytical model that define a complex equilibrium between monomer, polymer, and initiator were solved to investigate low ceiling temperature polymers for photolithographic applications. Both solutions calculate the molar and mass distribution of chain-growth polymer systems. Both methods show the system to be most accurately predicted by the term $K_{eq}[M]_0$ and not just K_{eq} as described by many polymer textbooks. This determination results in three distinct regions of a

chain-growth system: no appreciable polymerization ($K_{eq}[M]_0$ <1), a transition point ($K_{eq}[M]_0$ =1), and a region in which polymerization occurs ($K_{eq}[M]_0$ >1). The numerical and analytical were consistent with each other and with a VT-NMR experiment on a living PPHA system. The resulting data were consistent with the Van't Hoff equation, showed a change in slope when polymerization became energetically favorable, and exhibited a T_c consistent with phthalaldehyde's reported T_c. With the output of these models and VT-NMR, work will continue to exploit the chemical potential of T_c in lithographic applications.

4.7 ACKNOWLEDGMENTS

The authors would like to thank Steve Sorey and Dr. Ben Shoulders for their help with VT-NMR experiments as well as Willson group members, Michael Jacobsson, Dr. Saul Lee, and Dr. Elizabeth Costner, and Prof. Brent L. Iverson and Prof. Christopher W. Bielawski for their insightful discussions. We also appreciate the generous funding of the NSF (R05-0126), SRC (SA4840-78134), and the Applied Materials Graduate Fellowship.

4.8 REFERENCES

1. Odian, G. *Principles of Polymerization*; 4th ed.; Wiley-Interscience: New York, 2004, 279-282, 444-447.

2. http://www2.dupont.com/Plastics/en_US/Products/Delrin/Delrin.html. **2009**.

3. Vogl, O. *J. Polym. Sci., Part A: Polym. Chem.* **2004**, *42*, 795-818.

4. Vogl, O. *J. Polym. Sci., Part A: Polym. Chem.* **2000**, *38*, 2293-2299.

5. Vogl, O. *Makromol. Chem.* **1974**, *175*, 1281-1308.

6. Negulescu, I.; Vogl, O. *J. Polym. Sci., Polym. Chem. Ed.* **1976**, *14*, 2995-3012.

7. Negulescu, I.; Vogl, O. *J. Polym. Sci., Polym. Chem. Ed.* **1976**, *14*, 2415-2431.

8. Willson, C. G.; Ito, H.; Frechet, J. M. J.; Tessier, T. G.; Houlihan, F. M. *Journal of the Electrochemical Society* **1986**, *133*, 181-187.

9. Ito, H.; Willson, C. G. *Polym. Eng. Sci.* **1983**, *23*, 1012-1018.

10. Ito, H.; Ueda, M.; Schwalm, R. *J. Vac. Sci. Technol., B* **1988**, *6*, 2259-2263.

11. Ito, H.; Flores, E.; Renaldo, A. F. *J. Electrochem. Soc.* **1988**, *135*, 2328-2333.

12. Ito, H.; England, W. P.; Ueda, M. *J. Photopolym. Sci. Technol.* **1990**, *3*, 219-233.

13. Stevens, M. P. *Polymer Chemistry: An Introduction*; 3rd ed.; Oxford UP: New York, 1999, 191-194.

14. Allcock, H. *Contemporary Polymer Chemistry*; Prentice Hall: Upper Saddle River, 1990, 236-240.

15. Szwarc, M. *Carbanions Living Polymers and Electron Transfer Processes*; Interscience: New York, 1968, 104-150.

16. Flory, P. J. *Principles of Polymer Chemistry*; Cornell UP: New York, 1953, 102-105.

17. Anslyn, E. V. *Modern Physical Organic Chemistry*; University Science: Sausalito, 2004, 68-70.

18. Leyden, D. E., Cox, R. H *Analytical applications of NMR*; Wiley: New York, 1977, 260.

19. Gunther, H. *NMR spectroscopy : basic principles, concepts, and applications in chemistry*; 2nd ed.; Wiley: Chichester, NY, 1995.

Chapter 5: Block Copolymers for Nano-Imprint Lithography Templates

5.1 HARD DISK DRIVES

The semiconductor industry is not alone in its need for smaller and smaller features. While Moore's Law has driven IC features from the micron range to full-scale 32 nm production[1], the hard disk drive industry has also seen a necessity to decrease bit size. Figure 5.1 shows the areal density in Gbits/in^2 versus the product shipment year for Hitachi Global Storage Technologies.[2] Although not up to date, Figure 5.1 shows the linear increase on the logarithmic y-axis of areal density; a density of 1 Gbit/in^2 corresponds to 645,000 nm^2/bit while 1000 Gbits/in^2 means that on average a bit must be stored in 645 nm^2.

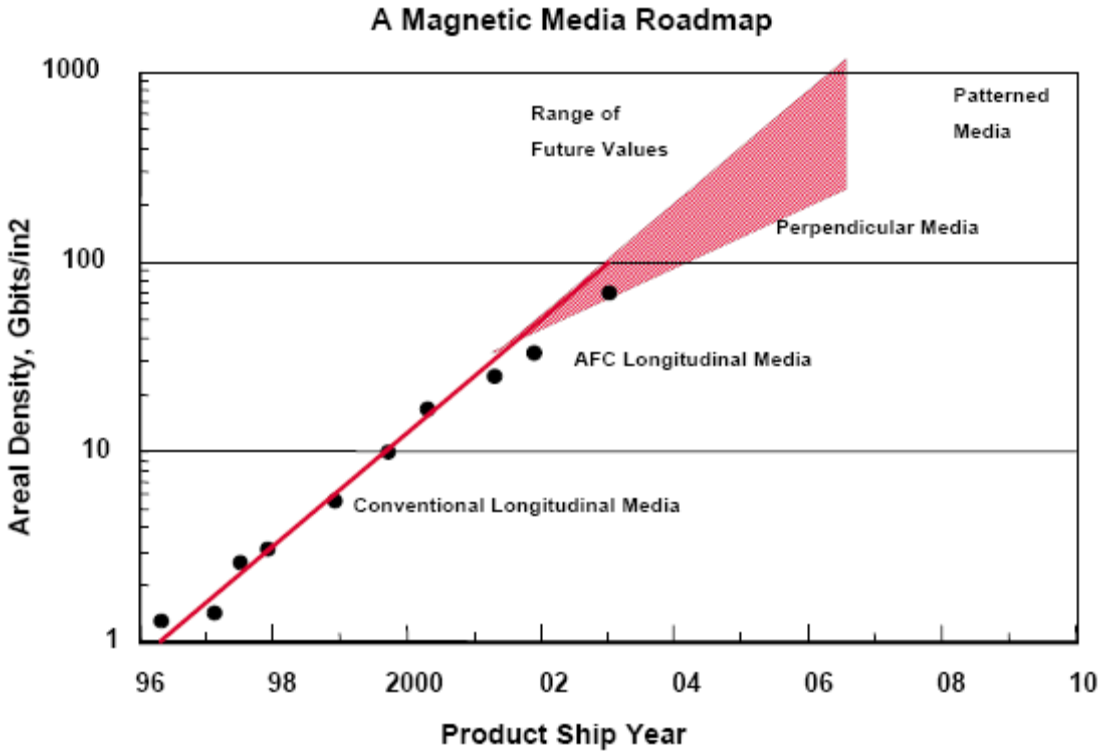

Figure 5.1: Hitachi data of areal density vs product ship year.[2]

It is the view of many that the current vertical recording on sputtered thin film stack technology is approaching a limit and will not extend beyond 1 Tbit/in^2 due to issues related to bit resolution and the superparamagnetic limit.[3,4] Bit Patterned Media (BPM) has the ability to overcome this fundamental limitation by separating individual bits into single domains (Figure 5.2). Both conventional multigrain media (CMM) and BPM rely on magnetic material with individual bits defined on concentric circular data tracks. The fundamental difference between the two is that the grains comprising bits in BPM act as isolated, strongly-coupled magnetic islands instead of intertwined, weakly-coupled fragments as in CMM. Therefore, the superparamagnetic limit is avoided because the volume of one BPM bit is roughly one hundred times greater than a CMM bit.

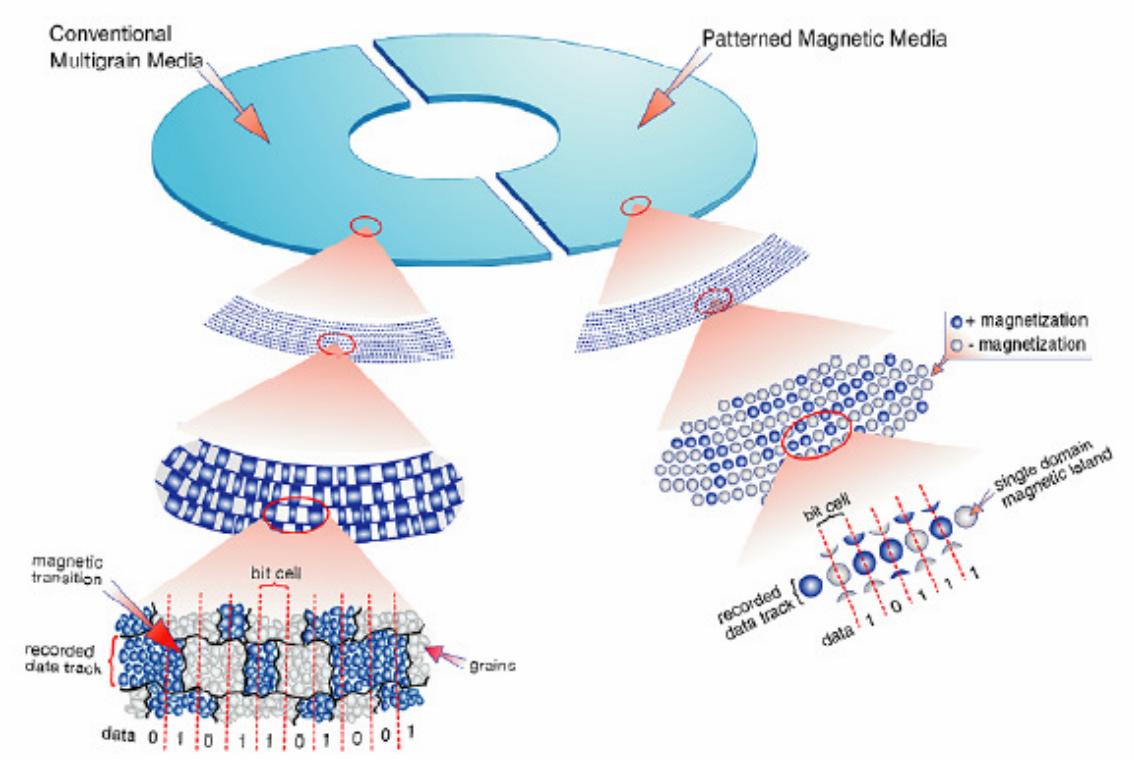

Figure 5.2: Conventional Mulitgrain Media vs Patterned Magnetic Media.[5]

While BPM is a noteworthy solution to some of the hard disk drive industry's problems, it is still a theoretical solution. Several issues arise with BPM, the biggest of which is feature size. To achieve areal densities at the 1 Terabit/nm^2 mark, individual domains must be on the scale of 5 to 20 nm in diameter; a scale that photolithography cannot pattern with current technologies.

5.2 NANO-IMPRINT LITHOGRAPHY

Nano-imprint lithography is a patterning technology that emerged as an alternative to photolithography in the latter half of the 1990s.[6] One particular version called Step and Flash Imprint Lithography (S-FIL®) has achieved commercial success, and its process steps are shown below (Figure 5.3). The first step involves dispensing a low viscosity monomer solution onto a substrate, followed by physically bringing a quartz template into contact with the solution. Once capillary action has filled the template features, the sample is irradiated with a mercury arc lamp. Upon photopolymerization, a hardened, cross-linked network forms on the substrate. The final step is removal of the template. Transfer etch processes can then proceed to pattern the inverse of the template features into the substrate.

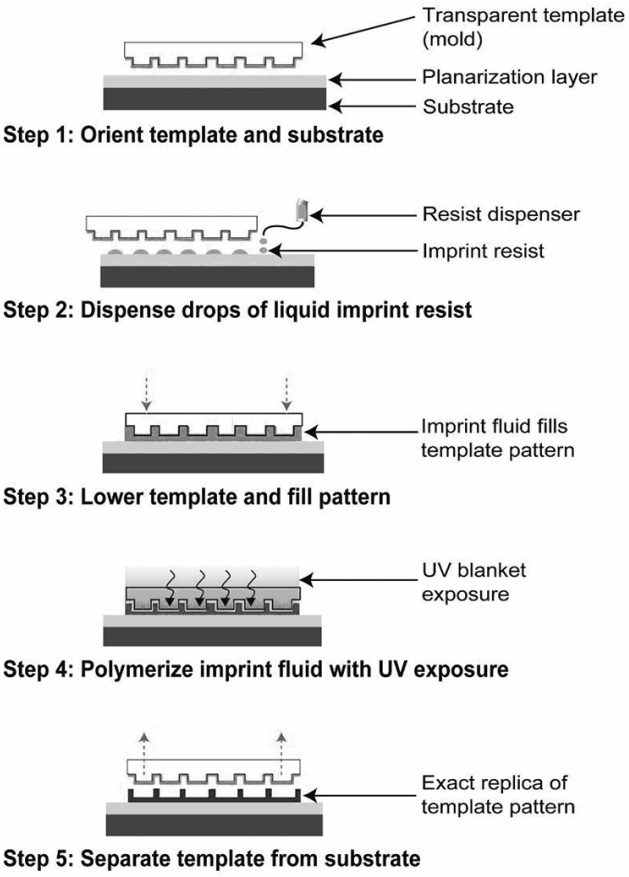

Figure 5.3: S-FIL® process.[6]

NIL reports have shown unparalleled resolution. In the early 2000s when photolithography was manufacturing 65 nm features and bringing 45 nm online, S-FIL® was showing the capability to produce dense 50 nm features and isolated 20 nm lines with very low LER as shown in Figure 5.4.[7,8] One report that has been well-cited (over 100 times at the time of this writing) showed that carbon nanotubes could be reproducibly imprinted using NIL techniques. AFM images in Figure 5.5 showed that features as small as three nanometers could be imprinted.[9]

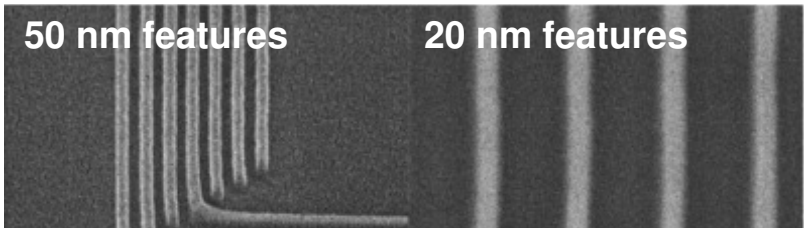

Figure 5.4: SEMs of S-FIL® images.[7,8]

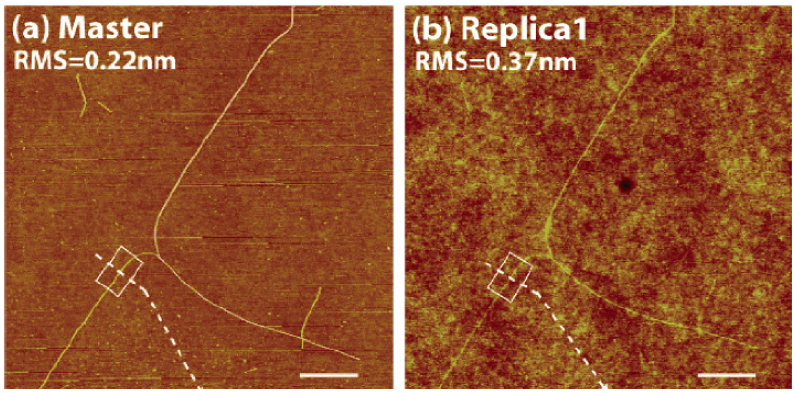

Figure 5.5: AFM images of master template with carbon nanotube (a) and the resulting imprint (b).[9]

5.3 TEMPLATE SPECIFICATIONS

A major issue that prevents NIL from being used to manufacture highly dense BPM devices is template fabrication. Challenges arise from the fact that NIL requires a master template that is exactly duplicated 1:1; ie, production of 1 Tbit/in^2 hard disk drives mandates a 1 Tbit/in^2 template. Current template fabrication involves electron-beam lithography (EBL), a very slow technique, to produce well-resolved features, and it has been estimated that it would take more than a month to fabricate a 95 mm patterned media disk at 1 Tbit/in^2.[10]

5.4 SELF-ASSEMBLED BLOCK COPOLYMERS

Due to the density and size of features needed for BPM, a technique must be found that does not require it to address each bit individually. A drastic improvement would be if the information to address each bit could be contained within the material itself. Block copolymers (BCs) seem to be an ideal way to achieve this as they spontaneously self-assemble into regular patterns with dimensions of tens of nanometers.

A block copolymer (BC) is comprised of a homopolymer covalently attached to another homopolymer. Research in BCs has rapidly expanded in the last few decades resulting in significant improvements in the synthesis, characterization, and self-assembly processes.[11] A Matsen diagram is shown below in Figure 5.6, which displays some of the unique self-assembly properties of BCs. The y-axis is the product of χ, the Flory-Huggins interaction parameter, and N, the number of volume segments for the entire BC, and the x-axis is the volume fraction of component a (f_a).[11-14] At low χN values, such as a dimer of MMA bonded to a dimer of styrene, the minimum energy state of the system is disordered. However as χN increases for symmetric diblock copolymers, specifically to χ>10.5, the system reaches a state where the favorable interactions of component a mixing with a and component b with b are greater than the entropic penalty of the organized microphase. Macrophase separation would ensue if two homopolymers were mixed under these conditions, but due to the covalent bond attaching these two unique chains, ordered microphases represent states where all forces are balanced.

Of particular interest to NIL template fabrication is the hexagonally packed cylindrical microphase. Each cylinder is envisioned as a dot on a template that would eventually pattern one bit. BCs self-assemble on the tens of nanometer scale, so these materials can provide the necessary feature density for hard disk drive applications.

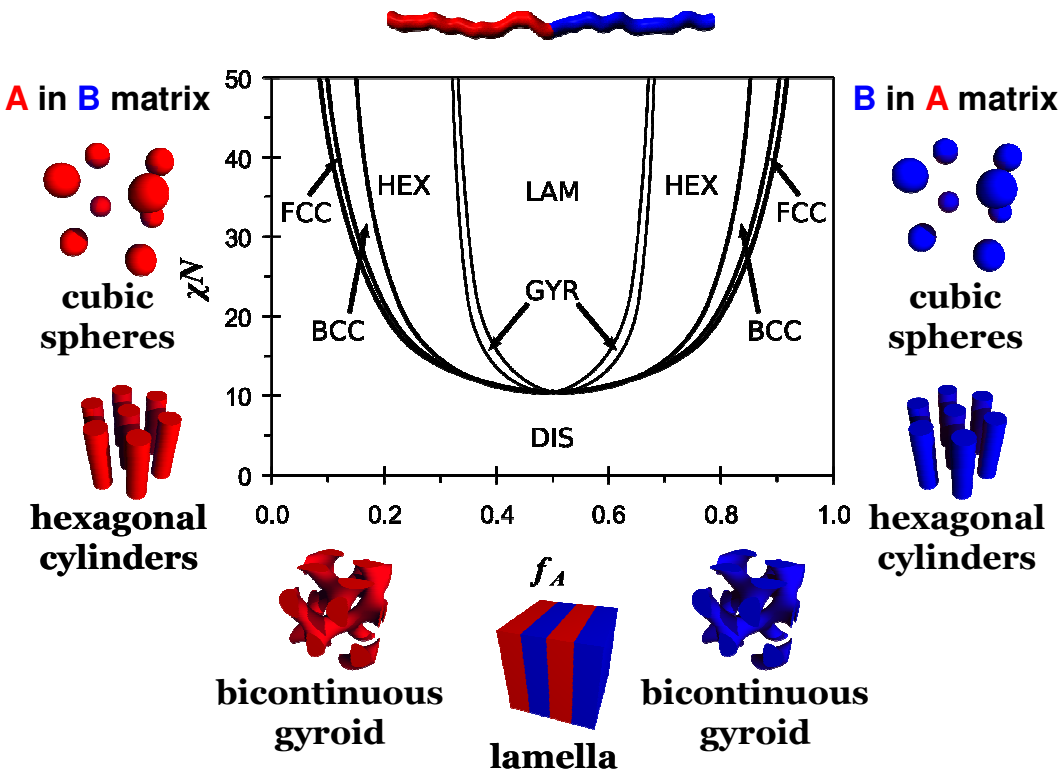

Figure 5.6: Matsen diagram.[14]

5.5 TEMPLATE FABRICATION PROCESS

With all pieces of this complex problem introduced, a process similar to that first outlined by Hawker and Russell was envisioned to produce NIL templates for BPM devices (Figure 5.7).[15] The first step involves treating the surface of a quartz substrate such that it will induce perpendicular orientation. The second step is coating a BC film to an appropriate thickness followed by annealing to produce hexagonally packed cylinders. Finally, the self-assembled features are subject to an O_2 RIE to produce 3-D cylinders at Giga - Teradot/in^2 densities.

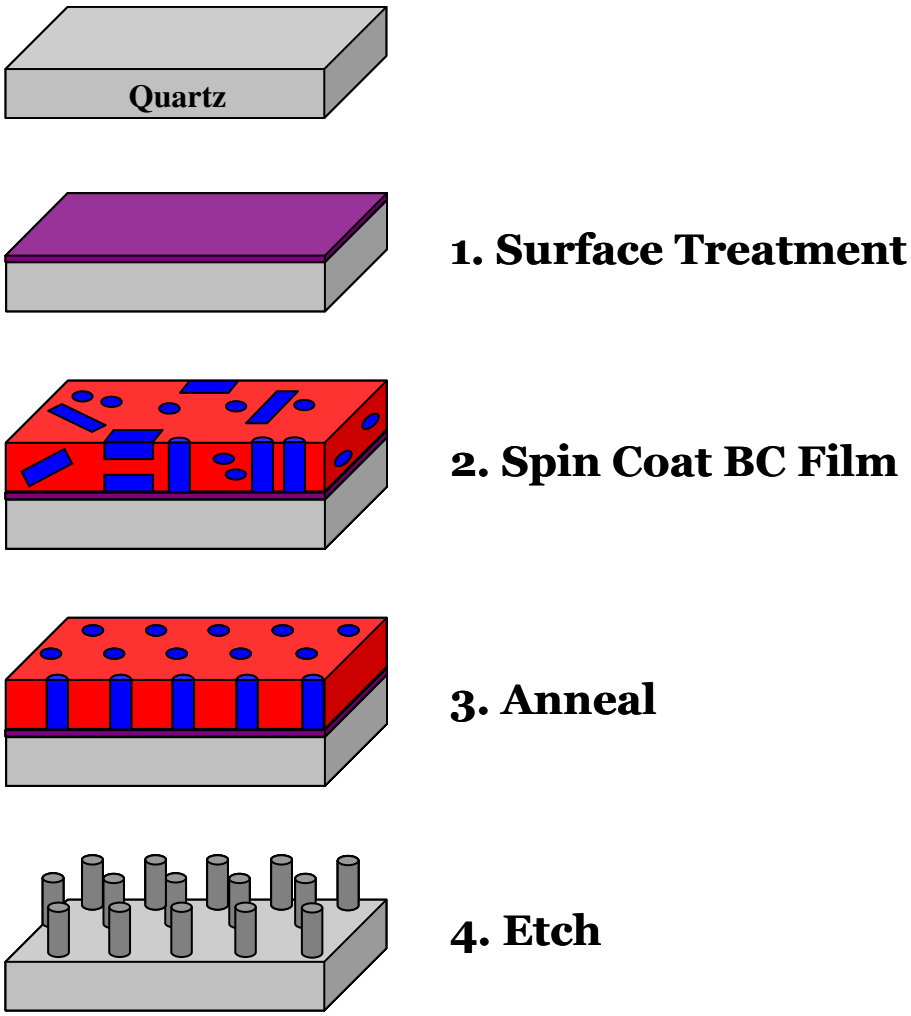

Figure 5.7: Process for NIL template fabrication for BPM.

5.6 BC ORIENTATION

For the hexagonally packed cylinders to function as dots for template fabrication, they must be oriented perpendicularly to the substrate. To achieve this orientation, multiple variables must be controlled; the two most important are film thickness and surface energy.

5.6.1 Film Thickness

As described by Russell and others, the MW of a BC determines its L_0, where L_0 is the bulk equilibrium period.[16,17] If a film is spin coated with a thickness, t, such that $t = nL_0$, where n is an integer, then features parallel to the surface are most commonly observed (Figure 5.8A). If the thickness is increased by varying the spin rate or concentration, t does not conform to nL_0 for n>1. This film produces islands and holes (B). For thin, noncommensurate films (L_0>t>0), the films tries to maintain a flat surface, but it does so at the cost of severe entropic penalties and chain packing (C). To minimize the free energy of the system, the BC changes its orientation to yield features perpendicular to the surface (D).[18,19]

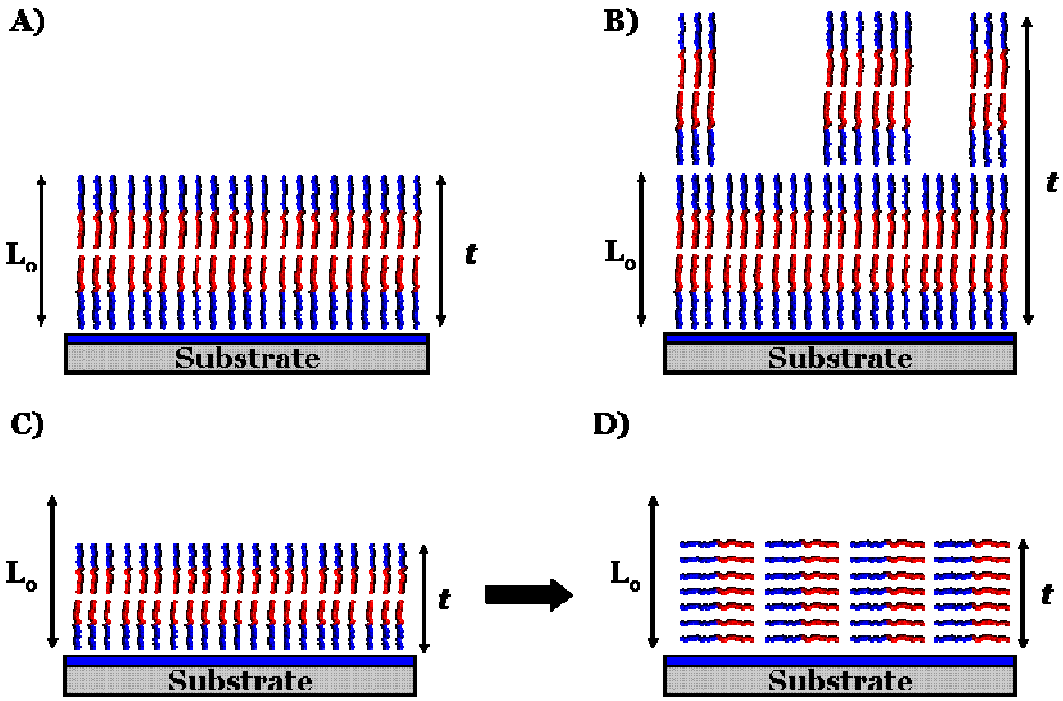

Figure 5.8: Thickness effects of BC orientation: A) $t = L_0$, parallel orientation B) $t>L_0$, islands and holes C) $t<L_0$, non-equilibrium chain packing D) $t<L_0$, perpendicular orientation.

5.6.2 Surface Energy

The second major variable in BC orientation is surface energy. Figure 5.9 displays how lamellae forming BCs can interact with a surface leading to either parallel or perpendicular orientation depending on preferential interactions between one of the blocks and a surface. In an oversimplified case, the PMMA block of a PS-b-PMMA BC will preferentially wet a surface with high surface energy leading to parallel lamellae because PMMA has a higher surface energy than PS. On the other hand, PS will wet a surface with a lower surface energy leading to the parallel lamellae as well. If the surface is neutral, meaning that and its surface energy falls in between that of the two blocks, then perpendicular lamellae will form.

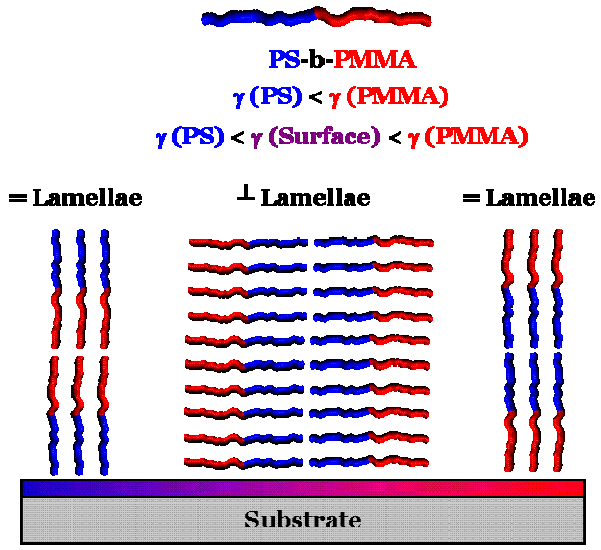

Figure 5.9: Preferential wetting of PS-b-PMMA on a gradient surface leads to = or ⊥ lamellae.

5.7 NEUTRAL SURFACE TECHNIQUES

Multiple techniques exist to achieve a neutral surface including surface treatment with alkyl chlorosilanes[20,21], solvent annealing[22,23], graphoepitaxy[10,24,25], and polymer brushes.[26-34] While all of these methods have shown success in achieving both

perpendicular and parallel orientation of some BCs, graphoepitaxy offers long range order on the order of microns. While this technique has made significant contributions in BC science, it is by far the most labor intensive and expensive as it requires e-beam exposure. Additionally, solvent annealing appears to be less well understood with very specific apparatus and conditions required. Therefore, alkyl chlorosilanes and polymer brushes were chosen as primary targets to investigate for this application.

5.8 SURFACE ENERGY AND CONTACT ANGLES

Before delving into chemistry, surface energy calculations must be addressed. Although multiple theories describe how best to determine surface energy from contact angles, the method described by van Oss, Good, and Chaudhury has been shown to be the most rigorous, most inclusive, and valid for a wide range of materials.[35-38] This model describes the inherent surface energy of a surface as the surface tension between two surfaces (γ_{12}) as the sum of the dispersion (γ_{12}^{LW}) and the acid-base components (γ_{12}^{AB}) as seen in eq (5.17). These two components are further separated as shown in eq (5.18) and eq (5.19) where γ_{1V}^{LW} is the dispersion force between a surface and a vacuum, and γ_{1V}^{p+} and γ_{1V}^{p-} are the Lewis-Acid and Lewis-Base forces between a surface and a vacuum, respectively.

$$\gamma_{12} = \gamma_{12}^{LW} + \gamma_{12}^{AB} \qquad (5.17)$$

$$\gamma_{12}^{LW} = (\sqrt{\gamma_{1V}^{LW}} - \sqrt{\gamma_{2V}^{LW}})^2 \qquad (5.18)$$

$$\gamma_{12}^{AB} = 2\,(\sqrt{\gamma_{1V}^{p+}\gamma_{1V}^{p-}} + \sqrt{\gamma_{2V}^{p+}\gamma_{2V}^{p-}} - \sqrt{\gamma_{1V}^{p+}\gamma_{2V}^{p-}} - \sqrt{\gamma_{1V}^{p-}\gamma_{2V}^{p+}}) \qquad (5.19)$$

The Young-Dupre equation describes the contact angle of a fluid with a substrate where γ_{LV} is the surface tension between the fluid and a vacuum, γ_{SV} is the surface energy between a surface and a vacuum, γ_{SL} is the interfacial energy between the liquid-solid, and π_{eq} is the equilibrium spreading pressure (eq (5.20)).

$$\gamma_{LV} \cos\theta = \gamma_{SV} - \gamma_{SL} - \pi_{eq} \quad (5.20)$$

Several variables in these equations can be related to each other and cancelled; $\gamma_{SL} = \gamma_{12}$, $\gamma_{SV} = \gamma_1$, and $\gamma_{LV} = \gamma_2$. With literature values of glycerol, water, and diiodomethane (Table 5.1) and assuming γ^{p+} and γ^{p-} are zero for diiodomethane, γ was solved using algebraic manipulations.

Table 5.1: Literature values of energy components for glycerol, water, and diiodomethane.[38]

Fluid	γ^{LW}	γ^{p+}	γ^{p-}	γ^{Total}
Glycerol	37.5	3.92	57.4	63.9
Water	21.8	25.6	25.4	72.8
Diiodomethane	50.8	0.7	0	50.8

5.9 CHLOROSILANES

Previous work by the Nealey group showed that an oxidized wafer can be treated with long alkyl monochlorosilanes leading to a low surface energy and hence parallel PS-b-PMMA orientation.[20] Upon exposure to x-rays, the alkyl surface was partially oxidized giving a surface that led to perpendicular BC orientation due to the higher surface energy. While this work showed the potential control for BC orientation by surface modification, the exact chemical species on the surface after x-ray exposure were not quantitatively investigated. A route was envisioned that started with known chemicals species already

on the chlorosilanes. This would remove the exposure step as well any uncertainty of the surface's chemical identity (Figure 5.10).

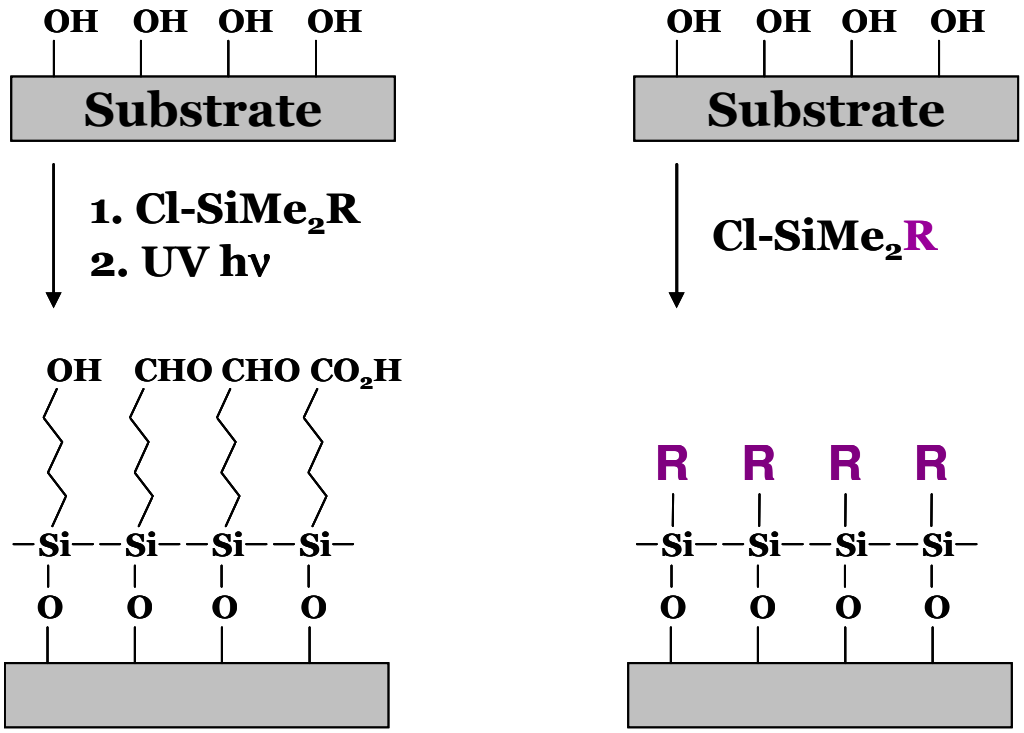

Figure 5.10: Nealey alklyl chlorosilane and oxidation technique (left) and proposed simplified route (right).

Fortunately, several monochlorosilanes are commercially available with various terminal functional groups. It is important to note that due to possible side reactions, only monochlorosilanes were chosen. It has been reported that di- and tri-chlorosilanes can lead to non-uniform multilayer treatments, which effect surface energy, film thickness, and film roughness.[39,40]

Desiring more polar terminal groups, several monochlorosilanes were synthesized via hydrosilylation chemistry on commercially available styrene derivatives (Scheme 5.1). While several compounds were subjected to the reaction conditions with dimethyl chlorosilane and Karstedt's catalyst, only the H, Cl, and Br derivatives were isolated and

fully characterized (6.1, 6.2, and 6.3). As with all hydrosilylation reactions, α and β isomers were isolated. Unfortunately, the Me, OMe, OAc, and t-Boc derivatives yielded no product via GC/MS or ^{1}H-NMR.

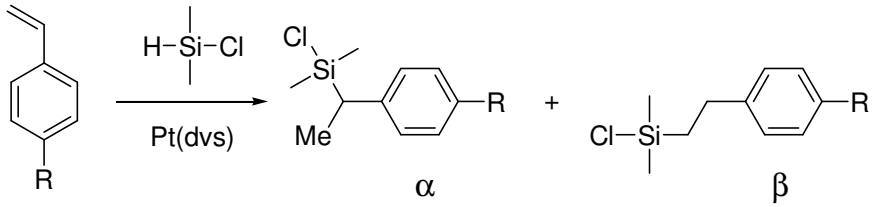

R = H; 5.1α, 5.1β, 65%
R = Cl; 5.2α, 5.2β, 81%
R = Br; 5.3α, 5.3β, 63%

Scheme 5.1: Synthesis of phenyl derivative chlorosilanes via hydrosilylation.

After vigorous oxidation with a piranha solution, wafers were treated with these compounds and other commercially available chlorosilanes, and their surface energy obtained via contact angle measurements. Several measurements were made on a wafer shard, and the error of the measurements was concluded to be +/- 3 dyne. As expected, the fluoroalkyl and alkyl chlorosilanes yielded surfaces with lower energies than those compounds with more polar groups such as the cyano and chloro compounds. Additionally, a wafer directly measured upon arrival had a surface energy 11 dyne/cm less than than one subjected to piranha. In regards to the styrene derivatives, bromo compound 5.3 yielded a surface with 47.9 dyne/cm, while 5.1 and 5.2 were both around 36 dyne/cm (Figure 5.11).

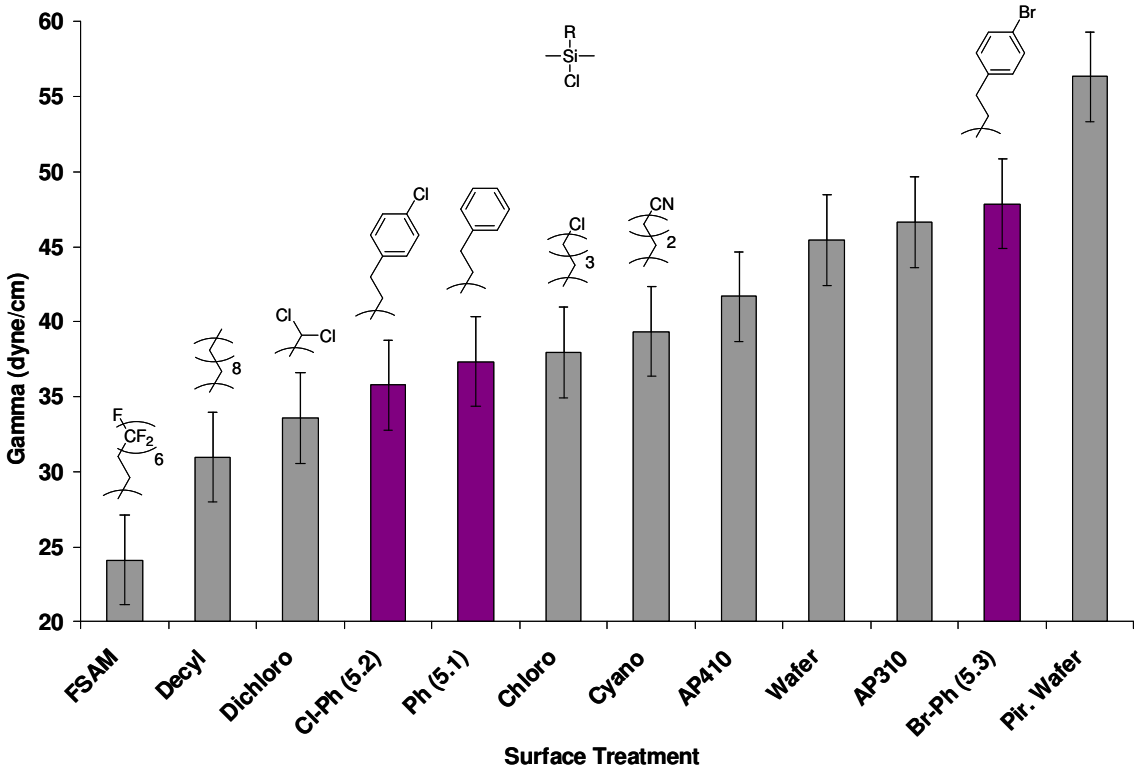

Figure 5.11: Surface energies of commercially available (gray) and synthesized (purple) chlorosilanes.

5.10 POLYMERIC CROSS-LINKED SURFACE TREATMENTS

Another commonly used technique to achieve neutral surfaces for perpendicular BC orientation is polymeric cross-linked surface treatments (PXSTs). Although not indicative of the architecture, the term 'polymer brush' was coined in 1991, and the name has persisted in the literature.[31] A PXST is a random copolymer made of one or two monomers that dictate the surface chemistry and a small amount of cross-linking monomer. A variety of functional groups have been reported to serve as the cross-linker: acrylates, epoxides, azides, and benzo cyclobutane. Additionally, a lone methyl hydroxyl group can be designed into the polymer brush that functions as an electrophile. Silanols of the wafer's surface then substitute this group. As can be expected, this method suffers

from long reaction times and poor surface coverage. A representative group of these PXSTs is shown in Scheme 5.2.[27-29,33]

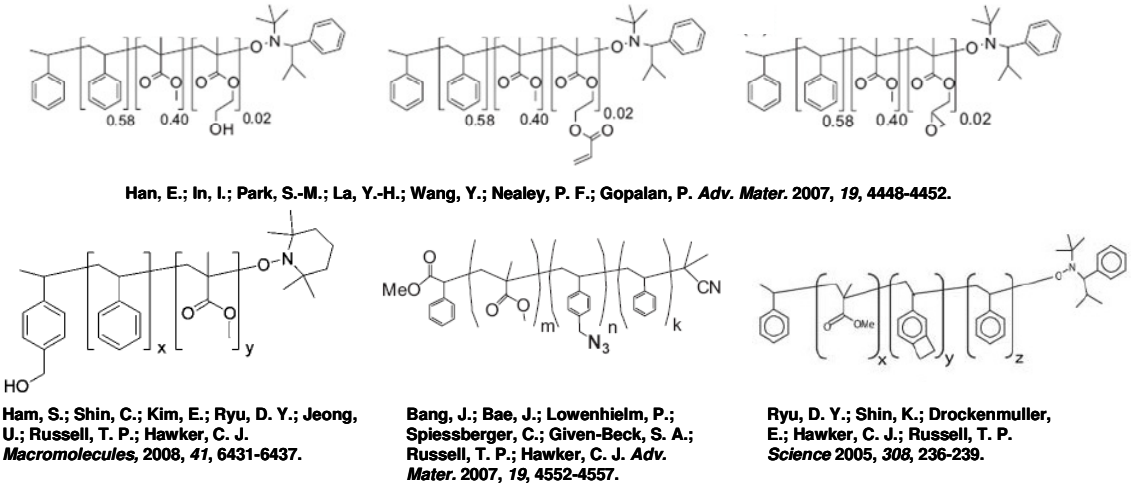

Han, E.; In, I.; Park, S.-M.; La, Y.-H.; Wang, Y.; Nealey, P. F.; Gopalan, P. *Adv. Mater.* 2007, *19*, 4448-4452.

Ham, S.; Shin, C.; Kim, E.; Ryu, D. Y.; Jeong, U.; Russell, T. P.; Hawker, C. J. *Macromolecules,* 2008, *41*, 6431-6437.

Bang, J.; Bae, J.; Lowenhielm, P.; Spiessberger, C.; Given-Beck, S. A.; Russell, T. P.; Hawker, C. J. *Adv. Mater.* 2007, *19*, 4552-4557.

Ryu, D. Y.; Shin, K.; Drockenmuller, E.; Hawker, C. J.; Russell, T. P. *Science* 2005, *308*, 236-239.

Scheme 5.2: Sample PXSTs used to control BC orientation.

Several observations can be made about these PXSTs. First, they are all drawn incorrectly in their respective reports. As drawn these polymers are block copolymers, but by the methods used to synthesize them, typically some form of living radical technique, the polymers are no doubt random copolymers. Secondly, MMA and styrene are the major components. The authors report that different PXST compositions lead to different BC orientation behavior[27,30,32], but they use PS-b-PMMA on top of essentially cross-linked PS-r-PMMA. Since the surface energy for PS is very close to PMMA according to the literature,[20,41,42] the control of BC orientation cannot be explained alone by the different surface energies due to molar compositions of the PXSTs. Desiring to further probe PXST surface energy and chemical structure effects on BC orientation, several styrene derivatives were copolymerized with vinyl benzyl chloride. Using benzyl azides in a manner similar to Hawker *et al*[29], nucleophilic substitution with sodium azide led to a small series of cross-linkable polymers (poly(5.5-R)) (Scheme 5.3). Each

polymer was characterized by GPC and ^{1}H-NMR, and the presence of the benzyl azide was confirmed by IR (Table 5.2).

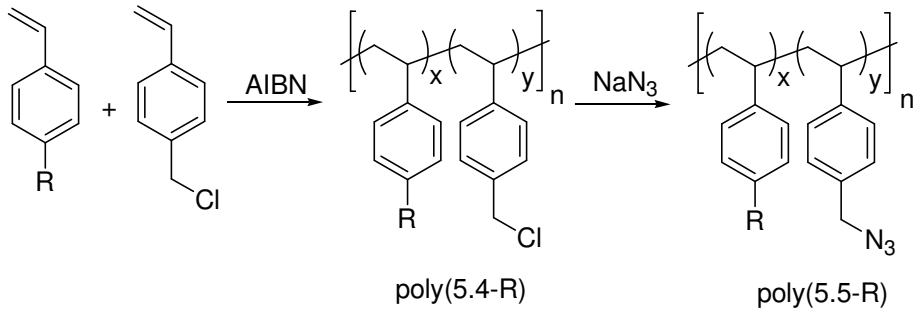

Scheme 5.3: Radical copolymerization and nucleophilic substitution to yield poly(5.5-R).

Table 5.2: Characterization of poly(5.5-R).

R	M_w (kDa)	M_n (kDa)	PDI	%BnAz (^{1}H-NMR)
H	26.6	15.5	1.71	7.7
Cl	30.2	17.3	1.75	8.9
Br	38.1	19.5	1.95	5.0
Me	36.6	21.8	1.68	8.1
tBu	32.0	17.6	1.81	7.0
OMe	26.5	14.3	1.85	8.0
OAc	48.1	27.1	1.67	4.6
tBoc	54.8	35.4	1.55	8.9
TMS	19.5	11.1	1.76	6.4
TBDMSO	17.9	11.0	1.63	13.7

As reported by Hawker and Russell, a PXST must be >5.5 nm to ensure complete coverage and display control of BC orientation.[34] Therefore, films >15 nm of poly(5.5-R) were spin-coated, heated to cross-link through the azide functionality, and thoroughly rinsed to remove any non-cross-linked materials. Surface energies of these films were obtained by goniometry with water, glycerol, and diiodomethane contact angles. The resulting surface energies are shown in Figure 5.12.

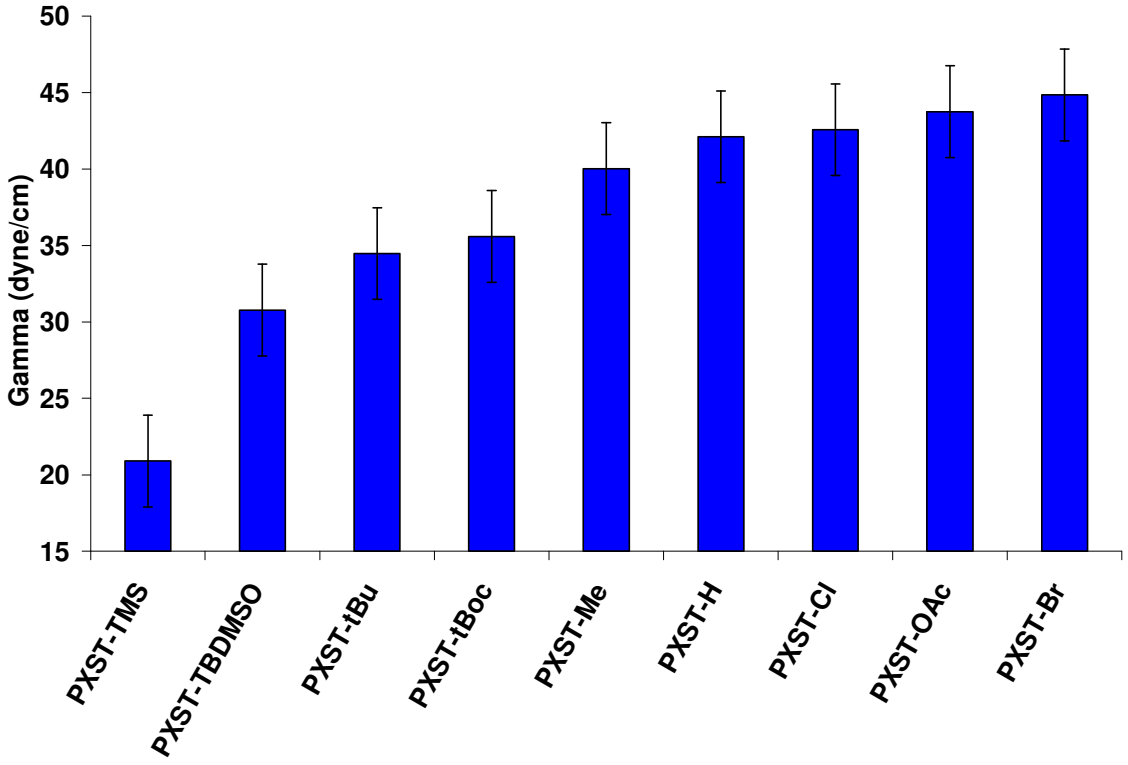

Figure 5.12: Surface energies of PXST-R.

5.11 ANIONIC SYNTHESIS OF PS-B-PMMA

With a variety of surfaces on hand via chlorosilanes and PXSTs, control of PS-b-PMMA orientation was investigated. This mandated the synthesis of PS-b-PMMA; several options were considered but due to previous experiences in our group with living radical techniques such as atom transfer radical polymerization (ATRP) and reversible addition fragmentation transfer (RAFT) polymerization, anionic techniques were chosen. While anionic polymerization suffers from limited functional group tolerance and requires extensive purification techniques, it is superior to radical techniques in regards to scale, percent conversion, yield, control of MW, polydispersity index (PDI), and reproducibility.

With the help of Prof. Christopher J. Ellison from the Chemical Engineering Department at the University of Texas at Austin, an anionic synthesis laboratory was setup including all of the necessary custom glassware (Appendix B).[43] After many hours removing impurities, distilling, and optimizing procedures, PS-b-PMMA was synthesized (Scheme 5.4). It began by initiating a living PS anion with sec-butyl lithium at -78 °C for 4 h to ensure complete conversion. After an aliquot was taken of the PS block, a five molar excess of 1,1'-diphenyl ethylene was reacted for 3 h to yield a dark red colored anion. This molecule functions to sterically encumber the polymer anion and has been shown to exclusively add 1,4 to methacrylates and not the terminating 1,2 addition.[44] Lastly, MMA was added to the reaction and stirred for 4 h followed by degassed methanol to quench the chain.

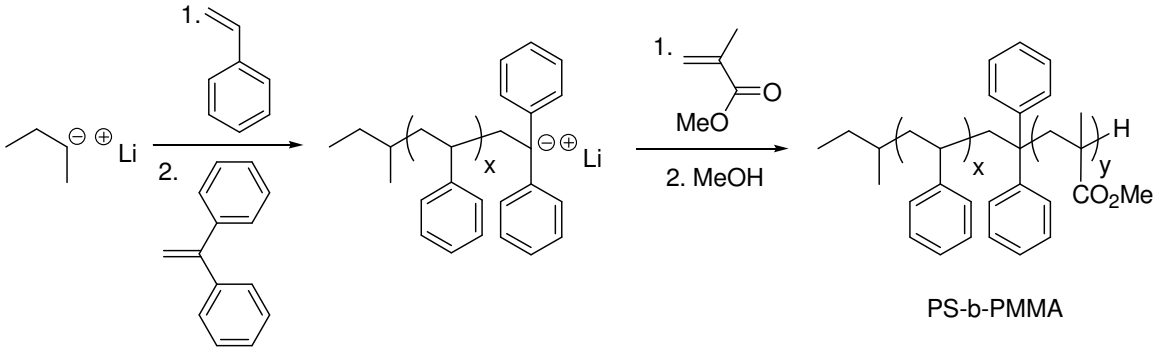

Scheme 5.4: Anionic Synthesis of PS-b-PMMA.

^{1}H-NMR showed the resulting polymer is 31 mol% PMMA, which corresponds to a volume fraction of 0.27.[12] This is within the range for cylinder morphology.[11] The M_n of the PS aliquot was 45.8 kDa with a PDI of 1.18; the total molecular weight was 65.6 kDa with a PDI of 1.18. Figure 5.13 shows GPC chromatograms of the PS aliquot and PS-b-PMMA.

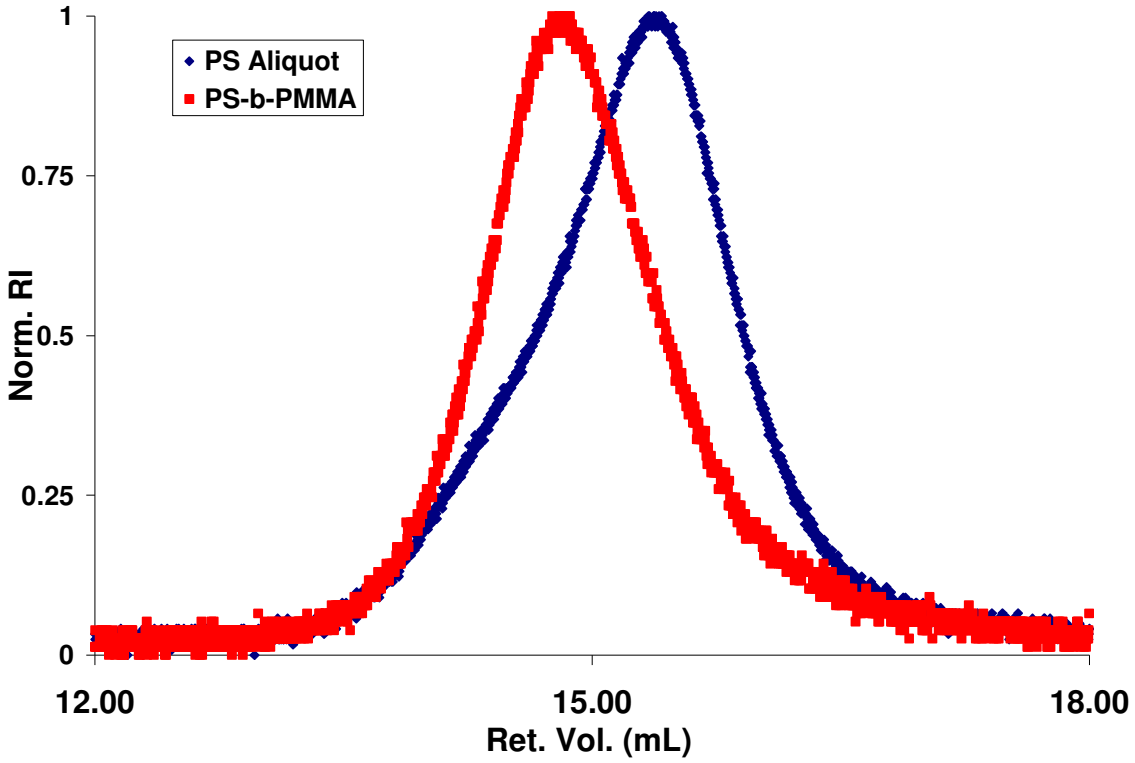

Figure 5.13: GPC chromatograms of PS aliquot (blue) and cylindrical PS-b-PMMA (red).

To confirm the bulk ordering, samples of this polymer were analyzed via small angle x-ray scattering (SAXS). Figure 5.14 shows the diffraction pattern of a sample of this polymer that was collected at 170 °C. Assigning the first major peak as q* and relating all other peaks to this value as shown in Table 5.3, this polymer's bulk ordering is consistent with hexagonally packed cylinders.

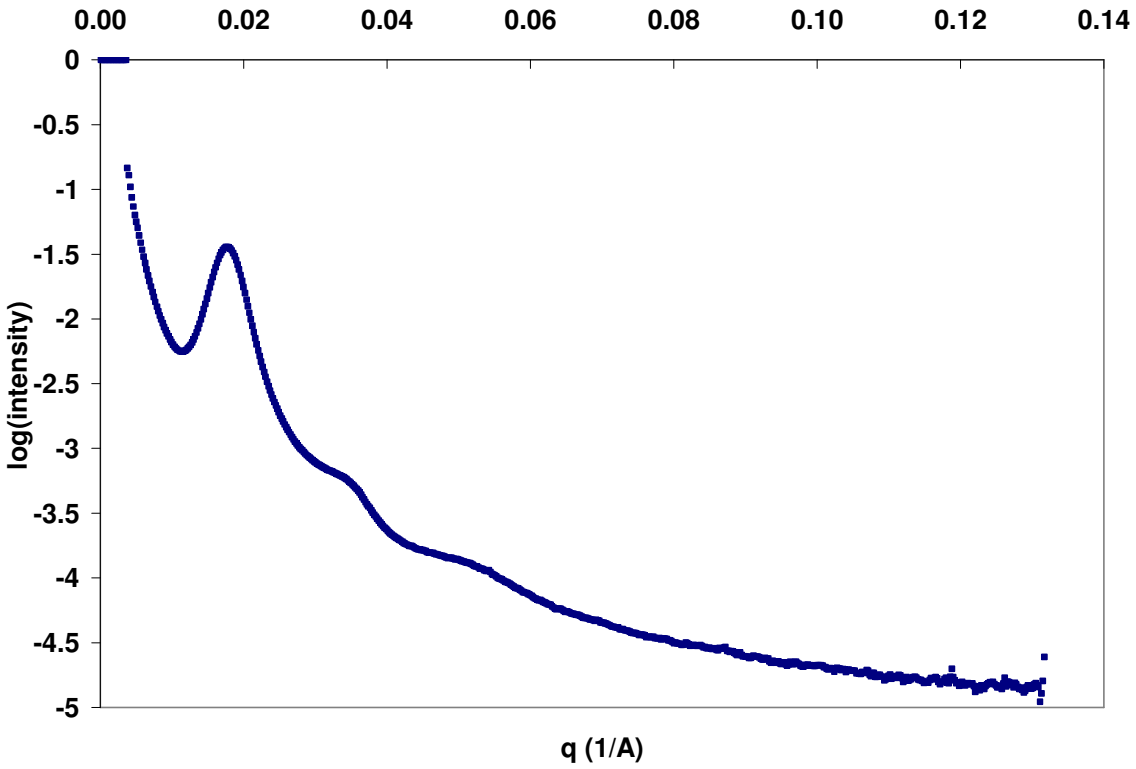

Figure 5.14: SAXS diffraction pattern of cylindrical PS-b-PMMA.

Table 5.3: SAXS peak assignment of cylindrical PS-b-PMMA.

q*	0.0181
domain spacing (nm)	34.7
peak 1	0.0339
peak 1/q*	1.8729
root 3	1.7321
peak 2	0.0358
peak 2/q*	1.9779
root 4	2.0000
peak 3	0.0548
peak 3/q*	3.0276
root 9	3.0000

In a similar fashion, lamellae forming PS-b-PMMA was synthesized. ^{1}H-NMR showed the resulting polymer is 54 mol% PMMA, which corresponds to a volume fraction of 0.49.[12] This is within the range for lamellar morphology.[11] The M_n of the PS aliquot was 30.8 kDa with a PDI of 1.02; the total molecular weight was 52.0 kDa with a PDI of 1.02. Figure 5.15 shows GPC chromatograms of the PS aliquot and PS-b-PMMA.

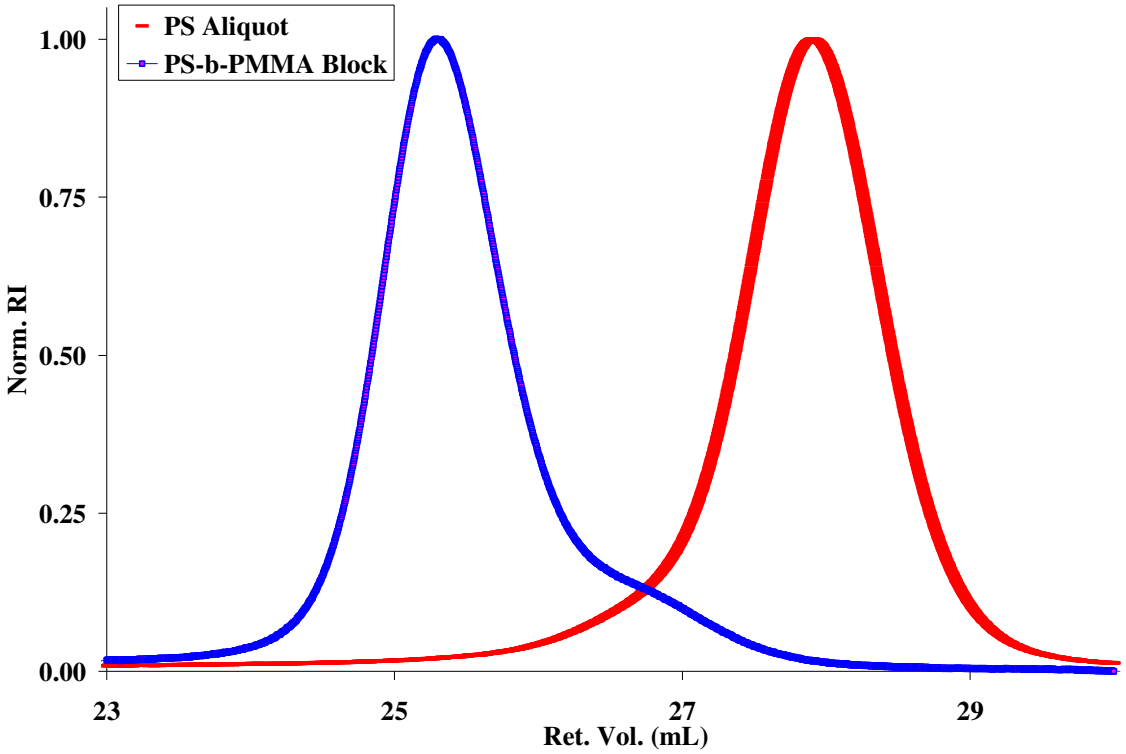

Figure 5.15: GPC chromatograms of PS aliquot (red) and lamellar PS-b-PMMA (blue).

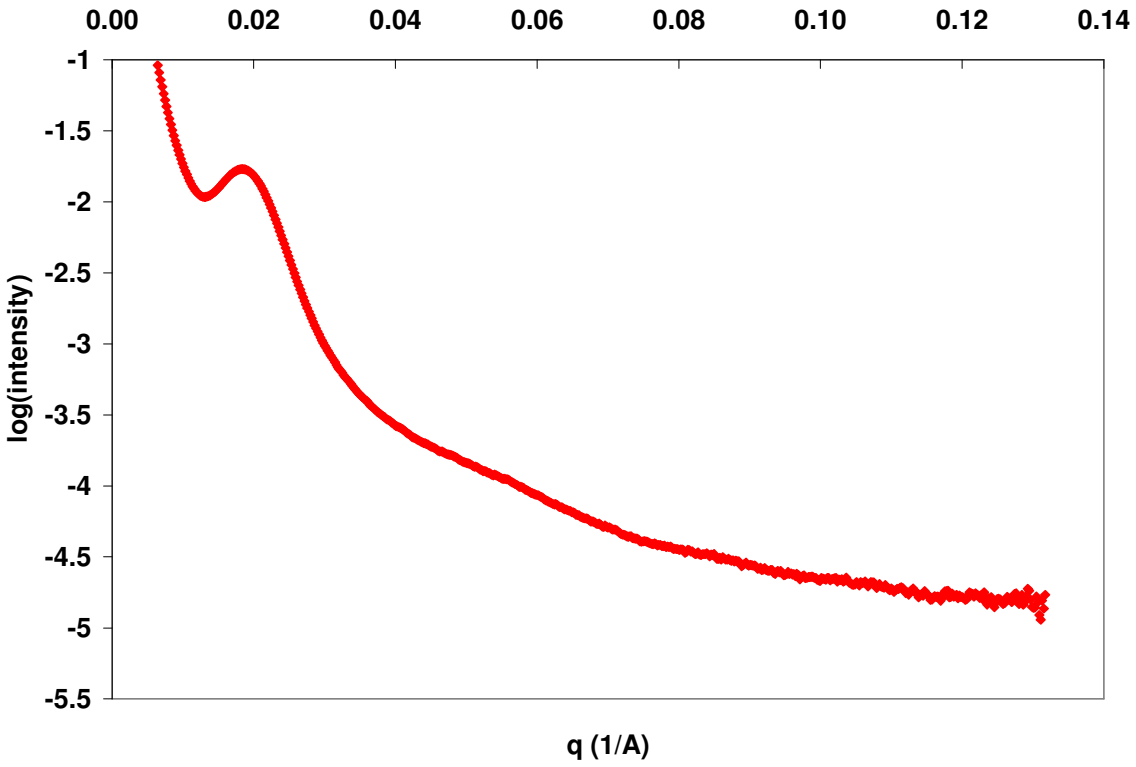

Figure 5.16: SAXS diffraction pattern for lamellar PS-b-PMMA.

Table 5.4: SAXS peak assignment of lamellar PS-b-PMMA.

q*	0.0194
domain spacing (nm)	32.4
peak 1	0.0561
peak 1/q*	3.0994
root 3	3.0000

5.12 PS-b-PMMA Cylinders on Chlorosilanes

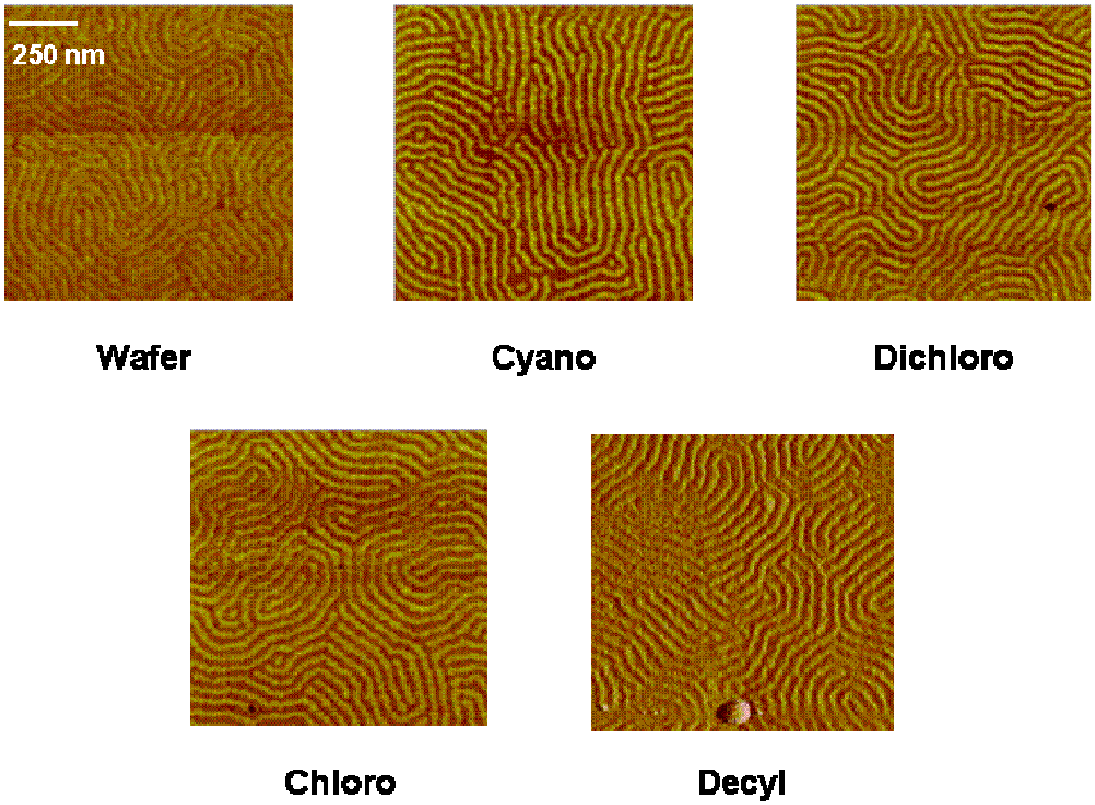

Figure 5.17: Representative AFM images of PS-b-PMMA cylinders on treated wafers.

Films of various thicknesses were coated onto treated wafers, annealed at 170 °C overnight in a vacuum oven, and analyzed via AFM in tapping mode. The representative images shown in Figure 5.17 display parallel cylinders. The cylinders are 20-25 nm in diameter and display no long range order. It was discovered that the BC orientation on top of these chlorosilanes is very sensitive to changes in film thickness. Films thicker or thinner than 5 nm from the optimized 40 nm led to featureless films.

PS-b-PMMA films were coated around 30 nm on surface treatment 5.1, the phenyl chlorosilane derivative. The resulting films displayed mixed morphology (Figure 5.18). Unfortunately, bulk perpendicular features were never observed, and as the film thickness was decreased, multiple defects were observed.

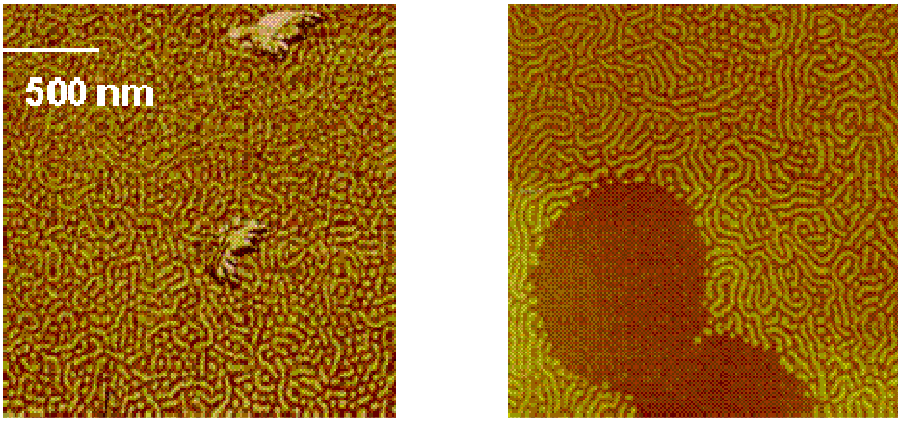

Figure 5.18: PS-b-PMMA cylinders on surface treatment 5.1.

PS-b-PMMA films coated on top of surface treatment 5.2, the chloro-phenyl derivative, displayed either parallel or mixed morphology depending on film thickness as shown in Figure 5.19. Films around 35 nm showed mixed morphology while films around 40 nm showed complete parallel orientation. When thinner films were coated, no features were observed.

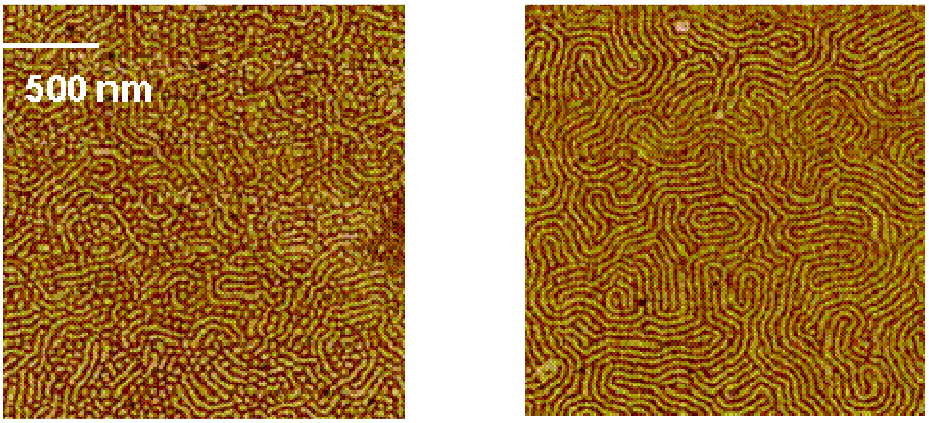

Figure 5.19: PS-b-PMMA films on surface treatment 5.2; mixed morphology (left) and parallel orientation (right).

As expected, PS-b-PMMA solutions did not wet FSAM treated wafers so its BC orientation control could not be investigated. Unfortunately, annealed films with a variety of thicknesses of PS-b-PMMA did not display any features, parallel or perpendicular, on wafers treated with bromo-phenyl derivative 5.3.

5.13 PS-b-PMMA Cylinders on PXSTs

PS-b-PMMA films of various thicknesses were then coated on the PXSTs, annealed, and investigated by AFM. PXST-Br resulted in perpendicular cylinder formation over a wide range of film thicknesses (20-40 nm). This process window result is similar to other polymeric surface treatments reported by Nealey[30] and Hawker and Russell.[28,32,34] Representative AFM images are shown in Figure 5.20. Additionally, the domain spacing of the AFM is 35-40 nm, which is consistent with the SAXS data. Assuming ideal hexagonally packing, this corresponds to an areal density of 500 Gdots/in^2.

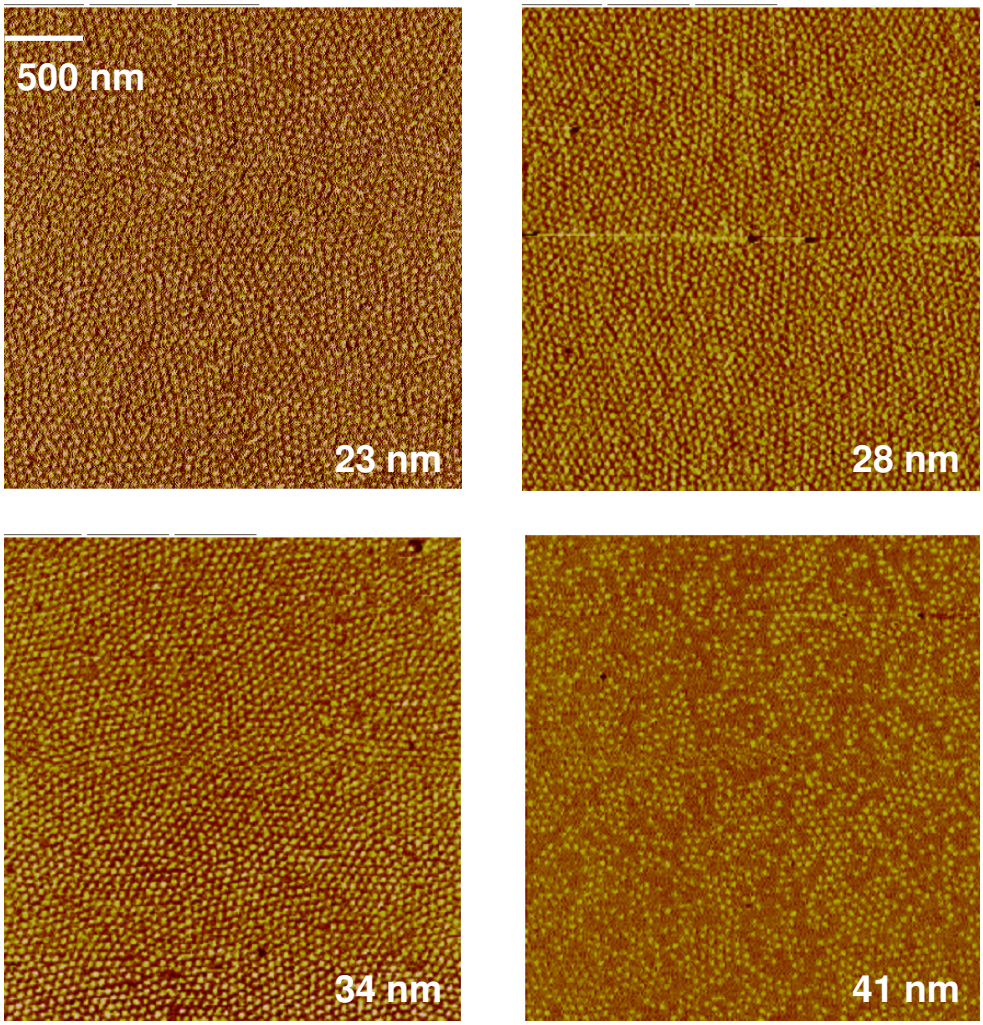

Figure 5.20: AFM images of PS-b-PMA cylinders on PXST-Br.

PS-b-PMMA cylinders on PXST-Cl consistently displayed mixed morphology with films 25-40 nm. A representative AFM is shown in Figure 5.21.

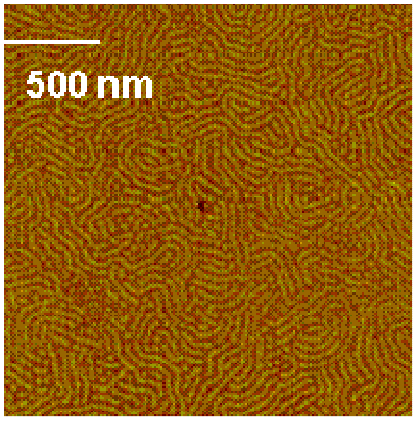

Figure 5.21: AFM image of PS-b-PMMA cylinders on PXST-Cl.

The most interesting data was observed with the PXST-H. With thin films around 20 nm, bulk parallel features were observed (A). As the film thickness was increased, AFM images showed rough surfaces associated with noncommensurate surfaces (B and C). Surprisingly, bulk perpendicular features were observed with films from 50-130 nm (D, E, and F). To our knowledge, this represents the thickest films that show bulk perpendicular orientation on a non-patterned substrate.

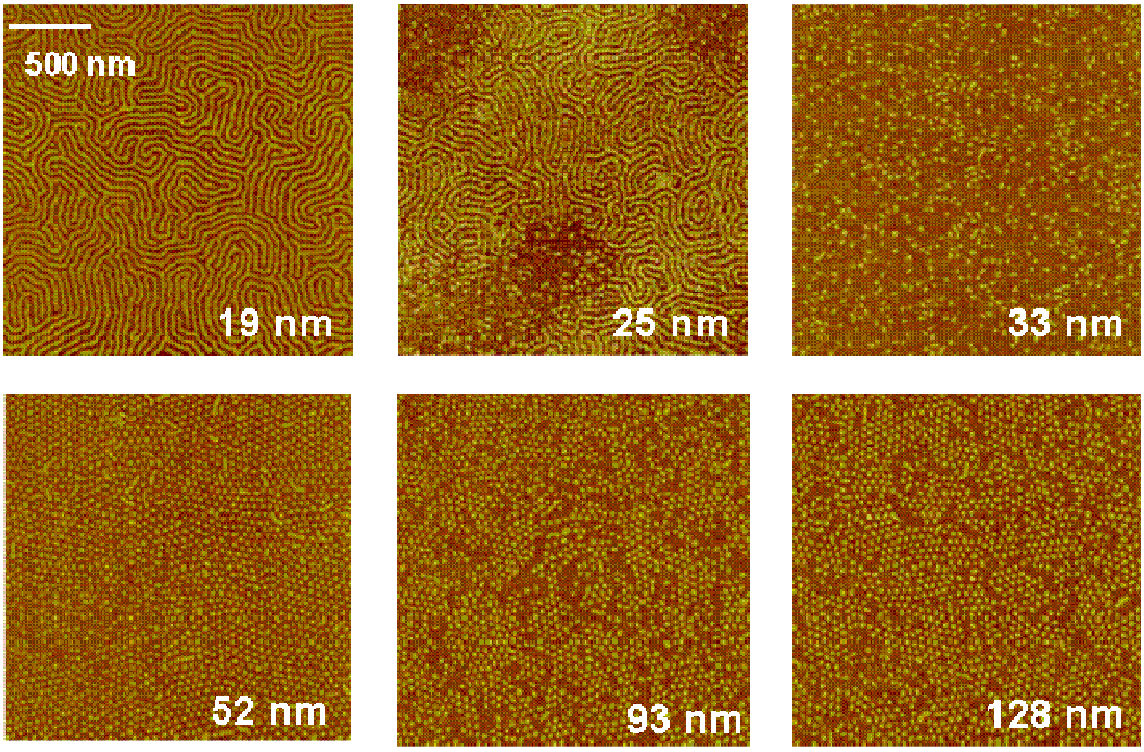

Figure 5.22: AFM images of PS-b-PMMA cylinders on PXST-H: A) 19 nm B) 25 nm C) 33 nm D) 52 nm E) 93 nm F) 128 nm.

PS-b-PMMA films coated onto cross-linked poly(5.5-Me) and poly(5.5-tBu) were reproducibly rough and optically poor. At the beginning of this study, laboratory techniques were thought to be the cause of this, but once compelling data was collected with other PXSTs using identical techniques, this result must be an effect of the phenyl substituent. Likewise, poly(5.5-tBoc) resulted in poor films that were optically blue after annealing. This is likely due to thermally induced deprotection of the tBoc group resulting in a rough surface not suitable for controlled BC orientation. Poly(5.5-OMe) and poly(5.5-OAc) led to smooth PXSTs, and the films were optically smooth after annealing with PS-b-PMMA. However, no features were observed despite varying the film thickness from 15-60 nm.

Combining all data from cylindrical PS-b-PMMA films, the process window for each PXST was gathered. As shown in Figure 5.23, PXST-Br yielded bulk perpendicular orientation over a 20 nm window, and PXST-Cl yielded mixed morphology over a similar window. The window is dominated by bulk perpendicular orientation on PXST-H. The conclusion from this data is that the monomers in the cross-linked surface treatment do not have to be the same as the monomers that comprise the BC.

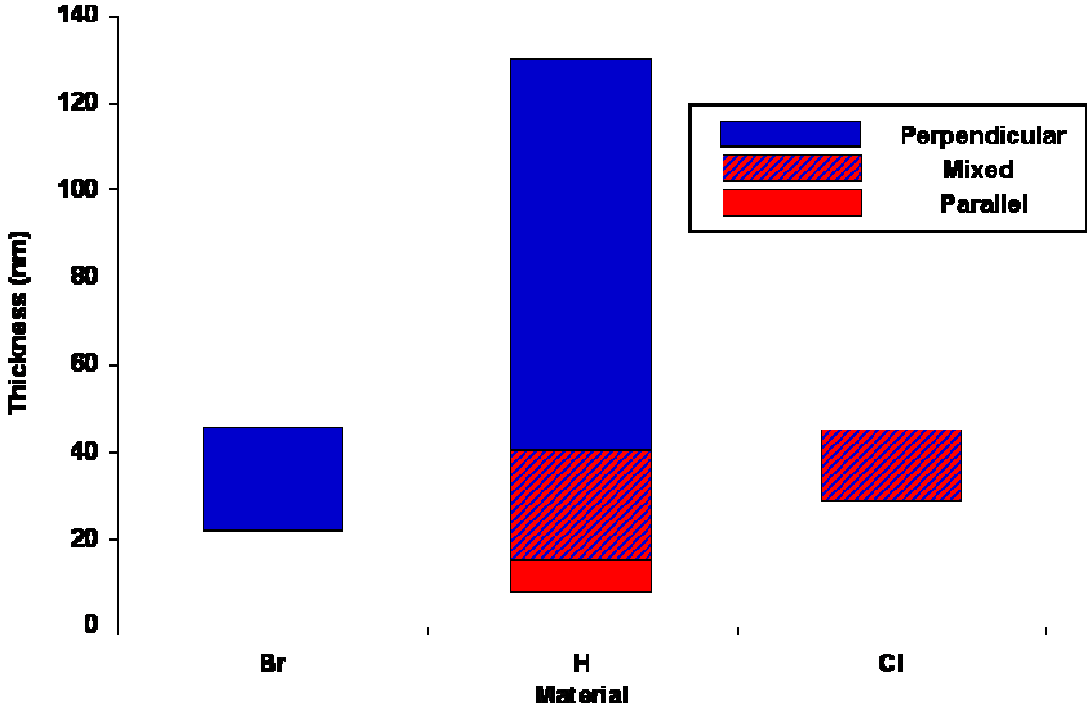

Figure 5.23: Process window for PS-b-PMMA cylinders on various PXSTs.

5.14 PS-b-PMMA Lamellae on PXSTs

With the success of the PXSTs on PS-b-PMMA cylinders, studies were then directed towards obtaining lamellar process window. Films on PXST-Br and PXST-Cl yielded perpendicular features over a very small window. Representative AFM images show the bulk ordering with an L_0 similar to that predicted by the SAXS data. Surprisingly, no features were ever isolated on PXST-H. This indicates that the free

energy of the system cannot be predicted alone by the surface energy of the PXST, BC, and film thickness, and studies will continue to investigate BC morphology on these PXSTs.

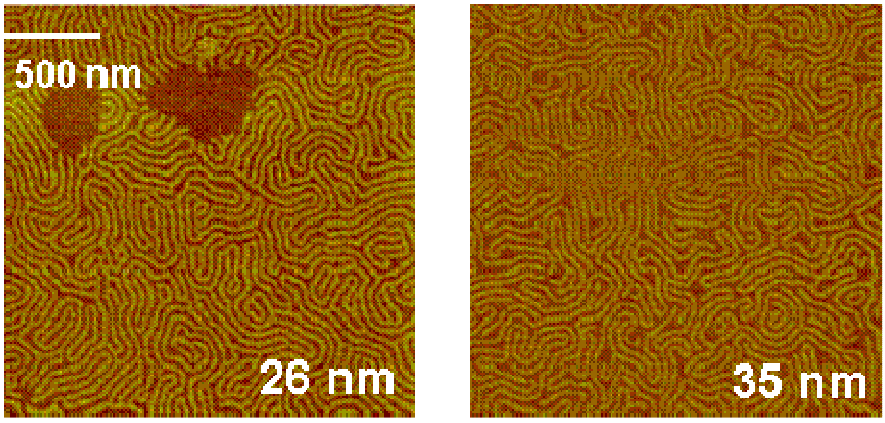

Figure 5.24: AFM images of PS-b-PMMA lamellae on PXST-Br (left) and PXST-Cl (right).

5.15 ETCH RESISTANCE

While the above techniques are an advancement in the BC field, PS-b-PMMA does not meet all of the material properties for the production of NIL templates. Of primary concern is the lack of etch selectivity because both blocks consist of hydrocarbons. Under typical oxygen reaction ion etch (O_2 RIE) conditions, poly(hydrocarbons) have etch rates that are very similar[45], and hence self-assembled PS-b-PMMA features are difficult to resolve.[46] For this application once the cylinders are oriented properly, we intend to remove one block to convert the smooth self-assembled film to an array of three dimensional features (Figure 5.7). Etch selectivity has been proposed to meet this requirement.

In a well-cited paper (over 70 times at the time of this writing), Colburn *et al* conducted a series of experiments that concluded a formulation with ≥12 wt% Si can

serve as an etch barrier under standard O_2 RIE conditions versus PS (Figure 5.25).[47] Therefore, a BC was designed that contained over 12 wt% silicon in one block but was all hydrocarbons in the other. This would provide the etch selectivity to yield a 3-D pattern of self-assembled features.

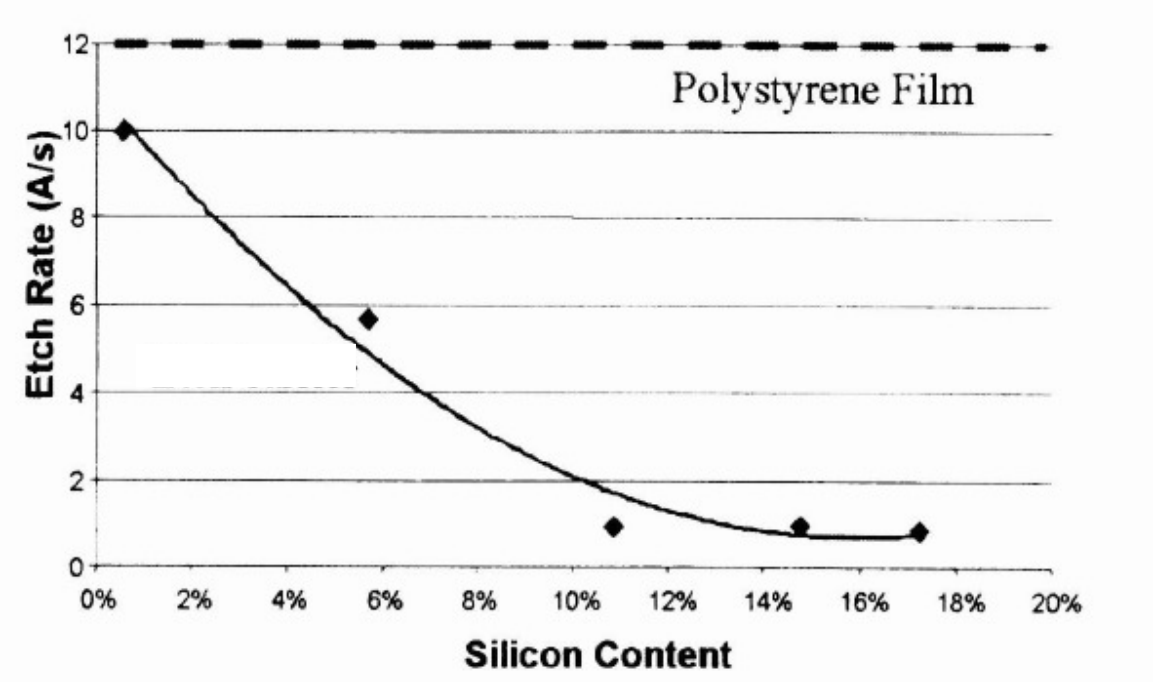

Figure 5.25: Etch rate data from Colburn on various Si wt% formulations.[47]

5.16 SILICON CONTAINING MONOMERS

Being limited by the functional group tolerance of anionic polymerizations, the most synthetically accessible silicon source was trimethyl silane. This group was incorporated into styrene via a Grignard reaction with commercially available 4-bromostyrene as shown in Scheme 5.5 to yield TMS-Sty (5.6). Additionally, a TBDMSO styrene derivative (TBDMSO-Sty) was synthesized via Scheme 5.6. It started with the silylation of commercially available 4-hydroxy benzaldehyde to yield 5.7.[48] This aldehyde was subjected to a Wittig reaction yielding monomer 5.8.[49]

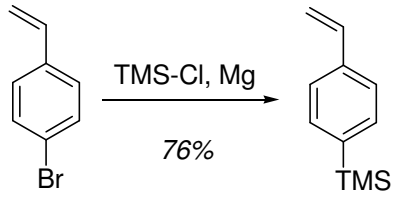

5.6

Scheme 5.5: Synthesis of TMS-Sty 5.6.

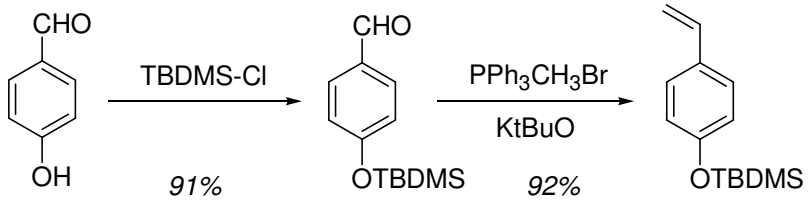

5.7 5.8

Scheme 5.6: 2-step synthesis of TBDMSO-Sty 5.8.

Desiring a non-styrene derivative with a lower boiling point for easier purification, isoprene derivative 5.9 (TMSI) was synthesized via a Kumada coupling according to a report by Sakurai (Scheme 5.7).[50]

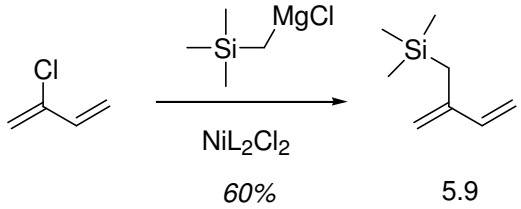

5.9

Scheme 5.7: Synthesis of TMSI 5.9.

5.17 O_2 RIE STUDY

Before expending the time and effort required for BC synthesis, the O_2 RIE properties of a variety of silicon containing monomers were investigated. Homopolymers of styrenes 5.6 and 5.8 were synthesize with AIBN. Films of these polymers were coated

along with PMMA and PS reference. Figure 5.26 displays the normalized etch depth vs time when these films were subjected to typical O_2 RIE conditions. As expected, PMMA and PSt are completely removed within four minutes while P(TMS-Sty) and P(TBDMSO-Sty) have over 92% of the original film remaining.

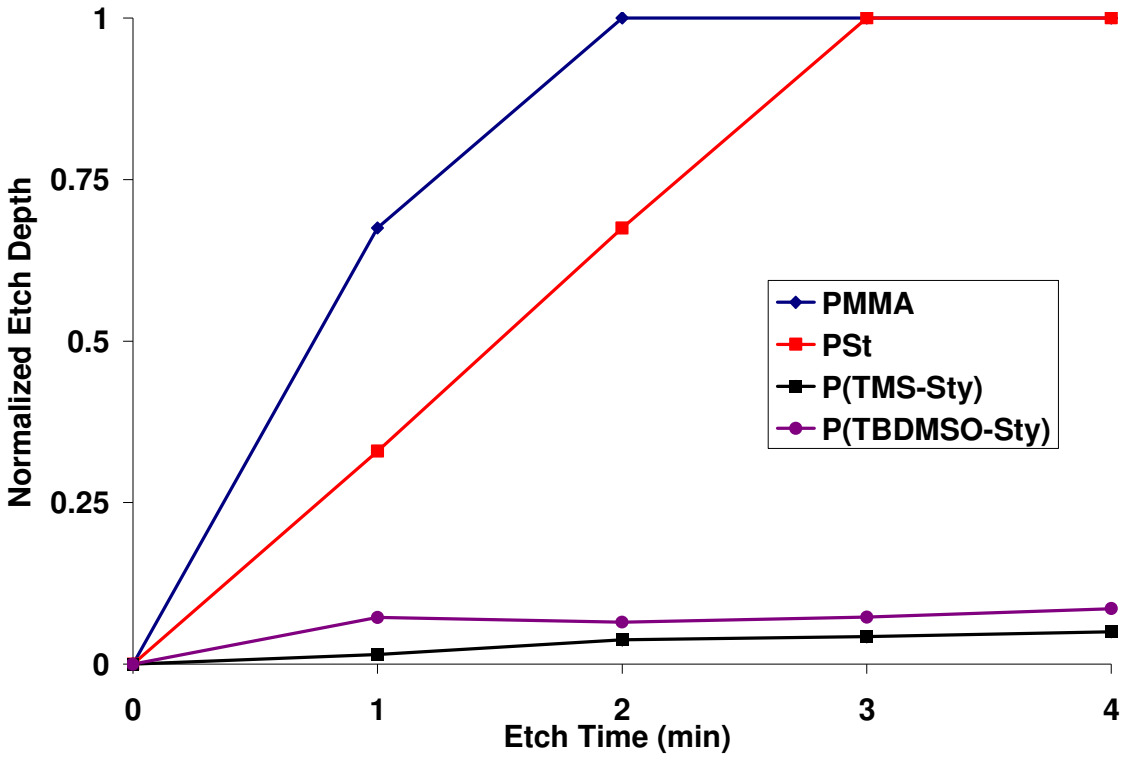

Figure 5.26: Etch study of poly(hydrocarbons) (red and blue) and silicon containing polymers (black and purple).

5.18 CF_4 Etch Rate Study

In a 2007 report describing work related to self-assembled polystyrene-block-polydimethylsiloxane (PS-b-PDMS) features, Jung noted that a wetting layer formed upon annealing.[41] This was attributed to the large surface energy difference between PS

and PDMS. To image the features, a short CF_4 etch was done to remove this wetting layer. Figure 5.27 shows images from this report.

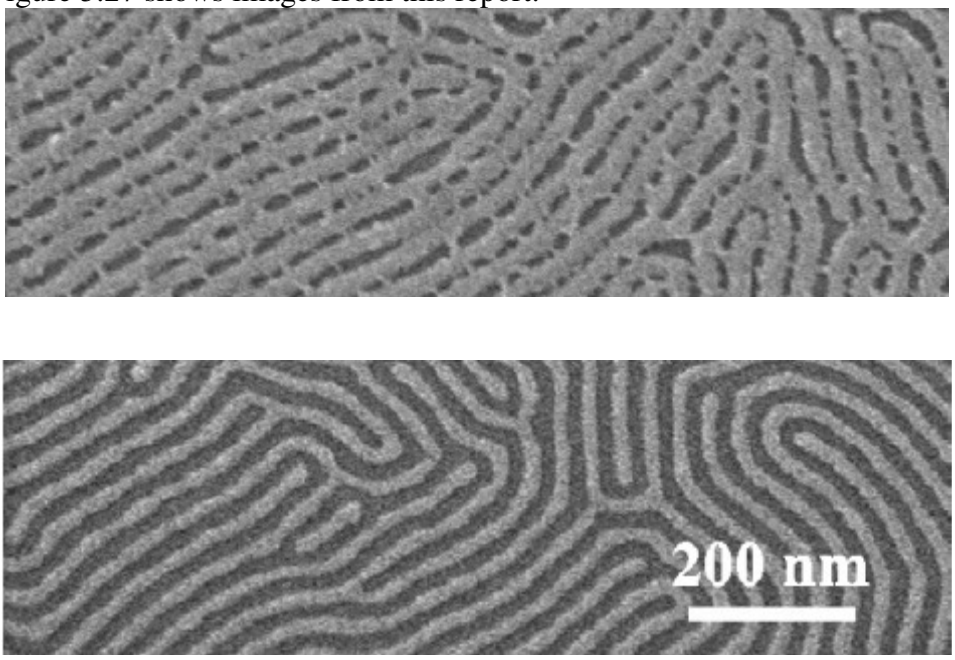

Figure 5.27: SEM images of annealed PS-b-PDMS before CF_4 etch (top) and after (bottom).[41]

Once the CF_4 plasma has etched through the wetting layer, it will come in contact with self-assembled BC cylinders. If the CF_4 selectively etches one block, then the resolution and aspect ratio of the cylinders in the final features will be negatively affected as shown in Figure 5.28.

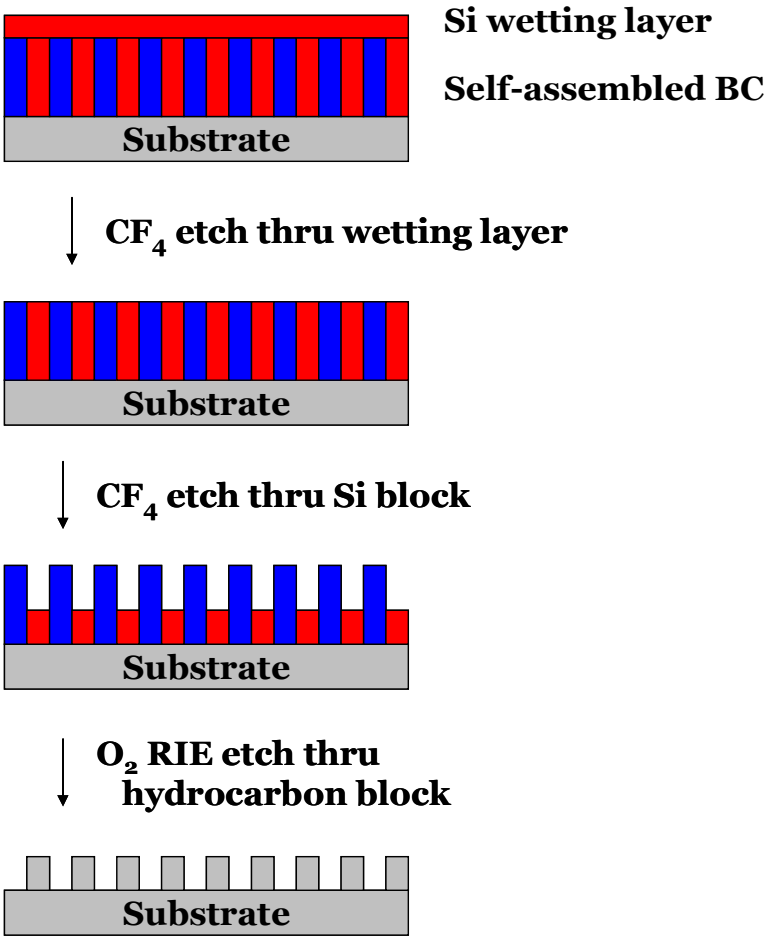

Figure 5.28: Cross-section of self-assembled BC during CF_4 and O_2 RIE etches.

Desiring a more quantified result regarding CF_4 etch rates of polyhydrocarbons and silicon containing polymers, a study was conducted on films of PSt and P(TBDMSO-Sty). Figure 5.29 displays the etch depth versus time for these two films, and the slope of the data corresponds to the etch rate. Under the conditions, PSt has an etch rate of 0.65 nm/sec while P(TBDMSO-Sty) had an etch rate of 0.69 nm/sec. Both lines show a high linear correlation. From these studies it was concluded that there was no appreciable etch rate differences between polyhydrocarbons and the silicon-containing polymers. This infers a CF_4 etch will remove a silicon wetting layer, but it will not preferentially remove

one block once through the wetting layer. This is important because if the CF_4 etch selectively removed the Si block, feature profiles and resolution could be negatively effected.

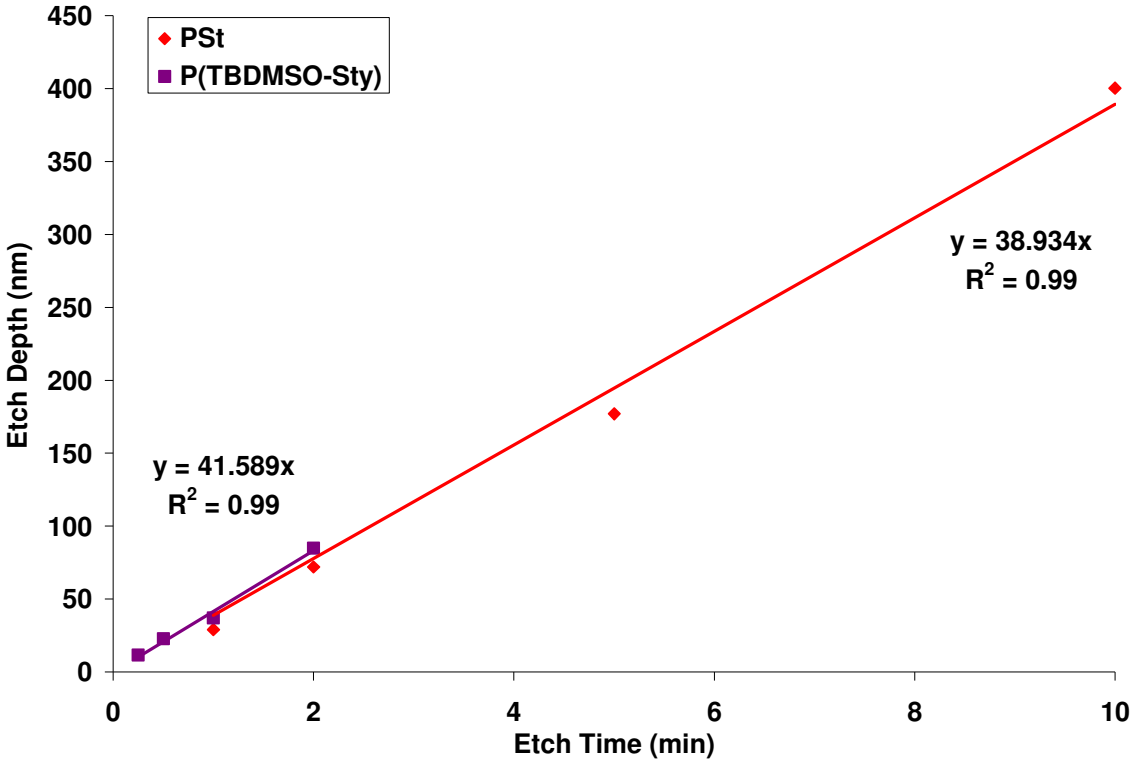

Figure 5.29: CF_4 etch study of PSty (red) and P(TBDMSO-Sty) (purple).

5.19 SILICON CONTAINING BLOCK COPOLYMERS

5.19.1 Styrene Monomers

The initial target for a silicon containing BC was P(TMS-Sty)-b-PMMA, however despite extensive purification, a living P(TMS-Sty) anion has not yet been achieved. Whether in THF at -78 °C or cyclohexane, the orange reaction solution would gradually turn colorless indicating no living anions. The isolated polymer would have a MW at

least three times greater than that intended and a PDI above 2. These observations point to an impurity that was not removed during the distillations and a termination reaction. Given the control of PS consistently achieved, a hypervalent silicon has been postulated as a possible source of this side reaction.

TBDMSO-Sty was then synthesized due to the larger steric bulk around the silicon and the lack of a Si-phenyl bond. Unfortunately, polymerization of it turned out to be very similar to TMS-Sty. Although control of the MW and PDI of this polymerization were much improved, there was still a side reaction that caused living chains to terminate.

5.19.2 Anionic Synthesis of PS-b-PTMSI

Due to the problems associated with styrene derivatives, monomer 5.9 was synthesized. After purification over nBuLi, isoprene 5.9 was successfully added on to a living PS anion in cyclohexane (Scheme 5.8). ^{1}H-NMR analysis showed a molar ratio of 83:17 Sty:TMSI by comparing the integrals of the aromatic peaks (red dot) to that of the vinyl peak assigned to the TMSI block (green dot) (Figure 5.30). The ratio of the vinyl peak (green dot) to the TMS peak (blue dot) was 1:9 indicating that there was no appreciable decomposition of the TMS group during the polymerization. Using the density of PS previously reported in the literature[12], and assuming the density of PTMSI is similar to that of polyisoprene (PI), the volume fraction of PS is approximated at 0.77. Small changes in the density of PTMSI produce relatively small changes in the volume fraction of PTMSI. According to existing literature[51], P(S-b-I) with f_{PI} = 0.24 produces cylinders of PI, therefore a cylindrical morphology is expected. GPC determined the PDI of the PS aliquot and PS-b-PTMSI to be 1.00 and 1.02, respectively with a total M_n of 65.7 kDa (Figure 5.31). DSC traces of the polymer showed two T_gs (Figure 5.32): one at 103 °C, which is consistent with reported PS values,[52] and another at -34 °C, which is

assumed to that of the PTMSI block. The reported T_g for PI is -73 °C,[52] but due to the steric bulk of the TMS group, this number seems to be reasonable.

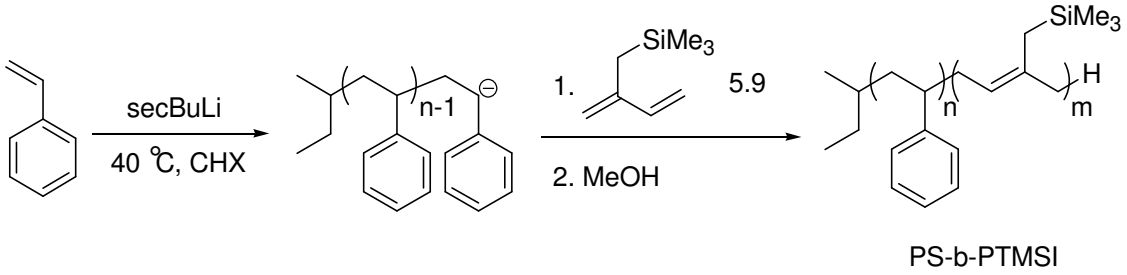

Scheme 5.8: Anionic synthesis of PS-b-PTMSI.

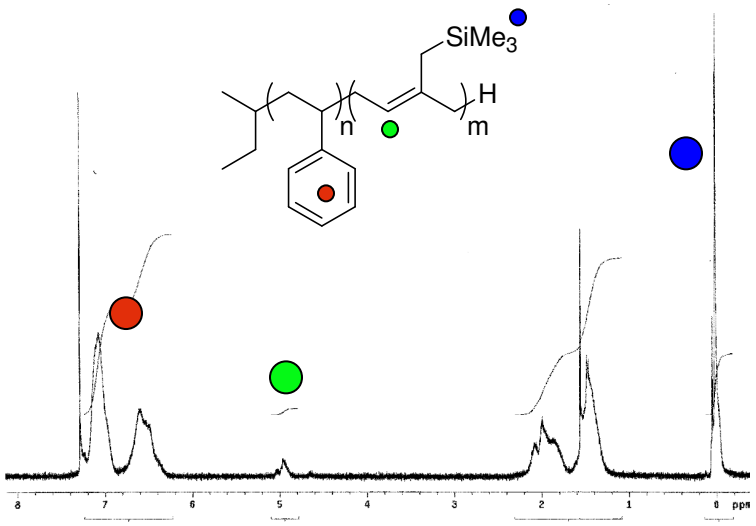

Figure 5.30: ^{1}H-NMR of PS-b-PTMSI.

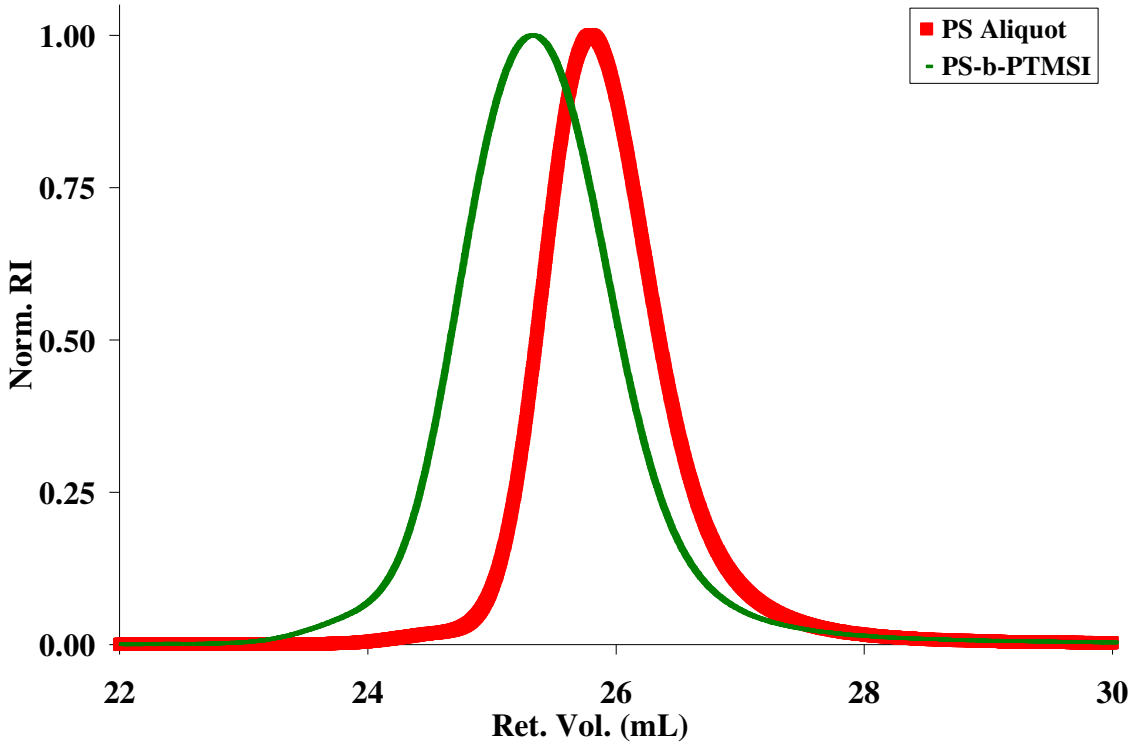

Figure 5.31: GPC chromatograms of PS aliquot (red) and PS-b-PTMSI (green).

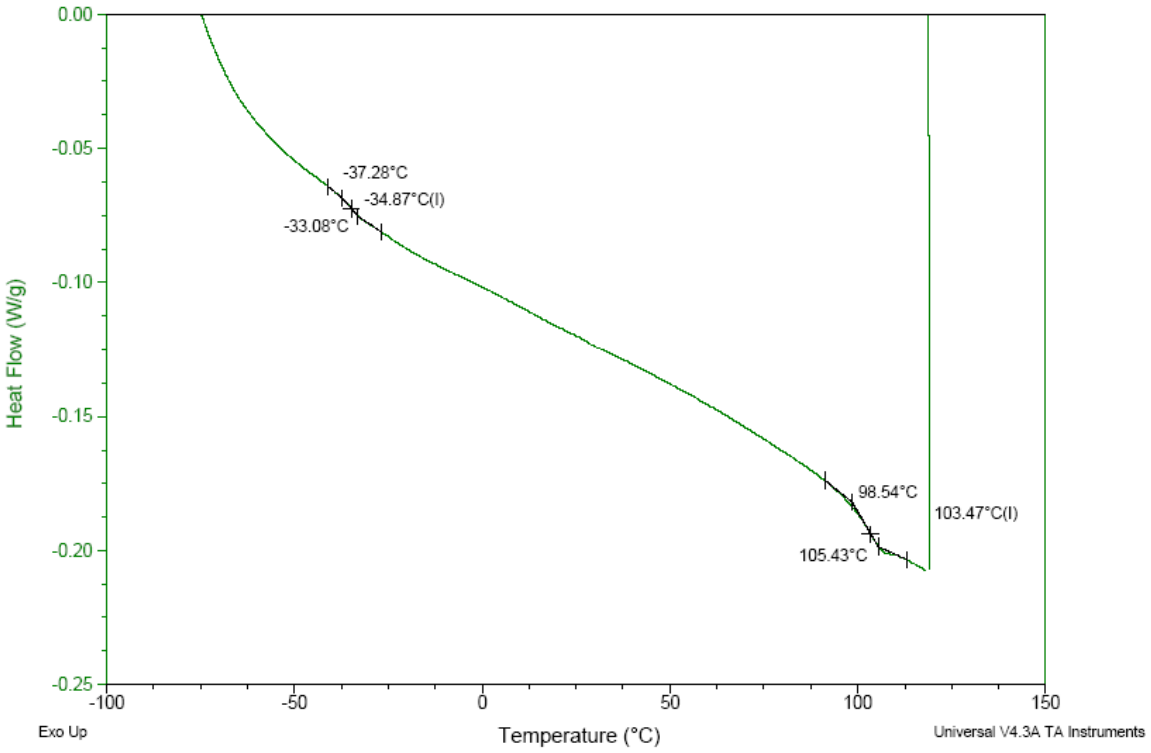

Figure 5.32: DSC trace of PS-b-PTMSI.

SAXS diffraction data was also collected on this polymer, and the resulting diffraction pattern is shown in Figure 5.33.

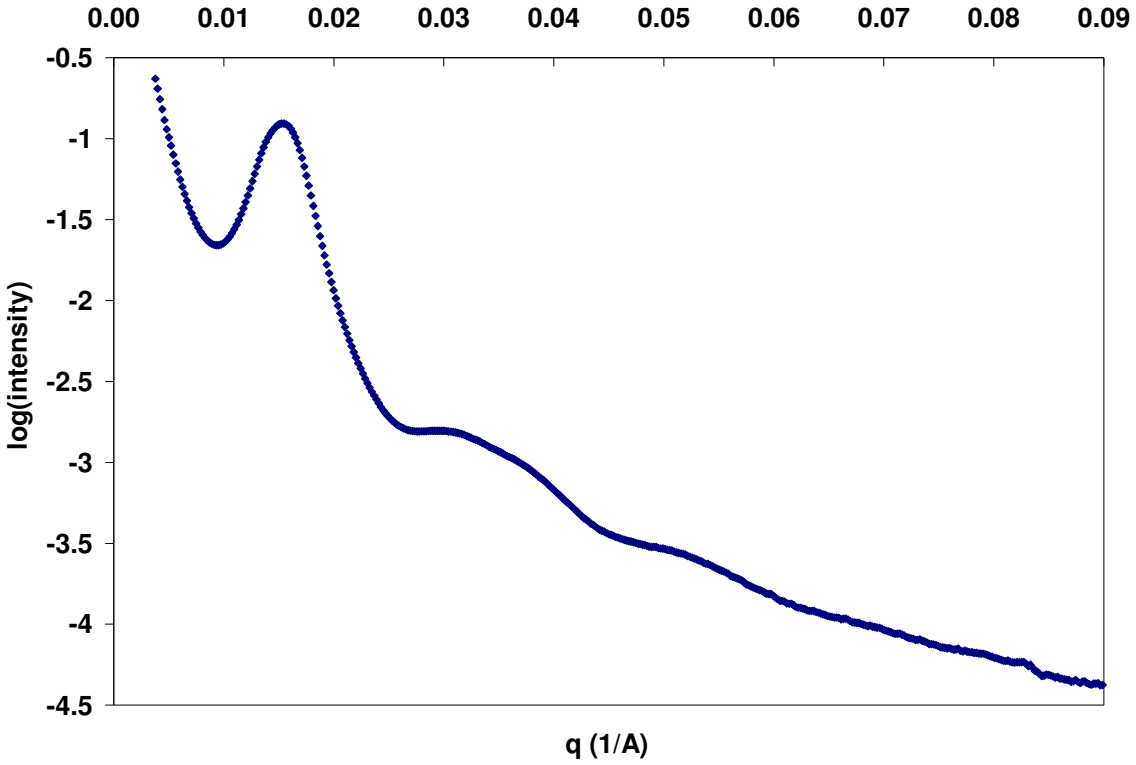

Figure 5.33: SAXS diffraction pattern on PS-b-PTMSI at 170 °C.

Bulk ordering is readily apparent with a q* value of 0.0157, and this corresponds to a domain spacing of 40 nm. Unfortunately, the diffraction peaks cannot be assigned to a known morphology. This can be due to several reasons including oxidative degradation, short annealing time, and metastable morphologies. Work is ongoing to account for these factors.

5.19.2.2 Thermal Studies of PS-b-PTMSI

Polyisoprene is known to be thermally unstable due to oxidative degradation of the olefin.[53] To investigate this issue with PS-b-PTMSI, samples were subjected to various temperatures under different atmospheres.

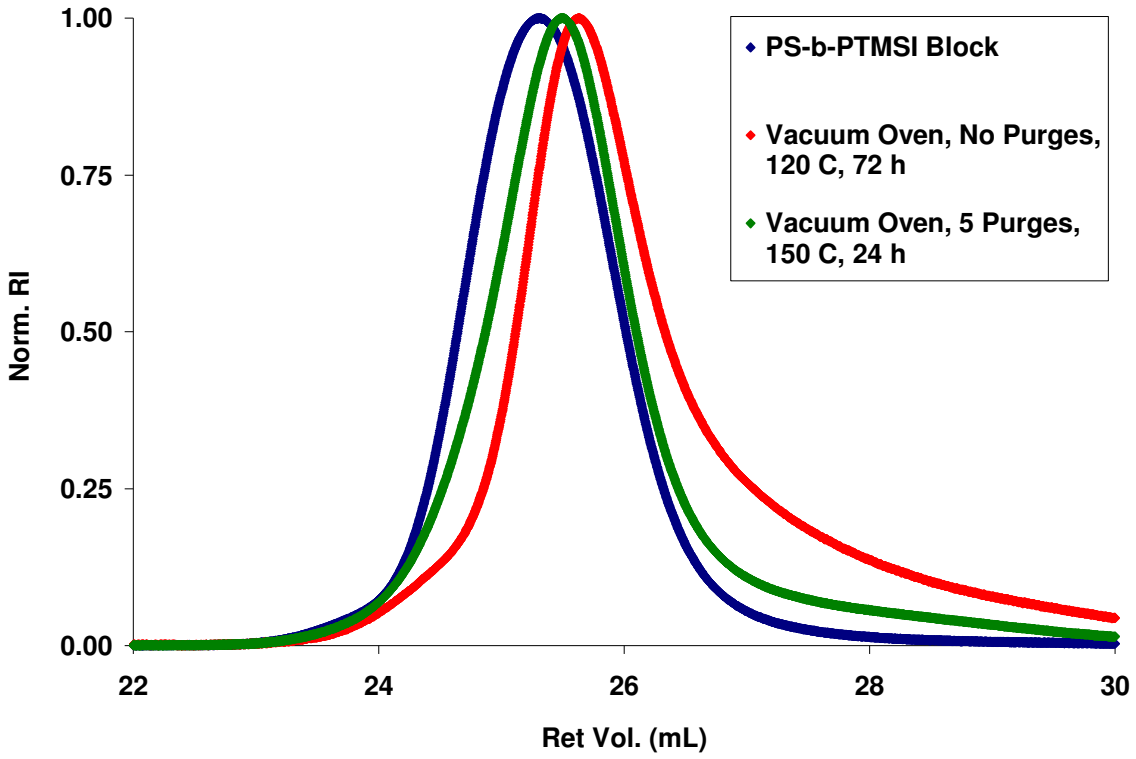

Figure 5.34: GPC traces of thermally annealed PS-b-PTMSI.

Figure 5.34 shows GPC chromatograms of the resulting materials. PS-b-PTMSI (blue) showed significant decomposition as evidenced by generation of a long low molecular weight tail when heated in a vacuum oven to 120 °C for 72 h (red). This was discouraging given the annealing temperature needs to be well above the T_g of PS to provide enough energy to induce alignment. To thoroughly remove oxygen from the atmosphere, the vacuum oven was taken through five pump purge cycles. This reduced the extent of decomposition, but degradation was still evident in the GPC when a sample was heated to 150 °C for 24 h(green).

5.19.2.3 Hydrogenation of PS-b-PTMSI

To remove the sensitivity of thermally induced oxidative degradation, reduction of the double bonds in the TMSI block was envisioned via hydrogenation. A tri-block copolymer of S-I-S provided by Prof. Christopher J. Ellison was studied as a model system. A ^{1}H-NMR spectrum of this material is shown in Figure 5.35, and from the integrals of the aromatic and vinyl regions, the ratios of styrene to isoprene as well as 1,4- to 3,4- isoprene addition were determined. The isoprene double bonds were hydrogenated with Wilkinson's catalyst as previously reported.[53] A ^{1}H-NMR spectrum of the resulting material, commonly referred to as S-PEP-S because the isoprene block can be viewed as an alternating copolymer of propylene-ethylene, is shown in Figure 5.36 that displays over 95% reduction of the vinyl peaks. Removal of BHT inhibitor by dissolving and re-precipitating the S-I-S proved to be essential for this reaction as well as degassing the dissolved polymer solution and pump-purging the Parr reactor. Unfortunately, reduction of PS-b-PTMSI was never observed despite increasing the catalyst loading, time, temperature, and hydrogen pressure.

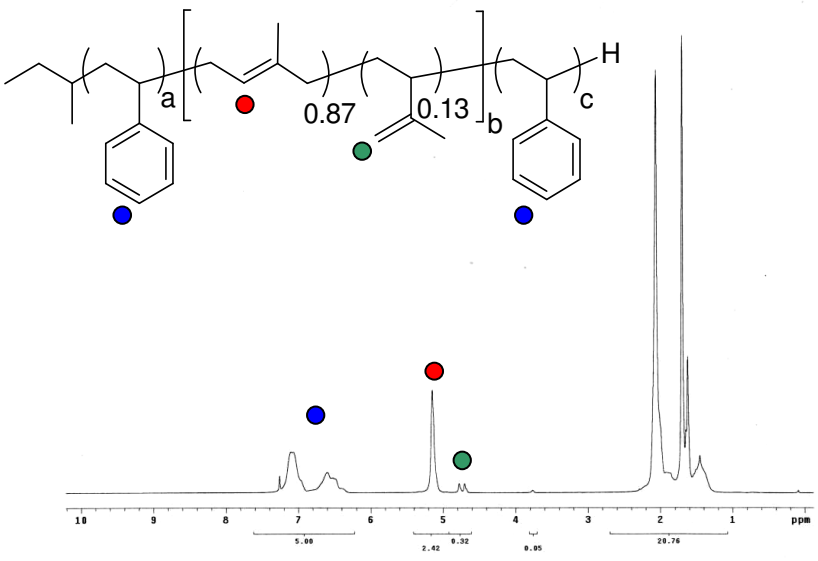

Figure 5.35: ^{1}H-NMR of S-I-S.

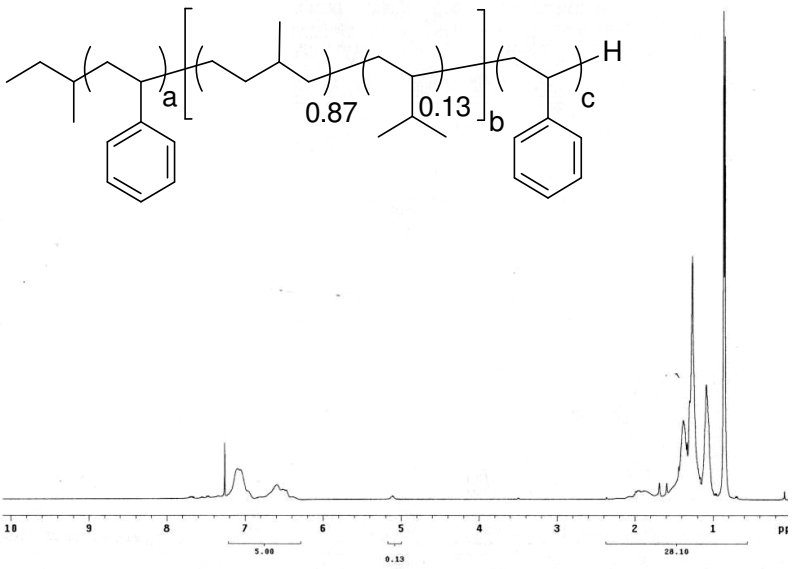

Figure 5.36: ^{1}H-NMR of S-PEP-S.

Fortunately, a sample of a non-commercially available Dow catalyst that is reported to exhaustively reduce styrene-isoprene polymers to their saturated analogs was received from Prof. Frank S. Bates of the University of Minnesota. Once again, S-I-S was used as a model system, and fully reduced product, commonly denoted C-PEP-C, was recovered when the polymer was dissolved in degassed cyclohexane with 10 wt% catalyst and placed under 600 psi of H_2 at 170 °C for 24 h. ^{1}H-NMR analysis displayed complete consumption of aryl and vinyl peaks (Figure 5.37).

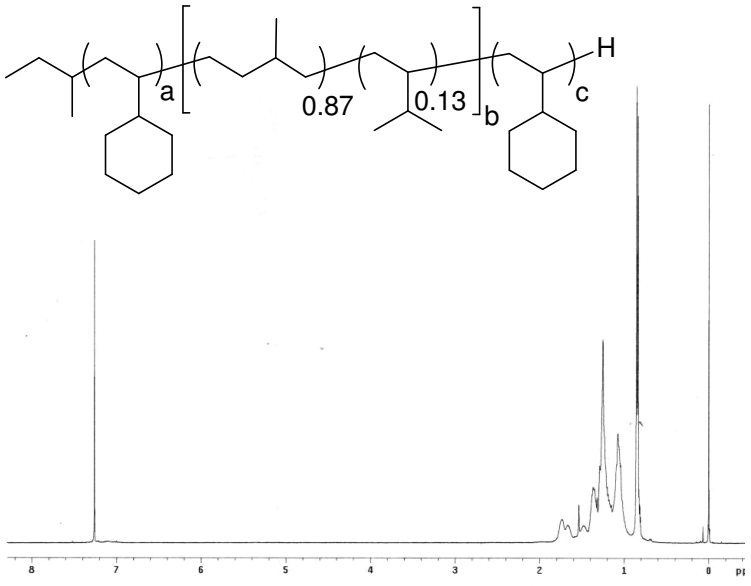

Figure 5.37: ^{1}H-NMR spectrum of C-PEP-C.

When submitted to the same reaction conditions that fully reduced S-I-S, PS-b-PTMSI was recovered without any reduction in aryl or vinyl protons via ^{1}H-NMR analysis. After increasing the catalyst loading, time, and hydrogen pressure, material was recovered that showed a 79% reduction of aromatic peaks and a 55% reduction of vinyl peaks by normalizing to the TMS group (Figure 5.38). Although this material would still be sensitive to oxidative degradation, this route is continuing to be pursued.

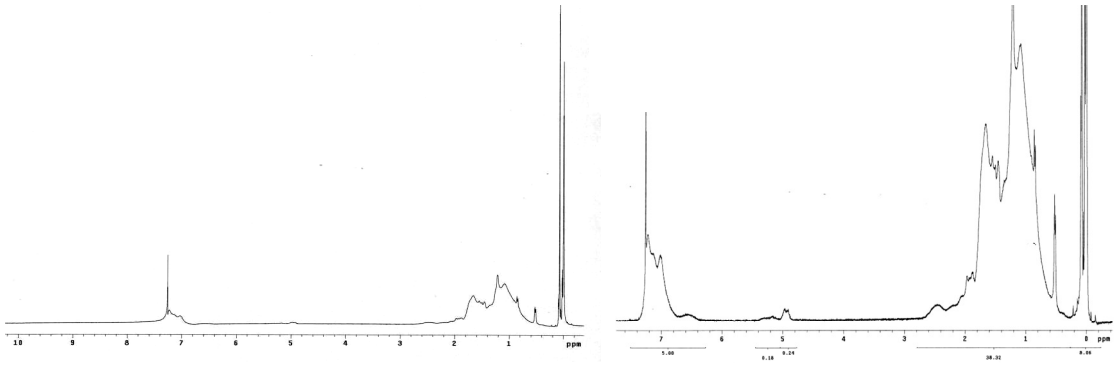

Figure 5.38: ^{1}H-NMR spectrum of partially reduced PS-b-PTMSI (left) and expanded spectrum (right).

5.19.3 Annealing PS-b-PTMSI

The surface energy of PS-b-PTMSI was determined to be 38.0 dyne/cm by contact angles. This lower energy is presumably due to the trimethylsilyl block. Films were coated on a variety of chlorosilane surfaces and PXSTs. Surface treatments were chosen to match the surface energy of the block and the chlorosilane/PXST. Due to the thermal instability of PS-b-PTMSI, all thermally annealed films did not show any features.

To remove the likelihood of oxidative degradation, films were annealed under saturated atmospheres of standard organic solvents: THF, toluene, and acetone. To this point, no features have been observed on films, but this technique is not well understood nor do reports give exact experimental conditions.[19,22,54,55] Therefore, this route will continue to be pursued.

5.19.4 Anionic Synthesis of PS-b-P(MTMSMA)

Fortunately, a silicon containing methacrylate (MTMSMA) is commercially available from Gelest, Inc. Due to its higher MW and boiling point compared to MMA,

the purification proved to be difficult. During the last distillation to remove alcohols, trioctylaluminum initiated MTMSMA polymerization. Attempts to remove alcohols by sodium hydride also led to polymerization. It was determined that alcohols could be removed when the monomer was passed through an alumina plug, and then subjected to freeze, pump, thaw cycles and distillation over calcium hydride. This monomer was successfully incorporated PS-b-P(MTMSMA) (Scheme 5.9).

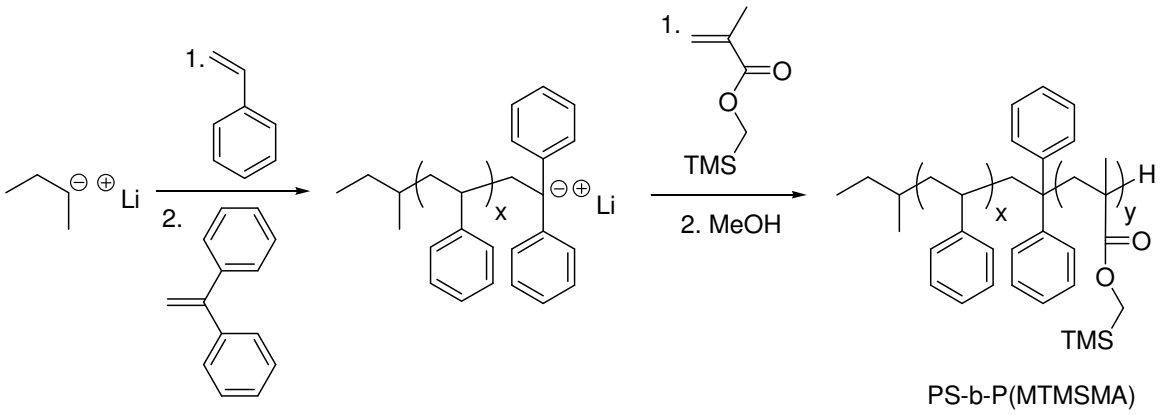

Scheme 5.9: Anionic synthesis of PS-b-P(MTMSMA).

^{1}H-NMR analysis showed a molar ratio of 73:27 Sty:MTMSMA by comparing the integral ratio of the aromatic peaks (red dot) to that of the oxy-methylene peak (green dot). (Figure 5.39). Additionally, the ratio of the oxy-methylene peak (green dot) to the TMS peak (blue dot) was 2:9 indicating there was no significant decomposition of the TMS group during polymerization. Using the density of PS previously reported in the literature[12] and assuming the density of PMTMSMA is similar to that of PMMA, the volume fraction of PS is approximately 0.66. Similarly to PS-b-PTMSI, small changes in the assumed density of P(MTMSMA) produce relatively small changes in the its volume fraction. According to the literature,[11] this volume fraction should yield a cylindrical morphology. GPC determined the PDI of the PS aliquot and PS-b-PTMSI both to be

1.17. The M_n of the PS aliquot and final precipitated block was 60.0 and 75.2 kDa, respectively (Figure 5.40).

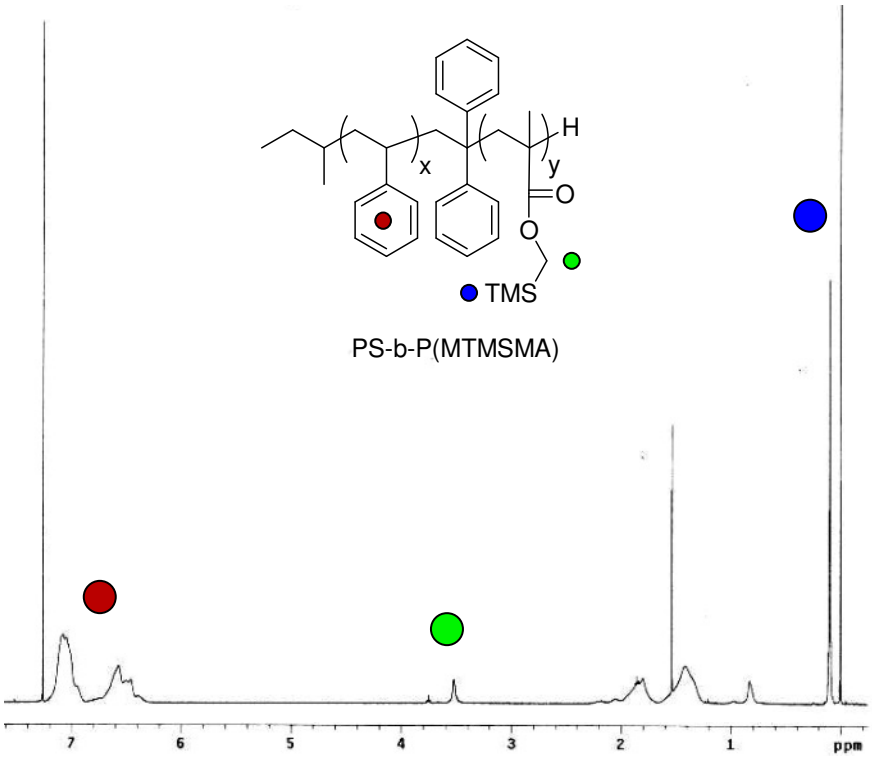

Figure 5.39: ^{1}H-NMR of PS-b-P(MTMSMA).

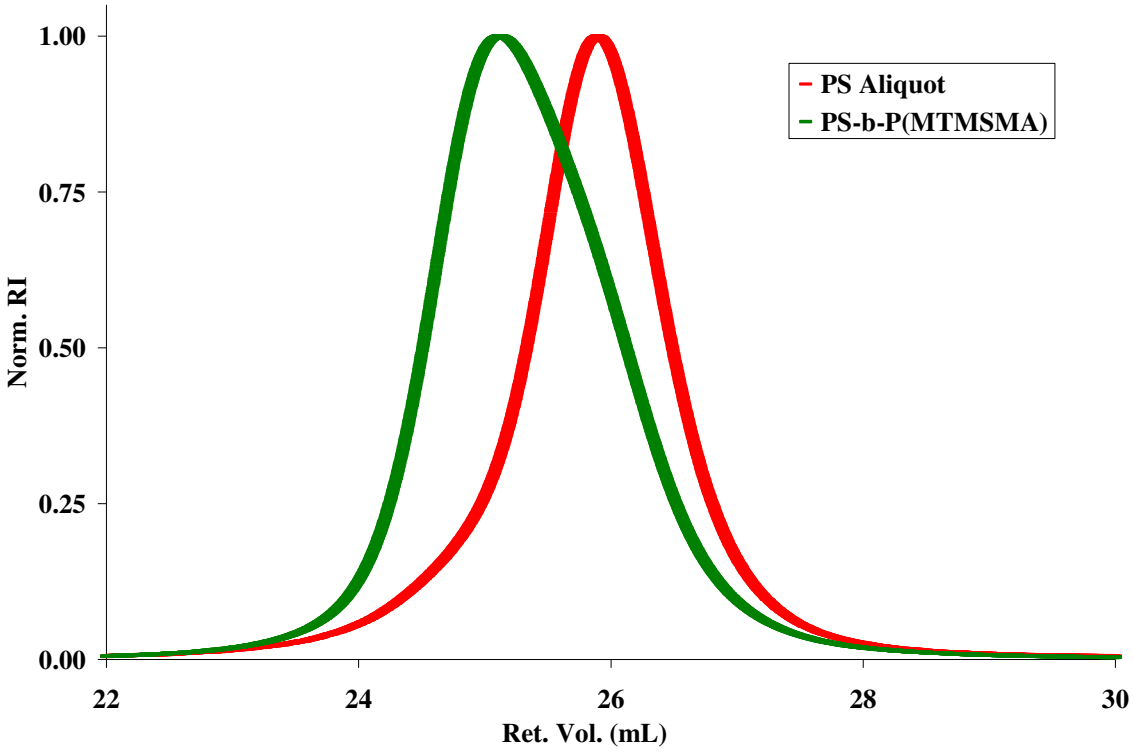

Figure 5.40: GPC chromatograms of PS aliquot (red) and PS-b-P(MTMSMA) (green).

SAXS data were collected on this polymer at 170 °C. The resulting diffraction pattern is shown in Figure 5.41. It shows bulk ordering, and the peak assignments are shown in Table 5.5. While the peaks are quite broad, there is good agreement of the $\sqrt{4}$ peak, and this is indicative of hexagonally packed morphology. The predicted domain spacing is 50 nm.

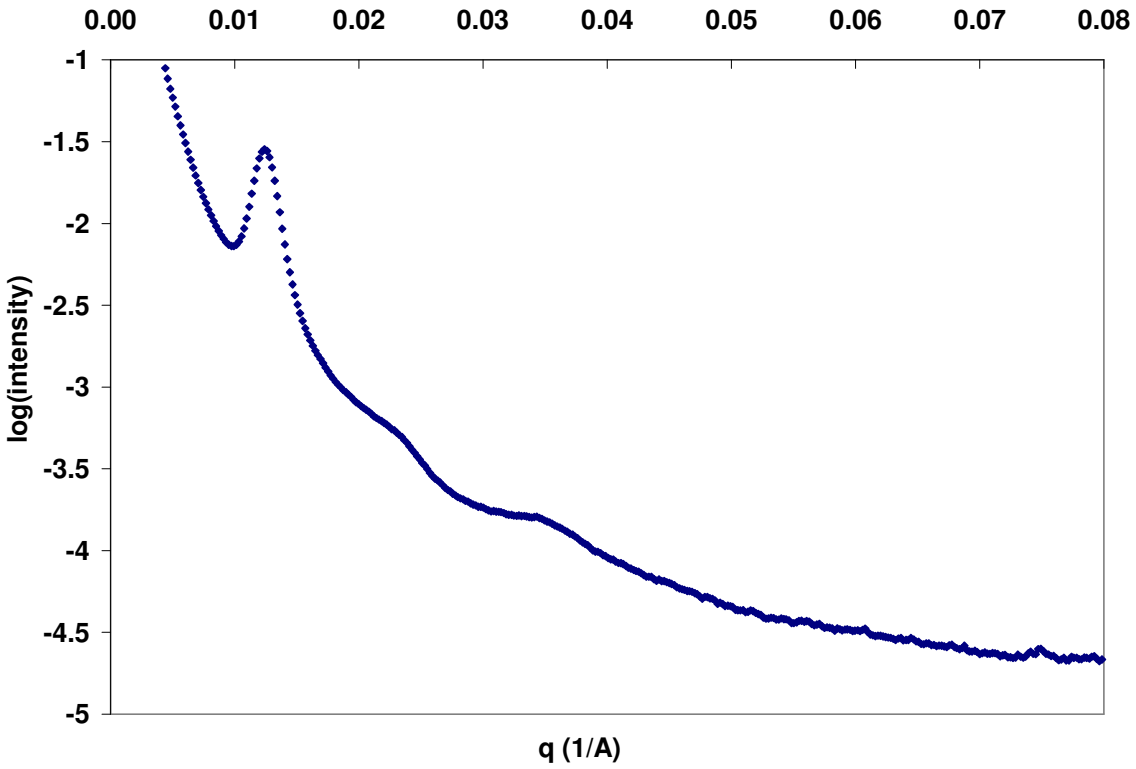

Figure 5.41: SAXS diffraction pattern of PS-b-PMTMSMA at 170 °C.

Table 5.5: SAXS peak assignment of PS-b-PMTMSMA at 170 °C.

q*	0.0126
domain spacing (nm)	50.0
peak 1	0.0231
peak 1/q*	1.8333
root 3	1.7321
peak 2	0.0249
peak 2/q*	1.9762
root 4	2.0000
peak 3	0.0345
peak 3/q*	2.7381
root 9	3.0000

5.19.5 Annealing PS-b-PMTMSMA

The surface energy of this polymer was determined to be 31.2 dyne/cm. This was much lower than PS-b-PMMA (45.8 dyne/cm) presumably due to the trimethyl silyl groups. Films were coated on PXSTs, and after thermal annealing, they showed classical dewetting behavior.[20,56]

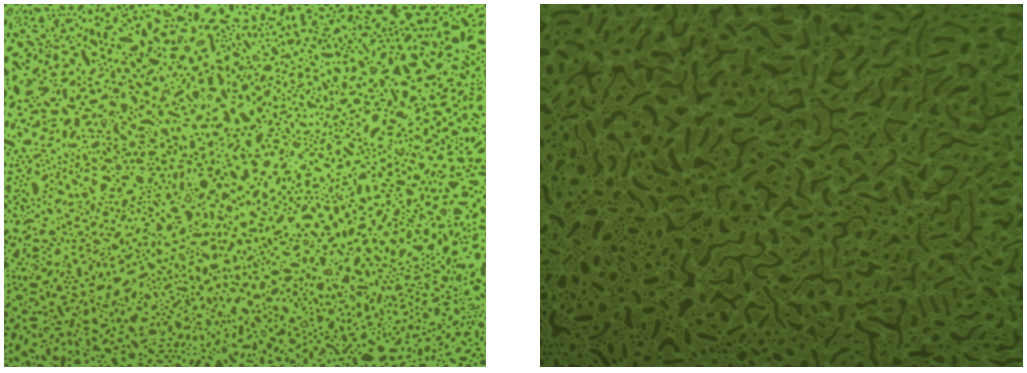

Figure 5.42: Optical microscope images of PS-b-PMTMSMA dewetting on PXST-Cl at 50x magnification (left) and PXST-OMe at 100x magnification (right).

Fortunately, films on decyl chlorosilane treated surfaces did not show any dewetting, and they were investigated via AFM. No features were found under standard 170 °C overnight annealing conditions, but it is known in the literature that higher temperatures and longer annealing times gives the film more energy to fix any frustrations. Therefore, the thermal stability of PS-b-PMTMSMA was investigated. Figure 5.43 is TGA data collected on this material, and it shows that the polymer has a significant decomposition rate at 230 and 250 °C. However, the polymer appears to be stable at 170 and 200 °C on this time scale.

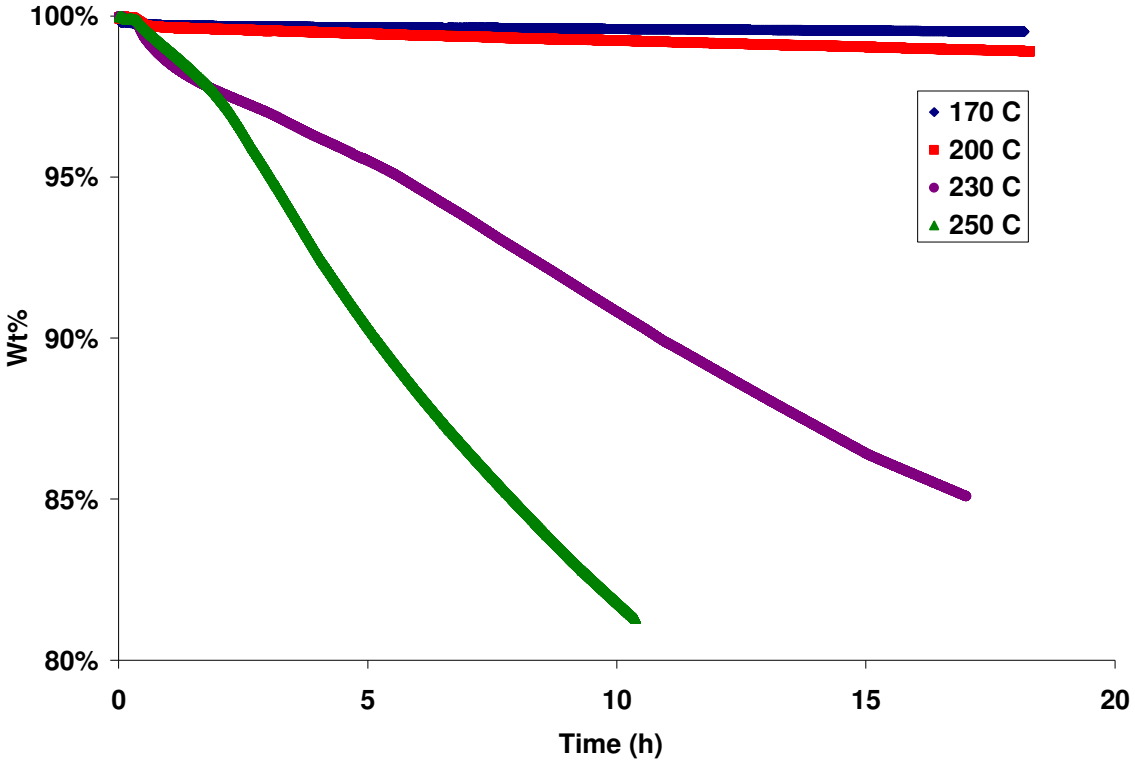

Figure 5.43: TGA data of PS-b-PMTMSMA at various temperatures.

With this data, films of various thicknesses were annealed at 200 °C in a vacuum oven for 5 days. Despite the higher temperatures and longer time, films did not show any bulk features. The films were consistently flat leading us to believe that dewetting was not a problem, so thermal annealing was abandoned as a route towards self-assembling this BC.

As discussed earlier, solvent annealing techniques are not well understood nor are the exact experimental details reported. Therefore initial attempts consisted of annealing BC films with a saturated atmosphere of a given solvent for various times. After optimizing variables such as solvent, time, film thickness, and surface treatment, AFM images were collected that displayed bulk ordering. The experimental setup involves a

standard glass petri dish and a twenty mL vial cap full of the solvent as shown in Figure 5.44.

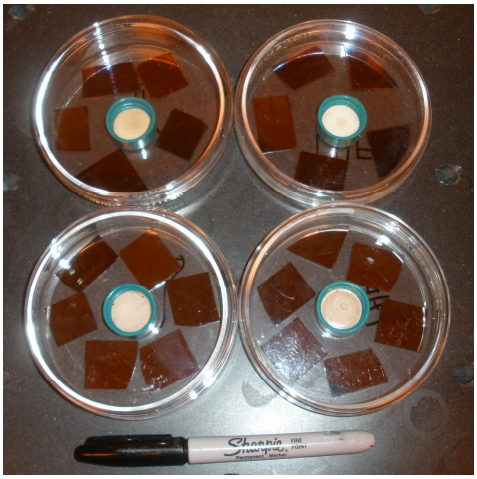

Figure 5.44: Picture of solvent annealing setup.

When a 15 nm films was annealed overnight with THF, parallel features were observed. Satisfyingly, the L_0 of these images matched that described by the SAXS data. Although this morphology did not cover the entire film surface like that observed with cylindrical and lamellar PS-b-PMMA, these are the first AFM images of this BC. As shown in AFM height image (Figure 5.45), the features assemble in the thinner regions of the film. The amplitude and phase images, indicative of the material's modulus, display adequate contrast of the parallel features.

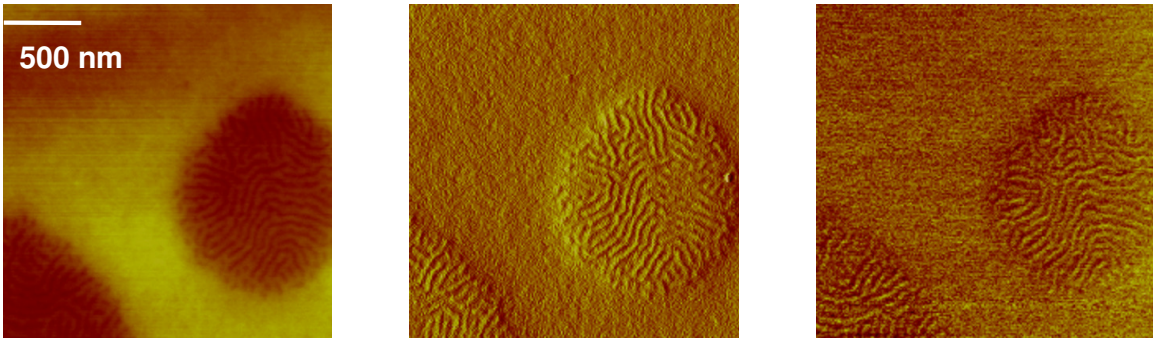

Figure 5.45: AFM images of THF annealed PS-b-PMTMSMA height (left), amplitude (middle), and phase (right).

When a similar film was annealed overnight in a saturated atmosphere of acetone, hexagonally packed perpendicular cylinders were observed (Figure 5.46). Although not perfectly packed, the height, amplitude, and phase images clearly display bulk ordering. With a domain spacing of 50 nm, this represents an areal density of 30 Gdots/in^2. Interestingly, the cylinders are physically raised from the surface as shown in Figure 5.47. This phenomenon has been reported with other sub-L_0 films by.[57]

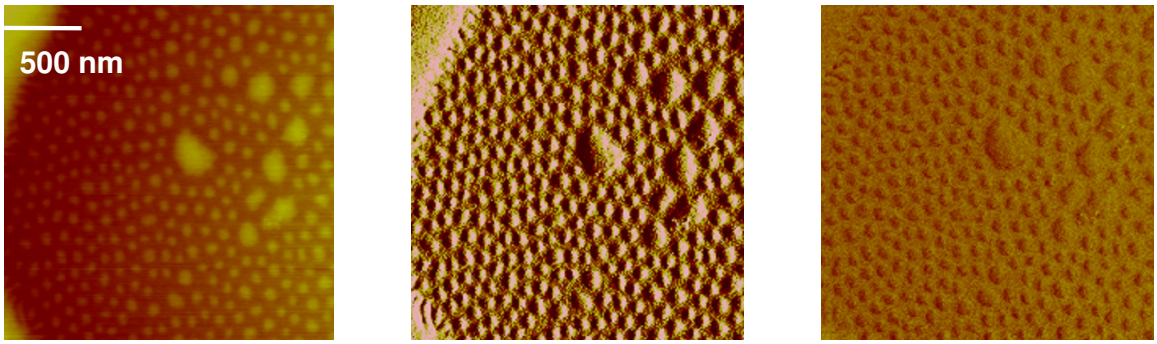

Figure 5.46: AFM images of acetone annealed PS-b-PMTMSMA height (left), amplitude (middle), and phase (right).

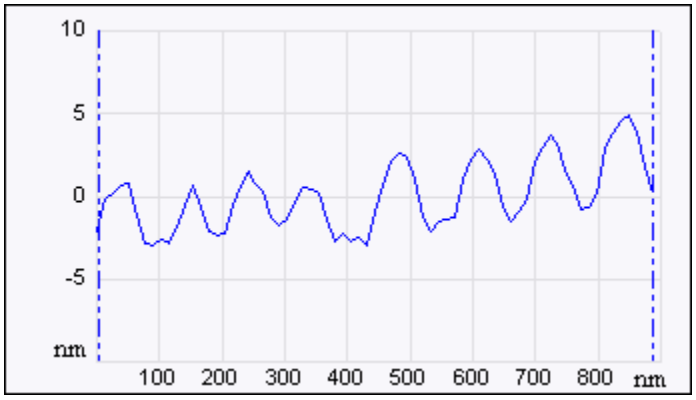

Figure 5.47: Cross-section of height data from AFM of acetone annealed PS-b-PMTMSMA.

5.20 CONCLUSION AND FUTURE WORK

Bit Patterned Media was introduced as the next generation technology for data storage. Nano Imprint Lithography is the only commercially viable technique to produce BPM, but the production of templates is a major concern for full commercialization. To pattern the high densities necessary for BPM, self-assembled block copolymers were chosen to be a cost-efficient method to produce highly regular structures over large areas.

Two techniques were investigated to control the surface energy necessary to achieve perpendicular orientation of BCs. Both commercially available and synthesized chlorosilanes were shown to give a wide range of surface energies. Additionally, a series of copolymers was synthesized with styrene derivatives and benzyl azide groups yielding Polymeric X-linked Surface Treatments.

Cylindrical and lamellar PS-b-PMMA were synthesized via anionic polymerization with excellent control of MW and PDI. Both the chlorosilanes and the aryl substituent of the PXST were shown to affect the process windows for cylindrical perpendicular orientation.

To achieve a 3-D pattern of the hexagonally packed cylinders, three silicon containing monomers were synthesized, and the TMS-isoprene derivative was successfully incorporated into a block copolymer. Although SAXS data was indicative of bulk order, both thermal and solvent annealed films have yet to yield any features via AFM. This is likely due to oxidative degradation of the isoprene block. A commercially available TMS methacrylate analog was successfully incorporated into a block copolymer. The bulk order of the SAXS pattern was confirmed by solvent annealing. Parallel features were observed with THF while acetone yielded perpendicular orientation on bare wafers.

To continue this work, the solvent annealing technique must be optimized to give bulk features over large areas. After a combination of CF_4 and oxygen etches, the 3-D features must be used as a template and display pattern transferring ability. In the larger picture, long range order of these features must be addressed by a patterned substrate. This will guide the cylinders to align and lead to NIL templates for BPM.

5.21 EXPERIMENTAL

General Materials and Methods. All reagents were purchased from Sigma-Aldrich Chemical Co. and used without further purification unless otherwise stated. AP410 and AP310 were purchased from AZ Clariant. THF was purchased from JT Baker. Chloroprene 50 wt% in xylenes was purchased from Pfaltz & Bauer. Cyclohexane was purified with a Pure Solv MD-2 solvent purification system. 4-Chlorobutyldimethylchlorosilane ("chloro"), (Dichloromethyl)dimethylchlorosilane ("dichloro"), 3-Cyanopropyldimethylchlorosilane ("cyano"), and n-Decyldimethyl chlorosilane ("decyl") were purchased from Gelest. 100 mm silicon wafers were purchased from Silicon Quest International.

^{1}H and ^{13}C NMR spectra were recorded on a Varian Unity Plus 400 MHz instrument. All chemical shifts are reported in ppm downfield from TMS using the residual protonated solvent as an internal standard ($CDCl_3$, ^{1}H 7.26 ppm and ^{13}C 77.0 ppm). HRMS (CI) was obtained on a VG analytical ZAB2-E instrument. IR data was recorded on a Nicolet Avatar 360 FT-IR and all peaks are reported in cm^{-1}. LRMS (GC/MS) were obtained on an Agilent 6890N Network GC Systtem and Agilent 5973N Mass Selective Detector.

All molecular weights were measured using an Agilent 1100 Series Isopump and Autosampler, and a Viscotek Model 302 TETRA Detector Platform with 3 I-series Mixed Bed High MW columns. Films were spin coated and baked on a Brewer CEE 100CB Spincoater & Hotplate. Polymer solutions were filtered with 0.20 µm PTFE filters prior to spin coating. Films were spin coated and baked on a Brewer CEE 100CB Spincoater & Hotplate. Film thicknesses were determined with a J.A. Woollam Co, Inc. VB 400 VASE Ellipsometer using wavelengths from 382 to 984 nm with a 70° angle of incidence. Contact angles were measured with a Ramé-Hart, inc. NRL C.A. Goniometer (Model #100-00). A Heraeus Vacutherm Type VT 6060 P from Kendro was used to thermally anneal the films under reduced pressure. A Digital Instruments Dimension 3100 atomic force microscope with NCHR Pointprobe® Non-Contact Mode tips with a force constant of 42 N/m was used to collect AFM images. Glass transition temperatures (T_g) were recorded on a TA Q100 Differential Scanning Calorimeter (DSC).

5.21.1 Surface Treatment with Chlorosilanes

Wafers were etched with piranha (2:1 sulfuric acid:30% hydrogen peroxide) for 1 h and rinsed with DI H_2O. After the wafers were submersed in toluene, the chlorosilane mixture (10 drops) and TEA (5 drops) were added to the bath and helt at rt without stirring for 1 h. Wafers were then rinsed with acetone, IPA, and DI H_2O, then blown dry.

5.21.2 Synthesis of Chlorosilanes

A 25 mL Schlenk tube was loaded with chloro-dimethyl-silane (2 mol eq.), DCM (20 mL), styrene derivative (1 mol eq.), platinum (0)-1,3-divinyl-1,1,3,3-tetramethyldisiloxane complex (3 drops), and a stir bar. After sealing the reaction vessel, the clear solution was stirred overnight at rt. Once the reaction was complete as determined by GC/MS, the slightly yellow reaction mixture was concentrated *in vacuo*. A mixture of α and β isomers were recovered as a clear liquid by distillation.

Chloro-dimethyl-(1-phenyl-ethyl)-silane, 5.1α

bp = 42-44°C, 0.24 torr, 64.7% yield. ^{1}H-NMR ($CDCl_3$) δ ppm = 7.320 (m, 2H), 7.225 (m, 2H), 7.171 (m, 1H), 2.466 (q, *J* = 7.2 Hz, 1H), 1.512 (d, *J* = 7.6 Hz, 3H), 0.365 (d, *J* = 8.0 Hz, 6H), ^{13}C-NMR ($CDCl_3$) δ ppm =142.713, 128.293, 127.445, 125.295, 31.584, 14.368, -0.253. Chloro-dimethyl-phenethyl-silane ***5.1β*** ^{1}H-NMR ($CDCl_3$) δ ppm = 7.320 (m, 2H), 7.225 (m, 2H), 7.171 (m, 1H), 2.797 (m, 2H), 1.240 (m, 2H), 0.445 (s, 6H), ^{13}C-NMR ($CDCl_3$) δ ppm = 143.747, 128.405, 127.840, 125.838, 29.047, 20.833, 1.630; IR (NaCl) cm^{-1} = 3063, 3027, 2961, 2930, 1603, 1496, 1454, 1255, 846, 698; HRMS (CI) = 198.0632 calc, 198.0633 found.

Chloro-[1-(4-chloro-phenyl)-ethyl]-dimethyl-silane, 5.2α

bp = 65-67 °C, 0.25 torr, 80.6% yield. ^{1}H-NMR ($CDCl_3$) δ ppm = 7.249 (d, *J* = 8.8 Hz, 2H), 7.049 (d, *J* = 8.4 Hz, 2H), 2.398 (q, *J* = 7.2, 1H), 1.442 (d, *J* = 7.6 Hz, 3H), 0.342 (s, 3H), 0.311 (s, 3H). Chloro-[2-(4-chloro-phenyl)-ethyl]-dimethyl-silane ***5.2β*** ^{1}H-NMR ($CDCl_3$) δ ppm = 7.249 (d, *J* = 8.8 Hz, 2H), 7.137 (d, *J* = 8.8 Hz, 2H), 2.722 (m, 2H), 1.160 (m, 2H), 0.410 (s, 6H), ^{13}C-NMR ($CDCl_3$) δ ppm = 142.192, 131.500, 129.201, 128.472, 28.482, 20.751, 1.645; IR (NaCl) cm^{-1} = 2959, 2929, 1491, 1407, 1093, 1060, 1014, 808, 784; HRMS (GC/CI) = 232.0242 calc, 232.0241 found, 232.0242 calc, 232.0235 found.

Chloro-[1-(4-bromo-phenyl)-ethyl]-dimethyl-silane, 5.3α

bp = 79-82 °C, 0.3 torr, 63.4% yield. ^{1}H-NMR ($CDCl_3$) δ ppm = 7.399 (d, *J* = 8.4 Hz, 2H), 6.994 (d, *J* = 8.4 Hz, 2H), 2.383 (q, *J* = 7.6, 1H), 1.438 (d, *J* = 7.6 Hz, 3H), 0.341 (s, 3H), 0.309 (s, 3H). Chloro-[2-(4-bromo-phenyl)-ethyl]-dimethyl-silane ***5.3β*** ^{1}H-NMR ($CDCl_3$) δ ppm = 7.399 (d, *J* = 8.4 Hz, 2H), 7.084 (d, *J* = 8.0 Hz, 2H), 2.704 (m, 2H), 1.156 (m, 2H), 0.409 (s, 6H), IR (NaCl) cm^{-1} = 2956, 2928, 1487, 1254, 1072, 1011, 802.

5.21.3 PXST Synthesis

poly(5.4-R) and poly(5.5-R)

In a procedure adopted from Hawker et al.[29], a substituted styrene (20 mmol) and vinyl benzyl chloride (0.62 mmol) were radically copolymerized in refluxing THF (20 mL) for 48 h with enough AIBN to obtain a theoretical MW of 25 kDa. Once poly(6.4-R) was precipitated in 0 °C MeOH, filtered, and dried *in vacuo*, the mol ratio of substituted styrene to vinyl benzyl chloride was determined by ^{1}H-NMR. Taking into account this ratio and the M_n as determined by GPC, poly(6.4-R) (1.0 g) and sodium azide (3 equiv/BnCl) were dissolved in DMF (20 mL) with THF (5 mL) and stirred overnight at rt. The polymer was precipitated in MeOH, filtered, re-dissolved in THF (10 mL), and stirred with H_2O (1 mL) to remove any unreacted salts. Finally, the polymer was isolated by precipitation in 0 °C MeOH, filtered, and dried *in vacuo* to yield white powder poly(6.5-R). Typical yields over these two steps were 50%; IR (KBr)≈2100 cm^{-1}. Complete characterization is shown in Table 5.2.

Trimethyl-(4-vinyl-phenyl)-silane, 5.6

A 500 mL RBF was charged with freshly ground Mg (5.3 g, 216.4 mmol), 1-chloro-4-vinyl-benzene (13.0 mL, 108.2 mmol), chlorotrimethyl silane (27.4 mL, 216.4 mmol), THF (130 mL), and a stir bar. After addition of a catalytic amount of

dibromoethane, the reaction was stirred overnight at rt. Once the reaction was complete as determined by TLC and GC/MS, the solution was quenched with H_2O (100 mL). After extracting the aqueous layer with ether (2 x 125 mL), the organic layers were combined, rinsed with brine, dried over $MgSO_4$, filtered, and concentrated *in vacuo*. Styrene 5.6 was recovered by flash column chromatography (Hex) as a colorless liquid in good yield (14.5 g, 75.8 %). ^{1}H NMR ($CDCl_3$) δ ppm: 7.568 (d, *J* = 7.2 Hz, 2H), 7.469 (d, *J* = 7.2 Hz, 2H), 6.789 (dd, *J* = 17.6, 11.6 Hz, 1 H), 5.852 (d, *J* = 17.6 Hz, 1H), 5.326 (d, *J* = 11.6, 1H), 0.350 (m, 9H);^{13}C NMR ($CDCl_3$) δ ppm: 140.101, 137.951, 136.872,0 133.546, 125.518, 114.053, -1.138; IR (NaCl) cm^{-1}: 3063, 3008, 2956, 2897, 1389, 1248, 1105, 989, 826; HRMS (CI) 177.1100 calc, 177.1104 found.

4-(tert-Butyl-dimethyl-silanyloxy)-benzaldehyde, 5.7

In a procedure adopted from Faler[48], a 1 L RBF was loaded with 4-hydroxy-benzaldehyde (20.0 g, 163.8 mmol), imidazole (33.4 g, 491.3 mmol), tert-butyl-dimethyl silyl chloride (34.6 g, 229.3 mmol), DCM (600 mL), and a stir bar. Once the reaction was complete as determined by TLC and GC/MS, the solution was quenched with H_2O (400 mL). After extracting the aqueous layer with DCM (2 x 150 mL), the organic layers were combined, rinsed with brine, dried over $MgSO_4$, filtered, and concentrated *in vacuo*. 5.7 was recovered as a clear liquid by distillation (104-106 °C, 2.0 torr) in excellent yield (35.1 g, 90.6 %); ^{1}H-NMR ($CDCl_3$) δ ppm = 9.884 (s, 1H), 7.786 (dt, *J* = 9.2, 2.4 Hz, 2H), 6.942 (dt, *J* = 9.2, 2.4 Hz, 2H), 0.990 (s, 9H), 0.246 (s, 6H); ^{13}C-NMR ($CDCl_3$) δ ppm = 190.889, 161.477, 131.887, 130.369, 120.451, 25.528, 18.229, -4.374; IR (NaCl) cm^{-1} = 2956, 2931, 2858, 1700, 1598, 1273, 1156, 908; HRMS (CI) = 237.1311 calc, 237.1313 found.

tert-Butyl-dimethyl-(4-vinyl-phenoxy)-silane, 5.8

In a procedure adopted from Megiatto[49], a 100 mL RBF was charged with KtBuO (15.2 g, 135.38 mmol, 95%) and THF (50 mL). This mixture was added dropwise to a solution of methyltriphenylphosphonium bromide (45.3 g, 126.9 mmol) in THF (400 mL) at 0 °C in a 1 L RBF. After stirring for 1 h, the yellow solution was cooled to -78 °C. Aldehyde 5.7 (10.0 g, 42.3 mmol) was then added to the yellow solution and stirred overnight at rt. The reaction was quenched with H_2O (300 mL), extracted with ether (2 x 200 mL), and the combined organics were rinsed with brine, dried over $MgSO_4$, filtered, and concentrated *in vacuo*. Styrene 5.8 was recovered as a clear liquid by flash column chromatography (Hex) in excellent yield (9.1 g, 91.7%). ^{1}H-NMR ($CDCl_3$) δ ppm = 7.285 (d, *J* = 6.4 Hz, 2H), 6.792 (d, *J* = 6.8 Hz, 2H), 6.653 (dd, *J* = 17.6, 10.6 Hz, 1H), 5.604 (d, *J* = 17.6 Hz, 1H), 5.123 (d, *J* = 10.0 Hz, 1H), 0.982 (s, 9H), 0.196 (s, 6H); ^{13}C-NMR ($CDCl_3$) δ ppm = 155.503, 136.307, 130.935, 127.296, 120.109, 111.664, 25.669, 18.222, -4.427; IR (NaCl) cm^{-1} = 2930, 2858, 1604, 1508, 1472, 1263, 915, 840, 780; HRMS (CI) = 235.1518 calc, 235.1519 found.

Synthesis of Trimethyl-(2-methylene-but-3-enyl)silane, 5.9

In a modified procedure from Sakurai[50], a 250 mL RBF with condenser was charged with freshly ground Mg (2.2 g, 92.2 mmol), a catalytic amount of dibromoethane, diethyl ether (100 mL), and a stir bar. After stirring for 15 min at rt, the reaction mixture was brought to reflux, and chloromethyltrimethylsilane (10.6 mL, 76.8 mmol) was added drop-wise over 30 min. In a separate 1 L RBF with addition funnel, a mixture of 1,3-Bis(diphenylphosphino)propane nickel (II) chloride (1.3 g, 2.3 mmol), freshly distilled chloroprene (9.0 mL, 97.6 mmol, bp = 58-61 °C, 760 torr), and diethyl ether (500 mL) was stirred at 0 °C. After nearly complete Mg consumption (2 h), the pale-gray Grignard solution was cooled, added drop-wise to the dark-red, chloroprene mixture over 30 min, and stirred overnight at rt. The yellow product was quenched with H_2O (500 mL) and

extracted with ether (3 x 250 mL); the organic layers were combined, dried over $MgSO_4$, filtered, and concentrated *in vacuo*. Monomer 5.9 was isolated by distillation (57-60 °C, 66 torr) as a clear liquid in moderate yield (6.5 g, 60%); ^{1}H NMR ($CDCl_3$) δ ppm: 6.380 (ddd, *J* = 17.6, 10.8, 0.4 Hz, 1H), 5.121 (dd, *J* = 17.6, 0.4 Hz, 1H), 5.052 (dd, *J* = 10.4, 0.4 Hz, 1H), 4.903 (m, 1H), 4.794 (s, 1H), 1.711 (d, *J* = 0.8 Hz, 2H), 0.007 (s, 9H); ^{13}C NMR ($CDCl_3$) δ ppm: 144.141, 139.915, 114.142, 113.606, 21.190, -1.250; IR (NaCl) cm^{-1}: 3084, 2955, 2897, 1588, 1248, 851; HRMS (CI) 140.1021 calc, 140.1023 found.

5.21.4 Etch Studies

Etching was conducted on a 790 Plasmatherm RIE Etcher/PECDV at the J.J. Pickle Research Center of the University of Texas at Austin Microelectronics Research Center. The oxygen pressure was 50 mTorr, and the oxygen flow rate was 40 sccm with a 120 W of power.

5.21.5 BC Purification

All reactions and purification were conducted under Ar atmosphere via standard Schlenk line techniques.[43] All glassware was flame dried and purged with argon five times prior to exposure to any solvent or monomer. Purification agents, n-butyllithium (2.5 M solution in hexanes, Aldrich), and dibutylmagnesium (1 M solution in heptane, Aldrich) were received as solutions, and the solvents were removed using vacuum, prior to mixing with monomers. Exposure to air was prevented by storing and handling the reagent bottles under argon atmosphere inside a dry-box. Lithium chloride (LiCl, Fluka) was stored in a 120 °C oven and repeatedly flame dried and purged when placed inside the reactor. 1,1'-Diphenylethylene (DPE) (97 %, Aldrich) was freeze-dried and vacuum-distilled twice over *n*-butyllithium and stored under argon atmosphere inside a dry-box. DPE, which is a high boiling liquid (bp 270-272 °C) was distilled at 140–160 °C under

continuous vacuum. High-purity Argon, used for maintain inert conditions, was passed through an OMI-2 organometallic Nanochem®resin indicator/purification column (Air Products). Methanol (reagent grade, Aldrich) used as termination reagent, was degassed by sparging with argon for 45 min for removing air (particularly oxygen), which can potentially couple "living" polymer chains leading to undesired products. All other chemicals were used as purchased.

Styrene (99 %, 10–15 ppm *p-tert*-butylcatechol inhibitor, Aldrich) was freeze-dried and then purified by two successive distillations from solvent-dried dibutylmagnesium (0.1 mmol/g styrene) at 40 °C for 2 h. The styrene burette was covered with aluminum foil to prevent photopolymerization and stored in a freezer. When ready for a reaction, the monomer was freeze-dried twice.

Methyl methacrylate (MMA) (99 % GC, hydroquinone stabilized, Fluka) was freeze-dried, and then dried over calcium hydride for at least 1 h at rt. It was finally titrated with trioctylaluminum at ambient temperature to remove alcohol residues (indicated by the formation of a yellow solution), before distilling it into a burette. The burette was covered with aluminum foil to prevent exposure to light and stored in a freezer.

Trimethyl-(2-methylene-but-3-enyl)silane was freeze-dried, and then dried over n-BuLi twice for at least 1 h at rt. After distilling a burrette, the monomer was freeze dried and used immediately.

Methacryloxymethyltrimethylsilane (Gelest, SIM6485.5) was filtered through basic alumina on a bench top open ot the air, and then freeze-dried in a solvent flask. After drying over calcium hydride two times for at least 1 h at rt, the monomer was distilled into a burrette. The monomer was covered in foil and stored in the freezer for up to two days.

5.21.6 PS-b-PMMA

A 500 mL reactor was loaded with a stir bar and 5 molar equivalents of LiCl to initiator. LiCl suppresses side reactions during MMA propagation.[44,58] Purified THF was added into the reactor via a solvent flask, and the reactor was cooled to -72 °C in a dry ice/IPA bath. The total volume of THF used was set to so that the final concentration was 5 wt% monomer. After the solution temperature was stabilized at -72 °C, secBuLi was added and stirred for 5 min. Approximately 20 drops of purified styrene was then added to the reaction via an airlock and a burrette. The color of the solution immediately turned orange, and after a 20 min seeding period, the remaining styrene was added. This was stirred for 4 h followed by addition of 5 molar equivalents of DPE to initiator. This addition turned the reaction a deep red. After 3 h of stirring, 20 drops of MMA was added to seed the MMA via the airlock and a burrette, and this caused the reaction to turn colorless. The reaction was stirred for 4 h after the remaining MMA was added. To quench the reaction, degassed methanol (5 mL) was added, and the resulting mixture was stirred for 45 min.

5.21.7 PS-b-PTMSI

A 500 mL reactor was loaded with a stir bar, flame dried, and cyclohexane was added into the reactor via a solvent flask. The total volume of cyclohexane used was set to so that the final concentration was 5 wt% monomer. After heating the reactor to 40 °C, sec-BuLi was added and stirred for 30 min to ensure a homogenous solution. Approximately 20 drops of purified styrene was then added to the reaction via an airlock and a burrette. The color of the solution slowly turned orange, and after a 20 min seeding period, the remaining styrene was added. After stirring overnight, 20 drops of TMSI was added via the airlock and a burrette. After a 20 min of seeding, the remaining TMSI was

added to the colorless reaction. To quench the reaction, degassed methanol (5 mL) was added, and the resulting mixture was for 30 min.

5.21.8 PS-b-P(MTMSMA)

PS-b-P(MTMSMA) was synthesized in an identical fashion to PS-b-PMMA as described above.

5.21.9 Surface Treatment with PXSTs

A film of poly(5.5-R) was spin coated from a 1.0 wt% solution in toluene at 3770 rpm for 30 sec onto a wafer that had been rinsed with IPA and acetone. The wafer was immediately baked at 250 °C for 5 min to cross-link the film. The wafer was then submerged in toluene for 2 min, blown dry, submerged again for 2 min, and blown dry. Typical film thicknesses as determined by ellipsometry were 15 - 20 nm.

5.21.10 BC Coating and Annealing

A clean, surface-treated wafer was spin coated with a film of PS-b-PMMA from toluene at various speeds and concentrations to give 20-70 nm films as determined by ellipsometry. Once cast, the wafer shards were annealed at 170 °C under reduced pressure for 12-18 h.

5.22 REFERENCES

1. Intel® 32nm Logic Technology. http://www.intel.com/technology/architecture-silicon/32nm/.

2. http://www.hitachigst.com/hdd/hddpdf/tech/hdd_technology2003.pdf. **2003**.

3. Ross, C. *Annu. Rev. Mater. Res.* **2001**, *31*, 203-235.

4. Service Robert, F. *Science* **2006**, *314*, 1868-1870.

5. http://www.hitachigst.com/hdd/research/storage/pm/index.html. **2004**.

6. Long, B. K.; Keitz, B. K.; Willson, C. G. *J. Mater. Chem.* **2007**, *17*, 3575-3580.

7. Resnick, D. J.; Mancini, D.; Dauksher, W. J.; Nordquist, K.; Bailey, T. C.; Johnson, S.; Sreenivasan, S. V.; Ekerdt, J. G.; Willson, C. G. *Microelectron. Eng.* **2003**, *69*, 412-419.

8. Stewart, M. D.; Johnson, S. C.; Sreenivasan, S. V.; Resnick, D. J.; Willson, C. G. *J. Microlithogr., Microfabr., Microsyst.* **2005**, *4*, 011002/011001-011002/011006.

9. Hua, F.; Sun, Y.; Gaur, A.; Meitl, M. A.; Bilhaut, L.; Rotkina, L.; Wang, J.; Geil, P.; Shim, M.; Rogers, J. A.; Shim, A. *Nano Lett.* **2004**, *4*, 2467-2471.

10. Ruiz, R.; Kang, H.; Detcheverry, F. A.; Dobisz, E.; Kercher, D. S.; Albrecht, T. R.; de Pablo, J. J.; Nealey, P. F. *Science (Washington, DC, U. S.)* **2008**, *321*, 936-939.

11. Bates, F. S.; Fredrickson, G. H. *Phys. Today* **1999**, *52*, 32-38.

12. Fetters, L. J.; Lohse, D. J.; Richter, D.; Witten, T. A.; Zirkel, A. *Macromolecules* **1994**, *27*, 4639-4647.

13. Cochran, E. W.; Morse, D. C.; Bates, F. S. *Macromolecules* **2003**, *36*, 782-792.

14. Cochran, E. W.; Garcia-Cervera, C. J.; Fredrickson, G. H. *Macromolecules* **2006**, *39*, 2449-2451.

15. Thurn-Albrecht, T.; Steiner, R.; DeRouchey, J.; Stafford, C. M.; Huang, E.; Bal, M.; Tuominen, M.; Hawker, C. J.; Russell, T. P. *Adv. Mater. (Weinheim, Ger.)* **2000**, *12*, 787-790.

16. Lambooy, P.; Russell, T. P.; Kellogg, G. J.; Mayers, A. M.; Gallagher, P. D.; Satija, S. K. *Phys. Rev. Lett.* **1994**, *72*, 2899-2902.

17. Walton, D. G.; Kellogg, G. J.; Mayes, A. M.; Lambooy, P.; Russell, T. P. *Macromolecules* **1994**, *27*, 6225-6228.

18. Meuler, A. J.; Hillmyer, M. A.; Bates, F. S. *Macromolecules (Washington, DC, U. S.)* **2009**, *42*, 7221-7250.

19. Kim, H.-C.; Park, S.-M.; Hinsberg, W. D. *Chem. Rev. (Washington, DC, U. S.)* **2010**, *110*, 146-177.

20. Peters, R. D.; Yang, X. M.; Kim, T. K.; Sohn, B. H.; Nealey, P. F. *Langmuir* **2000**, *16*, 4625-4631.

21. Niemz, A.; Bandyopadhyay, K.; Tan, E.; Cha, K.; Baker Shenda, M. *Langmuir* **2006**, *22*, 11092-11096.

22. Kim, S. H.; Misner, M. J.; Xu, T.; Kimura, M.; Russell, T. P. *Adv. Mater. (Weinheim, Ger.)* **2004**, *16*, 226-231.

23. Park, S.; Wang, J.-Y.; Kim, B.; Xu, J.; Russell, T. P. *ACS Nano* **2008**, *2*, 766-772.

24. Stoykovich, M. P.; Mueller, M.; Kim, S. O.; Solak, H. H.; Edwards, E. W.; de Pablo, J. J.; Nealey, P. F. *Science (Washington, DC, U. S.)* **2005**, *308*, 1442-1446.

25. Kim, S. O.; Kim, B. H.; Kim, K.; Koo, C. M.; Stoykovich, M. P.; Nealey, P. F.; Solak, H. H. *Macromolecules* **2006**, *39*, 5466-5470.

26. Mansky, P.; Liu, Y.; Huang, E.; Russell, T. P.; Hawker, C. *Science (Washington, D. C.)* **1997**, *275*, 1458-1460.

27. Han, E.; In, I.; Park, S.-M.; La, Y.-H.; Wang, Y.; Nealey, P. F.; Gopalan, P. *Adv. Mater. (Weinheim, Ger.)* **2007**, *19*, 4448-4452.

28. Ham, S.; Shin, C.; Kim, E.; Ryu, D. Y.; Jeong, U.; Russell, T. P.; Hawker, C. J. *Macromolecules (Washington, DC, U. S.)* **2008**, *41*, 6431-6437.

29. Bang, J.; Bae, J.; Lowenhielm, P.; Spiessberger, C.; Given-Beck, S. A.; Russell, T. P.; Hawker, C. J. *Adv. Mater. (Weinheim, Ger.)* **2007**, *19*, 4552-4557.

30. Han, E.; Stuen, K. O.; Leolukman, M.; Liu, C.-C.; Nealey, P. F.; Gopalan, P. *Macromolecules (Washington, DC, U. S.)* **2009**, *42*, 4896-4901.

31. Milner, S. T. *Science (Washington, D. C., 1883-)* **1991**, *251*, 905-914.

32. Ryu, D. Y.; Ham, S.; Kim, E.; Jeong, U.; Hawker, C. J.; Russell, T. P. *Macromolecules (Washington, DC, U. S.)* **2009**, *42*, 4902-4906.

33. Ryu, D. Y.; Shin, K.; Drockenmuller, E.; Hawker, C. J.; Russell, T. P. *Science (Washington, DC, U. S.)* **2005**, *308*, 236-239.

34. Ryu, D. Y.; Wang, J.-Y.; Lavery, K. A.; Drockenmuller, E.; Satija, S. K.; Hawker, C. J.; Russell, T. P. *Macromolecules (Washington, DC, U. S.)* **2007**, *40*, 4296-4300.

35. Van Oss, C. J.; Good, R. J.; Chaudhury, M. K. *Langmuir* **1988**, *4*, 884-891.

36. *Contact angle, wettability & adhesion*; VSP: Boston, 2002; Vol. 2,

37. Bailey, T. C., Dissertation, *Imprint template advances and surface modification, and defect analysis for step and flash imprint lithography*, The University of Texas at Austin, **2003**.

38. Colburn, M. E., Dissertation, *Step and flash imprint lithography: a low-pressure, room-temperature nanoimprint lithography*, The University of Texas at Austin, **2001**.

39. Brzoska, J. B.; Azouz, I. B.; Rondelez, F. *Langmuir* **1994**, *10*, 4367-4373.

40. Fadeev, A. Y.; McCarthy, T. J. *Langmuir* **2000**, *16*, 7268-7274.

41. Jung, Y. S.; Ross, C. A. *Nano Lett.* **2007**, *7*, 2046-2050.

42. *Polymer Handbook*; Wiley, 1989, 411-432.

43. Uhrig, D.; Mays, J. W. *J. Polym. Sci., Part A: Polym. Chem.* **2005**, *43*, 6179-6222.

44. Hsieh H. L., Q., R. P. *Anionic Polymerization: Principles and Practical Applications*; Marcel Dekker Inc.: New York, 1996,

45. Gokan, H.; Esho, S.; Ohnishi, Y. *J. Electrochem. Soc.* **1983**, *130*, 143-146.

46. Liu, C.-C.; Nealey, P. F.; Ting, Y.-H.; Wendt, A. E. *J. Vac. Sci. Technol., B: Microelectron. Nanometer Struct.--Process., Meas., Phenom.* **2007**, *25*, 1963-1968.

47. Colburn, M.; Grot, A.; Amistoso, M. N.; Choi, B. J.; Bailey, T. C.; Ekerdt, J. G.; Sreenivasan, S. V.; Hollenhorst, J.; Willson, C. G. *Proc. SPIE-Int. Soc. Opt. Eng.* **2000**, *3997*, 453-457.

48. Faler, C. A.; Joullie, M. M. *Org. Lett.* **2007**, *9*, 1987-1990.

49. Megiatto, J. D., Jr.; Schuster, D. I. *J. Am. Chem. Soc.* **2008**, *130*, 12872-12873.

50. Sakurai, H.; Hosomi, A.; Saito, M.; Sasaki, K.; Iguchi, H.; Sasaki, J.; Araki, Y. *Tetrahedron* **1983**, *39*, 883-894.

51. Khandpur, A. K.; Foerster, S.; Bates, F. S.; Hamley, I. W.; Ryan, A. J.; Bras, W.; Almdal, K.; Mortensen, K. *Macromolecules* **1995**, *28*, 8796-8806.

52. Odian, G. *Principles of Polymerization*; 4th ed.; Wiley-Interscience: New York, 2004, 31.

53. Singha, N. K.; De, P. P.; Sivaram, S. *J. Appl. Polym. Sci.* **1997**, *66*, 1647-1652.

54. Kim, G.; Libera, M. *Macromolecules* **1998**, *31*, 2569-2577.

55. Bosworth, J. K.; Paik, M. Y.; Ruiz, R.; Schwartz, E. L.; Huang, J. Q.; Ko, A. W.; Smilgies, D.-M.; Black, C. T.; Ober, C. K. *ACS Nano* **2008**, *2*, 1396-1402.

56. Li, Y.; Wang, X.; Sanchez, I. C.; Johnston, K. P.; Green, P. F. *J. Phys. Chem. B* **2007**, *111*, 16-25.

57. Spatz, J. P.; Moeller, M.; Noeske, M.; Behm, R. J.; Pietralla, M. *Macromolecules* **1997**, *30*, 3874-3880.

58. Allen, R. D.; Long, T. E.; McGrath, J. E. *Polym. Bull. (Berlin)* **1986**, *15*, 127-134.

Appendix A: Analytical Equations for Ceiling Temperature Equilibrium Calculations

A. 1 NUMERICAL SOLUTION

The following files were inserted into MathLab and used to solve the equations described in Chapter 3. This work would not be possible without the help of Colin C. Neikirk and Dr. Wei-Lun Jen.

A.1.1 File unzipSimSet

```
% polymerization / depolymerization kinetics analysis
% polymerization kinetics and simulation parameters inputs
function [ ] = unzipSimSet(  )



close all
clear all

% polymerization kinetic parameters
Keq = [.01; .02; .05; .1; .2; .5; 1; 2; 3; 5; 10; 15; 20; 50; 100];
Init = [.012];
Mono = [ 2];

% simulation parameters
maxCycle = 100000;
minChange = 0.00001;
maxPolymer = 1000;
```

```
tic;

% generate data
KeqSize = size(Keq, 1);
InitSize = size(Init, 1);
MonoSize = size(Mono, 1);
data = zeros((KeqSize * InitSize * MonoSize) , 5);
for i=1:1:KeqSize
   for j=1:1:InitSize
      for k=1:1:MonoSize
         [ M, currrentComposition ] = unzip( Keq(i), Init(j), Mono(k), maxCycle,
minChange, maxPolymer );
         data(i , 1) = Keq(i);
         data(i , 2) = Init(j);
         data(i , 3) = Mono(k);
         data(i , 4) = M;
         data(i , 5) = currrentComposition(1 , 1);
         mass = M;
         for l = 1:maxPolymer
            mass = M + l*currrentComposition(l, 1);
         end
         data(i , 6) = mass;
      end
   end
```

```
end
save('data.txt', 'data', '-ascii', '-tabs');

toc
% end of primary function
end
```

A.1.2 File Unzip

```
% polymerization / depolymerization kinetics analysis
function [ M, currrentComposition ] = unzip( Keq, Init, Mono, maxCycle, minChange, maxPolymer )

% function I/O:
% currrentComposition = an array of the molar concentrations of m-mers
% Keq = polymerization equilibrium constant
% Init = initiator molar concentration
% Mono = monomer molar concentration
% maxCycle = maximum number of simulation cycles
% minChange = minimun fraction of concentration change
% maxPolymer = maximum degree of polymerization

% initialize polymer composition array
currrentComposition = zeros(maxPolymer , 1);
currrentComposition(1 , 1) = Init;
M = Mono - Init;
for i=2:1:maxPolymer
```

```
    B = -((Keq * currrentComposition((i - 1) , 1)) + (Keq * M) + 1);
    C = (Keq * currrentComposition((i - 1) , 1) * M) - currrentComposition(i , 1);
    delta = (-B - sqrt((B ^ 2) - (4 * Keq * C))) / (2 * Keq);
    M = M - delta;
    currrentComposition((i - 1) , 1) = currrentComposition((i - 1) , 1) - delta;
    currrentComposition(i , 1) = delta;
  end
```

A.1.3 File unzipSingleRun

```
  % time step simulation of polymerization / depolymerization chain reaction
  referenceComposition = currrentComposition;
  for cycle=1:1:maxCycle
    for i=2:1:maxPolymer
      B = -((Keq * currrentComposition((i - 1) , 1)) + (Keq * M) + 1);
      C = (Keq * currrentComposition((i - 1) , 1) * M) - currrentComposition(i ,
1);
      delta = (-B - sqrt((B ^ 2) - (4 * Keq * C))) / (2 * Keq);
      M = M - delta;
      currrentComposition((i - 1) , 1) = currrentComposition((i - 1) , 1) - delta;
      currrentComposition(i , 1) = currrentComposition(i , 1) + delta;
    end
    if mod(cycle,10) == 0
      resume = 0;
      for j=1:1:maxPolymer
        if referenceComposition(j , 1) ~= 0
```

```
                    change = abs((currrentComposition(j , 1) - referenceComposition(j , 1))
/ referenceComposition(j , 1));
                    if change > minChange
                        referenceComposition = currrentComposition;
                        resume = 1;
                        break
                    end
                else
                    if currrentComposition(j , 1) ~= 0
                        referenceComposition = currrentComposition;
                        resume = 1;
                        break
                    end
                end
            end
            if resume == 0
                break
            end
        end
    end

    % end of the primary function
    end

    % polymerization / depolymerization kinetics analysis
```

```
% polymerization kinetics and simulation parameters inputs
function [ ] = unzipSingleRun(  )

tic;
close all
clear all

% polymerization kinetic parameters
Keq = 1;              % polymerization equilibrium constant
Init = 0.02;          % initiator molar concentration
Mono = 1;             % monomer molar concentration

% simulation parameters
maxCycle = 100000;      % maximum number of simulation cycles
minChange = 0.00001;          % minimun fraction of concentration change
maxPolymer = 200;       % maximum degree of polymerization

[ M, currrentComposition ] = unzip( Keq, Init, Mono, maxCycle, minChange,
maxPolymer );
M
currrentComposition(1 , 1)
save('data.txt', 'currrentComposition', '-ascii', '-tabs');


% end of primary function
```

end

A.2 ANALYTICAL DERIVATION

The following model was brought about by the efforts of a collaboration with Prof. Isaac Sanchez of the Department of Chemical Engineering at the University of Texas at Austin. The following equations would not have been derived by the author of this dissertation without his expertise of mathematics.

The model begins with the same basic chemical reactions as the numerical solution (eq. (4.1) and (4.5)), which yields the following recursive relation:

$$[M_{n+1}] = [M_1]\left\{K_{eq}[M]\right\}^n \equiv [M_1]x^n$$

where $x \equiv K_{eq}[M]$. Invoking mass balance yields

$$[M] = [M]_0 - \sum_{n=1}^{N} n[M_n] = [M]_0 - [M_1]\sum_{n=1}^{N} nx^{n-1} \qquad \text{(A.21)}$$

and

$$[M_1] = [I]_0 - \sum_{n=1}^{N-1}[M_{n+1}] = [I]_0 - [M_1]\sum_{n=1}^{N-1} x^n \equiv [I]_0 - [M_1]\left\{S_{N-1} - 1\right\} \qquad \text{(A.22)}$$

where S_{N-1} is the sum of a finite geometric series to terms of order $N-1$:

$$S_{N-1} = \sum_{n=0}^{N-1} x^n = \frac{1-x^N}{1-x} \qquad \text{(A.23)}$$

Note that eq. (A.22), can now be rewritten as:

$$[M_1] = \frac{[I]_0}{S_{N-1}} \quad \text{(A.24)}$$

Thus, the mass balance equation, eq. (A.21), becomes

$$[M] = [M]_0 - \frac{[I]_0}{S_{N-1}} \sum_{n=1}^{N} n x^{n-1} = [M]_0 - \frac{[I]_0}{S_{N-1}} \frac{dS_N}{dx} \qquad \text{(A.25)}$$

where

$$S_N \equiv S_{N-1} + x^N = \frac{1 - x^{N+1}}{1 - x} \qquad \text{(A.26)}$$

Defining

$$R_0 \equiv [I]_0 / [M]_0 \quad \text{and} \quad x_0 \equiv [M]_0 K_{eq} \qquad \text{(A.27)}$$

we have,

$$\frac{[M]}{[M]_0} \equiv \frac{x}{x_0} = 1 - \frac{R_0}{S_{N-1}} \frac{dS_N}{dx}$$

$$= 1 - R_0 \left\{ \frac{1}{1-x} - \frac{N x^N}{1 - x^N} \right\} \qquad \text{(A.28)}$$

For sufficiently large *N*, there are approximate solutions:

$$\frac{x}{x_0} \simeq 1 - R_0 \begin{cases} \dfrac{1}{1-x} & x < 1 \\ \\ N - \dfrac{1}{x-1} \simeq N & x > 1 \end{cases} \qquad \text{(A.29)}$$

or

$$\frac{x}{x_0} \simeq 1 - NR_0 \qquad x > 1 \qquad \text{(A.30)}$$

Note that the maximum value of N possible is given by

$$N_{\max} = [M]_0 / [I]_0 = 1 / R_0 \qquad \text{(A.31)}$$

so that $NR_0 \leq 1$.

For $x < 1$, eq. (A.29) is a quadratic equation in x and can be solved:

$$x = \frac{1}{2}\left[1 + x_0 - \sqrt{(1-x_0)^2 + 4R_0 x_0}\right] \qquad \text{(A.32)}$$

and as approximations ($R_0 << 1$)

$$x \simeq \begin{cases} x_0\left[1 - \dfrac{R_0}{1-x_0}\right] \Rightarrow \dfrac{[M]}{[M]_0} = \left[1 - \dfrac{R_0}{1-x_0}\right] & x_0 < 1 \\ \\ 1 - \sqrt{R_0} \Rightarrow [M]/[M]_0 = 1 - \sqrt{R_0} & x_0 = 1 \\ \\ 1 - \dfrac{R_0}{x_0 - 1} \Rightarrow [M] = \dfrac{1}{K_{eq}}\left[1 - \dfrac{R_0}{x_0 - 1}\right] & x_0 > 1 \end{cases} \qquad \text{(A.33)}$$

As can be seen from above, $x_0 = 1 = K_{eq}[M]_0$ is a transitional value and the character of the solution changes from $[M] \simeq [M]_0$ to one where $[M] \simeq 1/K_{eq}$. The condition $x_0 > 1$, corresponds to the most interesting regime for depolymerization kinetics.

For the particular initial conditions used in the numerical section, *viz.,*

$$[M]_0 = \text{unit molar} \qquad x_0 \equiv K_{eq}[M]_0 = K_{eq} \qquad R_0 \equiv [I]_0/[M]_0 = [I]_0 \tag{A.34}$$

eq. (A.32) becomes:

$$[M] = \frac{1}{2K_{eq}}\left[1 + K_{eq} - \sqrt{(K_{eq}-1)^2 + 4[I]_0 K_{eq}}\right] \tag{A.35}$$

The average degree of polymerization, $< n >$, is easily calculated:

$$< n > = \frac{\sum_{n=1}^{N} n[M_n]}{\sum_{n=1}^{N}[M_n]} = \frac{\sum_{n=1}^{N} nx^{n-1}}{\sum_{n=1}^{N} x^{n-1}} = \frac{\sum_{n=1}^{N} nx^{n-1}}{\sum_{n=0}^{N-1} x^{n}} = \frac{\sum_{n=1}^{N} nx^{n-1}}{S_{N-1}} = \frac{1}{S_{N-1}}\frac{dS_N}{dx}$$

$$= \frac{1}{1-x} - \frac{Nx^N}{1-x^N} \tag{A.36}$$

Thus,

$$< n > \simeq \begin{cases} \dfrac{1}{1-x} & x < 1 \\ \\ N - \dfrac{1}{x-1} & x > 1 \end{cases} \tag{A.37}$$

Notice that eq. (A.28) now takes on a simple form for all x:

$$\frac{x}{x_0} = \frac{[M]}{[M]_0} = 1 - R_0 < n > = 1 - \frac{< n >}{N_{\max}} \quad \text{(A.38)}$$

At the depolymerization-polymerization transition ($x = 1$), the degree of polymerization is given by

$$< n >_{x=1} = \lim_{x \to 1} \frac{1 - x^N - Nx^N(1-x)}{(1-x)(1-x^N)} = \frac{N+1}{2} \quad \text{(A.39)}$$

which is more clearly seen from the above definition of $< n >$:

$$< n >_{x=1} = \frac{\sum_{n=1}^{N} n}{\sum_{n=0}^{N-1} 1} = \frac{N(N+1)/2}{N} = \frac{N+1}{2} \cong \frac{N}{2} \quad \text{(A.40)}$$

For the initial values given in eq. (A.34), we have

$$< n > = \frac{1}{1 - K_{eq}[M]} = \frac{2}{1 - K_{eq} + \sqrt{(K_{eq} - 1)^2 + 4[I]_0 K_{eq}}} \quad \text{(A.41)}$$

For values of K_{eq} greater than unity, eq. (A.41) becomes

$$< n > \simeq \frac{K_{eq} - 1}{[I]_0 K_{eq}} \qquad K_{eq} > 1 \quad \text{(A.42)}$$

which becomes increasingly more accurate as K_{eq} gets larger.

Weight fractions are given by

$$W_n = \frac{n[M_n]}{\sum_{n=1}^{N} n[M_n]} = \frac{nx^n}{\sum_{n=1}^{N} nx^{n-1}} = \frac{nx^n}{\frac{dS_N}{dx}} \qquad \text{(A.43)}$$

which for large *N* and $x < 1$ yields

$$W_n = n(1-x)^2 x^n \qquad \text{(A.44)}$$

For the initial conditions in eq. (A.34), we have

$$W_n = \frac{n}{2^{n+2}}\left[1 + K_{eq} - \sqrt{(K_{eq}-1)^2 + 4[I]_0 K_{eq}}\right]^n \left[1 - K_{eq} + \sqrt{(K_{eq}-1)^2 + 4[I]_0 K_{eq}}\right]^2 \qquad \text{(A.45)}$$

For $K_{eq} > 1$, we have the approximation:

$$W_n \simeq n\left[1 - \frac{[I]_0 K_{eq}}{K_{eq}-1}\right]^n \left[\frac{[I]_0 K_{eq}}{K_{eq}-1}\right]^2, \quad K_{eq} > 1 \quad \text{(A.46)}$$

A maximum in W_n occurs at n^*:

$$n^* = -1/\ln\left\{\left[1+K_{eq}-\sqrt{(K_{eq}-1)^2+4[I]_0 K_{eq}}\right]/2\right\}$$

$$\simeq \frac{K_{eq}-1}{[I]_0 K_{eq}} \simeq < n > \qquad \text{(A.47)}$$

The polydispersity index (P_I) can also be calculated. Letting

$$\frac{dS_N}{dx} \equiv S_N^{'} \quad \text{and} \quad \frac{d^2 S_N}{dx^2} \equiv S_N^{''} \qquad \text{(A.48)}$$

we have

$$P_I \equiv \frac{< n^2 >}{< n >^2} = \frac{\sum_{n=1}^{N} n^2 x^{n-1} / \sum_{n=1}^{N} x^{n-1}}{\left[S_N^{'} / S_{N-1}\right]^2} = \frac{\frac{1}{S_{N-1}}\left[xS_N^{''} + S_N^{'}\right]}{\left[S_N^{'} / S_{N-1}\right]^2} = \frac{S_{N-1}}{S_N^{'}}\left[\frac{xS_N^{''}}{S_N^{'}} + 1\right]$$

$$= \frac{(x^N-1)\left\{x^N\left[\left[N(x-1)-1\right]^2 + x\right] - (x+1)\right\}}{\left\{x^N\left[N(x-1)-1\right]+1\right\}^2} \qquad \text{(A.49)}$$

$$\lim_{N\to\infty} P_I = \begin{cases} 1+x & x<1 \\ 4/3 & x=1 \\ 1 & x>1 \end{cases} \qquad \text{(A.50)}$$

Interestingly, the polydispersity ratio approaches 2 as $x \to 1$ from below just as it does for condensation polymerization, but anionic polymerization becomes ideally monodisperse for $x > 1$.

Appendix B: Custom Glassware for Anionic Block Copolymer Synthesis

B.1 REACTOR

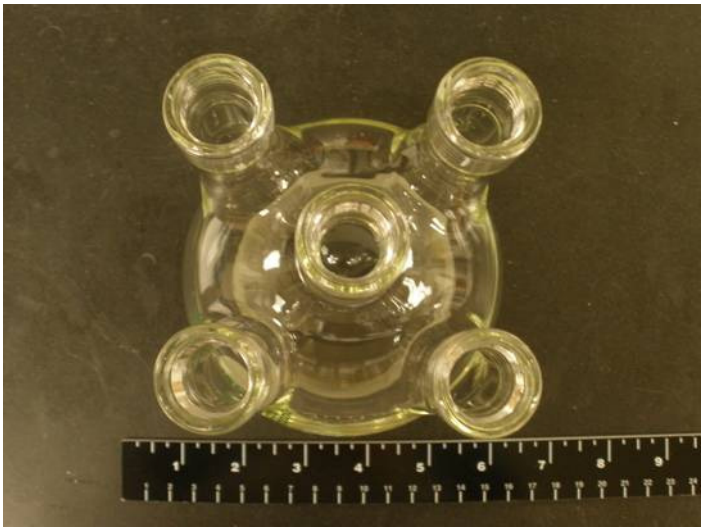

B.2 SOLVENT AND MONOMER FLASK

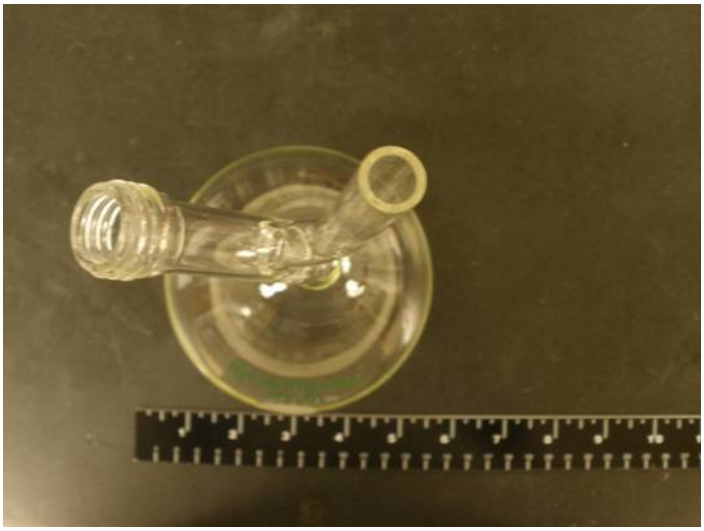

B.3 Short Path Distillation Head

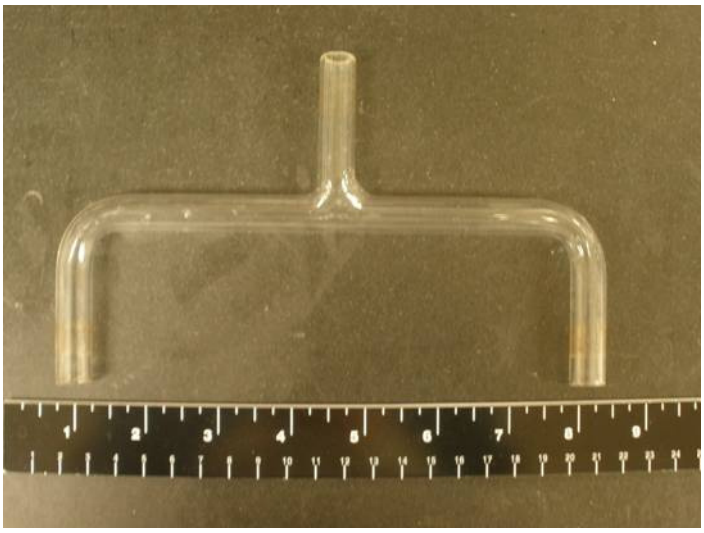

B.4 25 mL Burrette

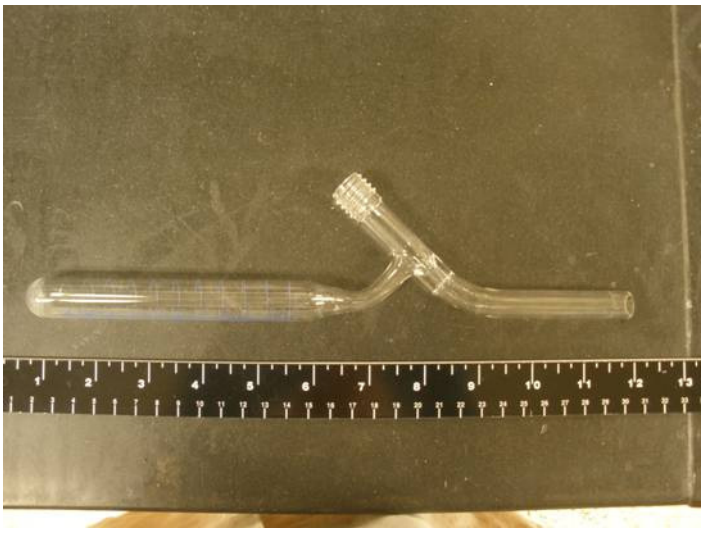

B.5 50 mL Burrette

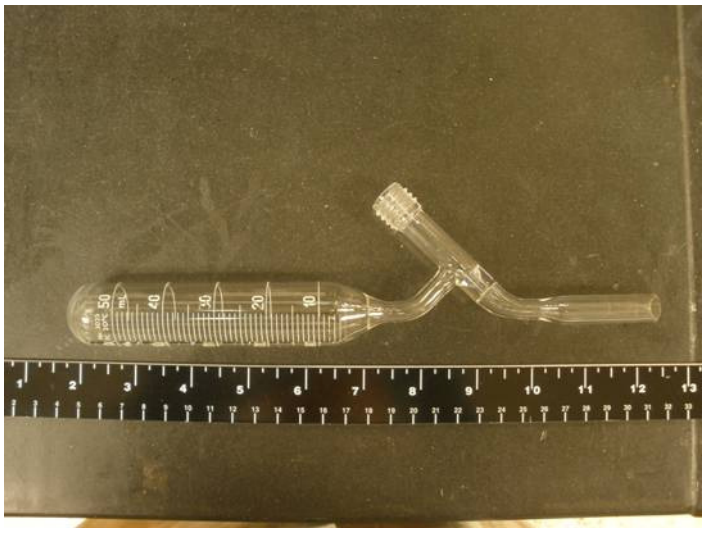

B.6 100 mL Burrette

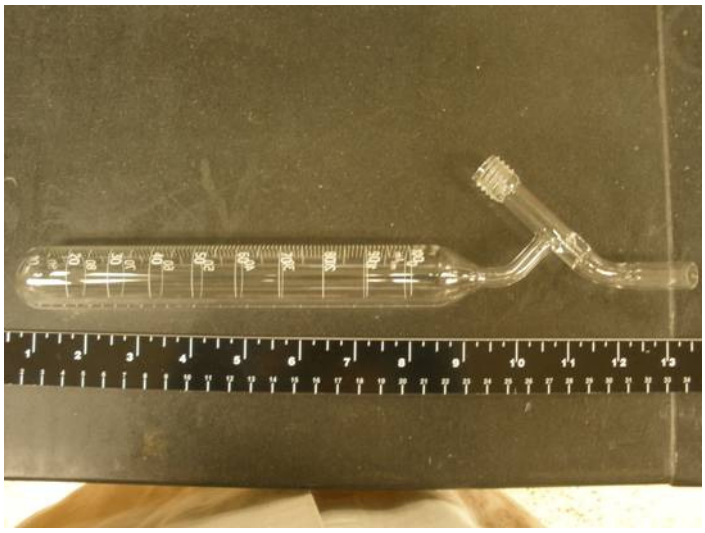

B.7 MANIFOLD

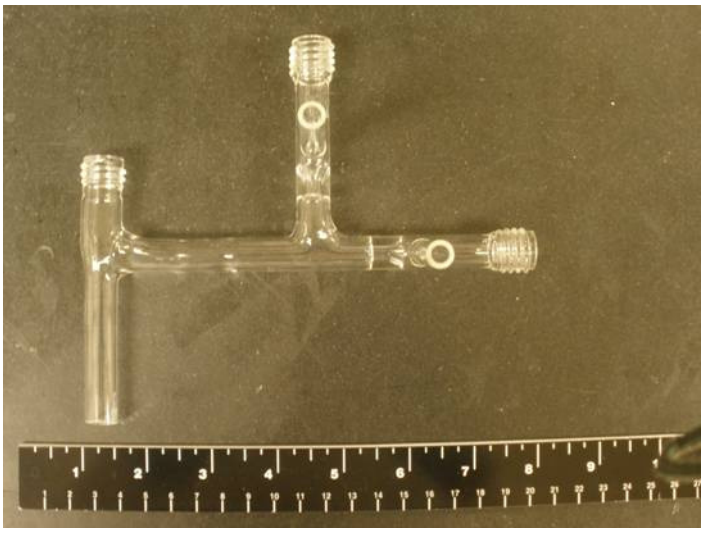

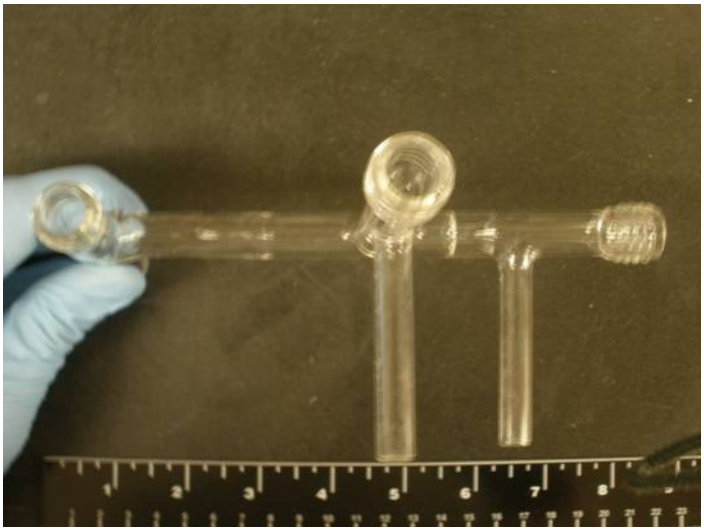

B.8 THERMOCOUPLE WELL

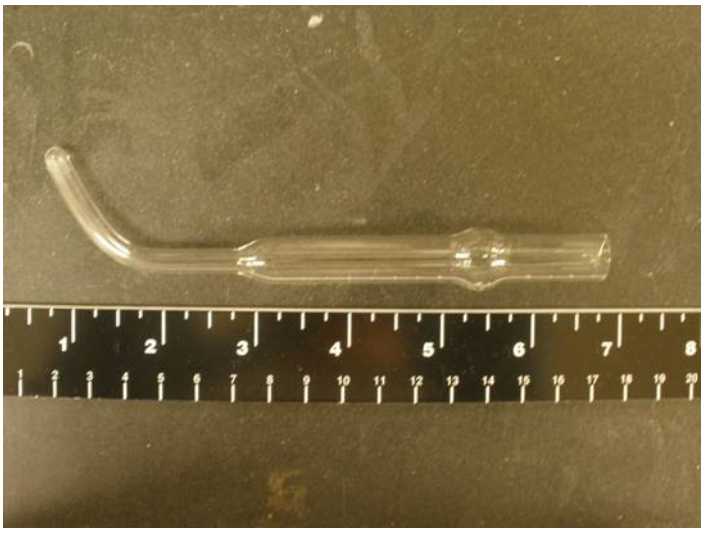

B.9 AIRLOCK

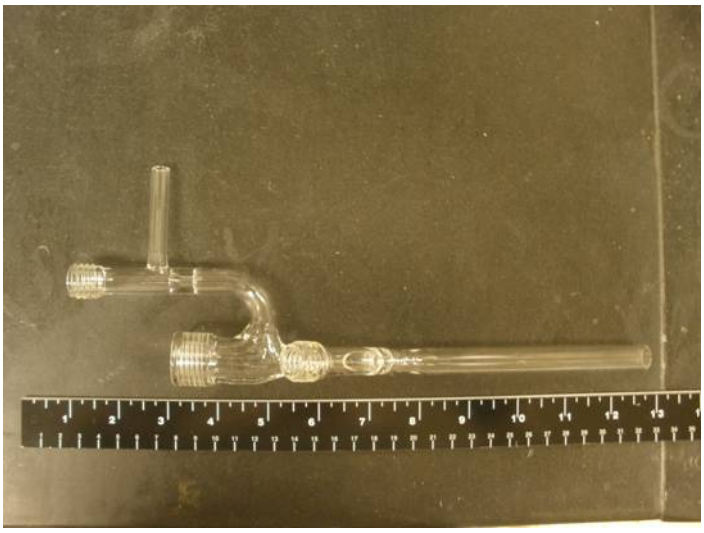

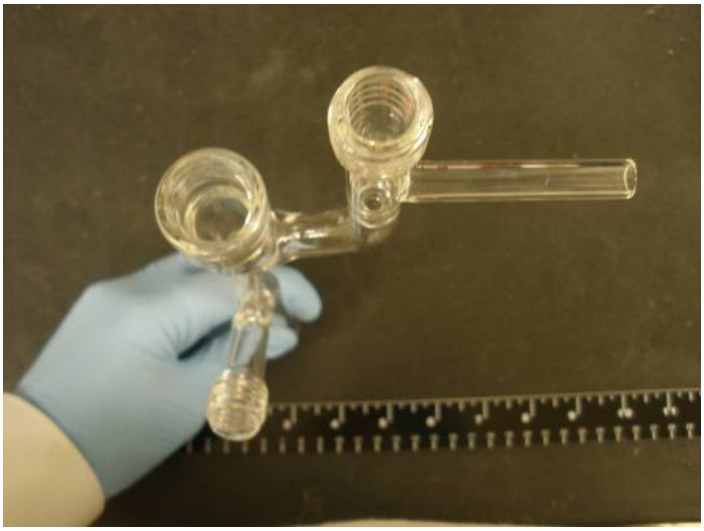

B.10 PLUG

Appendix C: Thermal Resist for Surface Plasmon Resonance Imaging

C.1 COLLABORATION

This project was done in collaboration with Dr. Peter Carmichael and Dr. Alex Liddle of the Center for Nanoscience Technology at the National Institute of Standards and Technology in Gaithersburg, MD.

C.2 BACKGROUND

When photons of the right momentum and incident angle collide with a metal's surface, they induce surface waves in the metal that consist of strongly coupled electromagnetic energy and excited surface states known as plasmons. This combination of light and excited material is called a polariton, and in particular, because of the special geometry of the surface wave that is formed, it is known as a surface-plasmon polariton (SPP).[1] SPPs affect many of the properties of metals, especially when the surface area of the metal is great, or when the size of the metal particle is so small that its relative surface area is large.[2]

Examples of how surface plasmons affect the optical properties of metals have been known since antiquity,[3] but recently researchers have been able to design and optimize surface plasmons for novel purposes. This area of research is broadly known as the field of plasmonics. It has roots in both optics and photonics, but it also bridges electronics because surface plasmons are typically formed on conductive metals. It bridges analytical chemistry and biology, because SPPs have found wide utility in solution-phase sensing of adsorption at metal interfaces.[4]

More recently, surface plasmons have shown potential in nanoscale lithography and manufacturing.[5] This is the result of two independent and synergistic effects. First,

the wavelength of excited SPPs can be made to be much shorter than the wavelength of the light that excites the SPP if the excitation wavelength is close to the resonant wavelength of the metal/dielectric.[6] Because dielectric silver has a resonance around 325 nm, UV light can be used to form plasmons that have very short wavelengths (down to lambda/20, or roughly 20 nm). SPP's thus allow near-UV light (365 nm) to act very much like DUV (193 nm), or EUV (13 nm) light, without the commensurate problems of having to produce, focus, and image light at these wavelengths.[7] The second effect comes from the fact that SPPs are entirely confined to the surface of the metal. This makes it easy to create well-defined two-dimensional interference effects. For example, if light is coupled into SPPs such that they propagate towards one another, a standing wave can be produced.[8] This technique has been used to create high resolution gratings in patternable media.[9] SPP interference also gives rise to unusual characteristics when it happens on periodic arrays of features. When light of the right wavelength radiates onto periodic holes in metal of just the right pitch and diameter, the amount of light transmitted through to the far-field can be greater than the amount originally incident on the holes.[10] This unexpected result is still under intensive research; however, high transmission masks that utilize this effect have already been designed and implemented.[11]

Near field scanning optical microscopy (NSOM) has been used to observe surface-plasmons directly. However, two issues make this an inadequate tool for doing metrology on SPPs. First, the tips have dimensions on the order of 50-150 nm, which is too big to see field variations that come about due to the small wavelength of SPPs. For metal surfaces with features such as holes, it is imperative to get field information at the edge of the holes where scattering takes place. Unfortunately, the tips are too big for this purpose.[12] Secondly, the metal cladding that surrounds the NSOM tip can support SPPs of its own, which can affect the nature of the field.[12]

A second approach for observing surface-plasmons is to coat the metal/dielectric surface with a photosensitive material whose photo-response can be measured by AFM. Commercially available photoresists have been used for this purpose.[13] However, such resists are pre-optimized to produce high contrast features. A linear photosystem that engenders a "gray-scale" response to the field strength might be better suited for metrology. Two other drawbacks of commercial photoresists are that they do not typically work in the visible range, and that they require spin-casting to produce high quality thin films. A visible light curing material would be quite useful for following surface plasmons on gold/dielectric interfaces that typically resonate in the visible. Although a novel azobenzene based composition has been reported to be useful for measuring visible fields,[14] this material actually produces a very small, nonlinear, and environmentally sensitive photoresponse. In cases where plasmonic structures have topologies that preclude spin-casting, new methods for applying the photosensitive material are needed.

In order for a photosenstive material to produce a photo-response that can be measured by AFM, the material must either undergo a conformational change upon exposure (i.e. the azobenzene type system), or it must undergo a photo-switch upon exposure which modulates the removal of the material upon development (photoresist type systems). The term "solubility switch" has for many years been used to describe the chemistry that occurs within commercial photoresists, but this term is specific to solvent developable systems. It seems that heat might be used as a developer instead of solvent. By analogy with photoresists, the chemistry that produces a "sublimation-switch" upon exposure must be found. Development of this novel material would involve bringing the temperature and pressure of the material between the sublimation points of the exposed and unexposed material.

A dry-developing photoresist that acts like a sublimation-switch has been used in direct-write NSOM and thermal lithography.[15] Fortuitously, this material also seems able to solve several of the previously mentioned problems associated with measuring SPPs. For example, the material can be dry-deposited over various topologies, forms <100 nm thin films, and is sensitive throughout the visible region.

C.3 SYNTHESIS

To continue the sublimation-switch chemistry put forward by Noach et al.,[15] a variety of 2,3-diamino-naphthoquinones was synthesized in an effort to investigate the role of aryl substituents on the material's absorbance, photochemistry, sublimation temperature, and sublimation rate. This was accomplished in a modular two step process in high yield (Scheme C.1).[16] These reactions were carried out on a multi-gram scale, and the products were fully characterized by ^{1}H-NMR, ^{13}C-NMR, IR, HRMS, and M_p. The λ_{max} and ε were also determined in DCM via a UV-vis spectrophotometer (Figure C.1). A shorthand nomenclature was developed that named compounds by the location and functional group of the aniline derivative and the substituent at the 3 position of the napthoquinone ring; IE, compounds C.1-6 were labeled #-R, Cl while C.7-12 were called #-R, pip.

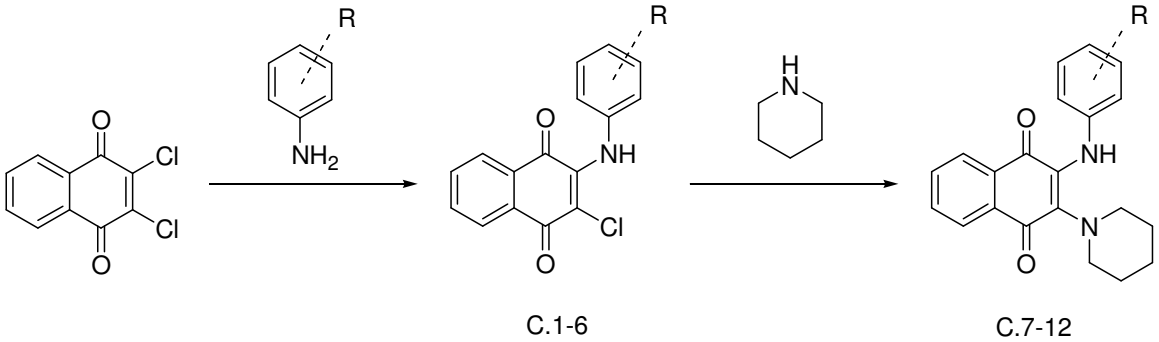

C.1-6 C.7-12

Scheme C.1: Two step synthesis of 2,3-diamino-naphthoquinones.

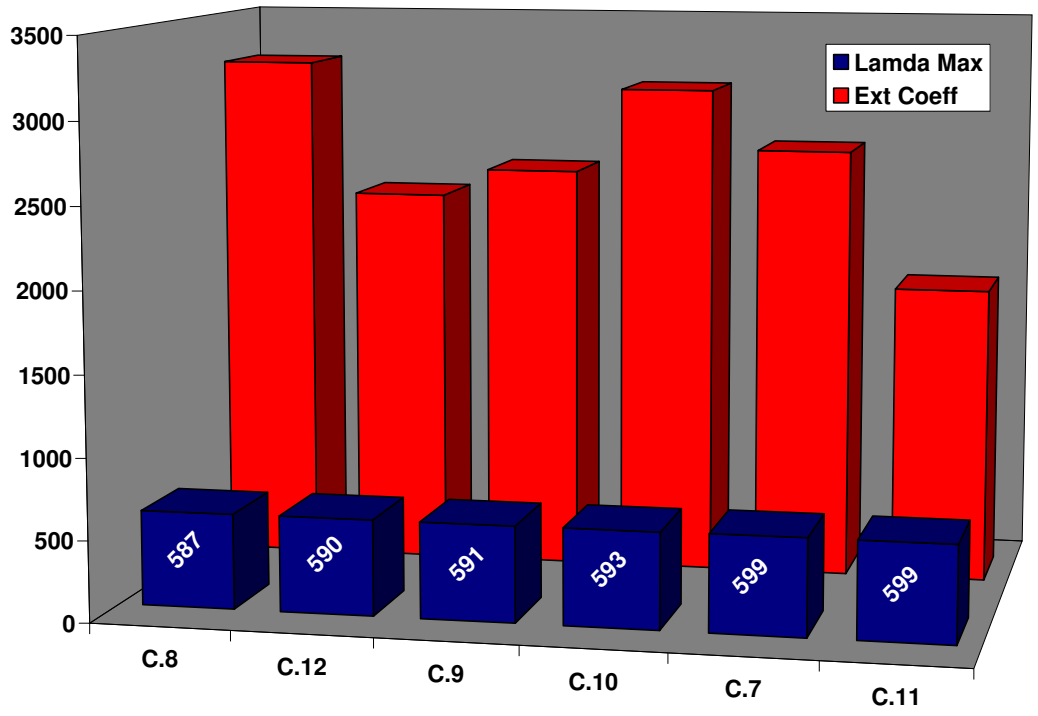

Figure C.1: UV-vis data of compounds C.7-12; Lamda max (blue), molar extinction coefficient (red).

C.4 THERMAL PROPERTIES

During the characterization of these compounds, an odd thermal property was noticed related to their melting points. Figure C.2 displays the DSC trace of commercially available dichlone. This trace shows the normal behavior of crystalline solids with sharp melting and freezing points.

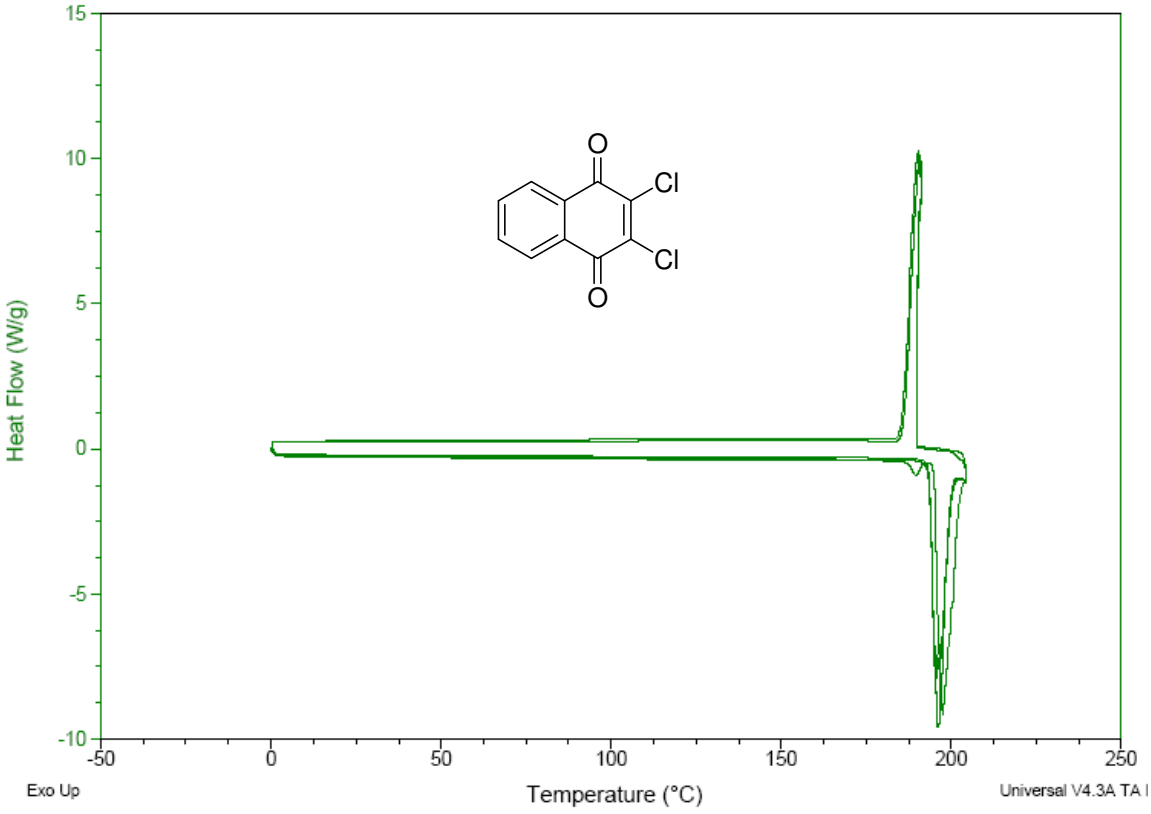

Figure C.2: DSC trace of dichlone.

Figures C.3 and C.4 show the DSC traces of compound C.1 and C.7. Compound C.1 displays a clear melting point transition over repeated heating and cooling cycles, but the freezing point is not regular like it is with dichlone. When the piperidine was substituted giving compound C.7, the DSC displayed a clear melting point during the first cycle. However after several cycles the melting point no longer appears and is replaced by a thermal transition around 15 °C. This transition is very similar to a glass transition temperature observed in polymers. Furthermore, this behavior was observed for all synthesized compounds, and the unique DSC traces are shown in the experimental section. The exact nature of the material during these heating and cooling cycles is not clear and can only be speculated as a glassy like substance. Regardless, the material

showed no decomposition by ^{1}H-NMR after cooling and heating cycles and was found suitable as a thermal sublimation switch resist.

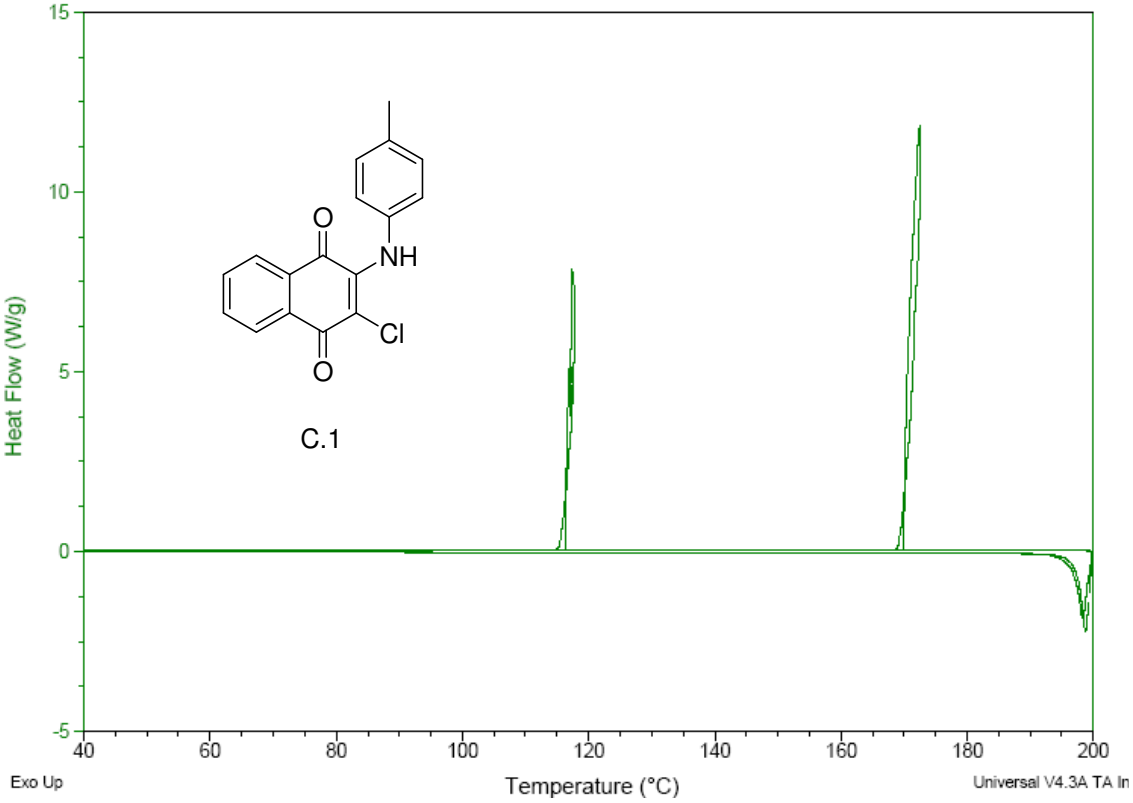

Figure C.3: DSC trace of 4-Me, Cl (C.1).

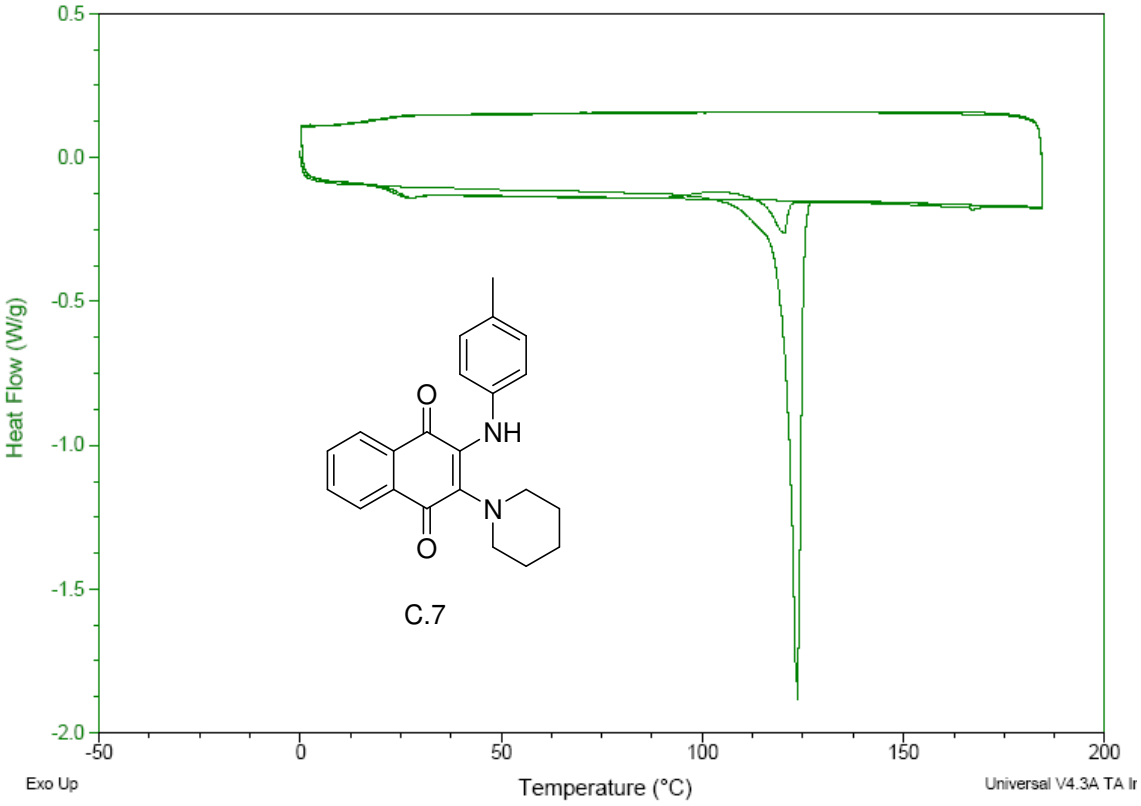

Figure C.4: DSC trace of 4-Me, pip (C.7).

C.5 ALKYNE INCORPORATION

During the course of these studies, a 2,3-diamino-naphthoquinone with an alkyne functionality was desired for use as a click chemistry substrate. This was accomplished by alkylating hydroxy compound C.9 with propargyl bromide (Scheme C.2). Unfortunately, this compound was not stable under ambient comditions, and another route proposed to install the terminal alkyne moiety.

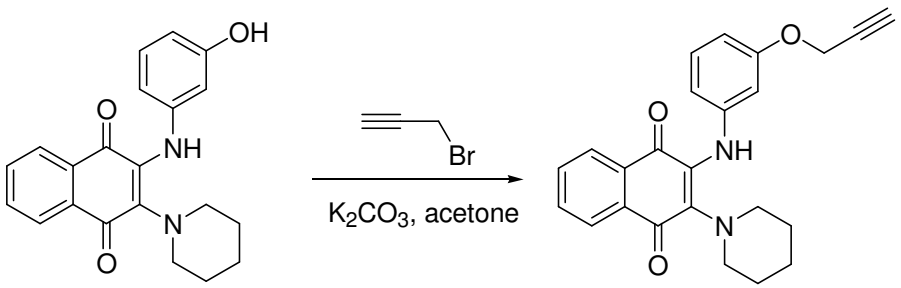

C.9 C.13

Scheme C.2: Alkylation of hydroxyl compound C.9.

Work was then directed at synthesizing aniline derivatives with an alkyne moiety according to literature procedures. Surprisingly, neither TMS protected C.14 nor unprotected C.15 yielded the desired adduct under our previously optimized reaction conditions (Scheme C.3).

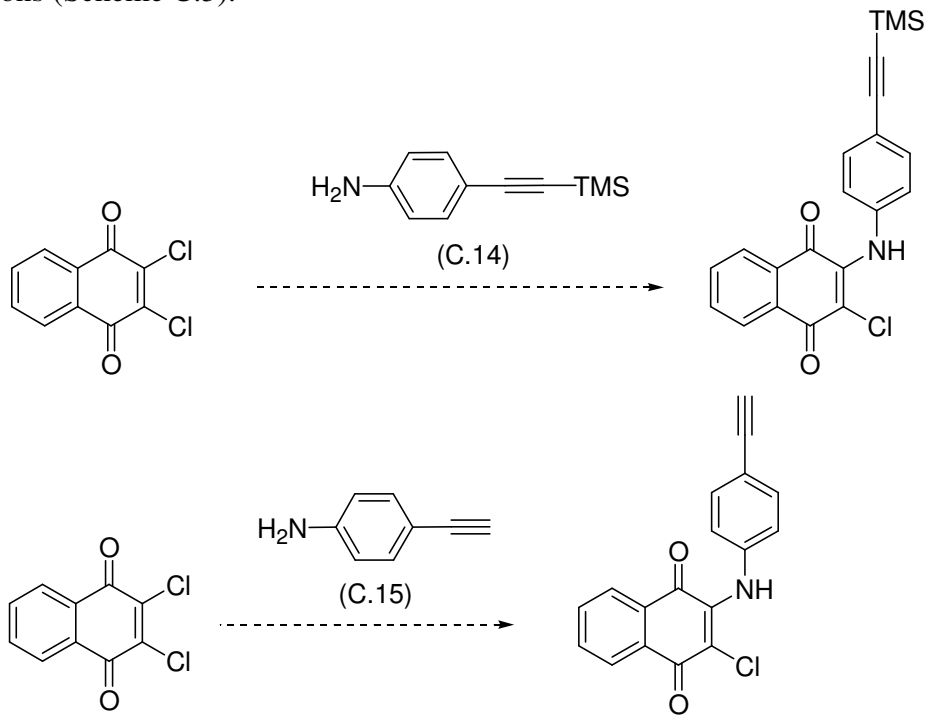

Scheme C.3: Michael addition of alkynl-anilines to dichlone.

Current work is directed at installing the alkyne functionality as the last step in the synthesis. Iodo,Cl (C.16) was synthesized in good yield followed by addition of piperidine to yield C.17. Songashira coupling and subsequent deprotection should yield the desired 2,3-diamino-naphthoquinone with an alykne moiety (Scheme C.4).

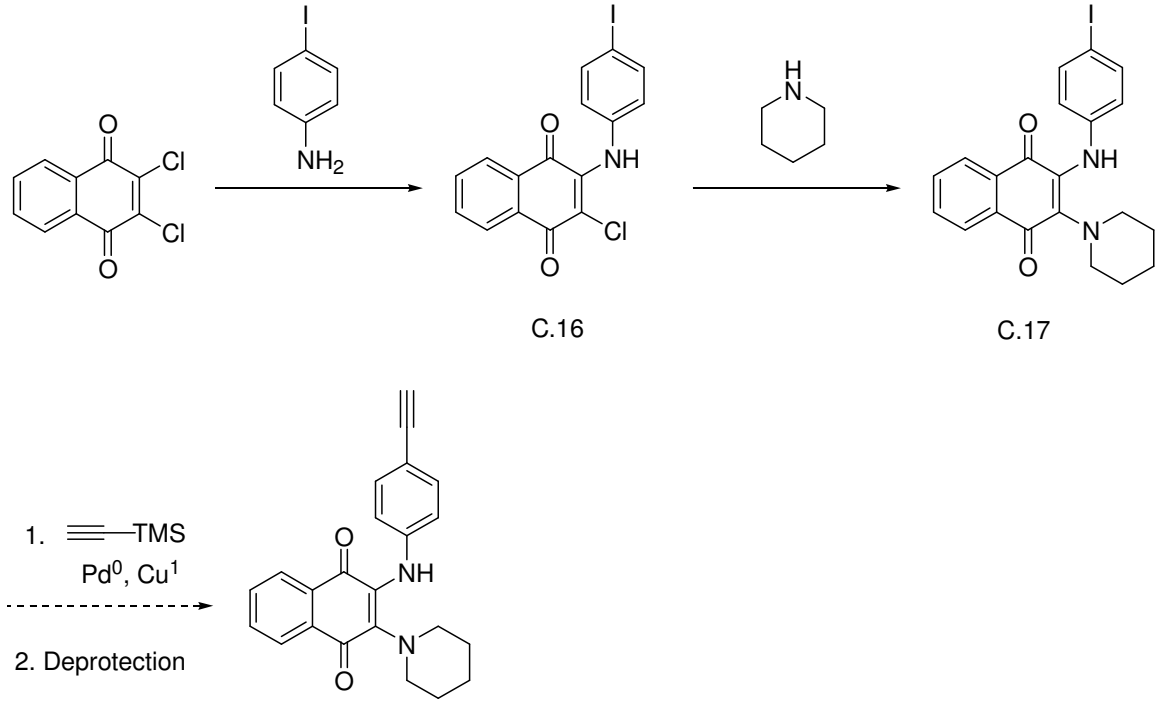

Scheme C.4: Syntheic route towards ethynyl 2,3-diamino-naphthoquinone derivative.

C.6 EXPERIMENTAL

All chemicals were purchased from Sigma-Aldrich and used as received unless otherwise stated. All reactions were conducted under a positive nitrogen atmosphere with oven-dried glassware unless otherwise stated. All ^{1}H and ^{13}C NMR spectra were recorded on a Varian Unity Plus 400 MHz instrument. All chemical shifts are reported in ppm downfield from TMS using the residual protonated solvent as an internal standard ($CDCl_3$, ^{1}H 7.26 ppm and ^{13}C 77.0 ppm; DMSO-d_6, ^{1}H 2.49 ppm and ^{13}C 39.5 ppm). HRMS (CI) was obtained on a VG analytical ZAB2-E instrument. IR data was recorded

on a Nicolet Avatar 360 FT-IR and all peaks are reported in cm^{-1}. Melting points and glass transition temperatures (T_g) were recorded on a TA Q100 Differential Scanning Calorimeter (DSC).

C.5.1 General Procedure for C.1-6

A 250 mL RBF with a condenser was charged with dichlone (5.0 g, 22.0 mmol), substituted aniline (66 mmol), EtOH (100 mL), and a stir bar. The solution was heated to 85 °C overnight and then cooled to rt. 2-aryl-amino-3-chloro napthoquinone was isolated by filtration in excellent yield.

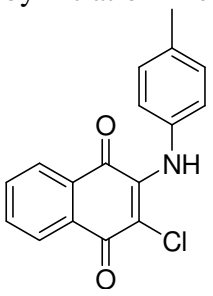

2-Chloro-3-p-tolylamino-[1,4]naphthoquinone, C.1

Deep red solid; yield (12.5 g, 97 %); Mp = 200 °C; ^{1}H NMR ($CDCl_3$) δ ppm: 8.181 (dt, *J* = 5.7, 0.6 Hz, 1H), 8.102 (dt, *J* = 5.7, 0.6 Hz, 1H), 7.759 (td, *J* = 5.7, 1.2 Hz, 1H), 7.675 (td, *J* = 5.7, 1.2 Hz, 1H), 7.655 (br s, 1H), 7.149 (d, *J* = 6.0, 2H), 6.984 (d, *J* = 6.0, 2H), 2.364 (s, 3H); ^{13}C NMR ($CDCl_3$) δ ppm: 180.554, 177.407, 141.597, 135.607, 134.990, 134.774, 132.839, 132.624, 129.811, 128.970, 127.066, 126.917, 124.328, 114.172, 21.012; IR (KBr) cm^{-1}: 3324, 1625, 1592, 1560, 1496, 1280, 816; HRMS (CI): 298.0635 calc, 298.0634 found.

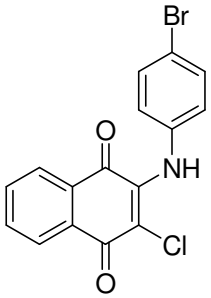

2-(4-Bromo-phenylamino)-3-chloro-[1,4]naphthoquinone, C.2

Deep red solid; Yield; (7.1 g, 99%); Mp = 264-265 °C; ^{1}H NMR (400 MHz) ($CDCl_3$) δ ppm: 9.342 (br s, 1H), 8.024 (d, *J* = 6.8 Hz, 2H), 7.858 (td, *J* = 7.6 Hz, 1.6 Hz, 1H), 7.799 (td, *J* = 7.6 Hz, 1.6 Hz, 1H), 7.471 (dd, *J* = 6.4 Hz, 2.0 Hz, 2H), 7.060 (dd, *J* = 6.8 Hz, 2.0 Hz, 2H); ^{13}C NMR ($CDCl_3$) δ ppm:; IR (KBr) cm^{-1}: 3243, 2353, 1675, 1637, 1600, 1566, 1505, 1483; HRMS (CI): 361.9588 calc, 361.9583 found.

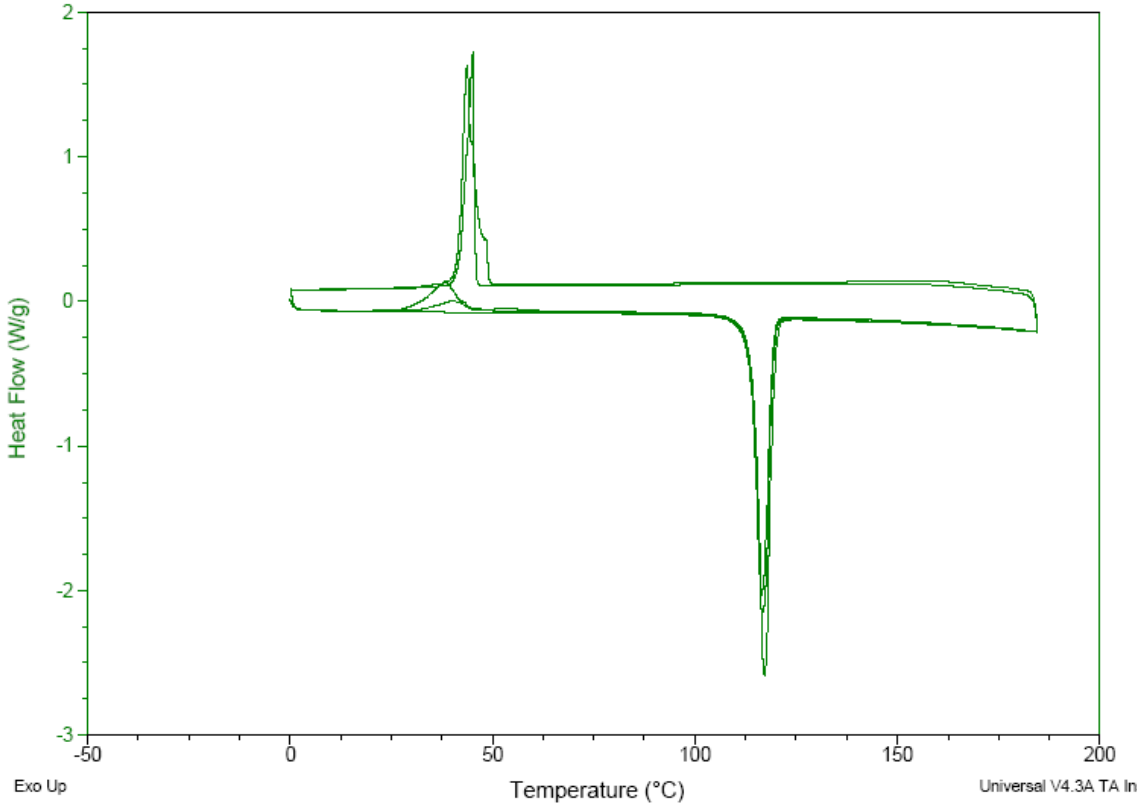

Figure C.5: DSC trace of 4-Br, Cl (C.2).

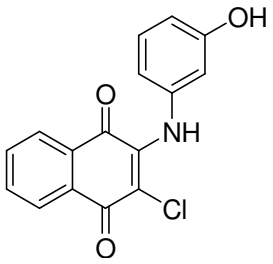

2-Chloro-3-(3-hydroxy-phenylamino)-[1,4]naphthoquinone, C.3

Deep red solid; Yield (6.3 g, 95%); ^{1}H NMR (400 MHz) ($CDCl_3$) δ ppm: 9.438 (br s, 1H), 9.181 (br s, 1H), 8.018 (d, *J* = 7.6 Hz, 2H), 7.855 (td, *J* = 7.6 Hz, 1.6 Hz, 1H), 7.793 (td, *J* = 7.6 Hz, 1.6 Hz, 1H), 7.065 (t, *J* = 7.6 Hz, 2H), 6.537 (m, 3H); ^{13}C NMR (1:1 DMSO-d_6:$CDCl_3$) δ ppm: 179.875, 176.468, 156.877, 142.376, 139.013, 134.348, 132.570, 131.841, 129.750, 128.136, 126.268, 125.971, 114.847, 113.940, 111.790, 111.068; IR (KBr) cm^{-1}: 3340, 3253, 2361, 1677, 1598, 1548, 1505, 1466; HRMS (CI): 300.0428 calc, 300.0427 found. Utilizing a benchtop apparatus, Mp = 220-222 °C, but by DSC traces of this compound did not show this Mp. It is believed the compound is subliming near this temperature.

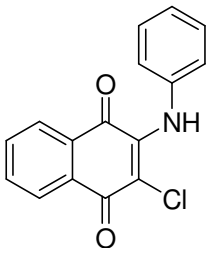

2-Chloro-3-phenylamino-[1,4]naphthoquinone, C.4

Deep red solid; yield (6.0 g, 96%); Mp = 210-212 °C; ^{1}H NMR (400 MHz) (DMSO-d_6) δ ppm: 9.304 (s, 1H), 8.022 (dt, J = 7.2, 1.2 Hz, 2H), 7.879 (td, J = 7.6, 1.6 Hz, 1H), 7.791 (td, J = 7.6, 1.2 Hz, 1H), 7.304 (t, J = 7.6 Hz, 2H), 7.117 (m, 3H); ^{13}C NMR (1:1 DMSO-d_6:$CDCl_3$) δ ppm: ; IR (KBr) cm^{-1}: 3238, 1675, 1562, 1444, 1289, 1140; HRMS (CI): 284.0478 calc, 284.0479 found.

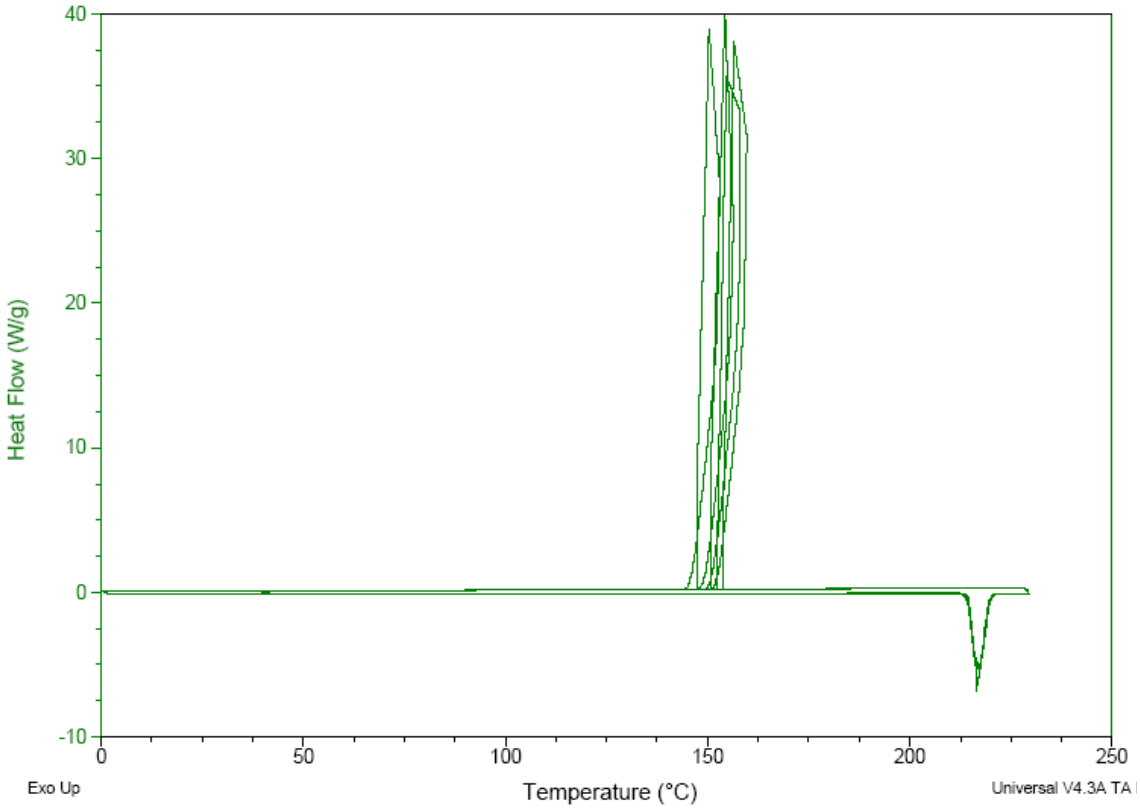

Figure C.6: DSC trace of 4-H, Cl (C.4).

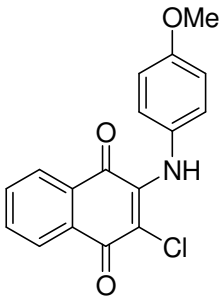

2-Chloro-3-(4-methoxy-phenylamino)-[1,4]naphthoquinone, C.5

Deep red solid; yield (6.8 g, 99%); ^{1}H-NMR (400 MHz) (CDCl3) δ ppm: 9.216 (br s, 1H), 8.021 (dd, J = 2.8 Hz, 0.8 Hz, 1H), 8.003 (dd, J = 3.2 Hz, 1.6 Hz, 1H), 7.847 (td, J = 7.6 Hz, 3.2 Hz, 1H), 7.778 (td, J = 7.6 Hz, 2.4 Hz, 1H), 7.078 (d, J = 6.8 Hz, 2H), 6.881 (d, J = 6.8 Hz, 2H), 3.747 (br s, 1H); ^{13}C-NMR (CDCl3) δ ppm:; IR (KBr) cm^{-1}: 3245, 1676, 1634, 1595, 1567, 1497, 1288, 1237; HRMS (CI): 314.0588 calc, 314.0584 found; Mp = 219-220 °C.

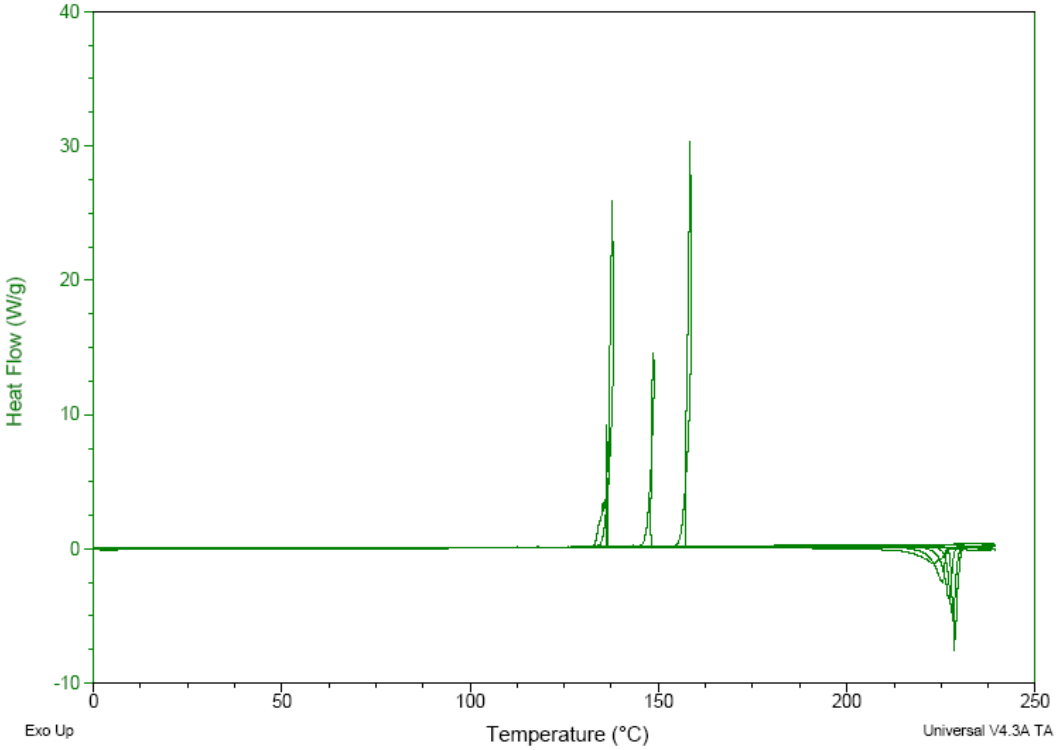

Figure C.7: DSC trace of 4-OMe, Cl (C.5).

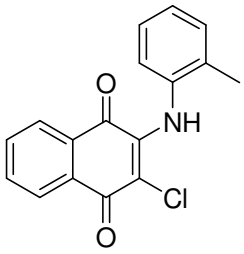

2-Chloro-3-o-tolylamino-[1,4]naphthoquinone, C.6

Dark red solid; yield (1.3 g, 98.3%); Mp = (dec.); ^{1}H NMR ($CDCl_3$) δ ppm: 8.186 (dd, *J* = 6.0, 1.2 Hz, 1H), 8.120 (dd, *J* = 5.7, 0.9 Hz, 1H), 7.768 (td, *J* = 5.4, 0.9 Hz, 1H), 7.686 (td, *J* = 5.4, 0.9 Hz, 1H), 7.477 (br s, 1H), 7.215 (m, 3H), 7.041 (m, 1H), 2.299 (s, 3H); ^{13}C NMR ($CDCl_3$) δ ppm: 180.435, 177.377, 142.110, 136.277, 135.042, 133.814, 132.817, 132.661, 130.302, 129.781, 127.081, 126.909, 126.798, 126.299, 125.868, 113.591, 18.184; IR (KBr) cm^{-1}:3247, 1674, 1637, 1507, 1481, 1287, 1143, 749; HRMS (CI): 298.0635 calc, 298.0635 found.

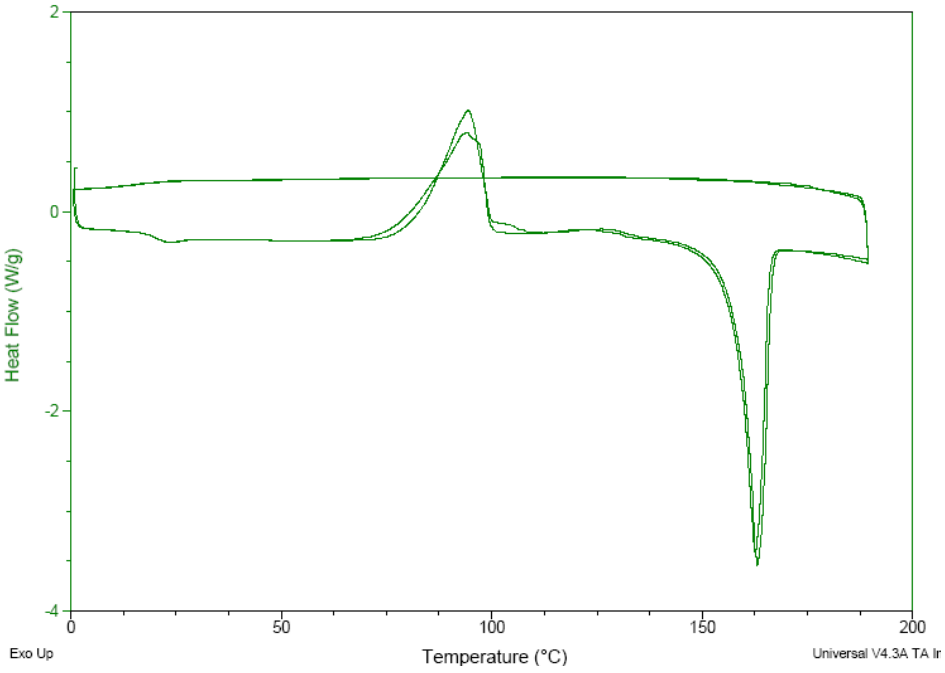

Figure C.8: DSC trace of 2-Me, Cl (C.6).

C.5.2 General Procedure for C.7-12

A 20 mL vial was charged with 2-Chloro-3-aryllamino-[1,4]naphthoquinone (5.0 mmol), freshly distilled piperidine (50 mmol), and a stir bar. After sealing the reaction vessel, it was stirred at 80 °C for 24 h. Upon cooling to rt, the dark green reaction mixture was diluted with DCM (200 mL), washed with 2 M HCl (3 x 75 mL), dried over $MgSO_4$, and concentrated *in vacuo*. Flash chromatography (7:3 Hex:EtOAc) yielded 2-Piperidin-3-arylamino-[1,4]naphthoquinone as a dark green solid in fair to excellent yield.

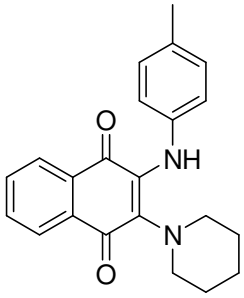

2-Piperidin-1-yl-3-p-tolylamino-[1,4]naphthoquinone, C.7

Yield: 96.6%; T_g= 15 °C, T_m = 123 °C ; ^{1}H NMR (600 MHz) ($CDCl_3$) δ ppm: 7.982 (ddd, *J* = 7.8, 1.8, 0.6 Hz, 1H), 7.964 (ddd, *J* = 7.2, 1.2, 0.6 Hz, 1H), 7.609 (td, *J* = 7.8, 1.8 Hz, 1H), 7.558 (td, *J* = 7.2, 1.2 Hz, 1H), 7.030 (d, *J* = 8.4 Hz, 2H), 6.755 (d, *J* = 6.6 Hz, 2H), 3.075 (m, 4H), 2.304 (s, 3H), 1.349 (m, 6H); ^{13}C NMR ($CDCl_3$) δ ppm: 182.310, 181.863, 137.274, 133.606, 133.412, 132.817, 132.438, 131.798, 130.831, 130.719, 128.725, 126.203, 125.459, 120.258, 49.739, 26.034, 24.204, 20.833; IR (KBr) cm^{-1}: 3312, 2931, 2844, 1653, 1636, 1516, 1405, 1287, 971; HRMS (CI): 347.1760 calc, 347.1756 found.

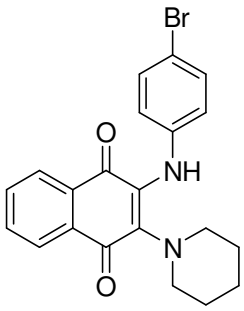

2-(4-Bromo-phenylamino)-3-piperidin-1-yl-[1,4]naphthoquinone, C.8

Yield: 69.5%; ^{1}H NMR (DMSO-d_6) δ ppm: 8.173 (s, 1H), 7.920 (m, 1H), 7.903 (m, 1H), 7.732 (dtd, *J* = 14.8, 7.6, 1.6 Hz, 2H), 7.319 (dt, *J* = 6.8, 2.8 Hz, 2H), 6.849 (dt, *J* = 6.8, 3.2 Hz, 2H), 3.044 (m, 4H), 1.298 (m, 6H) ;^{13}C NMR (DMSO-d_6) δ ppm: 181.356, 181.304, 140.405, 136.655, 133.545, 133.076, 132.176, 130.502, 130.427, 128.634, 125.948, 125.041, 120.606, 111.544, 49.343, 25.624, 23.801; IR (KBr) cm^{-1}: 3340, 2932, 2850, 1636, 1553, 1507, 1281; HRMS (CI): 411.0708 calc, 411.0702 found; T_d = 199 °C, $T_{90\%}$ = 208 °C, T_g = 43 °C, T_m = 142 °C.

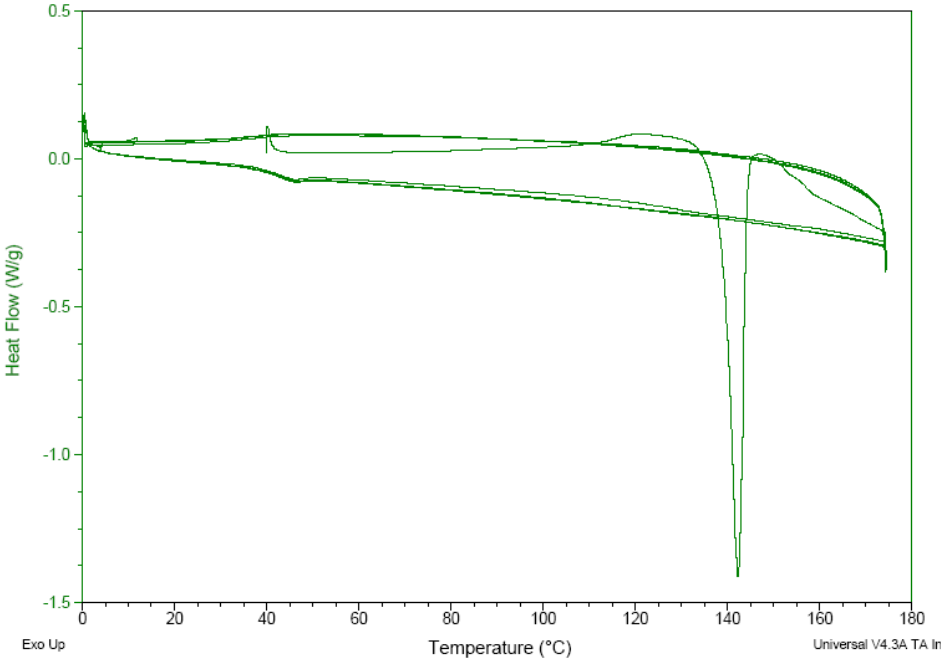

Figure C.9: DSC trace of 4-Br, pip (C.8).

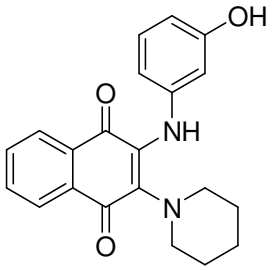

2-(3-Hydroxy-phenylamino)-3-piperidin-1-yl-[1,4]naphthoquinone, C.9

Yield: 69.7%; ^{1}H NMR (DMSO-d_6) δ ppm: 9.141 (br s, 1H), 7.892 (m, 3H), 7.719 (dtd, *J* = 15.6, 7.6, 1.6 Hz, 2H), 6.948 (t, *J* = 8.0 Hz, 1H), 6.390 dd, J = 7.2, 1.2 Hz, 1H), 6.296 (m, 3H)3.072 (m, 4H), 1.276 (m, 6H) ;^{13}C NMR (DMSO-d_6) δ ppm:181.505, 181.267, 157.242, 141.915, 135.859, 133.575, 132.994, 132.161, 130.405, 129.549, 128.493, 125.874, 125.033, 110.234, 107.913, 106.336, 49.306, 25.542, 23.905; IR (KBr) cm^{-1}: 3355, 3302, 2936, 2847, 1589, 1291; HRMS (CI): 349.1552 calc, 349.1551 found; T_d = 190 °C, $T_{90\%}$ = 200 °C, T_g = 70 °C, T_m = 147 °C.

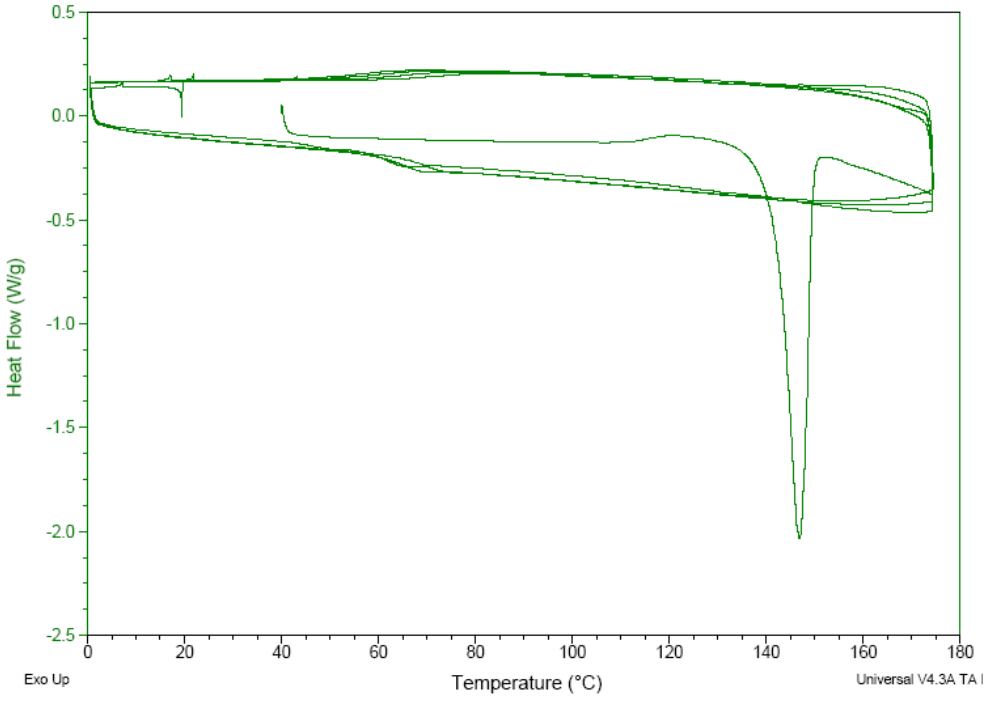

Figure C.10: DSC trace of 3-OH, pip (C.9).

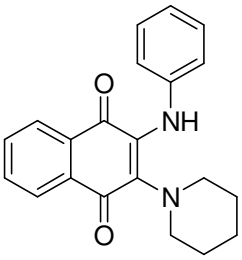

2-Phenylamino-3-piperidin-1-yl-[1,4]naphthoquinone, C.10

Yield: 84.5%; ^{1}H NMR (DMSO-d_6) δ ppm: 8.061 (s, 1H), 7.912 (dd, *J* = 7.2, 1.2 Hz, 2H), 7.731 (dtd, *J* = 17.6, 7.2, 1.2 Hz, 2H), 7.182 (t, *J* = 8.0 Hz, 2H), 6.894 (m, 3H), 3.015 (m, 4H), 1.238 (m, 6H) ;^{13}C NMR (DMSO-d_6) δ ppm:181.646, 181.155, 140.554, 135.316, 133.619, 132.942, 132.273, 130.390, 129.847, 127.816, 125.889, 125.033, 120.762, 119.334, 49.276, 25.416, 23.846; IR (KBr) cm^{-1}: 3309, 2990, 2918, 2835, 1638, 1553, 1407, 1280; HRMS (CI): 335.1760 calc, 335.1759 found; T_d = 192 °C, $T_{90\%}$ = 198 °C, T_g= 43 °C, T_m = 144 °C.

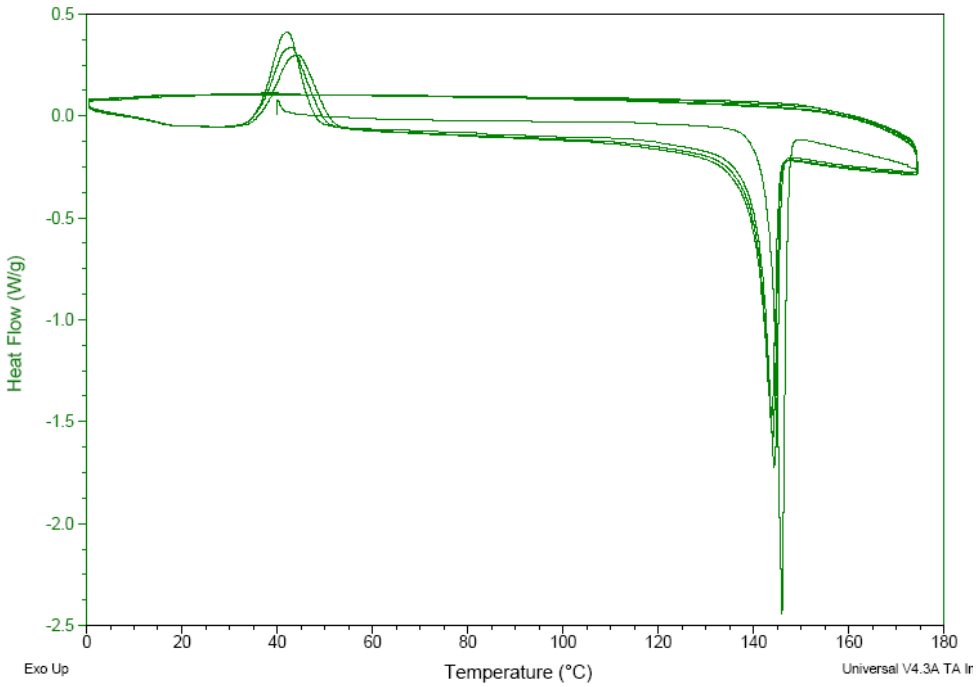

Figure C.11: DSC trace of 4-H, pip (C.10).

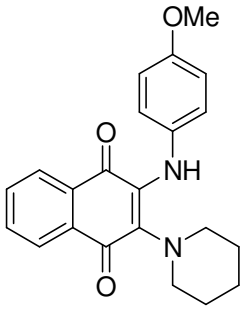

2-(4-Methoxy-phenylamino)-3-piperidin-1-yl-[1,4]naphthoquinone, C.11

Yield: 81.9%; ^{1}H NMR (DMSO-d_6) δ ppm: 8.051 (br s 1H), 7.901 (t, J = 1.6 Hz, 1H), 7.881 (t, J = 1.6 Hz, 1H), 7.743 (td, J = 7.7, 1.2 Hz, 1H), 7.684 (td, J = 7.7, 1.2 Hz, 1H), 6.891 (dd, J = 6.8, 2.0 Hz, 2H), 6.794 (dd, J = 6.8, 2.0 Hz, 2H), 2.933 (t, J = 5.2 Hz, 4H), 1.199 (m, 6H) ;^{13}C NMR (DMSO-d_6) δ ppm: 182.003, 180.694, 154.534, 133.798, 133.091, 132.637, 132.466, 132.354, 132.302, 130.249, 125.733, 125.026, 121.938, 112.973, 55.258, 49.336, 25.244, 23.838; IR (KBr) cm^{-1}: 3301, 3002, 2936, 2835, 2812, 1663, 1509, 1557, 1331, 1288, 1045, 970, 732; HRMS (CI): 363.1709 calc, 363.1707 found; T_d = 208 °C, $T_{90\%}$ = 220 °C, T_g = 21 °C, T_m = 126 °C.

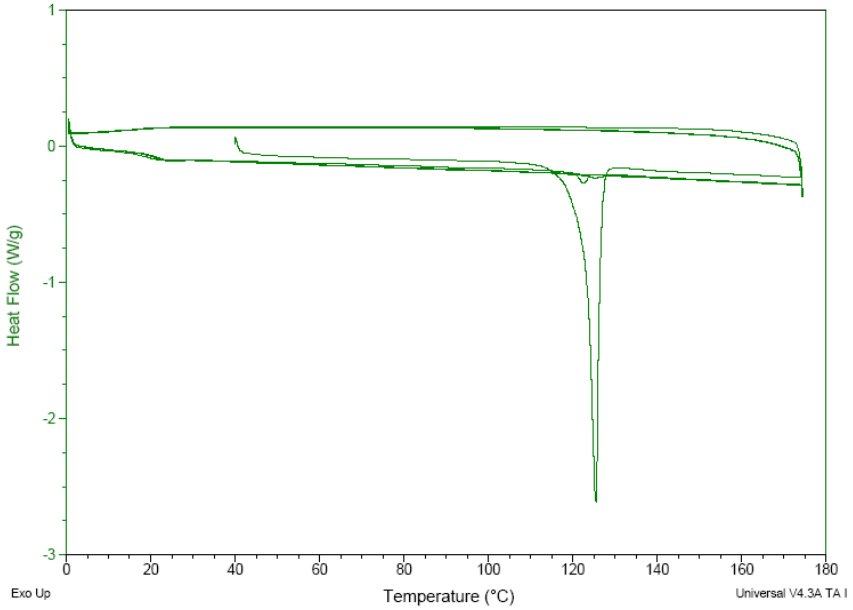

Figure C.12: DSC trace of 4-OMe, pip (C.11).

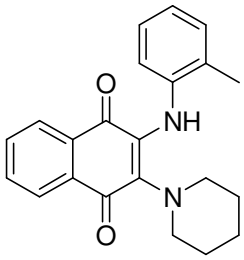

2-Piperidin-1-yl-3-o-tolylamino-[1,4]naphthoquinone, C.12

Yield: 98.9%; Tg= 23 °C, Tm = 117 °C; 1H NMR (400 MHz) (CDCl3) δ ppm: 8.003 (t, J = 7.2 Hz, 2H), 7.650 (t, J = 7.2 Hz, 1H), 7.594 (td, J = 7.6, 1.2 Hz, 1H), 7.167 (d, J = 7.2, 1H), 7.098 (t, J = 8.0 Hz, 1H), 6.975 (t, J = 7.2 Hz, 1H), 6.866 (br s, 1H), 6.673 (d, J = 8.0 Hz, 1H) 3.036 (m, 4H), 2.360 (s, 3H), 1.302 (m, 6H); ^{13}C NMR ($CDCl_3$) δ ppm:182.206, 181.819, 137.929, 133.412, 132.713, 132.363, 131.470, 130.555, 129.752, 128.978, 126.106, 126.032, 125.570, 125.392, 122.661, 120.585, 49.590, 25.803, 24.047, 17.954; IR (KBr) cm^{-1}: 3314, 2938, 2841, 1643, 1630, 1415, 1287, 971; HRMS (CI): 347.1760 calc, 347.1756 found.

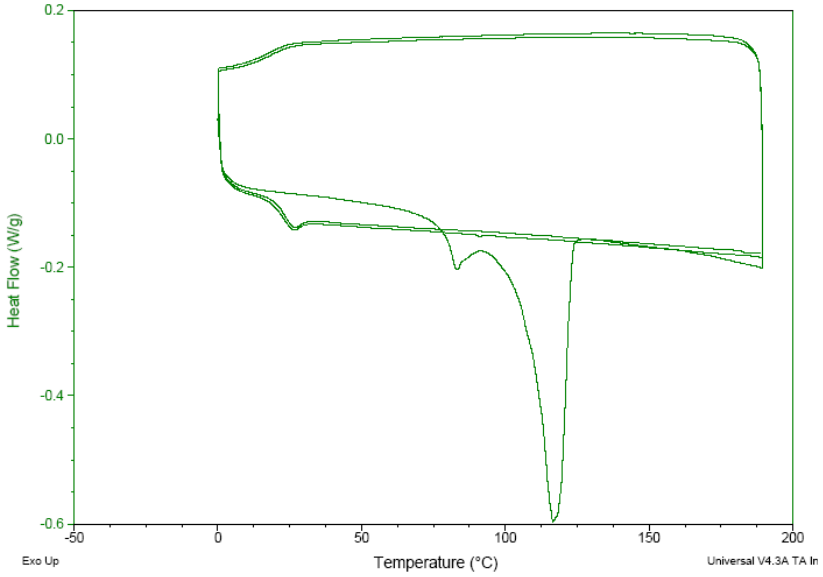

Figure C.13: DSC trace of 2-Me, pip (C.12).

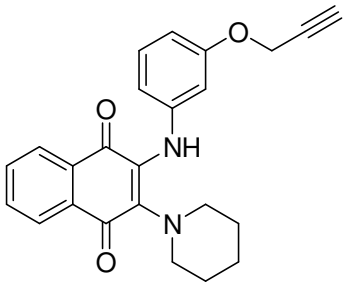

2-Piperidin-1-yl-3-(3-prop-2-ynyloxy-phenylamino)-[1,4]naphthoquinone, C.13

A 100 mL RBF was loaded with 2-(3-hydroxyphenylamino)-3-(piperidin-1-yl)naphthalene-1,4-dione (0.5 g, 1.4 mmol), potassium carbonate (0.5 g, 3.6 mmol) and a stir bar. The flask was put under vacuum and heated to 50 °C for 2 h, and then put under an inert atmosphere. Propargyl bromide (0.5 g, 3.4 mmol, 80% in toluene) and acetone (7 mL, freshly distilled over 4 Å molecular sieves) were injected into the reaction flask. A condenser was added, and the reaction was heated to reflux for 12 d. The reaction was reduced *in vacuo* and subjected to flash chromatography (3:7 Hex:EtOAc) to give 2-(piperidin-1-yl)-3-(3-(prop-2-ynyloxy)phenylamino)naphthalene-1,4-dione in moderate yield (0.45 g, 81%) as a dark green solid. T_g = 20 °C, T_m = decomp., T_d = 199 °C, $T_{90\%}$ = 212 °C; ^{1}H-NMR ($CDCl_3$) δ ppm = 8.018 (m, 2H), 7.673 (m, 2H), 7.176 (t, J = 10.4 Hz, 1H), 7.084 (s, 1H), 6.639 (dd, J = 12.0, 2.0 Hz, 1H), 6.545 (dd, J = 12.0, 2.0 Hz, 1H), 6.488 (t, J = 2.8 Hz, 1H), 4.696 (m, 2H), 3.191 (s, 4H), 2.524 (t, J = 3.2 Hz, 1H), 1.412 (s, 6H); ^{13}C NMR ($CDCl_3$) δ ppm: 182.089, 157.871, 141.442, 135.081, 133.370, 132.670, 130.691, 129.151, 128.928, 126.324, 125.483, 113.318, 107.820, 107.187, 78.609, 75.492, 55.849, 49.719, 26.133, 24.221; IR (NaCl) cm^{-1}: 3298, 2934, 2851, 2120, 1637, 1590, 1506, 1286, 1203, 1155, 1043, 977; HRMS (CI) = 387.1709 calc., 387.1711 found.

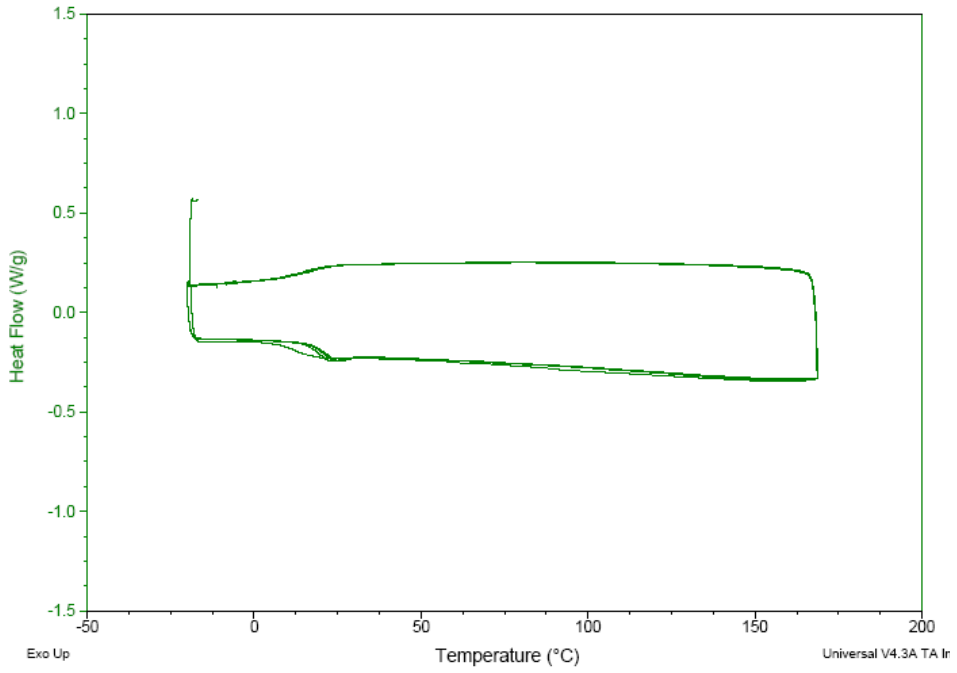

Figure C.14: DSC trace of 3-propargyl, Cl (C.13).

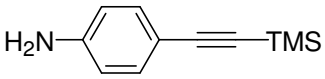

4-Trimethylsilanylethynyl-phenylamine, C.14

In a procedure modified from Long[17], a 250 mL RBF was loaded with TEA (16 mL, 114.1 mmol), THF (105 mL), and TMS-acetylene (4 mL, 28.5 mmol). The flask was then subjected to three freeze, pump, thaw cycles and kept under inert atmosphere. A second 250 mL RBF under inert atmosphere was loaded with 4-iodoaniline (2.5 g, 11.4 mmol), CuI (109 mg, 0.6 mmol), $PdCl_2(PPh_3)_2$ (0.8 g, 1.1 mmol), and a stir bar. The liquids from the first flask were transferred to the solids in the second flask via a cannula to yield a dark red solution upon stirring. A condenser was added and the reaction was heated to 60°C for 4 h, at which point the reaction was determined complete by GC/MS. The black reaction mixture was removed from heat and concentrated *in vacuo*. The

reaction was diluted with ether and washed one time each with water then brine. The combined organic layers were dried over $MgSO_4$, filtered, and concentrated *in vacuo*. The resulting viscous solution was immediately loaded for flash chromatography. Flash chromatography (7:3 Hex:EtOAc) yielded 4-(trimethylsilylethynyl)aniline as a yellow/brown solid in moderate yield (1.5 g, 69% yield); T_m = decomp.; ^{1}H NMR ($CDCl_3$) δ ppm: 7.272 (d, J = 9.2 Hz, 2H), 6.572 (d, J = 8.8 Hz, 2H), 3.788 (br, s, 2H), 0.226 (s, 9H); ^{13}C NMR ($CDCl_3$) δ ppm: 146.753, 133.360, 114.507, 112.483, 105.965, 91.360, 0.127; IR (KBr) cm^{-1}: 3456, 3372, 2957, 2143, 1622, 1510, 1248, 838; HRMS (CI) = 190.1052 calc, 190.1053 found.

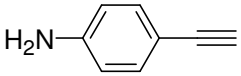

4-Ethynyl-phenylamine, C.15

In a procedure modified from Long, a 100 mL RBF was loaded with K_2CO_3 (2.7 g, 19.8 mmol), 4-trimethylsilanylethynyl-phenylamine (1.3 g, 6.6 mmol), MeOH (50 mL), and a stir bar. The reaction was stirred at rt for 4 h at which point the reaction was complete by TLC. The reaction was concentrated *in vacuo,* and 4-ethynyl-phenylamine was isolated by column chromatography (7:3 Hex:EtOAc) as a yellow solid in moderate yield (470 mg, 61%). T_m = decomp.; ^{1}H-NMR ($CDCl_3$) δ ppm = 7.2045 (d, *J* = 8.4 Hz, 2H), 6.4885 (d, *J* = 8.4 Hz, 2H), 3.726 (br, s, 2H), 2.880 (s, 1H), ^{13}C NMR ($CDCl_3$) δ ppm: 146.968, 133.404, 114.524, 111.201, 84.355, 74.884; IR (KBr) cm^{-1}: 3483, 3388, 3261, 2337, 2097, 1617, 1512, 1305, 1215, 1178, 828; HRMS (CI) = 118.0657 calc, 118.0654 found.

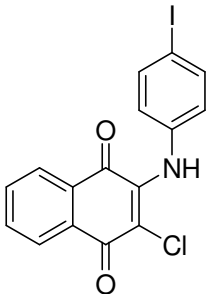

2-Chloro-3-(4-iodo-phenylamino)-[1,4]naphthoquinone, C.16

Yield: 85%; T_m = decomp.; T_d = 267 °C, $T_{90\%}$ = 287 °C; ^{1}H-NMR (DMSO) δ ppm = 9.318 (s, 1H), 8.015 (d, *J* = 7.6 Hz, 2H), 7.820 (dtd, *J* = 24, 7.2, 1.2 Hz, 2H), 7.614 (d, *J* = 8.4 Hz, 2H), 6.914 (d, *J* = 8.4 Hz, 2H); ^{13}C NMR (DMSO) δ ppm: 180.022, 176.722, 142.923, 138.954, 136.521, 134.752, 133.266, 131.890, 130.346, 126.522, 126.092, 125.714, 115.401, 88.258; IR (KBr) cm^{-1}: 3261, 2921, 1674, 1639, 1599, 1364, 1301, 1294, 1242, 1140; HRMS (CI) = 408.9367 calc., 408.9367 found.

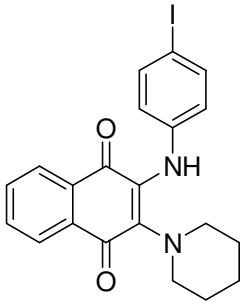

2-(4-Iodo-phenylamino)-3-piperidin-1-yl-[1,4]naphthoquinone, C.17

Yield: 45%; T_g = 46.9 °C, T_m = 147 °C, T_d = 204 °C, $T_{90\%}$ = 225 °C; ^{1}H-NMR ($CDCl_3$) δ ppm = 7.934 (m, 2H), 7.557 (m, 2H), 7.455 (dt, *J* = 8.8, 2.4 Hz, 2H), 6.956 (s, 1H), 6.543 (dt, *J* = 8.8, 2.4 Hz, 2H), 3.065 (s, 4H), 1.360 (s, 6H); ^{13}C NMR ($CDCl_3$) δ ppm: 181.947, 139.865, 137.082, 135.088, 133.474, 132.804, 132.588, 130.639, 128.413, 126.413, 125.543, 121.480, 84.137, 49.711, 26.200, 24.146; IR (KBr) cm^{-1}: 3294, 2915, 2850, 1633, 1548, 1495, 1388, 1280, 1251; HRMS (CI) = 458.0491 calc., 458.0491 found.

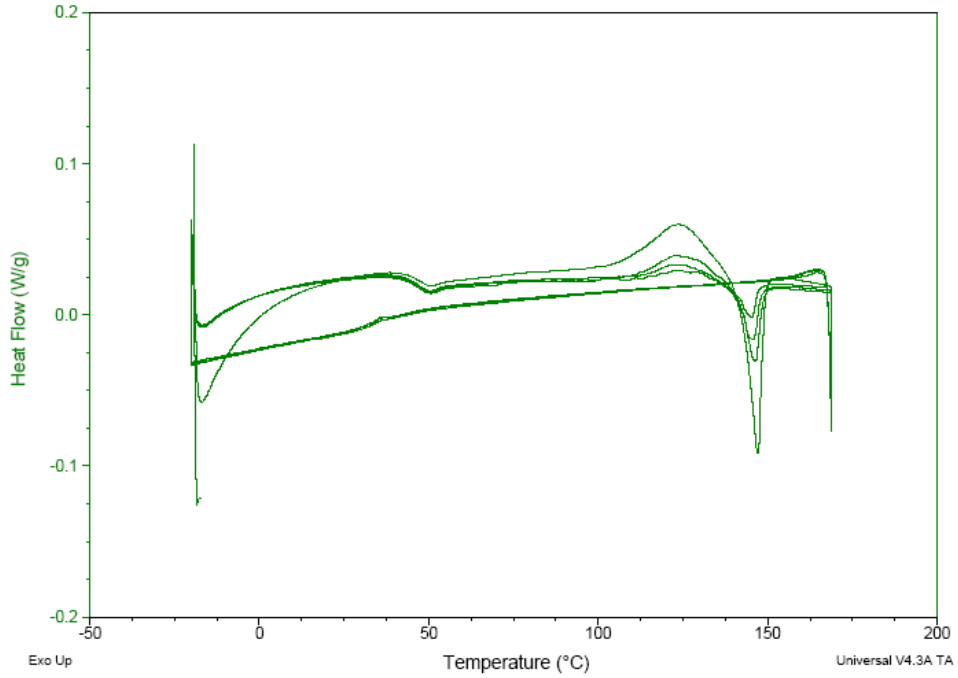

Figure C.15: DSC trace of 4-I, pip (C.17).

C.6 CONCLUSION

A series of compounds was synthesized to function as a thermal resist responsive to visible wavelengths of light. The photoproducts of these 2,3-diamino-naphthoquinones should have a sublimation temperature well above that of the starting material, and future work will be directed at identifying these photoproducts, material properties related to thin film deposition, and surface plasmon imaging.

C.7 REFERENCES

1. Huang, C.-P.; Zhu, Y.-Y. In *Active and Passive Electronic Components* 2007; Vol. 1, p 1-13.

2. Sanders, E. W., *Optical Properties of Metallic Nanoparticles*, Yale University, **2007**.

3. Maier, S. A.; Atwater, H. A. *J. Appl. Phys.* **2005**, *98*, 011101/011101-011101/011110.

4. Jain, P. K.; Huang, X.; El-Sayed, I. H.; El-Sayed, M. A. *Plasmonics* **2007**, *2*, 107-118.

5. Srituravanich, W.; Fang, N.; Sun, C.; Luo, Q.; Zhang, X. *Nano Lett.* **2004**, *4*, 1085-1088.

6. Luo, X.; Ishihara, T. *Opt Express* **2004**, *12*, 3055-3065.

7. Srituravanich, W.; Durant, S.; Lee, H.; Sun, C.; Zhang, X. *J. Vac. Sci. Technol., B: Microelectron. Nanometer Struct.--Process., Meas., Phenom.* **2005**, *23*, 2636-2639.

8. Luo, X.; Ishihara, T. *Appl. Phys. Lett.* **2004**, *84*, 4780-4782.

9. Liu, Z.-W.; Wei, Q.-H.; Zhang, X. *Nano Lett.* **2005**, *5*, 957-961.

10. Dintinger, J.; Degiron, A.; Ebbesen, T. W. *MRS Bull.* **2005**, *30*, 381-384.

11. Kanyogoro, E.; Peckerar, M.; Hughes, H.; Liu, M. *Solid-State Electron.* **2008**, *52*, 1555-1562.

12. Personal Communication, Lezec, H., *Surface Plasmon*, **2004.**

13. Wang, L.; Jin Eric, X.; Uppuluri Sreemanth, M.; Xu, X. *Opt Express* **2006**, *14*, 9902-9908.

14. Chun, C. *Organic Holographic Materials and Applications III*, 2005, 5939.

15. Noach, S.; Manevich, M.; Eisenberg, N.; Fokin, E. P.; Mihalina, T. V. *Nanotechnology* **2005**, *16*, 775-778.

16. Win, T.; Yerushalmi, S.; Bittner, S. *Synthesis* **2005**, 1631-1634.

17. Long, B. K.; Keitz, B. K.; Webb, R. C.; Wilson, C. G. *Polym. Prepr. (Am. Chem. Soc., Div. Polym. Chem.)* **2008**, *49*, 264-265.

Glossary

AFM	Atomic force microscopy
BC	Block copolymer
CAR	Chemically amplified resists
DIBAL-H	Diisobutyl aluminum hydride
DCM	Dichloromethane
DNQ	Diazonapthoquinone
DSC	Differential scanning calorimetry
EBL	electron beam lithography
EUV	Extreme ultraviolet
GPC	Gel permeation chromatography
HRMS	High resolution mass spectroscopy
IC	Integrated circuit
IPA	isopropyl alcohol
IR	Infrared
ITRS	International technology roadmap for semiconductors
LAH	Lithium aluminum hydride
LER	Line edge roughness
MIBK	Methyl isobutyl ketone
MMA	Methyl methacrylate
M_n	Number average molecular weight
M_w	Weight average molecular weight
MW	Molecular weight
NBA	*o*-nitro benzyl alcohol

NCAR	Non-chemically amplified resists
NIL	Nanoimprint lithography
NMR	Nuclear magnetic resonance
PAB	Post apply bake
PAG	Photoacid generator
PCC	Pyridinium chlorochromate
PDI	Polydispersity Index
PDI	Polymeric dissolution inhibitor (Chapters 3 & 4)
PEB	Post exposure bake
PGMEA	Propylene glycol monomethyl ether acetate
PMMA	Poly(methyl methacrylate)
PNBHFA	Poly(norbornenehexafluoroalcohol)
PPHA	Polyphthalaldehyde
PS	Polystyrene
RI	Refractive index
RIE	Reactive ion etch
SAXS	Small angle x-ray scattering
SEM	Scanning electron microscope
SFIL	Step and flash imprint lithography
TBDMS	*tert*-butyl dimethyl silane
t-BOC	*tert*-Butyl carbonate
T_c	Ceiling temperature
TEA	Triethyl amine
T_g	Glass transition temperature
TGA	Thermal gravimetric analysis

THF	Tetrahydrofuran
TMAH	Tetramethyl ammonium hydroxide
TMS	Trimethyl silyl
UV	Ultraviolet

Bibliography

1. http://www.computerhistory.org/timeline/?year=1947. **2006**.

2. www.nobelprize.org. **2010**.

3. http://inventors.about.com/od/istartinventions/a/intergrated_circuit.htm.

4. http://www.itrs.net/reports.html. **2007**.

5. http://www.hitachigst.com/hdd/research/storage/pm/index.html. **2004**.

6. https://asml.picturepark.com/Website/Publisher.aspx?Page=ASML. **2010**.

7. *Contact angle, wettability & adhesion*; VSP: Boston, 2002; Vol. 2,

8. http://www2.dupont.com/Plastics/en_US/Products/Delrin/Delrin.html. **2009**.

9. http://www.intel.com/technology/architecture-silicon/32nm/.

10. *Polymer Handbook*; Wiley, 1989, 411-432.

11. http://www.pbs.org/transistor/index.html. **1999**.

12. http://www.intel.com/technology/architecture-silicon/2billion.htm. **2009**.

13. Akue-Gedu, R.; Rigo, B. *Tetrahedron Lett.* **2004**, *45*, 1829-1832.

14. Allcock, H. *Contemporary Polymer Chemistry*; Prentice Hall: Upper Saddle River, 1990, 236-240.

15. Allen, R. D.; Long, T. E.; McGrath, J. E. *Polym. Bull. (Berlin)* **1986**, *15*, 127-134.

16. Anslyn, E. V. *Modern Physical Organic Chemistry*; University Science: Sausalito, 2004, 68-70.

17. Auriemma, F.; De Rosa, C.; Corradini, P. *Adv. Polym. Sci.* **2005**, *181*, 1-74.

18. Bailey, T. C., Dissertation, *Imprint template advances and surface modification, and defect analysis for step and flash imprint lithography*, The University of Texas at Austin, **2003**.

19. Bang, J.; Bae, J.; Lowenhielm, P.; Spiessberger, C.; Given-Beck, S. A.; Russell, T. P.; Hawker, C. J. *Adv. Mater. (Weinheim, Ger.)* **2007**, *19*, 4552-4557.

20. Bates, F. S.; Fredrickson, G. H. *Phys. Today* **1999**, *52*, 32-38.

21. Blanc, A.; Bochet, C. G. *Org. Lett.* **2007**, *9*, 2649-2651.

22. Bosworth, J. K.; Paik, M. Y.; Ruiz, R.; Schwartz, E. L.; Huang, J. Q.; Ko, A. W.; Smilgies, D.-M.; Black, C. T.; Ober, C. K. *ACS Nano* **2008**, *2*, 1396-1402.

23. Brandrup, J. *Polymer Handbook*; 4th ed.; Wiley-Interscience, 1999, 432.

24. Brzoska, J. B.; Azouz, I. B.; Rondelez, F. *Langmuir* **1994**, *10*, 4367-4373.

25. Chen, C.-Y.; Pittman, C. U., Jr.; Helbert, J. N. *J. Polym. Sci., Polym. Chem. Ed.* **1980**, *18*, 169-178.

26. Chun, C. *Organic Holographic Materials and Applications III*, 2005, 5939.

27. Cochran, E. W.; Garcia-Cervera, C. J.; Fredrickson, G. H. *Macromolecules* **2006**, *39*, 2449-2451.

28. Cochran, E. W.; Morse, D. C.; Bates, F. S. *Macromolecules* **2003**, *36*, 782-792.

29. Colburn, M.; Grot, A.; Amistoso, M. N.; Choi, B. J.; Bailey, T. C.; Ekerdt, J. G.; Sreenivasan, S. V.; Hollenhorst, J.; Willson, C. G. *Proc. SPIE-Int. Soc. Opt. Eng.* **2000**, *3997*, 453-457.

30. Colburn, M. E., Dissertation, *Step and flash imprint lithography: a low-pressure, room-temperature nanoimprint lithography*, The University of Texas at Austin, **2001**.

31. Coleman, M. M.; Graf, J. F.; Painter, P. C. *Specific Interactions and the Miscibility of Polymer Blends*; Technomic: Landcaster, 1991, 1-45.

32. Crivello, J. V. *J. Polym. Sci., Part A: Polym. Chem.* **1999**, *37*, 4241-4254.

33. Delaire, J. A.; Lagarde, M.; Broussoux, D.; Dubois, J. C. *J. Vac. Sci. Technol., B* **1990**, *8*, 33-38.

34. Dintinger, J.; Degiron, A.; Ebbesen, T. W. *MRS Bull.* **2005**, *30*, 381-384.

35. Emmanuvel, L.; Shaikh, T. M. A.; Sudalai, A. *Org. Lett.* **2005**, *7*, 5071-5074.

36. Fadeev, A. Y.; McCarthy, T. J. *Langmuir* **2000**, *16*, 7268-7274.

37. Faler, C. A.; Joullie, M. M. *Org. Lett.* **2007**, *9*, 1987-1990.

38. Falvey, D. E.; Sundararajan, C. *Photochem. Photobiol. Sci.* **2004**, *3*, 831-838.

39. Fetters, L. J.; Lohse, D. J.; Richter, D.; Witten, T. A.; Zirkel, A. *Macromolecules* **1994**, *27*, 4639-4647.

40. Flory, P. J. *Principles of Polymer Chemistry*; Cornell UP: New York, 1953, 102-105.

41. Frechet, J. M. J.; Eichler, E.; Ito, H.; Willson, C. G. *Polymer* **1983**, *24*, 995-1000.

42. Fuchikami, T.; Yamanouchi, A.; Ojima, I. *Synthesis* **1984**, 766-768.

43. Gagis, A.; Fusco, A.; Benedict, J. T. *J. Org. Chem.* **1972**, *37*, 3181-3182.

44. Gokan, H.; Esho, S.; Ohnishi, Y. *J. Electrochem. Soc.* **1983**, *130*, 143-146.

45. Gorgues, A.; Simon, A.; Le Coq, A.; Hercouet, A.; Corre, F. *Tetrahedron* **1986**, *42*, 351-370.

46. Grayson, S. M.; Long, B. K.; Kusomoto, S.; Osborn, B. P.; Callahan, R. P.; Chambers, C. R.; Willson, C. G. *J. Org. Chem.* **2006**, *71*, 341-344.

47. http://www.hitachigst.com/hdd/hddpdf/tech/hdd_technology2003.pdf. **2003**.

48. Gronheid, R.; Fonseca, C.; Leeson, M. J.; Adams, J. R.; Strahan, J. R.; Willson, C. G.; Smith, B. W. *Proc. SPIE* **2009**, *7273*, 727332/727331-727332/727338.

49. Gunther, H. *NMR spectroscopy : basic principles, concepts, and applications in chemistry*; 2nd ed.; Wiley: Chichester, NY, 1995,

50. Ham, S.; Shin, C.; Kim, E.; Ryu, D. Y.; Jeong, U.; Russell, T. P.; Hawker, C. J. *Macromolecules (Washington, DC, U. S.)* **2008**, *41*, 6431-6437.

51. Han, E.; In, I.; Park, S.-M.; La, Y.-H.; Wang, Y.; Nealey, P. F.; Gopalan, P. *Adv. Mater. (Weinheim, Ger.)* **2007**, *19*, 4448-4452.

52. Han, E.; Stuen, K. O.; Leolukman, M.; Liu, C.-C.; Nealey, P. F.; Gopalan, P. *Macromolecules (Washington, DC, U. S.)* **2009**, *42*, 4896-4901.

53. Heath, W. H., Dissertation, *Design, synthesis, and evaluation of materials for microelectronics applications*, The University of Texas at Austin, **2006**.

54. Helbert, J. N.; Chen, C.-Y.; Pittman, C. U., Jr.; Hagnauer, G. L. *Macromolecules* **1978**, *11*, 1104-1109.

55. Hibbs, M. S. *Microlithography: Science and Technology*; Marcel Dekker: New York, 1998, 1-108.

56. Hsieh H. L., Q., R. P. *Anionic Polymerization: Principles and Practical Applications*; Marcel Dekker Inc.: New York, 1996,

57. Hua, F.; Sun, Y.; Gaur, A.; Meitl, M. A.; Bilhaut, L.; Rotkina, L.; Wang, J.; Geil, P.; Shim, M.; Rogers, J. A.; Shim, A. *Nano Lett.* **2004**, *4*, 2467-2471.

58. Huang, C.-P.; Zhu, Y.-Y. In *Active and Passive Electronic Components* 2007; Vol. 1, p 1-13.

59. Hufford, D. L.; Tarbell, D. S.; Koszalka, T. R. *J. Am. Chem. Soc.* **1952**, *74*, 3014-3018.

60. Ichikawa, R.; Hata, M.; Okimoto, N.; Oikawa-Handa, S.; Tsuda, M. *J. Polym. Sci., Part A: Polym. Chem.* **1998**, *36*, 1035-1042.

61. Isemura, T.; Kakita, R.; Kawahara, K. *J. Chromatogr., A* **2004**, *1026*, 109-116.

62. Ito, H.; England, W. P.; Ueda, M. *J. Photopolym. Sci. Technol.* **1990**, *3*, 219-233.

63. Ito, H.; Flores, E.; Renaldo, A. F. *J. Electrochem. Soc.* **1988**, *135*, 2328-2333.

64. Ito, H.; Schwalm, R. *Recent Adv. Anionic Polym., Proc. Int. Symp.* **1987**, 421-430.

65. Ito, H.; Ueda, M.; Schwalm, R. *J. Vac. Sci. Technol., B* **1988**, *6*, 2259-2263.

66. Ito, H.; Willson, C. G. *Polym. Eng. Sci.* **1983**, *23*, 1012-1018.

67. Jain, P. K.; Huang, X.; El-Sayed, I. H.; El-Sayed, M. A. *Plasmonics* **2007**, *2*, 107-118.

68. Jiang, X.; Lavender, C. A.; Woodcock, J. W.; Zhao, B. *Macromolecules (Washington, DC, U. S.)* **2008**, *41*, 2632-2643.

69. Johnson, J. A.; Baskin, J. M.; Bertozzi, C. R.; Koberstein, J. T.; Turro, N. J. *Chem. Commun. (Cambridge, U. K.)* **2008**, 3064-3066.

70. Jung, Y. S.; Ross, C. A. *Nano Lett.* **2007**, *7*, 2046-2050.

71. Kanyogoro, E.; Peckerar, M.; Hughes, H.; Liu, M. *Solid-State Electron.* **2008**, *52*, 1555-1562.

72. Kevwitch, R. M.; McGrath, D. V. *Synthesis* **2002**, 1171-1176.

73. Khandpur, A. K.; Foerster, S.; Bates, F. S.; Hamley, I. W.; Ryan, A. J.; Bras, W.; Almdal, K.; Mortensen, K. *Macromolecules* **1995**, *28*, 8796-8806.

74. Khramov, D. M., Dissertation, *Novel N-heterocyclic carbenes: Applications in materials chemistry and catalysis*, The University of Texas at Austin, **2008**.

75. Kim, G.; Libera, M. *Macromolecules* **1998**, *31*, 2569-2577.

76. Kim, H.-C.; Park, S.-M.; Hinsberg, W. D. *Chem. Rev. (Washington, DC, U. S.)* **2010**, *110*, 146-177.

77. Kim, S. H.; Misner, M. J.; Xu, T.; Kimura, M.; Russell, T. P. *Adv. Mater. (Weinheim, Ger.)* **2004**, *16*, 226-231.

78. Kim, S. O.; Kim, B. H.; Kim, K.; Koo, C. M.; Stoykovich, M. P.; Nealey, P. F.; Solak, H. H. *Macromolecules* **2006**, *39*, 5466-5470.

79. Lambooy, P.; Russell, T. P.; Kellogg, G. J.; Mayers, A. M.; Gallagher, P. D.; Satija, S. K. *Phys. Rev. Lett.* **1994**, *72*, 2899-2902.

80. LaPedus, M. In *EE Times* 2008, p 1-5.

81. Leunissen, L. H. A.; Lawrence, W. G.; Ercken, M. *Microelectron. Eng.* **2004**, *73-74*, 265-270.

82. Leyden, D. E., Cox, R. H *Analytical applications of NMR*; Wiley: New York, 1977, 260.

83. Personal Communication, Lezec, H., *Surface Plasmon*, **2004.**

84. Li, Y.; Wang, X.; Sanchez, I. C.; Johnston, K. P.; Green, P. F. *J. Phys. Chem. B* **2007**, *111*, 16-25.

85. Liu, C.-C.; Nealey, P. F.; Ting, Y.-H.; Wendt, A. E. *J. Vac. Sci. Technol., B: Microelectron. Nanometer Struct.--Process., Meas., Phenom.* **2007**, *25*, 1963-1968.

86. Liu, Z.-W.; Wei, Q.-H.; Zhang, X. *Nano Lett.* **2005**, *5*, 957-961.

87. Long, B. K.; Keitz, B. K.; Webb, R. C.; Wilson, C. G. *Polym. Prepr. (Am. Chem. Soc., Div. Polym. Chem.)* **2008**, *49*, 264-265.

88. Long, B. K.; Keitz, B. K.; Willson, C. G. *J. Mater. Chem.* **2007**, *17*, 3575-3580.

89. Luo, X.; Ishihara, T. *Opt Express* **2004**, *12*, 3055-3065.

90. Luo, X.; Ishihara, T. *Appl. Phys. Lett.* **2004**, *84*, 4780-4782.

91. Maier, S. A.; Atwater, H. A. *J. Appl. Phys.* **2005**, *98*, 011101/011101-011101/011110.

92. Mansky, P.; Liu, Y.; Huang, E.; Russell, T. P.; Hawker, C. *Science (Washington, D. C.)* **1997**, *275*, 1458-1460.

93. Medeiros, D. R.; Aviram, A.; Guarnieri, T. C.; Huang, W.-S.; Kwong, R.; Magg, C. K.; Mahorowala, A. P.; Moreau, W. M.; Petrillo, K. E.; Angelopoulos, M. *IBM J. Res. Dev.* **2001**, *45*, 639-650.

94. Megiatto, J. D., Jr.; Schuster, D. I. *J. Am. Chem. Soc.* **2008**, *130*, 12872-12873.

95. Meiring, J. E., Dissertation, *Mesoscale simulation of the photoresist process and hydrogel biosensor array platform indexed by shape*, The University of Texas at Austin, **2005**.

96. Meuler, A. J.; Hillmyer, M. A.; Bates, F. S. *Macromolecules (Washington, DC, U. S.)* **2009**, *42*, 7221-7250.

97. Milner, S. T. *Science (Washington, D. C., 1883-)* **1991**, *251*, 905-914.

98. Moore, G. In *Electronics Magazine* 1965.

99. Moore, J. D.; Byrne, R. J.; Vedantham, P.; Flynn, D. L.; Hanson, P. R. *Org. Lett.* **2003**, *5*, 4241-4244.

100. Moreau, W. M. *Semiconductor Lithography: Principles, Practices, and Materials*; Pelnum Press: New York, 1998,

101. Munk, P.; Aminabhavi, T. M. *Introduction to Macromolecular Science*; 2nd ed.; John Wiley and Sons: New York, 2001, 241-250.

102. Narita, T.; Hagiwara, T.; Hamana, H.; Maesaka, S. *Polym. J. (Tokyo)* **1988**, *20*, 519-523.

103. Narita, T.; Hagiwara, T.; Hamana, H.; Nara, T. *Makromol. Chem., Rapid Commun.* **1985**, *6*, 301-304.

104. Narita, T.; Hagiwara, T.; Hamana, H.; Nara, T. *Polym. J. (Tokyo)* **1988**, *20*, 277-279.

105. Negulescu, I.; Vogl, O. *J. Polym. Sci., Polym. Chem. Ed.* **1976**, *14*, 2415-2431.

106. Negulescu, I.; Vogl, O. *J. Polym. Sci., Polym. Chem. Ed.* **1976**, *14*, 2995-3012.

107. Netopilik, M.; Kratochvil, P. *Polymer* **2003**, *44*, 3431-3436.

108. Niemz, A.; Bandyopadhyay, K.; Tan, E.; Cha, K.; Baker Shenda, M. *Langmuir* **2006**, *22*, 11092-11096.

109. Nishida, T.; Notomi, M.; Iga, R.; Tamamura, T. *Jpn. J. Appl. Phys., Part 1* **1992**, *31*, 4508-4514.

110. Noach, S.; Manevich, M.; Eisenberg, N.; Fokin, E. P.; Mihalina, T. V. *Nanotechnology* **2005**, *16*, 775-778.

111. Odian, G. *Principles of Polymerization*; 4th ed.; Wiley-Interscience: New York, 2004, 279-282, 444-447.

112. Orji, N. G.; Vorburger, T. V.; Fu, J.; Dixson, R. G.; Nguyen, C. V.; Raja, J. *Meas. Sci. Technol.* **2005**, *16*, 2147-2154.

113. Osborn, B. P., Dissertation, *Vacuum ultraviolet directed design, synthesis and development of 157 nm photoresist materials*, The University of Texas at Austin, **2004**.

114. Park, S.; Wang, J.-Y.; Kim, B.; Xu, J.; Russell, T. P. *ACS Nano* **2008**, *2*, 766-772.

115. Pelliccioli Anna, P.; Wirz, J. *Photochem Photobiol Sci* **2002**, *1*, 441-458.

116. Peters, R. D.; Yang, X. M.; Kim, T. K.; Sohn, B. H.; Nealey, P. F. *Langmuir* **2000**, *16*, 4625-4631.

117. Pinnow, M. J., Dissertation, *Design and synthesis of materials for 157 nm photoresists applications*, The University of Texas at Austin, **2005**.

118. Pollex, A.; Millet, A.; Mueller, J.; Hiersemann, M.; Abraham, L. *J. Org. Chem.* **2005**, *70*, 5579-5591.

119. Resnick, D. J.; Mancini, D.; Dauksher, W. J.; Nordquist, K.; Bailey, T. C.; Johnson, S.; Sreenivasan, S. V.; Ekerdt, J. G.; Willson, C. G. *Microelectron. Eng.* **2003**, *69*, 412-419.

120. Personal Communication, Rigo, B., *Hydrolysis of acetal with formic acid*, **2006.**

121. Romack, T. J.; Harrison, Z. J.; French, D. V.; Amin, D. H.; Hartsell, J. L.; Meyer, J. D. *Macromolecules (Washington, DC, U. S.)* **2007**, *40*, 7180-7183.

122. Ross, C. *Annu. Rev. Mater. Res.* **2001**, *31*, 203-235.

123. Ruiz, R.; Kang, H.; Detcheverry, F. A.; Dobisz, E.; Kercher, D. S.; Albrecht, T. R.; de Pablo, J. J.; Nealey, P. F. *Science (Washington, DC, U. S.)* **2008**, *321*, 936-939.

124. Ryu, D. Y.; Ham, S.; Kim, E.; Jeong, U.; Hawker, C. J.; Russell, T. P. *Macromolecules (Washington, DC, U. S.)* **2009**, *42*, 4902-4906.

125. Ryu, D. Y.; Shin, K.; Drockenmuller, E.; Hawker, C. J.; Russell, T. P. *Science (Washington, DC, U. S.)* **2005**, *308*, 236-239.

126. Ryu, D. Y.; Wang, J.-Y.; Lavery, K. A.; Drockenmuller, E.; Satija, S. K.; Hawker, C. J.; Russell, T. P. *Macromolecules (Washington, DC, U. S.)* **2007**, *40*, 4296-4300.

127. Sakurai, H.; Hosomi, A.; Saito, M.; Sasaki, K.; Iguchi, H.; Sasaki, J.; Araki, Y. *Tetrahedron* **1983**, *39*, 883-894.

128. Sanders, E. W., *Optical Properties of Metallic Nanoparticles*, Yale University, **2007**.

129. Personal Communication, Satoshi Kikichi, Y. S., *Central Glass Polymerization of TFETFMA*, **2006.**

130. Schmid, G. M., Dissertation, *Understanding molecular scale effects during photoresist processing*, The University of Texas at Austin, **2003**.

131. Service Robert, F. *Science* **2006**, *314*, 1868-1870.

132. Singha, N. K.; De, P. P.; Sivaram, S. *J. Appl. Polym. Sci.* **1997**, *66*, 1647-1652.

133. Slot, E.; Wieland, M. J.; de Boer, G.; Kruit, P.; ten Berge, G. F.; Houkes, A. M. C.; Jager, R.; van de Peut, T.; Peijster, J. J. M.; Steenbrink, S. W. H. K.; Teepen, T. F.; van Veen, A. H. V.; Kampherbeek, B. J. *Proc. SPIE* **2008**, *6921*, 69211P/69211-69211P/69219.

134. Spatz, J. P.; Moeller, M.; Noeske, M.; Behm, R. J.; Pietralla, M. *Macromolecules* **1997**, *30*, 3874-3880.

135. Srituravanich, W.; Durant, S.; Lee, H.; Sun, C.; Zhang, X. *J. Vac. Sci. Technol., B: Microelectron. Nanometer Struct.--Process., Meas., Phenom.* **2005**, *23*, 2636-2639.

136. Srituravanich, W.; Fang, N.; Sun, C.; Luo, Q.; Zhang, X. *Nano Lett.* **2004**, *4*, 1085-1088.

137. Stevens, M. P. *Polymer Chemistry: An Introduction*; 3rd ed.; Oxford UP: New York, 1999, 191-194.

138. Stewart, M. D., Dissertation, *Catalyst diffusion in positive-tone chemically amplified photoresists*, The University of Texas at Austin, **2003**.

139. Stewart, M. D.; Johnson, S. C.; Sreenivasan, S. V.; Resnick, D. J.; Willson, C. G. *J. Microlithogr., Microfabr., Microsyst.* **2005**, *4*, 011002/011001-011002/011006.

140. Stoykovich, M. P.; Mueller, M.; Kim, S. O.; Solak, H. H.; Edwards, E. W.; de Pablo, J. J.; Nealey, P. F. *Science (Washington, DC, U. S.)* **2005**, *308*, 1442-1446.

141. Szwarc, M. *Carbanions Living Polymers and Electron Transfer Processes*; Interscience: New York, 1968, 104-150.

142. Tanaka, A.; Hozumi, Y.; Hatada, K.; Endo, S.; Fujishige, R. *J. Polym. Sci.* **1964**, *2*, 181-186.

143. Taylor, J. C., Dissertation, *Advanced lithographic patterning technologies: Materials and processes*, The University of Texas at Austin, **2007**.

144. Thompson, L. F.; Willson, C. G.; Bowden, M. J.; Editors *ACS Symposium Series, Vol. 219: Introduction to Microlithography: Theory, Materials, and Processing*, 1983, 139-267.

145. Thurn-Albrecht, T.; Steiner, R.; DeRouchey, J.; Stafford, C. M.; Huang, E.; Bal, M.; Tuominen, M.; Hawker, C. J.; Russell, T. P. *Adv. Mater. (Weinheim, Ger.)* **2000**, *12*, 787-790.

146. Trinque, B. C., Dissertation, *Synthesis, copolymerization studies and 157 nm photolithography applications of 2-trifluoromethylacrylates*, The University of Texas at Austin, **2003**.

147. Uhrig, D.; Mays, J. W. *J. Polym. Sci., Part A: Polym. Chem.* **2005**, *43*, 6179-6222.

148. Umino, Y.; Narita, T.; Hamana, H. *J. Polym. Sci., Part A: Polym. Chem.* **2008**, *46*, 7011-7021.

149. Van Oss, C. J.; Good, R. J.; Chaudhury, M. K. *Langmuir* **1988**, *4*, 884-891.

150. Personal Communication, Viscotek, *Solvents for Fluorinated Polymers*, **2008.**

151. Vogl, O. *J. Polym. Sci., Part A: Polym. Chem.* **2000**, *38*, 2293-2299.

152. Vogl, O. *Makromol. Chem.* **1974**, *175*, 1281-1308.

153. Vogl, O. *J. Polym. Sci., Part A: Polym. Chem.* **2004**, *42*, 795-818.

154. Walton, D. G.; Kellogg, G. J.; Mayes, A. M.; Lambooy, P.; Russell, T. P. *Macromolecules* **1994**, *27*, 6225-6228.

155. Wang, J.-L.; Grimaud, T.; Matyjaszewski, K. *Macromolecules* **1997**, *30*, 6507-6512.

156. Wang, J.-L.; Grimaud, T.; Shipp, D. A.; Matyjaszewski, K. *Macromolecules* **1998**, *31*, 1527-1534.

157. Wang, L.; Jin Eric, X.; Uppuluri Sreemanth, M.; Xu, X. *Opt Express* **2006**, *14*, 9902-9908.

158. http://www.inc.com/news/articles/200707/computers.html. **2007**.

159. Willson, C. G.; Dammel, R. A.; Reiser, A. *Proc. SPIE-Int. Soc. Opt. Eng.* **1997**, *3050*, 38-51.

160. Willson, C. G.; Ito, H.; Frechet, J. M. J.; Tessier, T. G.; Houlihan, F. M. *Journal of the Electrochemical Society* **1986**, *133*, 181-187.

161. Willson, C. G.; Ito, H.; Miller, D. C.; Tessier, T. G. *Polym. Eng. Sci.* **1983**, *23*, 1000-1003.

162. Win, T.; Yerushalmi, S.; Bittner, S. *Synthesis* **2005**, 1631-1634.

163. Wuensch, B.; Zott, M. *Synthesis* **1992**, 927-928.

164. Yeo, J.; Kim, H.; Eynon, B. *Proc. SPIE* **2008**, *6921*, 692107/692101-692107/692109.

Vita

Jeffrey Ryan Strahan was born on March 18th, 1983 in San Antonio, TX to parents James William and Victoria Lynn Strahan. After short periods in Dallas, TX and Salt Lake City, UT, Jeff grew up in the suburbs of Nashville, TN where he graduated from Franklin High School in 2001. Jeff attended Gonzaga University and conducted undergraduate research with Prof. Jennifer Shepherd for the latter half of his studies, including a summer internship at the University of California Los Angeles with Prof. Catherine Clarke. After receiving a B.S. in chemistry from Gonzaga University 2005, Jeff continued his studies at the University of Texas at Austin under Prof. C. Grant Willson, which included a summer internship at the National Institute of Standards and Technology under Dr. James Liddle. Jeff received his Ph.D. in organic chemistry in 2010 and will join the research and development team of Milliken and Company in Spartanburg, SC.

Permanent address: 27620 Olde Nantucket, San Antonio, TX 78015

This dissertation was typed by Jeffrey Ryan Strahan.